Cannabinoids delivery systems based on supramolecular inclusion complexes and polymeric nanocapsules for treatment of neuropathic pain

Fanny Astruc Astruc-Diaz

N° d'ordre : **99-2012** Année 2012

THESE DE L'UNIVERSITE DE LYON

Délivrée par

L'UNIVERSITE CLAUDE BERNARD LYON 1

ECOLE DOCTORALE DE CHIMIE

DIPLOME DE DOCTORAT

(arrêté du 7 août 2006)

soutenue publiquement le 9 Juillet 2012

par

Mme. ASTRUC-DIAZ Fanny

CANNABINOIDS DELIVERY SYSTEMS BASED ON SUPRAMOLECULAR INCLUSION COMPLEXES AND POLYMERIC NANOCAPSULES FOR TREATMENT OF NEUROPATHIC PAIN

Jury	Mme. DUCKI Sylvie	Rapporteur
	M. VIERLING Pierre	Rapporteur
	M. DUTASTA Jean-Pierre	Examinateur
	M. PAROLA Stéphane	Directeur de thèse
	M. THOMPSON Charles	Examinateur

To Matteo and Maxime,

To Philippe,

ACKNOWLEGEMENTS

I would like to give my sincere gratitude to my advisor, Dr. Stephane Parola, for his confidence and for giving me the opportunity of conducting this Ph.D research.
I wish to give my profoundness appreciation to Dr. Philippe Diaz for his excellence guidance, patience, caring and time to complete this work.
I would like to thank Dr. Charles Thompson for generously giving me the time and the support to achieve this project.
I would also like to thank my Jury members for their time to review my dissertation.
I am appreciative of the help I've received from my colleagues at the University of Montana, Steven McDaniel for the cyclodextrin molecular modeling, Dr. James Driver for conducting the nanocapsules morphological studies, Dr. Christopher Palmer for his guidance with the use of the GC-MS, Dr. Ravil Petrov for his help and practical experience in the laboratory, and Dr. Nicolas Guilloteau and Dr. Yamina Belabassi for their warm words of encouragement. I am also appreciative for my co-workers at MD Anderson Cancer Center and Dr. Mohamed Naguib for giving me the opportunity to work in his laboratory, Dr. Gabriel Lopez-Berestein for teaching me how to make non ionic liposomes and Dr. Pablo Vivas-Mejia for his help preparing them. I would like to give my gratitude to Dr. Jon Nagy and Ryan Holly for hosting me in their laboratory and assisting me with particle sizing studies.
Finally, I would like to thank my friend, Agnes, and my family, my mum and my sister Melanie for their unconditional trust and support through all this difficult and rewarding experience, and my dad who passed away before the completion of this thesis. I am grateful to my parents in law, Nelly and Mario for their gentleness and their help taking care of my sons while I was busy preparing my seminar. I would also like to thank my sons for their love and patience even when I was frustrated and not available for them. Most of all, I would like to thank my husband who loved me when I deserved it the least but when I needed the most.

TABLE OF CONTENTS

LIST OF ABBREVIATIONS

A	
AC	Adenylate cyclase
AEA	Anandamine
2-AG	2-arachidonylglycerol
AIDS	Acquired immunodeficiency syndrome
AUC	Area under curve
B	
BCS	Biopharmaceutics Classification System
BSA	Bovine serum albumin
BSCB	Blood-spinal cord barrier
C	
CBD	Cannabidiol
CBs	Cannabinoids
CB1	Cannabinoid receptor 1
CB2	Cannabinoid receptor 2
CCI	Chronic constriction nerve injury
CDs	Cyclodextrins
CE	Complexation efficiency
CIPN	Chemotherapy-induced peripheral neuropathy
CMC	Critical micelle concentration
CNS	Central Nervous System
CrELP	Cremophor™ ELP
CB[n]	Cucurbituril
CV	Coefficient of variation
D	
DDS	Drug delivery system
DLS	Dynamic Light Scattering
DMF	Drug master file
dPN	Diabetic peripheral neuropathy
DMSO	Dimethyl sulfoxide
DMPC	Dimyristoylphosphatidyl choline
DPN	Distal peripheral neuropathy
DRG	Dorsal root ganglia
DSE	Depolarization-Induced Suppression of Excitation

DSI	Depolarization-Induced Suppression of Inhibition
E	
(E)-BCP	Beta-caryophyllene
ε	Dielectric constant
EC_{50}	Half maximal effective concentration
ECs	Endocannbinoids system
eCBs	Endocannabinoids
EE	Entrapment efficiency
EMEA	European Medicines Agency
EMT	Enzyme membrane transporter
EPR	Enhanced Permeability and Retention
ERK1/2	Extracellular signal-regulated kinase-1 and -2
ESI-MS	Electrospray mass spectrometry
EtOH	Ethanol
Eud	Eudragit
F	
FAAH	Fatty acid amide hydrolase
FLAT	FAAH-like anandamide transporter
FDA	Food and Drug Administration
FTIR	Fourier transform infrared spectroscopy
G	
GALT	Gut-associated lymphoid tissue
δ	Hildebrand solubility parameter
GRAS	Generally regarded as safe
GC-MS	Gas chromatography–mass spectrometry
GDP	Guanosine diphosphate
GI	Gastrointestinal
GIRK	Inwardly rectifying potassium channels
GIT	Gastrointestinal tract
Gln	Glutamine
Glu	Glutamate
GTP	Guanosine triphosphate
H	
HLB	Hydrophilic lipophylic balance
$(5\text{-HT})_3$	Serotonin receptor
HPβCD	Hydroxypropyl-β-cyclodextrin
HPγCD	Hydroxypropyl-γ-cyclodextrin

HPLC	High performance liquid chromatography
I	
IC_{50}	Median inhibition concentration
IENF	Intraepidermal nerve fibers
IIG	Inactive Ingredient Guide
i.m.	Intramuscular
i.p.	Intraperitoneal
i.v.	Intravenous
J	
JNK	c-Jun N terminal kinase
K	
K_I	Inhibition constant
L	
LC/MS/MS	liquid chromatography/tandem mass spectrometric
LD_{50}	Half lethal dose
Log P	Partition Coefficient
M	
MA	Maleic acid
MAGL	Monoacylglycerol lipase
MAPK	Mitogen-activated protein kinases
MeOH	Methanol
MLVs	Multilamellar vesicles
MS	Multiple sclerosis
MPS	Mononuclear Phagocytic System
N	
nACh	Acetylcholine Receptor
NADA	N-Arachidonoyldopamine
NAGly	N-arachidonylglycine
NAPE	N-acyl-phosphatidylethanolamine
NAPE-PLD	N-acyl-phosphatidylethanolamine hydrolyzing phospholipase D
NCE	New chemical entity
NMDA	N-Methyl-D-aspartate receptor
NMP	N-methyl-2-pyrrolidone
NMR	Nuclear magnetic resonance
NO	Nitric oxide
NOESY	Nuclear Overhauser effect spectroscopy
NP	Neuropathic pain

NPs	Nanoparticles
NS	Nanosuspension
O	
OEA	N-oleoylethanolamine
OLVs	Oligolamellar vesicles
OR	Ostwald ripening
P	
P80	Polysorbate 80
PAA	N-palmitoylethanolamine-preferring acid amidase
PBS	Phosphate buffer saline
PC	Phosphatidylcholine
pCBs	Phytocannabinoids
PCS	Photon Correlation Spectroscopy
PD	Pharmacodynamy
PDA	Photo diode array
PDI	Polydispersity index
PEA	N-palmitoylethanolamine
PEG	Polyethylene glycol
PG	Propylene glycol
PI3K	Phosphoinositide 3-kinase
PIN	Paclitaxel-induced neuropathy
PK	Pharmacokinetic
PLA	Poly(lactic acid)
PLGA	Poly(lactic-co-glycolic acid)
PNS	Peripheral nervous system
pol/Φ_{solv}.	Polymer to solvent ratio
PPAR	Peroxisome proliferator-activated receptors
χ	Solvent/non-solvent interaction parameter
R	
RES	ReticuloEndothelial System
R_f	Retention factor
RMβCD	Randomly methylated β-cyclodextrin
ROESY	Rotating-frame NOE spectroscopy
S	
SBEβCD	Sulfobutylether-β-cyclodextrin sodium salt
SEDDS	Self-Emulsifying Drug Delivery System
s.c.	Subcutaneous

SEM	Scanning Electron microscopy
SNL	Spinal nerve ligation
T	
TBOA	DL-threo-β-benzyloxyaspartate
TEM	Transmission Electron Miscroscopy
THC	Tetrahydrocannabinol
THF	Tetrahydrofuran
TLC	Thin layer chromatography
TRPV1	Transient Receptor Potential Vanilloid type-1
U	
UNODC	United Nations Office on Drugs and Crimes
USP	Pharmacopeia of the United States
Z	
Z-average	Mean diameter of particles

INTRODUCTION AND OBJECTIVES

Up to 8%[5] of the European population and approximately 3.8 million individuals in the United States[6] are affected by Neuropathic pain (NP). NP is generally chronic and disabling and challenging to treat with only 40-60% of patients achieving partial relief[7]. Neuropathic pain may arise as a consequence of a lesion or disease affecting the somatosensory system and could be CNS or PNS related[8]. The management of patients with chronic NP is complex and response to existing treatments often inadequate[9]. Common therapeutics include antidepressants, antiepileptic, opioids and tramadol. The therapeutic potential of cannabinoids has recently been investigated following the discovery of the endocannabinoid system and is gaining clinical acceptance to improve NP outcomes, particularly for CB2 receptors agonists which have shown to produce antinociception without psychotropic effect[10-14]. Synthetic and natural cannabinoids compounds are generally lipophilic in nature and evidence indicates that lipophilicity may be of importance for potentializing their therapeutic activity[15-16]. Furthermore, pharmacological activity of a drug is the result of affinity and interaction with its biological target but also optimum and reliable exposure at the target site. Appropriate drug delivery system (DDS) are thereby required to deliver the drug at a sufficient concentration to the site of action. The goals of this research project were 1) to design, develop and study an early drug delivery system allowing *in vivo* PK and PD studies of a selective CB2 agonist recently synthesized in our laboratory, 2) to design and elaborate a DDS based on cationic nanocapsules for a highly lipophilic natural CB2 agonist for future theragnostic applications.

Chapter I is a bibliography review defining the endocannabinoid system i.e. receptors, endocannabinoids, enzymes, transporters and its signaling pathway as well as an overview of the family of synthetic and natural cannabinnoid compounds and their therapeutical use. Finally, pain and neuropathic pain mechanisms are approached and their potential treatment using CB2 agonists discussed.

In **Chapter II**, we designed and characterized different DDS for CB2 agonists synthesized in our laboratory namely, co-solvent/surfactant micellar system, self-emulsifying drug delivery system (SEDDS), cyclodextrin inclusion complexes and liposomal suspension, to support *in vivo* PK/PD studies. We also compared their influence on the activity of our lead compound MDA7 on a model of neuropathic pain in rats. A thorough investigation of MDA7-hydroxypropyl cyclodextrin complexes formation has been conducted to afford a better understanding of this promising and efficient DDS for the delivery of lipophilic cannabinoids.

In **Chapter III**, we designed and characterized cationic drug-loaded polymeric nanocapsules obtained by a nanoprecipitation method, for the delivery of a model drug, a natural CB2 agonist, beta-caryophyllene [(E)-BCP]. We investigated the impact of various factors and operating conditions on the formation of nanocapsules, and optimize their size, size distribution and drug entrapment efficiency. The aim was to develop a protective and mucoadhesive colloidal carrier for the oral delivery of the oxidation sensitive (E)-BCP, applicable to other cannabinoids for *in vivo* administration.

Using the well characterized cationic nanocapsules developed, we generated preliminary results on the feasibility and characterization of macrocycles-nanocapsules complexes formation, based on host-guest/electrostatic interactions and counterionic condensation with respectively cucurbituril and sulfobutyl ether-beta-cyclodextrins. Fluorescent dye has also been incorporated in order to further use these complexes as sensitive and highly-specific probes providing a unique concept of theragnostic combining diagnostic/imaging to assess the efficiency of drug delivery and possible mechanisms of nanocapsules bioabsorption, and therapeutic activity.

CHAPTER I BIBLIOGRAPHY

1. Cannabis.

Cannabinoids have been used as therapeutic agent for more than 4000 years in China and across many ancient cultures. The two most referenced cannabinoids preparations, named differently depending on the culture, are marijuana and hashish. Both preparations are derived from the hemp plant *Cannabis sativa L.,* (Cannabaceae). Hashish is composed of cannabis resin secreted by glands called Trichomes. The ethymology of this word is still debated and associated from the Middle ages with a chiite sect called hashishins. In India, Hashish has been used for centuries for religious and medicinal purpose and is called Charas. Marijuana is dried leaves and female flower heads. Cannabis was included in the earliest Chinese Pharmacopeia Shen-nung pen ts'ao ching (divine Husbandman's material medica)[17].

Innumerable indications for cannabis therapeutic uses have been reported such as analgesic, anticonvulsant, hypnotic, tranquilizer, anesthetic, anti-inflammatory, antibiotic, antiparasite, antispasmodic, digestive, appetite stimulant, diuretic, aphrodisiac or anaphrodisiac, antitussive, expectorant and others[18]. The introduction of cannabis in European medicine and then in North America occurred in the midst of the 19th century. Pharmaceuticals laboratories (i.e. Merck, Bristol-Meyers, Eli Lilly) commercialized cannabis extracts or tinctures.

From the early 20th century to the current phase III clinical trial in USA or the recent approval in Europe and Canada of Sativex (GW Pharmaceuticals), the use of cannabis derivatives as medicinal agent has been the subject of controversy. Despite its therapeutic potential, cannabis is today considered as a potential drug of abuse which has been hampering the development of new cannabinoids derivatives as therapeutics. Potential side effects are discussed in section 8.

Cannabis extracts contains more than 460 compounds of which around 70 are considered as phytocannabinoids[19]. The primary psychoactive phytocannabinoid of cannabis is delta-9-tetrahydrocannabinol, commonly known as Δ^9-THC, and scheduled I by the DEA. Despite early intense use, medicinal cannabis use declined likely because of

readily available aspirin and opioids treatments and cannabis criminalization (i.e.1937 in the United States, 1970 in France, 1971 in UK).

2. Endocannabinoid system.

In recent years, several endogenous lipids, named endocannabinoids (eCBs), have been shown to activate cannabinoid receptors (CBs), which are also the molecular targets of phytocannabinoids such as the Δ^9-THC. The identification of an endogenous cannabinoids system (ECs) renewed in the late 20th century the interest for cannabinoids as potential therapeutics. The ECs is defined as the signaling system consisting of eCBs together with their target receptors, the presumed endocannabinoid membrane transporters and the enzymes and other proteins regulating the tissue levels of eCBs. The ECs plays a key role in mediating and modulating numerous fundamental physiological processes involving CNS and autonomic nervous system, immune, endocrine, reproductive and cardiovascular activity[20-22]. Imbalance in the ECs results in the impairment of various processes including neuroinflammation, immunomodulation and food control. Because of the modulation of these processes, ECs has been involved in different pathologies such as Alzheimer disease[23-24], multiple sclerosis[25-26], Parkinson disease,[27] chronic and inflammatory pain[11,28-32], cancer[33-34], nausea vomiting[35], obesity[36-37], epilepsy[38] ,glaucoma[39] ,asthma[40], mood disorders[41-42].

Table 1[43]: Chronology of selected discoveries on the field of cannabinoids. The identification of the cannabinoid receptor in 1988 and anandamide in 1992 marked the initiation of a tide of research findings that led to the discovery of the endogenous cannabinoid system and to the first clinical application of an endocannabinoid-based therapy in less than 20 years.

Year	Discovery	Citation
1964	Identification of the chemical structure of Δ^9-tetrahydrocannabinol	44
1984	First proof that cannabinoids decrease cyclic adenosine monophosphate, suggesting mediation by a Gi/o-coupled receptor	45
1988	Identification of the CB1 receptor	46
1990	Molecular cloning and mapping of CB1	47-48
1992	Identification of the first endogenous ligand on CB receptors: arachidonyl ethanolamine (anandamide, AEA)	49
1993	Identification of the CB2 receptor	50
1994	Development of SR141716A (rimonabant)	51
1994	Mechanisms of cannabinoid biosynthesis	52
1995	2-arachidonoyl glycerol, a second endocannabinoid	53-54
1996	Fatty acid amidohydrolase, the first enzyme degradating endocannabinoids	55
1997	Evidence for anandamide transport	56
1997	Neurobiology of cannabinoid dependence and withdrawal	57
1999	Generation of CB1-receptor knockout mice	58
2001	Functional role for CB1 receptors in drug self-administration and relapse	59-60
2001	First demonstration that endocannabinoids modulate synaptic transmission in the brain	61-63

Year	Discovery	Citation
2001	First evidence for the existence of further cannabinoid receptors	64
2002	Endocannabinoids mediate extinction of aversive memories	65
2003	Anandamide degradation and anxiety	66
2005	First clinical indication for cannabinoid CB1 receptor antagonists	67

3. Cannabinoid receptors.

The two different cannabinoid receptors named CB1 and CB2 belong to the family of seven transmembrane Guanosine binding Protein-Coupled Receptors family (GPCR) and are Gαi/o protein-coupled. In 1990, the first cannabinoid receptor CB1 has been characterized and cloned from a rat cerebral cortex by Matsuda[48].CB2 was isolated from human myeloid cells and cloned more recently by Munro in 1993[50]. CB1 and CB2 exhibit 48% of amino acid sequence identity[50]. Human and rat CB1 and CB2 receptors show 97% and 81% amino-acid sequence identity, respectively[48, 68-69]. These receptors are widely expressed and distinguished by their functions, localizations and signaling mechanisms. CB1 is expressed in the CNS in neurons but also in immune cells. CB2 was thought to be expressed only in immune cells but recent evidences show that it's also express in CNS on glial cells and neurons[70-73]. Low expression of CB2 under normal physiological conditions in the CNS could explain why it was considered first as a peripheral CB receptor. CB1 and CB2 stimulation result in central and peripheral activities. CB1 receptor is likely involved in the regulation of cognition, memory, motor activity, appetite, wake/sleep cycles, affective response, thermogenesis and nociception[22] while the CB2 receptor has been described to be involved in the regulation of immune responses and/or inflammatory reactions, modulating immune cells migration, cytokines release and antigen presentation within the CNS and outside[74-76]. Neurologic function of CB2 has been less studied than CB1[72, 77-78]. Neuronal CB1 receptor, is a pre-synaptic localized receptor, with highest density in the hippocampus, cerebellum, striatum, basal ganglia and cortex. CB1 is also expressed in immune cells and involved in immunomodulation. CB1 expressed in peripheral tissues/organs is responsible for

energy metabolism such as in liver, gastrointestinal tract, pancreas, white and brown adipose tissue or skeletal muscle[79-80]. In less extent CB1 is present in adrenal gland, bone marrow, heart, lung, prostate and testicles/ovaries[81].

CB2 receptors are expressed mainly on immune tissues and cells such as spleen, tonsils, monocytes, and B and T lymphocytes, macrophages, natural killer cells, but also in skeletal muscle. Importantly, CB2 is expressed in the CNS immune cells, microglia[82], cerebromicrovascular endothelial cells[83] and possibly astrocytes[84] and its expression is increased after inflammation. Onaivi was one of the pioneers[85] to demonstrate that CB2 receptors and their gene transcripts are also widely distributed in the CNS under normal physiologic conditions. The expression of CB2 receptors in glial but also neuronal cells in the brain suggests that CB2 receptors may play broader roles in the CNS than previously appreciated[71-72,86-88]. CB2 has been subject to less investigation than CB1 and since it has no or less severe psychoactive effect, it is emerging as a new phamocological target for the treatment of schizophrenia[89-90] or addiction[91].

These two receptors are capable of binding a variety of endogenous and exogenous chemical ligands acting as agonist or antagonist which arise new development strategies for treatment of diseases.

4. Endocannabinoids.

The best studied and the most active eCBs as yet described are anandamide (AEA)[49] an ethanolamide derivative of arachidonic acid derived from sanskrit word ananda meaning bliss, and 2-arachidonylglycerol (2-AG)[53-54] (Fig. 1). AEA and 2-AG and eCBs in general are ligands at both of CB1 and CB2 with higher affinity for CB1[92]. AEA is also described as a partial agonist at CB1[93], a weak CB2 agonist and can activate the non CB capsaicin/vanilloid receptor named transient receptor potential vanilloid type-1 (TRPV1) channel. 2-AG is a full agonist at both CB1 and CB2 receptors, more efficacious and 170 to 1000-fold more concentrated than AEA in the brain[54,94-95]. Due to their lipophilic nature, eCBs are local mediators, biosynthetized on-demand and released immediately from cells. In the CNS, eCBs act as retrograde neuromodulators, released from post-synaptic neurons and acting at CB1 on pre-synaptic axon terminals[96], modulating the release or reuptake of neurotransmitters to prevent the development of excessive neuronal activity.

Thereby, eCBs maintain homeostasis in the CNS under physiological and pathological conditions[97].

CB2 activation in brain microglial cells[82, 98-99], astrocytes[100] and oligodendrocytes[101-102] regulate neuroinflammation and provide neuroprotection by attenuating proinflammatory agents release such IL-1β, TNFα or nitric oxide (NO) as well as inhibiting other inflammatory mediators[23, 103-104]. CB2 cell distribution has remained controversial due to uncertainty of experimental approaches used or specificity of some methodological tools available such as anti-CB2 antibody[105]. Several additional eCBs have been identified, among them are two additional analogues of anandamide namely homo-γ-linolenylethanolmide and docosotetraenylethanolamide[106-107] triggering comparable pharmacological effects as anandamide. Other eCBs have been studied such as the non hydrolysable 2-AG analogue noladin ether (2-arachidonyl glycerol ether)[108] displaying a CB1 agonist profile, Virodhamine (0-arachidonoyl-ethanolamine)[109] showing CB1 antagonist or partial agonist activity and full agonist activity at CB2, and NADA (N-Arachidonoyldopamine)[110] an endogenous ligand for CB1 and a potent agonist at TRPV1. In addition, two endogenous peptides analogues of hemopressin have been newly discovered and described as CB1 agonists[111-112]. Otherwise, other eCB-related compounds have also been described[113] (see a non exhaustive list in Fig.1). They present high structural similarity with eCBs and may potentiate the eCBs effect, a so called “entourage effect”, by inhibiting their degradation[2]. Among the latter substances, which display cannabimimetic activity whereas less active or even inactive at CBs, are mentioned *N*-palmitoylethanolamine (PEA) claimed to possess anti-inflammatory, anticonvulsant, and antiproliferative activities[114], N-stearoylethanolamine reported to induce apoptosis of glioma cells[115], N-oleoylethanolamine (OEA) described to act as an appetite suppressor[116] and N-arachidonylglycine (NAGly) presented to suppress tonic inflammatory pain[117].

These eCBs congeners which play a biological function by activating non-CB1 and non-CB2 receptors, are more abundant than eCBs. Their range of activity remains still obscure and need to be investigated.

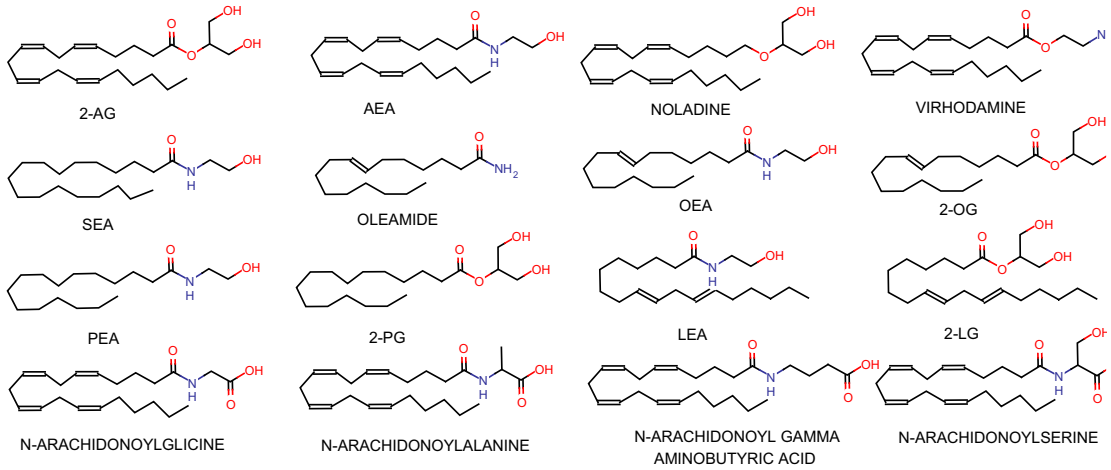

Figure 1: Endocannabinoid-related compounds. SEA: steroylethanolamide; OEA:oleoylethanolamide; 2-OG: 2-oleoylglycerol; PEA:palmitoyethanolamide; 2-PG: 2-palmitoylglycerol; LEA: linoleoyethanolamide; 2-LG: 2-linoleoylglycerol.

5. Enzymes

The enzymes responsible for catabolic and the biosynthetic pathways of AEA and 2-AG have been an attractive target for the synthetic chemists. Drugs that interfere with these enzymes can pharmacologically regulate the eCBs levels and thereby the CB receptors without interacting with them. AEA and 2-AG are produced on demand through multiple biosynthetic pathways, which encompasses N-acyl-phosphatidylethanolamine (NAPE)-hydrolyzing phospholipase D (NAPE-PLD) for AEA,[118] and sn-1-specific diacylglycerol lipase and phospholipase C for 2-AG[119]. The degradation of eCBs occurs through different pathways including the major hydrolytic enzymes fatty acid amide hydrolase (FAAH) for AEA. Although 2-AG also acts as a substrate for FAAH, monoacylglycerol lipase (MAGL) is considered the primary enzyme of 2-AG degradation[120]. To a lesser extent other intracellular enzymes have a role in the AEA and 2-AG degradation including *N*-palmitoylethanolamine-preferring acid amidase (PAA), cyclooxygenase-2, lipoxygenases and cytochrome P450. Recently, two additional enzymes have been described to be responsible of a portion of 2-AG hydrolysis, ABHD6[121], and ABHD12. MAGL, ABHD6 and ABHD12 collectively account for at least 98% of the total 2-AG hydrolase activity in brain but each enzyme exhibits a distinct subcellular distribution, suggesting that they may regulate distinct pools of 2-AG in the nervous system[122]. These enzymes are intracellular and require the reuptake of eCBs implying a putative

transporter (EMT)[123-125] for metabolism. A variant of the anandamide-degrading enzyme fatty acid amide hydrolase (FAAH), termed FAAH-like anandamide transporter (FLAT), that lacked amidase activity but bound anandamide with low micromolar affinity and facilitated its translocation into cells has been recently identified as the first EMT[126]. These biosynthetic or degradative enzymes allow metabolic control of the endogenous tone of eCBs, and hence they regulate the biological activities of these substances.

The number of members of ECs is still increasing and might soon include non-CB1 non-CB2 receptors for endocannabinoids, endocannabinoid-related molecules with little activity at CB1 and CB2 receptors, and new enzymes for the biosynthesis and degradation of these molecules. The ECs can be described as a pleiotropic and locally acting pro-homeostatic signaling system activated 'on demand' following perturbation of cell homeostasis[2].

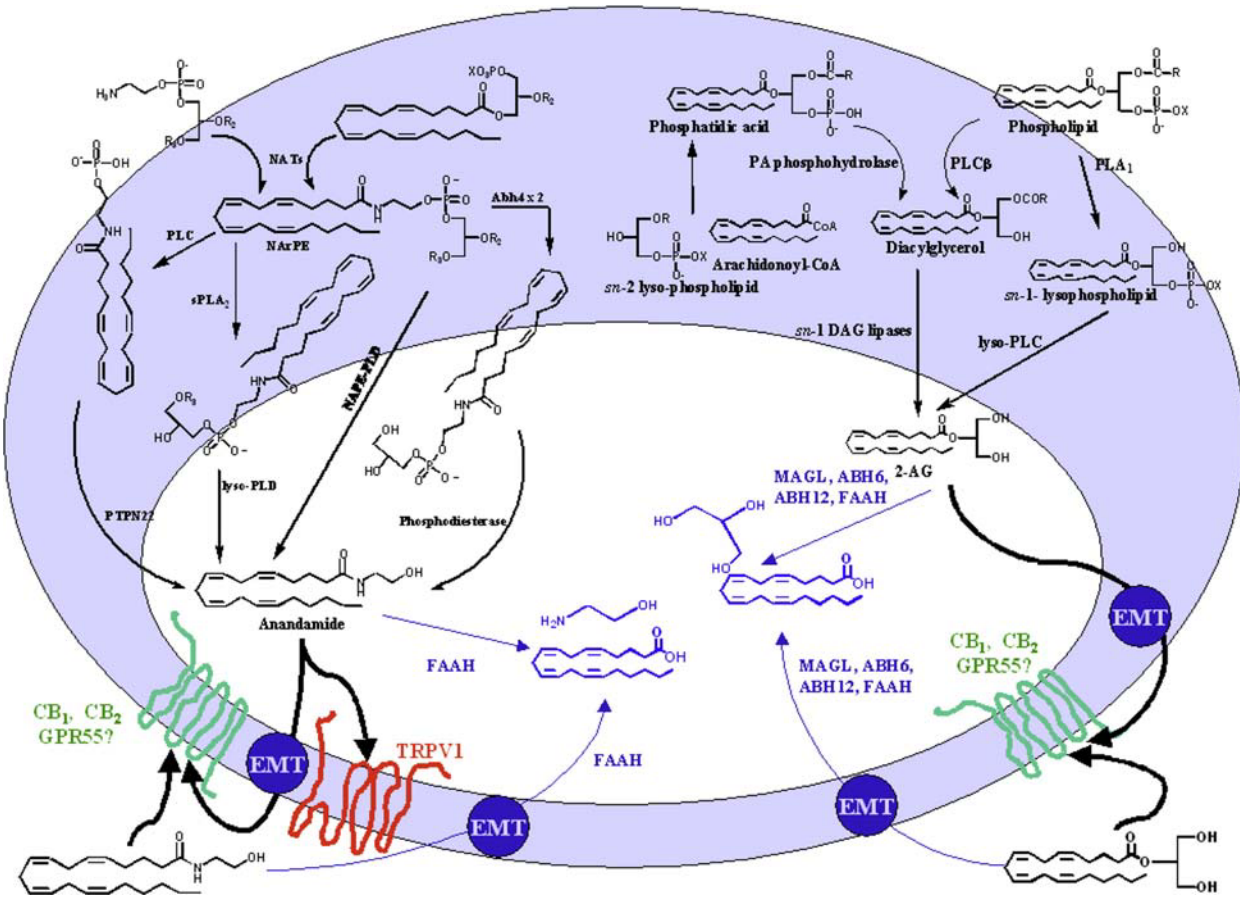

Figure 2[2]: Biosynthesis, action, and inactivation of the two best-studied endocannabinoids, anandamide and 2-arachidonoylglycerol (2-AG). Several pathways might exist for both the formation and catabolism of anandamide and 2-AG. The former originates from a phospholipid precursor, *N*-arachidonoyl-phosphatidyl-ethanolamine (NArPE), formed from the *N*-arachidoylation of phosphatidylethanolamine via *N*-acyltransferases(NATs). NArPE is transformed into anandamide via four possible alternative pathways, the most direct of which is catalysed by an *N*-acyl-phosphatidylethanolamine-selective phosphodiesterase (NAPE-PLD). 2-AG is produced almost exclusively via the hydrolysis of diacylglycerols (DAGs) via *sn*-1-selective DAG lipases (DAGLs) α and β. After cellular re-uptake via a specific and yet-to-be characterized mechanism (EMT), which appears to also mediate the release of de-novo biosynthesized endocannabinoids, anandamide is metabolized via fatty acid amide hydrolase-1 (FAAH) and 2-AG via several monoacylglycerol lipases (MAGLs). 2-AG can also be degraded by FAAH. Both endocannabinoids activate CB_1 and CB_2 receptors with different affinities (anandamide being the one with highest affinity in both cases) and efficacies (2-AG being the one with highest efficacy in both cases). Anandamide can also activate transient receptor potential vanilloid type-1 (TRPV1) channels at an intracellular site, and interact with several other molecular targets, whereas both compounds were recently reported by some authors, but not by others, to interact with GPR55, an orphan G-protein-coupled receptor. Abh4,6,12, α-β-hydrolases 4, 6, 12; PLD, phospholipase D; $PLA_{1/2}$, phospholipase A_1/A_2; PTPN22, protein tyrosine phosphatase N22. Biosynthetic pathways are shown in black, degradative ones in blue. Thick arrows denote movement or action.

6. Cannabinoid receptor-mediated intracellular signal pathways.

Depolarization and subsequent calcium influx triggers the biosynthesis and the release of eCBs that can act as fast retrograde signaling molecules that activate presynaptic CB1 receptors. Activation of these receptors can transiently inhibit the release of neurotransmitters such as GABA or glutamate in processes termed depolarization-induced suppression of inhibition (DSI) or excitation (DSE). Activation of CB receptors promotes their interaction with G proteins, resulting in guanosine diphosphate (GDP)/guanosine triphosphate (GTP) exchange and subsequent dissociation of the α and βγ subunits. These units regulate the activity of multiple effector proteins which induce biological functions[127]. When both CB1 and CB2 receptors are engaged, multiple intracellular signal transduction pathways are activated. It is well established that CB1 and CB2 activation regulate multiple effectors through both G-protein-dependent and G-protein-independent signal transduction pathways[128]. GPCRs are capable of adopting more than one active conformation, in which each active state is capable of stimulating an overlapping yet distinct group of downstream effectors[129-130]. This may allow signaling through the receptor to be directed through one pathway over the others through either strength-of-signal or biased agonism (also called functional selectivity) effects[131].

The most referred pathway is the coupling with $G_{i/o}$ proteins (Fig. 3) which results in inhibition of adenylate cyclase (AC) and subsequent cAMP response, and in activation of mitogen-activated protein kinases (MAPK), phosphoinositide 3-kinase (PI3K)-Akt pathways[132-134].

Activation of mitogen-activated protein kinases (MAPK) cascade i.e. c-Jun N terminal kinase (JNK), p38 MAPK and extracellular signal-regulated kinase-1 and -2 (ERK1/2), also leads to changes in phosphorylation and so in the function of many cellular molecules, including several transcription factors, cell proliferation, survival/death and glucose metabolism regulation. CB1 also inhibits voltage-gated calcium channels in neurons and modulate A-type and inwardly rectifying potassium channels (GIRK), causing a reduced neurotransmitter release through reduced intra-cellular Ca^{2+} and a hyperpolarized membrane potential resulting in a higher depolarizing stimulus. This is the mechanism by which eCBs can serve as retrograde neuromodulators in both short-term and long-term forms of synaptic plasticity, including DSI and DSE, long term potentiation and depression, and long-term depression of inhibition that suppresses neurotransmitter

release for extended duration[21,135-138]. Besides, CB1 may occasionally signal through stimulatory G_s protein to increase AC and G_q protein to increase intracellular Ca^{2+} but some additional studies are needed to determine the physiological significance of this dual coupling[139-140].

Since both CB1 and CB2 are GPCRs, the type of signaling pathway modulated by CB receptors activation appears to depend on the type of agonist under study as well as the tissue or organ involved. 2-AG preferentially activates the MAPK-ERK pathway, while noladin and the synthetic cannabinoid CP-55,940 preferentially inhibits adenylyl cyclase. Like noladin, the synthetic ligand CP-55,940 has also been shown to preferentially inhibits adenylyl cyclase in CB_2 receptors[141]. Together, these results support the emerging concept of agonist-directed trafficking at the cannabinoid receptors.

In addition to the effects of G proteins and downstream effectors, it has been found that most GPCRs form homodimers and heterodimers with other GPCRs (i.e. D2 dopamine receptor, the μ-, κ- and δ-opioid receptors, the orexin-1 receptor, the A2A adenosine receptor and the β2AR) and that these interactions influence many aspects of receptor function[142]. In response to prolonged activation, CB receptor signaling is subject to regulation via receptor desensitization and internalization. Internalized receptors are subsequently recycled to the plasma membrane or degraded.

Thus even though the overall effect of activating a GPCR which is coupled to a $G_{i/o}$ protein can impact different signaling pathways depending on the ligand, the overall effect of activating CB receptors, is to apply a biochemical “brake” to the functions of the cell.

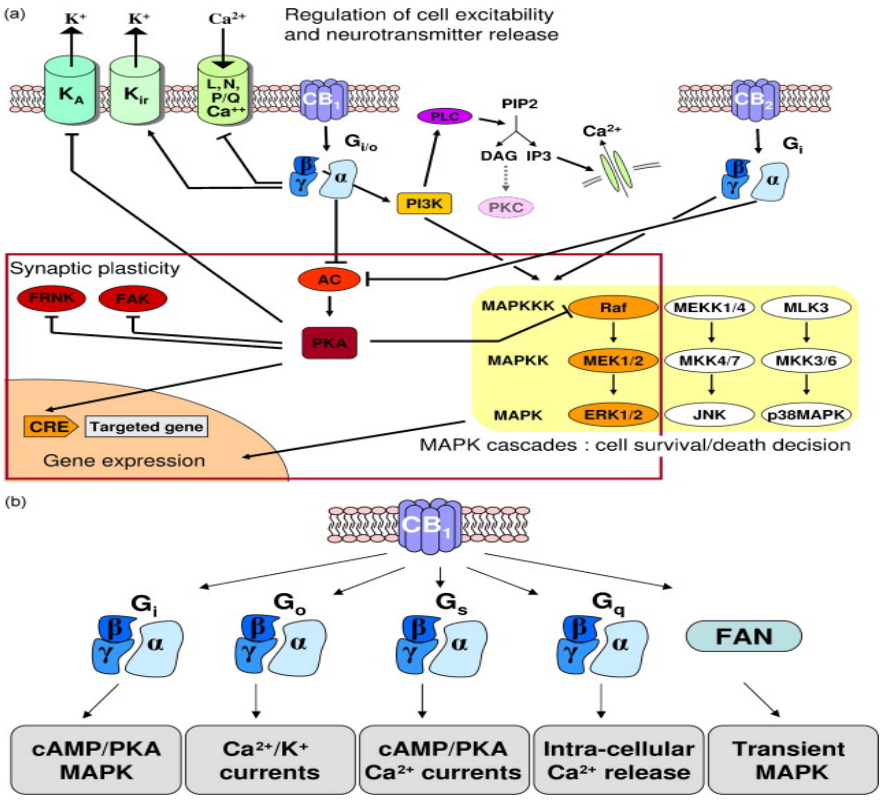

Figure 3[1]: Complexity at cannabinoid receptor signalling. Both CB_1 and CB_2 cannabinoid receptors are associated with $G\alpha_{i/o}$-dependent inhibition of adenylyl cyclase activity and Gβγ-dependent activation of the different MAPK cascades (a). In addition, the CB_1 cannabinoid receptor negatively regulates voltage-gated Ca^{2+} channels and positively regulates inwardly rectifying K+ channels. Finally, the CB1 receptor induces elevation of intracellular free Ca^{2+} through Gβγ-dependent activation of PLC. Cross-talks between signalling pathways are illustrated by the variety of responses requiring cannabinoid-mediated inhibition of PKA. Reduction of PKA activity is related to a reduction of gene expression through decreasing cAMP response element (CRE) activity. In addition, reduction of PKA activity leads to a decrease in constitutive inhibitory phosphorylation of c-Raf and a consecutive activation of ERK1/2. Similarly, reduction of voltage-dependent K+ A channel and focal-adhesion kinase (pp125 FAK and FRNK) phosphorylations through inhibition of PKA lead to activation of these different effectors. Several of these signalling pathways are directly related to the variety of functions regulated by cannabinoid receptors. Besides, it is now demonstrated that activation of CB1 cannabinoid receptors also leads to activation or Gs and Gq proteins (B). In addition the CB1 cannabinoid receptor also signals trough non-G protein partners such as the adaptor protein FAN. Preferential activation of different intracellular effectors by each G protein contributes to diversity and selectivity of responses regulated by cannabinoid receptors.

7. Interactions of cannabinoids with some other receptor systems.

Endogenous and exogenous cannabinoids or cannabinoids-like compounds can activate different signaling pathways engaging non-CB1 and non-CB2 receptors. Some of the

behavioural effects of cannabinoids may occur through other receptors or a synergic action of CB receptors with these other receptors. The most established non-CB1 non-CB2 receptor mediating some of the pharmacological effects of AEA, NADA and THC[110] is the transient receptor potential vanilloid type-1 (TRPV1) receptor, a non selective cation channel. TRPV1 is the natural target of capsaicin and is also activated by noxious heat and acidic pH. Distributed in the peripheral and central terminals of the sensory neurons[143], TRPV1 has been suggested as a potential target for the development of antinociceptive, antiinflammatory[144-145] and antiepileptogenesis agents[146].

The deorphanized G protein-coupled receptor GPR55 first discovered by Sawzdargo et al.[147] shares low sequence homology, respectively 13.5% and 14.4% to CB1 and CB2[148]. GPR55 has recently been suggested as a third additional member of the cannabinoid receptor family since several cannabinoid receptor ligands also bind GPR55[148-153]. Cannabidiol (CBD), the main non-psychoactive component of *Cannabis sativa*, appears to be an antagonist of this receptor[151,154] and OEA an agonist. AEA and 2-AG show no activation of GPR55[152, 155]. It is thought to be involved in pain signaling[156] and to produce anti-inflammatory effects in microglia[157], in obesity in humans[158], in breast cancer cells migration[159]. In addition, GPR55 -/- mice have been shown to experience less pain in different models of neuropathic pain validating this receptor as a promising therapeutic target[156].

Additional targets of eCBs and some of their metabolites are the peroxisome proliferator-activated receptors (PPAR)-α,- γ, δ, a class of nuclear receptors that control the expression of several genes involved particularly in lipid and glucose metabolism[160] and immune/inflammatory responses[161]. It is thought that 2-AG, AEA, PEA, CBD mediate part of their pharmacological activity through various isotypes of PPARs[162].

Abnormal cannabiniol vasodilatory effect is mediated by an endothelial receptor called abnormal cannabidiol receptor. Recent investigations support the hypothesis that GPR18 also named N-arachidonoyl glycine (NAGly) receptor, is the putative molecular target in the CNS of abnormal cannabiniol and NAGly a metabolite of AEA. Through activation, GPR18 initiates microglial migration[163].

GPR119 has been suggested to be stimulated by oleylethanolamide (OEA) and be, at least in part, implied in reducing food intake and body weight gain, a hypothesis that is supported by the localization of the receptor in brain, pancreas, and gastrointestinal tract[164].

T-type Ca^{2+} channels presents in nerves, heart, smooth and skeletal muscles and endocrine tissues[165] have been suggested as interesting target in the regulation of sleep[166], nociception[167], epilepsy[168-169] pain[170-171] and neuropathic pain[172-173]. Interestingly, several endocannabinoids such as AEA[174], phytocannabinoids (Δ9-THC, CBD)[175] and synthetic cannabinoids[171] can directly block T-type calcium channels.

Cannabinoids have also been suggested as modulators of for others receptors[133] such as serotonin receptor $(5\text{-HT})_3$[176-177], acetylcholine receptor (nACh)[178], glutamate receptor (NMDA)[179], TASK-1 channel[180] and Na^+ channel[181].

8. Drug of abuse.

Hashish or marijuana are the most world used illicit drugs according to the U.S. National Institute on Drug Abuse and UNODC (United Nations Office on Drugs and Crimes) http://www.unodc.org/unodc/en/data-and-analysis/WDR-2010.html. Even though cannabis derivatives exhibited a very high LD_{50}, long term and high frequency of cannabis use might result in various side effects. Cannabinoid literature has mainly focused on the CB1 receptor and its pharmacological responses. The complex array of behavioral effects exhibited by the cannabinoids acting at the CB1 receptor have been characterized in numerous animal species, including human. Drug discrimination tests, dog static ataxia, mouse tetrad models and many others have been used in order to demonstrate the psychoactive effects of the CB1 cannabinoids. Cannabis consumption is associated with a variety of possible impairment of mental and bodily functions including memory and concentration, movement coordination, pleasure, pain tolerance, appetite and induction of psychiatric illness[182-183] such as Schizophrenia. Although the association between cannabis and Schizophrenia is still controversial, many authors have emphasized that cannabis abuse may influence the development of schizophrenic

psychosis in predisposed people or the neurodevelopment of normal brain during adolescence leading to Schizophrenia[184-188].

Different synthetic cannabinoid derivatives are now commercially available and increasingly popular recreational drugs. Labelled “Herbal incense”, Spice®, K2® and others have been intentionally adulterated with synthetic cannabinoids to produce effects similar to cannabis while circumventing drug legislation. JWH-018[189-190] one of the most commonly use of these synthetic compounds is a potent full agonist at CB1 and CB2 with higher binding affinities at CB receptors than Δ^9–THC. Little is known about its pharmacology and toxicology in humans. Recent reports seem to correlate its use with an increased risk of psychosis[191] and abuse[192]. These aversive effects are putatively attenuated with cannabis which contains phytocannabinoids which could be CB2 antagonists such as CBD[191]. CBD has been ascribed to inhibit the metabolism of Δ^9–THC to the more psychoactive 11-OH- Δ9–THC[193] and/or to antagonize Δ^9–THC *in vivo* side effects[194-196]. Despite contradictory findings regarding the interactions between CBD and Δ^9–THC[197-198], this discovery allowed scientists to compare the effect of a full CB1/CB2 agonist with cannabis derivatives which includes CB1 partial agonist like Δ9–THC but also potential CB2 antagonists such as CBD.

9. Therapeutic cannabinoid derivatives on the market.

Only few cannabinoids-based pharmaceutical products have reached the market. Sativex®, a (1:1) Δ^9–THC and CBD mixture, developed by GW Pharmaceuticals is the first cannabis-based prescription medicine in UK, Spain, Czech Republic, Canada, Germany, Denmark and New Zealand as a treatment of Multiple Sclerosis (MS) spasticity. The product is also in Phase III clinical development for treatment of cancer pain (Canada). In addition, GW Pharmaceuticals has submitted an application under the European Mutual Recognition Procedure to seek marketing authorization for Sativex® in other selected European member states, including France. In the US, Sativex® is still an investigational drug (Phase IIIb) being developed as an adjunctive analgesic treatment for patients with advanced cancer.

There are currently two synthetic CB1 agonists marketed, Marinol® (Dronabinol, synthetic Δ^9–THC) and Cesamet® (Nabilone, synthetic analog of Δ9–THC) manufactured respectively by Solvay Pharmaceuticals and Valeant Pharmaceuticals International,

respectively. Dronabinol is used as an appetite stimulant in acquired immunodeficiency syndrome (AIDS) patients and for nausea and vomiting associated with cancer chemotherapy. Nabilone is used as an anti-emetic drug against nausea and vomiting caused by cancer chemotherapy[199].

Rimonabant® (Sanofi-Aventis) was the first selective CB1 receptor antagonist developed as an appetite suppressant and anti-obesity agent. Never approved in the US, it has been officially withdrawn by the EMEA (European Medicines Agency) in 2009 because of severe depression and anxiety side effects[200-201].

10. Phytocannabinoids.

The term phytocannabinoid (pCB) promiscuously refers to lipophilic molecules naturally occurring in the *cannabis sativa L.* with similar chemical structures as Δ^9–THC[19,202-203]. More than 70 of these compounds have been isolated and just a few of them have the ECs as a pharmacological target. Recently several plant natural products have been described as CB receptors ligands and/or exhibiting cannabimimetic effects. It might be more accurate to define the pCBs as "any plant-derived natural product capable of either directly interacting with CB receptors on orthosteric or allosteric sites and/or indirectly modulating eCBs enzymes and subsequently eCBs levels[204-205]. Whereas Δ^9–THC is still the most prevalent pCB studied, its psychotropic activity, subserved pharmacology and potential therapeutic effect investigations of other pCBs[206-208]. The most common described pCBs which have been reported to interact with the eCbs are Δ^9–THC and its analogs such as Cannabidiol (CBD), cannabigerol (CBG), Δ^9–tetrahydrocannabivarin (Δ^9-THCV), cannabidavirin (CBDV) and cannabinol (CBN). They have particularly shown interesting *in vivo* activity in models of CNS disorders[202]. CBD is currently the only pCB other than Δ^9–THC that has been investigated for anticonvulsant effects in humans,[202] in addition to its reported effects as alleviating the unwanted side effects from Δ^9–THC (i.e. sativex®). Promising evidence support further investigations for CBD as a main or adjunctive therapeutic agent. Other "herbal cannabimimetics", N-alkylamides (alkamides) from *Echinacea* spp. (E. purpurea, E. pallida and E. angustifolia), have been proved to interact functionally with high affinity to the human CB2 receptor[209] and to show some anti-inflammatory activity[210]. The main alkamides are the isomeric dodeca-2E,4E,8Z, 10E/Z-tetraenoic acid isobutylamides (see Table 2)[204].

β-caryophyllene [(E)-BCP] (see Table 2), a bicyclic sesquiterpene, is a predominant volatile constituent of numerous of essential oils, especially cloves *Syzygium aromaticum*[211] and cannabis[212] and contributes also to the spiciness of black pepper *Piper Nigrum*[213]. This FDA approved food additive[214] has been shown to selectively target the CB2 receptor at nanomolar concentrations (*K*i= 155 nM) and to act as a full agonist[215]. Although (E)-BCP pharmacokinetic and toxicity profiles need further investigations, (E)-BCP has been evidenced to exert significant cannabimimetic activity including anti-inflammatory[215-217], local anaesthetic[211], anti-carcinogenic activity[218-220] and to reduce neuropathic pain[204]. No psychotropic effect has been ascribed to (E)-BCP which doesn't bind to CB1 receptor. (E)-BCP is an attractive candidate for clinical trials targeting the CB2 receptor.

Table 2: Examples of different families of phytocannabinoids[221].

Structure	Name	Origin	CB receptor affinity	Other targets (ECS)	References
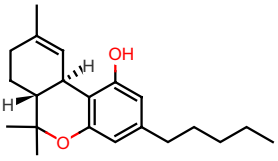	Δ^9-THC	*Cannabis sativa* L.	Non-selective CB_1 and CB_2 affinity (K_i values <50 nM) (human)	GPR55 PPARs Different ion channels	222,223
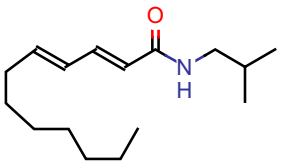	*N*-alkylamide	*Echinacea* spp.	Selective CB_2affinity (K_i value <100 nM) (human)	PPAR-γ Inhibition of AEA transport Partial FAAH inhibtion	224-225
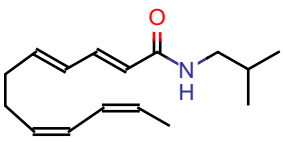	*N*-alkylamide	*Echinacea* spp.	Selective CB_2affinity (K_i value <100 nM) (human)	PPAR-γ Inhibition of AEA transport Parial FAAH inhibition	224-225

Structure	Name	Origin	CB receptor affinity	Other targets (ECS)	References
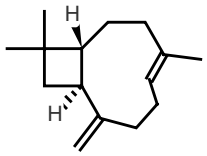	β-caryophyllene	Widespread in plants	Selective CB_2affinity (K_i value<200 nM) (human)	No data	221

11. Pain.

11.1. Physiological pain.

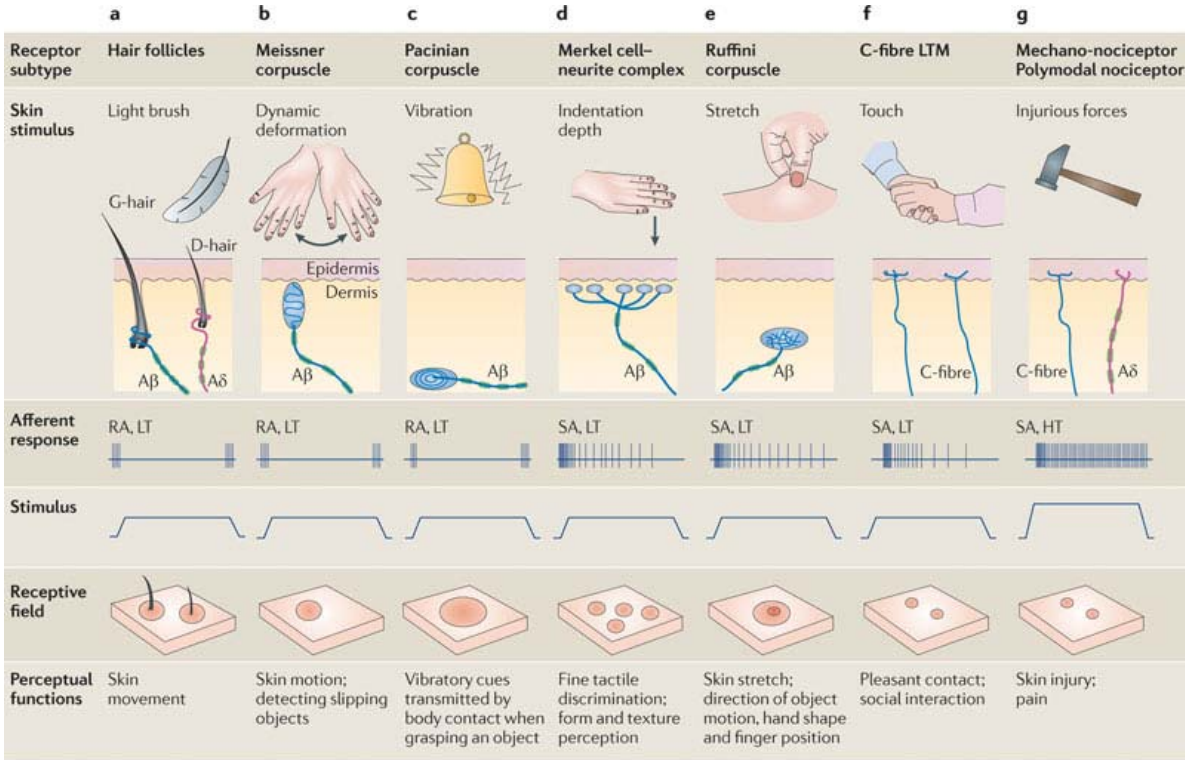

Figure 4: Cutaneous mechanosensory neurons differentiate into many functionally distinct subtypes — with specific threshold sensitivities and encoding capabilities — each of which is thought to transduce specific kinds of mechanical stimuli. Rapid adaptation (RA), slow adaptation (SA), low threshold (LT), high threshold (HT)[4].

Pain is defined as an unpleasant sensory and emotional experience associated with tissue damage or described in terms of such damage, by the International Association for the Study of Pain. Pain is essential to warn living organism to a damaging stimulus even

though pain is unpleasant and can be associated with suffering. Pain is required for survival since avoiding harm is crucial to maintain the integrity of the organism. Persons with congenital insensitivity to pain lack protective warning and show extensive scarring and, tend to die early[226].

In mammals, innocuous mechanical stimuli are detected by sensitive touch receptors or mechanoreceptors located in the nerve fiber of mechanosensory neurons (Fig. 4 and Fig. 5)[4]. The activation of these mechanoreceptors generates a depolarizing current. An action potential follows the initial receptor activation if the current is sufficient. Four mechanoreceptors detect light mechanical sensation, Meissner corpuscle, Pacinian corpuscle Merkel's disk and Ruffini corpuscle. These receptors show progressive loss of response even though the stimulation is maintained. After initial stimulation, these receptors can exhibit fast adaptation, if the resulting action potential can decrease as fast as stimulation is maintained (e.g. pant pressing a hair on your leg continuously) or slow adaptation if the action potential is maintained.

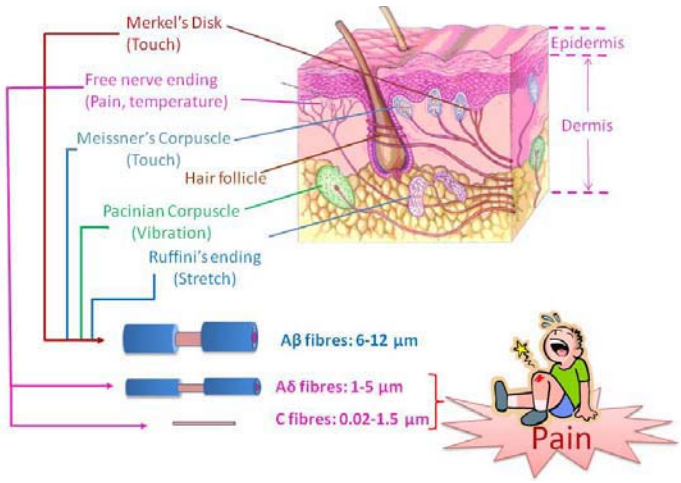

Figure 5 : Receptors in skin and fibers that link receptors to the CNS. Adapted from [1].

By contrast, detection of pain, heat and cold is performed by nerve endings of specialized mechanosensory neurons that are activated by noxious stimuli. These unipolar neurons are primary afferent neurons which have their cell body located in trigeminal (innervates region of the head) and dorsal root ganglia (DRG) and project axon to the skin and to deeper body structures. Umyelinated slowly conducting C-fibers and more rapidly conducting Aδ-fibers are polymodal nociceptors responding to respectively noxious, thermal and chemical stimuli or to mechanical and thermal stimuli (Fig. 5). Nociceptors respond to these acute tissue-damaging stimuli through direct activation of transient receptor potential (TRP) channels such as TRPV1 (temperature > 43°C) or the cool-sensing receptor TRPM8 as well as activation of the acid-sensing ion channels ASIC. In addition an indirect mechanism can

result from activation of TRP channels (TRPV3) on keratinocytes or release of intermediates molecules activating sensory neurons receptors such as ATP[3].

The high threshold of nociceptor terminal can be decreased as a result of the production and release of chemical inflammatory mediators and neurotrophic factors from non-neuronal cells. This phenomenon termed heterosensitization will result in a reduction of depolarization required to initiate the action potential. In addition, the reduction of the threshold of nociceptors can also result from an increase of sensitivity or changes in transducers as a result of prior activation (autosensitization)[227].

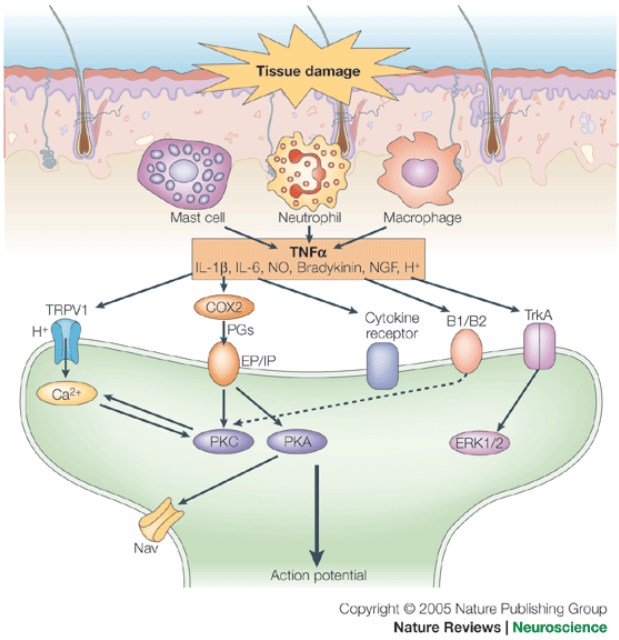

Figure 6: After tissue damage, mast cells and macrophages are activated and some blood-borne immune cells, including neutrophils, may be recruited. Various immune mediators are released (such as TNF, IL-1, IL-6, NO, bradykinin, NGF and protons), which exert their algesic effects by acting directly on nociceptors or indirectly through the release of other mediators, most notably prostanoids[3].

After tissue damage, inflammation results in recruitment of immune cells such as mast cells, resident or recruited activated macrophage and neutrophils infiltrating from the blood. This local inflammation will result in the release of an “inflammatory soup” including peptides such as bradykinin, lipids such as prostaglandins, neurotransmitters (serotonin), neurotrophin (NGF), cytokines (e.g. TNF, IL-1) and chemokines (e.g. CCL2, CXL8) (Fig. 6). All these pro-inflammatory agents will produce pain but also hyperalgesia

through the activation of the corresponding receptors expressed by nociceptive terminals.

The action potential is transmitted to the CNS by glutamate release from nociceptor terminal thereby activating AMPA and kainate ligand-gated ion channels of dorsal horn neurons.

Pain information can be blocked by neurons from the brainstem. The descending pain modulation pathway is used by the brain to inhibit spinal pain signaling. Periaqueductal grey-neurons send endorphin-containing axons which stimulate neurons in the medulla which send serotonin-containing axons to the spinal cord which in turn will activate inhibitory GABAergic neurons.

11.2. Neuropathic pain.

Pain is a leading health problem worldwide with 20% of Americans suffering from chronic pain. The chronic pathological pain state, such as neuropathic pain persists beyond the resolution of the source of pain seriously disrupting quality of life. In 2003 the lost of worker productivity was estimated at $61.2 billion in the United States[228]. Neuropathic pain can be induced after an injury to the nervous system such as peripheral nerve injury or induced by diabetes or chemotherapeutic agent treatments. Chemotherapy-induced peripheral neuropathy (CIPN) is an adverse reaction that becomes a dose-limiting toxicity of chemotherapy that accompanies the administration of taxanes (paclitaxel), platinum-containing drugs and vinca alkaloids. In most cases, sensory symptoms resolve within months after paclitaxel treatment is discontinued, but the sensory abnormalities and pain can become chronic[229]. Distal peripheral neuropathy (DPN) is the most common form of symmetric sensory polyneuropathy one of several distinct syndromes of diabetic neuropathy. Despite recent advances in the treatment of patients with diabetes, neuropathy remains among the most common of complications of diabetes, affecting up to 50% of patients. There is no effective treatment to prevent or reverse neuropathic pain[230].

In contrast with physiological pain where tissue injury and/or inflammation induce reversible adaptative changes in the sensory nervous system leading to protective sensitization, in neuropathic pain changes in sensitivity become persistent or chronic. In neuropathic pain the nervous system, peripheral or central is injured. The resulting

changes in pain processing can occur spontaneously or as a result of exposure to mildly painful stimuli (hyperalgesia) or stimuli not normally perceived as painful (allodynia). Neuropathic pain management is currently aimed only at reducing symptoms. The treatment of chronic pain remains an unmet clinical need, with only half of patients receiving adequate pain relief using drugs with adverse central nervous system (CNS) side effects. Comorbidities such as sleep disorders, depression and anxiety compromise the quality of life of neuropathic pain patients[231].

Dynamic changes in the neural matrix and in the peripheral nervous system induced by the release of cytokines, chemokines and neurotrophic factors occur over several temporal scales. Negative symptoms such as numbness or elevated heat threshold are the first indication of damage to the somatosensory system. Upon nerve injury, resident immune cells, mast cells and macrophages are activated (Fig. 7A). Blood-born neutrophiles, monocytes and T-cells will be recruited and accumulate to the site of injury[232]. All these immune cells release proinflammatory cytokines such as IL-1β and TNFα, chemokines and proinflammatory mediators (e.g. prostaglandins) which trigger inflammation resulting in peripheral nociceptive sensitization. Peripheral sensitization results in reduction of threshold and an increase in the excitability of the peripheral afferents leading to allodynia and hyperalgesia. These changes in pain processing are also mediated by posttranslational changes, trafficking and expression changes of ion channels such as TRP channels, T-type calcium channels or voltage-gated calcium channels[233]. In addition, TNFα is transported along the afferent fiber to the spinal cord.

Hyperexcitability of peripheral nerves results in generation of ectopic action potential discharge leading to spontaneous pain. Uninjured fibers neighboring the site of injury can be recruited increasing ectopic activity. Ectopic activity seems to be crucial in the development of neuropathic pain. Human clinical studies and animal models indicate that the altered central processing associated with pain is maintained dynamically by ongoing peripheral input[234]. It is likely that pain resulting from a variety of causes, including diabetic peripheral neuropathy (dPN), chemotherapeutic-induced neuropathy (CIPN), and after nerve injury, becomes chronic as a result of the initial inflammatory reaction to damaged primary afferent fibers and neurons, recruitment of non-involved peripheral nerves and engagement of central mechanism resulting in central sensitization[235].

Central sensitization might develop as a consequence of ectopic activity in primary nociceptive afferent fibers and where structural damage within the CNS is not necessarily

involved. It now becomes evident that abnormal hyperactivity of damaged primary afferent fibers of the peripheral nervous system (PNS) induces and maintains hyperalgesia and allodynia in chronic neuropathic pain caused by paclitaxel administration[236], diabetes[237] and nerve injury[238-239].

Intraepidermal nerve fibers (IENF) are nerve endings arising from nociceptors within the dermis and reduced density of IENF (Fig. 7A) and abnormalities of somatosensory fibers have been clearly identified in DPN[240]. In paclitaxel-induced neuropathy (PIN), axonal degeneration at the level of the peripheral nerve was not observed. In contrast, reduced density of IENFs was observed in both DPN and PIN[241] and could explain abnormal spontaneous afferent discharge observed in these two pathologies[236,242]. The output of pain processing in the spinal cord is a balance between excitatory and inhibitory processes involving excitatory glutamatergic neurons and GABAergic and glycinergic inhibitory interneurons (Fig. 7C). Loss of function and reduced number of inhibitory interneurons in the dorsal horn for neuropathic pain has been now clearly established[233].

Enhancement of pain transmission in the central nervous system following central sensitization is triggered by peripheral nervous system input. Abnormal ectopic activity in primary nociceptive afferent fibers induces central sensitization through NMDA channels recruitment and activation after suppression of Mg^{2+} blockade. In addition, gating of NMDA channels are enhanced through GPCR activations such as NK1, EP or mGlu receptors or MAPK phosphorylation. PKC activation also enhances NMDA receptor function after TrkB activation by BDNF (Fig. 7B).

AMPA receptors containing GluR2 are calcium impermeable. These receptors are converted to AMPA lacking GluR2 and become calcium permeable after trafficking and degradation of GluR2.

The homeostasis of glutamate (Glu) in the nervous system is regulated through Glu uptake by glutamate transporters[243]. EAAT1 and EAAT2 have been shown to be the major Glu transporters in the CNS for Glu uptake under normal physiological condition. They are responsible of the Glu transport into the astrocytes where it is converted to glutamine (Gln) by Gln synthetase. Gln is then shuttled to the neuron through glutamine transporters SN1 and SNAT2. In the neuron Gln is converted to Glu by phosphate-activated glutaminase (Fig. 7B).

Expression and uptake activity of EAATs are altered and contribute to neuropathic pain after chronic constriction nerve injury (CCI) in rats[244]. After an initial upregulation of

EAATs within the first 5 days post CCI within the ipsalateral spinal cord dorsal horn, EAATs downregulation was observed by Western blot and immunohistochemistry resulting in a decrease Glu uptake. Treatment with Riluzole a positive EAAT activity regulator attenuated neuropathic pain behavior by restoring Glu uptake in CCI rats. In addition blockade of spinal glutamate transporters by glutamate transporter blockers DL-threo-β-benzyloxyaspartate (TBOA) and dihydrokainate produced excitatory behavioral responses, including spontaneous pain behaviors and hypersensitivity, in response to thermal and mechanical stimulation in naive rats.

In contrast, intrathecal administration of the glutamate transporter inhibitors TBOA, dihydrokainate, and DL-threo-β-hydroxyaspartate reduced formalin-evoked pain behaviors in the second phase[245]. Intrathecal TBOA also attenuated CFA-induced thermal hyperalgesia after CFA injection. The antinociceptive effects of TBOA were blocked by co-administration of a selective group III mGluR antagonist, (RS)-α-methylserine-O-phosphate[245] suggesting the involvement of spinal inhibitory pre-synaptic group III mGluRs. In addition, inhibition of GLT-1 by the transporter inhibitor trans-pyrrolidine-2,4-dicarboxylic acid resulted in a significant reduction of nociceptive behavior in the rat formalin assay. This effect was confirmed in naïve adult rats following antisense knockdown of EAAT-2[246]. Similarly, decreased pain behaviors after formalin injection in experimental autoimmune encephalomyelitis mice was normalized with the promoter of glutamate transporter activity, MS-153[247]. By treating EAE mice with the selective group II mGluR antagonist, LY-341495 prior to formalin stimulation, formalin responses was restored back to control levels indicating the involvement of pre-synaptic inhibitory mGluRs. Therefore, in contrast with normal physiological conditions, inhibition of glutamate uptake in pathological pain state seems to be associated with a decrease of pain sensation[248]. At the moment, it is difficult to understand the involvement and the effects of Glu transporters modulations on neuropathic pain. A central reorganization of A-fiber terminals which sprout from dorsal horn deep lamina invading the C-fiber terminals region is also observed.

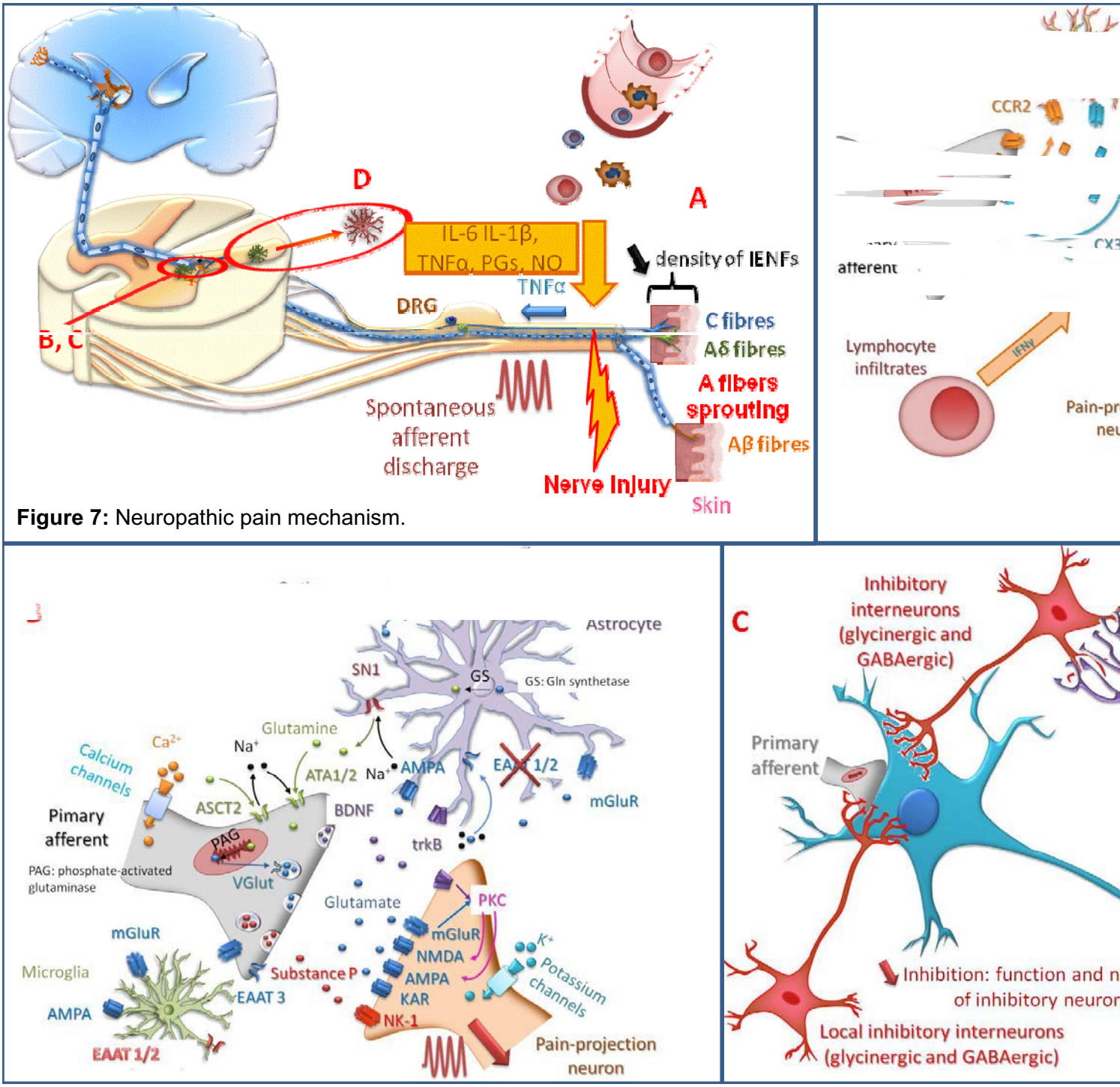

Figure 7: Neuropathic pain mechanism.

Chemokines CX3CL1 and CCL2 and their cognate receptors CX3CR1 and CCR2 are the most studied chemokines and receptors in neuropathic pain. After Glu stimulation, CX3L1 is expressed and released by neurons thereby activating CX3CR1 receptors expressed in glial cells (Fig. 7D). CX3R1 activation results in activation and chemotaxis activity of glial cells[249]. Similarly, microglia CCR2 activation by CCL2 possibly released by afferent nerve terminal induces microglia activation. CCR2 appears to be expressed by astrocytes and primary afferent terminal as well as pain-projection neurons. Therefore the effect of CCL2 after activating CCR2 is still a debate.

12. CB2 receptors: a target for Neuropathic Pain treatment?

Selective CB2 agonists have shown considerable efficacy in a variety of animal models of neuropathic pain[14,30,250-252] without evidence of psychoactivity. Different strategies have been attempted to investigate the role of CB2 receptor in pain modulation using non-selective CB1/CB2 agonists, or selective CB2 agonists and inhibitors of enzymes that degrade endocannabinoids[253]. **Results from these studies support the potential development of selective CB2 receptor agonists for the treatment of both acute and neuropathic pain**[254]. Mechanisms involved in the antinociceptive activity of CB2 agonists and distribution of CB2 receptors are still controversial and under investigation. CB2 receptors are primary described to be expressed in immune cells[50,255-256] of both PNS and CNS[257] and it is well accepted that CB2 is present in microglia during neuroinflammation. There is also evidence for their expression in human primary afferent nociceptors which are critical for pain modulation[77,253,258]. CB2 receptors have a chemotactic effect on immune cells modulating their migration, antigen presentation and release of inflammation mediators[75] (i.e. NGF, cytokines, chemokines, ATP, histamine, prostanoids, etc.) which can be of importance upon peripheral injury, and subsequent primary afferent sensitization. In case of neuropathic pain resulting from nerve injury, CB2 agonists may reduce neuroinflammation and sensitization at the peripheral nerve. CB2 located in CNS may also play a role[259] possibly acting on the microglia activation[260] or by a direct neuronal action on pain neurotransmitter[77] thereby decreasing central sensitization. Effect of CB2 agonists within the CNS on microglia activation and migration, or the activity of the glial derived and deleterious substances such as

proinflamatory cytokines (e.g.IL-β, IL-6, TNF-α) and other cytotoxic agents[74,260], can result in a decrease of neuropathic pain symptoms. However, 2-AG, a full CB1/CB2 endocannabinoid agonist triggers microglial migration while synthetic CB2 ligands whether agonist or antagonist, inhibit 2-AG-induced chemotaxis[75, 260]. CB2 agonist has been shown to either increase or decrease cell migration, and be either pro- or anti-inflammatory[75] depending on the animal model, the cell type[261] or the class of CB2 ligand involved. Different classes of CB2 ligands can produce diverse physiological effects due to activation of distinct signaling pathways or to functional selectivity[141,262], emphasizing that each CB2 ligand needs to be separately evaluated for therapeutic efficacy. At a cellular level, CB2 agonists act differently on internalization and desensitization processes and a greater understanding of the cellular compensations that occur during chronic drug administration will also be necessary[257] to fully understand the therapeutic benefits of CB2 agonists.

Recently, the selectivity of CB2 agonists reported in the literature and tested in models of analgesia has been questioned. In the majority of these studies, some weak but measurable CB1 activity[28] may have conducted to a synergistic effect of CB1/CB2 activities, since even weak CB1 binding was ascribed to produce substantial agonism[263]. Other group such as Sain et al.[264] demonstrated that non-selective CB1/CB2 agonists produced antinociceptive activity in different models of inflammatory and neuropathic pain which was abolished in CB1 knockout mice but not in CB2 knockout mice. It should be noted that the doses used for this study were low, possibly favoring CB1 agonist activity. It is extremely difficult to conclusively establish if CB2 or off-target activity of compounds which were claimed to be CB2 agonist (or antagonist) were responsible of their effect in *in vivo* models of neuropathic pain[73] since endocannabinoids and phytocannabinoids have been shown to modulate different receptors and ion channels.

Despite CB2 agonists show considerable efficacy in various preclinical models, further pharmacological investigations are yet needed to be conducted on their peculiar signaling pathways and potential polypharmacology, in order to successfully develop efficacious drugs with reduced side effects for the treatment of neuropathic pain or others neurodegenerative diseases.

9 REFERENCES.

1. Bosier, B.; Muccioli, G. G.; Hermans, E.; Lambert, D. M., Functionally selective cannabinoid receptor signalling: Therapeutic implications and opportunities. *Biochemical Pharmacology* **2010,** 80, (1), 1-12.
2. De Petrocellis, L.; Di Marzo, V., An introduction to the endocannabinoid system: from the early to the latest concepts. *Best Pract. Res. Clin. Endoc. Metab.* **2009,** 23, (1), 1-15.
3. Marchand, F.; Perretti, M.; McMahon, S. B., Role of the Immune system in chronic pain. *Nat Rev Neurosci* **2005,** 6, (7), 521-532.
4. Delmas, P.; Hao, J.; Rodat-Despoix, L., Molecular mechanisms of mechanotransduction in mammalian sensory neurons. *Nat Rev Neurosci* **2011,** 12, (3), 139-153.
5. Bouhassira, D.; Lantéri-Minet, M.; Attal, N.; Laurent, B.; Touboul, C., Prevalence of chronic pain with neuropathic characteristics in the general population. *Pain* **2008,** 136, (3), 380-387.
6. Galluzzi, K. E., Managing Neuropathic Pain. *JAOA: Journal of the American Osteopathic Association* **2007,** 107, (suppl 6), ES39-ES48.
7. Dworkin, R. H.; O'Connor, A. B.; Backonja, M.; Farrar, J. T.; Finnerup, N. B.; Jensen, T. S.; Kalso, E. A.; Loeser, J. D.; Miaskowski, C.; Nurmikko, T. J.; Portenoy, R. K.; Rice, A. S.; Stacey, B. R.; Treede, R. D.; Turk, D. C.; Wallace, M. S., Pharmacologic management of neuropathic pain: evidence-based recommendations. *Pain* **2007,** 132, (3), 237-51.
8. Treede, R. D.; Jensen, T. S.; Campbell, J. N.; Cruccu, G.; Dostrovsky, J. O.; Griffin, J. W.; Hansson, P.; Hughes, R.; Nurmikko, T.; Serra, J., Neuropathic pain: redefinition and a grading system for clinical and research purposes. *Neurology* **2008,** 70, (18), 1630-5.
9. Dworkin, R. H.; O'Connor, A. B.; Backonja, M.; Farrar, J. T.; Finnerup, N. B.; Jensen, T. S.; Kalso, E. A.; Loeser, J. D.; Miaskowski, C.; Nurmikko, T. J.; Portenoy, R. K.; Rice, A. S. C.; Stacey, B. R.; Treede, R.-D.; Turk, D. C.; Wallace, M. S., Pharmacologic management of neuropathic pain: Evidence-based recommendations. *Pain* **2007,** 132, (3), 237-251.
10. Yamamoto, W.; Mikami, T.; Iwamura, H., Involvement of central cannabinoid CB2 receptor in reducing mechanical allodynia in a mouse model of neuropathic pain. *Eur J Pharmacol* **2008,** 583, (1), 56-61.
11. Diaz, P.; Phatak, S. S.; Xu, J. J.; Fronczek, F. R.; Astruc-Diaz, F.; Thompson, C. M.; Cavasotto, C. N.; Naguib, M., 2,3-Dihydro-1-Benzofuran Derivatives as a Series of Potent Selective Cannabinoid Receptor 2 Agonists: Design, Synthesis, and Binding Mode Prediction through Ligand-Steered Modeling. *ChemMedChem* **2009,** 4, (10), 1615-1629.
12. Naguib, M.; Diaz, P.; Xu, J. J.; Astruc-Diaz, F.; Craig, S.; Vivas-Mejia, P.; Brown, D. L., MDA7: a novel selective agonist for CB2 receptors that prevents allodynia in rat neuropathic pain models. *British Journal of Pharmacology* **2008,** 155, (7), 1104-16.
13. Toth, C. C.; Jedrzejewski, N. M.; Ellis, C. L.; Frey, W. H., 2nd, Cannabinoid-mediated modulation of neuropathic pain and microglial accumulation in a model of murine type I diabetic peripheral neuropathic pain. *Mol Pain* **2010,** 6, 16.

14. Ibrahim, M. M.; Deng, H.; Zvonok, A.; Cockayne, D. A.; Kwan, J.; Mata, H. P.; Vanderah, T. W.; Lai, J.; Porreca, F.; Makriyannis, A.; Malan, T. P., Jr., Activation of CB2 cannabinoid receptors by AM1241 inhibits experimental neuropathic pain: pain inhibition by receptors not present in the CNS. *Proc Natl Acad Sci U S A* **2003,** 100, (18), 10529-33.
15. Lichtman, A. H.; Smith, P. B.; Martin, B. R., The antinociceptive effects of intrathecally administered cannabinoids are influenced by lipophilicity. *Pain* **1992,** 51, (1), 19-26.
16. Paton, R. G. P. D. T. W. D. M., *The general pharmacology of cannabinoids*. Oxford University Press: London, 1972; p 50-75.
17. Medicine, U. S. N. L. o. Classics of Traditional Chinese Medicine: from the History of Medicine Division National Library of Medicine. http://www.nlm.nih.gov/exhibition/chinesemedicine/emperors.html
18. Zuardi, A. W., History of cannabis as a medicine: a review. *Rev Bras Psiquiatr* **2006,** 28, (2), 153-7.
19. Elsohly, M. A.; Slade, D., Chemical constituents of marijuana: the complex mixture of natural cannabinoids. *Life Sci* **2005,** 78, (5), 539-48.
20. Di Marzo, V., Endocannabinoid System. In *eLS*, John Wiley & Sons, Ltd: 2001.
21. Piomelli, D., The molecular logic of endocannabinoid signalling. *Nat Rev Neurosci* **2003,** 4, (11), 873-84.
22. Mackie, K., Cannabinoid Receptors: Where They are and What They do. *Journal of Neuroendocrinology* **2008,** 20, 10-14.
23. Benito, C.; Romero, J. P.; Tolon, R. M.; Clemente, D.; Docagne, F.; Hillard, C. J.; Guaza, C.; Romero, J., Cannabinoid CB1 and CB2 receptors and fatty acid amide hydrolase are specific markers of plaque cell subtypes in human multiple sclerosis. *J Neurosci* **2007,** 27, (9), 2396-402.
24. Tolon, R. M.; Nunez, E.; Pazos, M. R.; Benito, C.; Castillo, A. I.; Martinez-Orgado, J. A.; Romero, J., The activation of cannabinoid CB2 receptors stimulates in situ and in vitro beta-amyloid removal by human macrophages. *Brain Res* **2009,** 1283, 148-54.
25. Zajicek, J. P.; Apostu, V. I., Role of cannabinoids in multiple sclerosis. *Cns Drugs* **2011,** 25, (3), 187-201.
26. Sanchez, A. J.; Garcia-Merino, A., Neuroprotective agents: cannabinoids. *Clin Immunol* **2012,** 142, (1), 57-67.
27. Garcia-Arencibia, M.; Garcia, C.; Fernandez-Ruiz, J., Cannabinoids and Parkinson's disease. *CNS Neurol Disord Drug Targets* **2009,** 8, (6), 432-9.
28. Beltramo, M., [The cannabinoid system and pain: towards new drugs?]. *J Soc Biol* **2009,** 203, (1), 99-106.
29. Manzanares, J.; Julian, M.; Carrascosa, A., Role of the cannabinoid system in pain control and therapeutic implications for the management of acute and chronic pain episodes. *Curr Neuropharmacol* **2006,** 4, (3), 239-57.
30. Naguib, M.; Diaz, P.; Xu, J. J.; Astruc-Diaz, F.; Craig, S.; Vivas-Mejia, P.; Brown, D. L., MDA7: a novel selective agonist for CB2 receptors that prevents allodynia in rat neuropathic pain models. *Br J Pharmacol* **2008,** 155, (7), 1104-16.
31. Diaz, P.; Phatak, S. S.; Xu, J.; Astruc-Diaz, F.; Cavasotto, C. N.; Naguib, M., 6-Methoxy-N-alkyl isatin acylhydrazone derivatives as a novel series of potent selective cannabinoid receptor 2 inverse agonists: design, synthesis, and binding mode prediction. *J Med Chem* **2009,** 52, (2), 433-44.

32. Diaz, P.; Xu, J. J.; Astruc-Diaz, F.; Pan, H. M.; Brown, D. L.; Naguib, M., Design and synthesis of a novel series of N-alkyl isatin acylhydrazone derivatives that act as selective cannabinoid receptor 2 agonists for the treatment of neuropathic pain. *Journal of Medicinal Chemistry* **2008,** 51, (16), 4932-4947.
33. Proto, M. C.; Gazzerro, P.; Di Croce, L.; Santoro, A.; Malfitano, A. M.; Pisanti, S.; Laezza, C.; Bifulco, M., Interaction of endocannabinoid system and steroid hormones in the control of colon cancer cell growth. *J Cell Physiol* **2012,** 227, (1), 250-8.
34. Malfitano, A. M.; Ciaglia, E.; Gangemi, G.; Gazzerro, P.; Laezza, C.; Bifulco, M., Update on the endocannabinoid system as an anticancer target. *Expert Opin Ther Targets* **2011,** 15, (3), 297-308.
35. Parker, L. A.; Rock, E. M.; Limebeer, C. L., Regulation of nausea and vomiting by cannabinoids. *Br J Pharmacol* **2011,** 163, (7), 1411-22.
36. Engeli, S., Central and peripheral cannabinoid receptors as therapeutic targets in the control of food intake and body weight. *Handb Exp Pharmacol* **2012,** 209, 357-81.
37. Valenzuela, C.; Aguirre, C.; Castillo, V.; Ronco, A. M.; Llanos, M., [A role for the endocannabinoid system in obesity]. *Rev Med Chil* **2010,** 138, (5), 621-9.
38. Hofmann, M. E.; Frazier, C. J., Marijuana, endocannabinoids, and epilepsy: Potential and challenges for improved therapeutic intervention. *Exp Neurol* **2011**.
39. Nucci, C.; Bari, M.; Spano, A.; Corasaniti, M.; Bagetta, G.; Maccarrone, M.; Morrone, L. A., Potential roles of (endo)cannabinoids in the treatment of glaucoma: from intraocular pressure control to neuroprotection. *Prog Brain Res* **2008,** 173, 451-64.
40. Braun, A.; Engel, T.; Aguilar-Pimentel, J. A.; Zimmer, A.; Jakob, T.; Behrendt, H.; Mempel, M., Beneficial effects of cannabinoids (CB) in a murine model of allergen-induced airway inflammation: Role of CB(1)/CB(2) receptors. *Immunobiology* **2011,** 216, (4), 466-476.
41. Ashton, C. H.; Moore, P. B., Endocannabinoid system dysfunction in mood and related disorders. *Acta Psychiatr Scand* **2011,** 124, (4), 250-61.
42. Esteban, S.; Garcia-Sevilla, J. A., Effects induced by cannabinoids on monoaminergic systems in the brain and their implications for psychiatric disorders. *Prog Neuropsychopharmacol Biol Psychiatry* **2011**.
43. Rodriguez De Fonseca, F.; Schneider, M., GUEST EDITORIAL: The endogenous cannabinoid system and drug addiction: 20 years after the discovery of the CB1 receptor. *Addiction Biology* **2008,** 13, (2), 143-146.
44. Gaoni, Y.; Mechoulam, R., Isolation, Structure, and Partial Synthesis of an Active Constituent of Hashish. *Journal of the American Chemical Society* **1964,** 86, (8), 1646-1647.
45. Howlett, A. C.; Fleming, R. M., Cannabinoid inhibition of adenylate cyclase. Pharmacology of the response in neuroblastoma cell membranes. *Mol Pharmacol* **1984,** 26, (3), 532-8.
46. Devane, W. A.; Dysarz, F. A., 3rd; Johnson, M. R.; Melvin, L. S.; Howlett, A. C., Determination and characterization of a cannabinoid receptor in rat brain. *Mol Pharmacol* **1988,** 34, (5), 605-13.
47. Herkenham, M.; Lynn, A. B.; Little, M. D.; Johnson, M. R.; Melvin, L. S.; de Costa, B. R.; Rice, K. C., Cannabinoid receptor localization in brain. *Proc Natl Acad Sci U S A* **1990,** 87, (5), 1932-6.

48. Matsuda, L. A.; Lolait, S. J.; Brownstein, M. J.; Young, A. C.; Bonner, T. I., Structure of a cannabinoid receptor and functional expression of the cloned cDNA. *Nature* **1990,** 346, (6284), 561-564.
49. Devane, W. A.; Hanus, L.; Breuer, A.; Pertwee, R. G.; Stevenson, L. A.; Griffin, G.; Gibson, D.; Mandelbaum, A.; Etinger, A.; Mechoulam, R., Isolation and structure of a brain constituent that binds to the cannabinoid receptor. *Science* **1992,** 258, (5090), 1946-9.
50. Munro, S.; Thomas, K. L.; Abushaar, M., Molecular Characterization of a Peripheral Receptor for Cannabinoids. *Nature* **1993,** 365, (6441), 61-65.
51. Rinaldi-Carmona, M.; Barth, F.; Heaulme, M.; Shire, D.; Calandra, B.; Congy, C.; Martinez, S.; Maruani, J.; Neliat, G.; Caput, D.; et al., SR141716A, a potent and selective antagonist of the brain cannabinoid receptor. *FEBS Lett* **1994,** 350, (2-3), 240-4.
52. Di Marzo, V.; Fontana, A.; Cadas, H.; Schinelli, S.; Cimino, G.; Schwartz, J.-C.; Piomelli, D., Formation and inactivation of endogenous cannabinoid anandamide in central neurons. *Nature* **1994,** 372, (6507), 686-691.
53. Mechoulam, R.; Ben-Shabat, S.; Hanus, L.; Ligumsky, M.; Kaminski, N. E.; Schatz, A. R.; Gopher, A.; Almog, S.; Martin, B. R.; Compton, D. R.; Pertwee, R. G.; Griffin, G.; Bayewitch, M.; Barg, J.; Vogel, Z., Identification of an endogenous 2-monoglyceride, present in canine gut, that binds to cannabinoid receptors. *Biochemical Pharmacology* **1995,** 50, (1), 83-90.
54. Sugiura, T.; Kondo, S.; Sukagawa, A.; Nakane, S.; Shinoda, A.; Itoh, K.; Yamashita, A.; Waku, K., 2-Arachidonoylglycerol: a possible endogenous cannabinoid receptor ligand in brain. *Biochem Biophys Res Commun* **1995,** 215, (1), 89-97.
55. Cravatt, B. F.; Giang, D. K.; Mayfield, S. P.; Boger, D. L.; Lerner, R. A.; Gilula, N. B., Molecular characterization of an enzyme that degrades neuromodulatory fatty-acid amides. *Nature* **1996,** 384, (6604), 83-87.
56. Beltramo, M.; Stella, N.; Calignano, A.; Lin, S. Y.; Makriyannis, A.; Piomelli, D., Functional role of high-affinity anandamide transport, as revealed by selective inhibition. *Science* **1997,** 277, (5329), 1094-1097.
57. Rodriguez de Fonseca, F.; Carrera, M. R.; Navarro, M.; Koob, G. F.; Weiss, F., Activation of corticotropin-releasing factor in the limbic system during cannabinoid withdrawal. *Science* **1997,** 276, (5321), 2050-4.
58. Ledent, C.; Valverde, O.; Cossu, G.; Petitet, F.; Aubert, J. F.; Beslot, F.; Bohme, G. A.; Imperato, A.; Pedrazzini, T.; Roques, B. P.; Vassart, G.; Fratta, W.; Parmentier, M., Unresponsiveness to cannabinoids and reduced addictive effects of opiates in CB1 receptor knockout mice. *Science* **1999,** 283, (5400), 401-4.
59. De Vries, T. J.; Shaham, Y.; Homberg, J. R.; Crombag, H.; Schuurman, K.; Dieben, J.; Vanderschuren, L. J.; Schoffelmeer, A. N., A cannabinoid mechanism in relapse to cocaine seeking. *Nat Med* **2001,** 7, (10), 1151-4.
60. Navarro, M.; Carrera, M. R. A.; Fratta, W.; Valverde, O.; Cossu, G.; Fattore, L.; Chowen, J. A.; Gomez, R.; del Arco, I.; Villanua, M. A.; Maldonado, R.; Koob, G. F.; de Fonseca, F. R., Functional interaction between opioid and cannabinoid receptors in drug self-administration. *Journal of Neuroscience* **2001,** 21, (14), 5344-5350.
61. Kreitzer, A. C.; Regehr, W. G., Retrograde Inhibition of Presynaptic Calcium Influx by Endogenous Cannabinoids at Excitatory Synapses onto Purkinje Cells. *Neuron* **2001,** 29, (3), 717-727.

62. Ohno-Shosaku, T.; Maejima, T.; Kano, M., Endogenous Cannabinoids Mediate Retrograde Signals from Depolarized Postsynaptic Neurons to Presynaptic Terminals. *Neuron* **2001,** 29, (3), 729-738.
63. Wilson, R. I.; Nicoll, R. A., Endogenous cannabinoids mediate retrograde signalling at hippocampal synapses. *Nature* **2001,** 410, (6828), 588-592.
64. Hájos, N.; Ledent, C.; Freund, T. F., Novel cannabinoid-sensitive receptor mediates inhibition of glutamatergic synaptic transmission in the hippocampus. *Neuroscience* **2001,** 106, (1), 1-4.
65. Marsicano, G.; Wotjak, C. T.; Azad, S. C.; Bisogno, T.; Rammes, G.; Cascio, M. G.; Hermann, H.; Tang, J.; Hofmann, C.; Zieglgansberger, W.; Di Marzo, V.; Lutz, B., The endogenous cannabinoid system controls extinction of aversive memories. *Nature* **2002,** 418, (6897), 530-534.
66. Kathuria, S.; Gaetani, S.; Fegley, D.; Valino, F.; Duranti, A.; Tontini, A.; Mor, M.; Tarzia, G.; La Rana, G.; Calignano, A.; Giustino, A.; Tattoli, M.; Palmery, M.; Cuomo, V.; Piomelli, D., Modulation of anxiety through blockade of anandamide hydrolysis. *Nature Medicine* **2003,** 9, (1), 76-81.
67. Van Gaal, L. F.; Rissanen, A. M.; Scheen, A. J.; Ziegler, O.; Rössner, S., Effects of the cannabinoid-1 receptor blocker rimonabant on weight reduction and cardiovascular risk factors in overweight patients: 1-year experience from the RIO-Europe study. *The Lancet* **2005,** 365, (9468), 1389-1397.
68. Reggio, P. H., Pharmacophores for ligand recognition and activation/inactivation of the cannabinoid receptors. *Curr Pharm Des* **2003,** 9, (20), 1607-33.
69. Gerard, C. M.; Mollereau, C.; Vassart, G.; Parmentier, M., Molecular cloning of a human cannabinoid receptor which is also expressed in testis. *Biochem J* **1991,** 279 (Pt 1), 129-34.
70. Zhang, J.; Hoffert, C.; Vu, H. K.; Groblewski, T.; Ahmad, S.; O'Donnell, D., Induction of CB2 receptor expression in the rat spinal cord of neuropathic but not inflammatory chronic pain models. *European Journal of Neuroscience* **2003,** 17, (12), 2750-2754.
71. Van Sickle, M. D.; Duncan, M.; Kingsley, P. J.; Mouihate, A.; Urbani, P.; Mackie, K.; Stella, N.; Makriyannis, A.; Piomelli, D.; Davison, J. S.; Marnett, L. J.; Di Marzo, V.; Pittman, Q. J.; Patel, K. D.; Sharkey, K. A., Identification and functional characterization of brainstem cannabinoid CB2 receptors. *Science* **2005,** 310, (5746), 329-32.
72. Gong, J. P.; Onaivi, E. S.; Ishiguro, H.; Liu, Q. R.; Tagliaferro, P. A.; Brusco, A.; Uhl, G. R., Cannabinoid CB2 receptors: immunohistochemical localization in rat brain. *Brain Res* **2006,** 1071, (1), 10-23.
73. Atwood, B. K.; Mackie, K., CB2: a cannabinoid receptor with an identity crisis. *British Journal of Pharmacology* **2010,** 160, (3), 467-479.
74. Ashton, J. C.; Glass, M., The cannabinoid CB2 receptor as a target for inflammation-dependent neurodegeneration. *Current Neuropharmacology* **2007,** 5, (2), 73-80.
75. Miller, A. M.; Stella, N., CB2 receptor-mediated migration of immune cells: it can go either way. *British Journal of Pharmacology* **2008,** 153, (2), 299-308.
76. Cabral, G. A.; Griffin-Thomas, L., Emerging role of the cannabinoid receptor CB2 in immune regulation: therapeutic prospects for neuroinflammation. *Expert Rev Mol Med* **2009,** 11, e3.

77. Beltramo, M.; Bernardini, N.; Bertorelli, R.; Campanella, M.; Nicolussi, E.; Fredduzzi, S.; Reggiani, A., CB2 receptor-mediated antihyperalgesia: possible direct involvement of neural mechanisms. *Eur J Neurosci* **2006,** 23, (6), 1530-8.
78. Baek, J. H.; Zheng, Y.; Darlington, C. L.; Smith, P. F., Cannabinoid CB2 receptor expression in the rat brainstem cochlear and vestibular nuclei. *Acta Otolaryngol* **2008,** 128, (9), 961-7.
79. Path, M. E., Rehashing endocannabinoid antagonists: can we selectively target the periphery to safely treat obesity and type 2 diabetes? *Journal of Clinical Investigation* **2010,** 120, (8), 2646-2648.
80. Pang, Z.; Wu, N. N.; Zhao, W.; Chain, D. C.; Schaffer, E.; Zhang, X.; Yamdagni, P.; Palejwala, V. A.; Fan, C.; Favara, S. G.; Dressler, H. M.; Economides, K. D.; Weinstock, D.; Cavallo, J. S.; Naimi, S.; Galzin, A. M.; Guillot, E.; Pruniaux, M. P.; Tocci, M. J.; Polites, H. G., The central cannabinoid CB1 receptor is required for diet-induced obesity and rimonabant's antiobesity effects in mice. *Obesity (Silver Spring)* **2011,** 19, (10), 1923-34.
81. Pertwee, R. G., Pharmacology of cannabinoid CB1 and CB2 receptors. *Pharmacol Ther* **1997,** 74, (2), 129-80.
82. Nunez, E.; Benito, C.; Pazos, M. R.; Barbachano, A.; Fajardo, O.; Gonzalez, S.; Tolon, R. M.; Romero, J., Cannabinoid CB2 receptors are expressed by perivascular microglial cells in the human brain: an immunohistochemical study. *Synapse* **2004,** 53, (4), 208-13.
83. Golech, S. A.; McCarron, R. M.; Chen, Y.; Bembry, J.; Lenz, F.; Mechoulam, R.; Shohami, E.; Spatz, M., Human brain endothelium: coexpression and function of vanilloid and endocannabinoid receptors. *Mol Brain Res* **2004,** 132, (1), 87-92.
84. Rivers, J. R.; Ashton, J. C., The development of cannabinoid CBII receptor agonists for the treatment of central neuropathies. *Cent Nerv Syst Agents Med Chem* **2010,** 10, (1), 47-64.
85. Onaivi, E. S.; Leonard, C. M.; Ishiguro, H.; Zhang, P. W.; Lin, Z.; Akinshola, B. E.; Uhl, G. R., Endocannabinoids and cannabinoid receptor genetics. *Prog Neurobiol* **2002,** 66, (5), 307-44.
86. Brusco, A.; Tagliaferro, P. A.; Saez, T.; Onaivi, E. S., Ultrastructural localization of neuronal brain CB2 cannabinoid receptors. *Ann N Y Acad Sci* **2008,** 1139, 450-7.
87. Hsieh, G. C.; Pai, M.; Chandran, P.; Hooker, B. A.; Zhu, C. Z.; Salyers, A. K.; Wensink, E. J.; Zhan, C.; Carroll, W. A.; Dart, M. J.; Yao, B. B.; Honore, P.; Meyer, M. D., Central and peripheral sites of action for CB2 receptor mediated analgesic activity in chronic inflammatory and neuropathic pain models in rats. *British Journal of Pharmacology* **2011,** 162, (2), 428-440.
88. Onaivi, E. S.; Carpio, O.; Ishiguro, H.; Schanz, N.; Uhl, G. R.; Benno, R., Behavioral Effects of CB2 Cannabinoid Receptor Activation and Its Influence on Food and Alcohol Consumption. *Annals of the New York Academy of Sciences* **2008,** 1139, (1), 426-433.
89. Ishiguro, H.; Horiuchi, Y.; Ishikawa, M.; Koga, M.; Imai, K.; Suzuki, Y.; Morikawa, M.; Inada, T.; Watanabe, Y.; Takahashi, M.; Someya, T.; Ujike, H.; Iwata, N.; Ozaki, N.; Onaivi, E. S.; Kunugi, H.; Sasaki, T.; Itokawa, M.; Arai, M.; Niizato, K.; Iritani, S.; Naka, I.; Ohashi, J.; Kakita, A.; Takahashi, H.; Nawa, H.; Arinami, T., Brain cannabinoid CB2 receptor in schizophrenia. *Biol Psychiatry* **2010,** 67, (10), 974-82.

90. Ortega-Alvaro, A.; Aracil-Fernandez, A.; Garcia-Gutierrez, M. S.; Navarrete, F.; Manzanares, J., Deletion of CB2 Cannabinoid Receptor Induces Schizophrenia-Related Behaviors in Mice. *Neuropsychopharmacology* **2011,** 36, (7), 1489-1504.
91. Xi, Z.-X.; Peng, X.-Q.; Li, X.; Song, R.; Zhang, H.-Y.; Liu, Q.-R.; Yang, H.-J.; Bi, G.-H.; Li, J.; Gardner, E. L., Brain cannabinoid CB2 receptors modulate cocaine's actions in mice. *Nat Neurosci* **2011,** 14, (9), 1160-1166.
92. Pertwee, R. G.; Howlett, A. C.; Abood, M. E.; Alexander, S. P. H.; Di Marzo, V.; Elphick, M. R.; Greasley, P. J.; Hansen, H. S.; Kunos, G.; Mackie, K.; Mechoulam, R.; Ross, R. A., International Union of Basic and Clinical Pharmacology. LXXIX. Cannabinoid Receptors and Their Ligands: Beyond CB(1) and CB(2). *Pharmacol Rev* **2010,** 62, (4), 588-631.
93. Howlett, A. C., The cannabinoid receptors. *Prostaglandins Other Lipid Mediat* **2002,** 68-69, 619-31.
94. Stella, N.; Schweitzer, P.; Piomelli, D., A second endogenous cannabinoid that modulates long-term potentiation. *Nature* **1997,** 388, (6644), 773-778.
95. Sugiura, T.; Waku, K., 2-Arachidonoylglycerol and the cannabinoid receptors. *Chem Phys Lipids* **2000,** 108, (1-2), 89-106.
96. Katona, I.; Freund, T. F., Endocannabinoid signaling as a synaptic circuit breaker in neurological disease. *Nature Medicine* **2008,** 14, (9), 923-930.
97. Pertwee, R. G., Ligands that target cannabinoid receptors in the brain: from THC to anandamide and beyond. *Addict Biol* **2008,** 13, (2), 147-59.
98. Maresz, K.; Carrier, E. J.; Ponomarev, E. D.; Hillard, C. J.; Dittel, B. N., Modulation of the cannabinoid CB2 receptor in microglial cells in response to inflammatory stimuli. *Journal of Neurochemistry* **2005,** 95, (2), 437-445.
99. Stella, N., Cannabinoid signaling in glial cells. *Glia* **2004,** 48, (4), 267-277.
100. Fernández-Ruiz, J.; Pazos, M. R.; García-Arencibia, M.; Sagredo, O.; Ramos, J. A., Role of CB2 receptors in neuroprotective effects of cannabinoids. *Molecular and Cellular Endocrinology* **2008,** 286, (1–2, Supplement 1), S91-S96.
101. Gomez, O.; Sanchez-Rodriguez, A.; Le, M.; Sanchez-Caro, C.; Molina-Holgado, F.; Molina-Holgado, E., Cannabinoid receptor agonists modulate oligodendrocyte differentiation by activating PI3K/Akt and the mammalian target of rapamycin (mTOR) pathways. *Br J Pharmacol* **2011,** 163, (7), 1520-32.
102. Molina-Holgado, E.; Vela, J. M.; Arevalo-Martin, A.; Almazan, G.; Molina-Holgado, F.; Borrell, J.; Guaza, C., Cannabinoids promote oligodendrocyte progenitor survival: involvement of cannabinoid receptors and phosphatidylinositol-3 kinase/Akt signaling. *J Neurosci* **2002,** 22, (22), 9742-53.
103. Ehrhart, J.; Obregon, D.; Mori, T.; Hou, H.; Sun, N.; Bai, Y.; Klein, T.; Fernandez, F.; Tan, J.; Shytle, R. D., Stimulation of cannabinoid receptor 2 (CB2) suppresses microglial activation. *J Neuroinflammation* **2005,** 2, 29.
104. Ramirez, B. G.; Blazquez, C.; Gomez del Pulgar, T.; Guzman, M.; de Ceballos, M. L., Prevention of Alzheimer's disease pathology by cannabinoids: neuroprotection mediated by blockade of microglial activation. *J Neurosci* **2005,** 25, (8), 1904-13.
105. Brownjohn, P. W.; Ashton, J. C., Spinal cannabinoid CB2 receptors as a target for neuropathic pain: an investigation using chronic constriction injury. *Neuroscience* **2012,** 203, 180-93.
106. Hanus, L.; Gopher, A.; Almog, S.; Mechoulam, R., Two new unsaturated fatty acid ethanolamides in brain that bind to the cannabinoid receptor. *J Med Chem* **1993,** 36, (20), 3032-4.

107. Pertwee, R.; Griffin, G.; Hanus, L.; Mechoulam, R., Effects of two endogenous fatty acid ethanolamides on mouse vasa deferentia. *Eur J Pharmacol* **1994,** 259, (2), 115-20.
108. Hanuš, L.; Abu-Lafi, S.; Fride, E.; Breuer, A.; Vogel, Z.; Shalev, D. E.; Kustanovich, I.; Mechoulam, R., 2-Arachidonyl glyceryl ether, an endogenous agonist of the cannabinoid CB1 receptor. *Proceedings of the National Academy of Sciences* **2001,** 98, (7), 3662-3665.
109. Porter, A. C.; Sauer, J.-M.; Knierman, M. D.; Becker, G. W.; Berna, M. J.; Bao, J.; Nomikos, G. G.; Carter, P.; Bymaster, F. P.; Leese, A. B.; Felder, C. C., Characterization of a Novel Endocannabinoid, Virodhamine, with Antagonist Activity at the CB1 Receptor. *Journal of Pharmacology and Experimental Therapeutics* **2002,** 301, (3), 1020-1024.
110. Huang, S. M.; Bisogno, T.; Trevisani, M.; Al-Hayani, A.; De Petrocellis, L.; Fezza, F.; Tognetto, M.; Petros, T. J.; Krey, J. F.; Chu, C. J.; Miller, J. D.; Davies, S. N.; Geppetti, P.; Walker, J. M.; Di Marzo, V., An endogenous capsaicin-like substance with high potency at recombinant and native vanilloid VR1 receptors. *Proceedings of the National Academy of Sciences* **2002,** 99, (12), 8400-8405.
111. Gomes, I.; Grushko, J. S.; Golebiewska, U.; Hoogendoorn, S.; Gupta, A.; Heimann, A. S.; Ferro, E. S.; Scarlata, S.; Fricker, L. D.; Devi, L. A., Novel endogenous peptide agonists of cannabinoid receptors. *FASEB J* **2009,** 23, (9), 3020-9.
112. Richter, F.; Meurers, B. H.; Zhu, C.; Medvedeva, V. P.; Chesselet, M. F., Neurons express hemoglobin alpha- and beta-chains in rat and human brains. *J Comp Neurol* **2009,** 515, (5), 538-47.
113. Kogan, N. M.; Mechoulam, R., The chemistry of endocannabinoids. *J Endocrinol Invest* **2006,** 29, (3 Suppl), 3-14.
114. Lambert, D. M.; Vandevoorde, S.; Diependaele, G.; Govaerts, S. J.; Robert, A. R., Anticonvulsant activity of N-palmitoylethanolamide, a putative endocannabinoid, in mice. *Epilepsia* **2001,** 42, (3), 321-7.
115. Maccarrone, M.; Pauselli, R.; Di Rienzo, M.; Finazzi-Agro, A., Binding, degradation and apoptotic activity of stearoylethanolamide in rat C6 glioma cells. *Biochem J* **2002,** 366, (Pt 1), 137-44.
116. Fu, J.; Kim, J.; Oveisi, F.; Astarita, G.; Piomelli, D., Targeted enhancement of oleoylethanolamide production in proximal small intestine induces across-meal satiety in rats. *Am J Physiol Regul Integr Comp Physiol* **2008,** 295, (1), R45-50.
117. Huang, S. M.; Bisogno, T.; Petros, T. J.; Chang, S. Y.; Zavitsanos, P. A.; Zipkin, R. E.; Sivakumar, R.; Coop, A.; Maeda, D. Y.; De Petrocellis, L.; Burstein, S.; Di Marzo, V.; Walker, J. M., Identification of a new class of molecules, the arachidonyl amino acids, and characterization of one member that inhibits pain. *J Biol Chem* **2001,** 276, (46), 42639-44.
118. Okamoto, Y.; Morishita, J.; Tsuboi, K.; Tonai, T.; Ueda, N., Molecular characterization of a phospholipase D generating anandamide and its congeners. *J Biol Chem* **2004,** 279, (7), 5298-305.
119. Bisogno, T.; Howell, F.; Williams, G.; Minassi, A.; Cascio, M. G.; Ligresti, A.; Matias, I.; Schiano-Moriello, A.; Paul, P.; Williams, E. J.; Gangadharan, U.; Hobbs, C.; Di Marzo, V.; Doherty, P., Cloning of the first sn1-DAG lipases points to the spatial and temporal regulation of endocannabinoid signaling in the brain. *J Cell Biol* **2003,** 163, (3), 463-8.

120. Ahn, K.; McKinney, M. K.; Cravatt, B. F., Enzymatic pathways that regulate endocannabinoid signaling in the nervous system. *Chemical Reviews* **2008,** 108, (5), 1687-1707.
121. Marrs, W. R.; Blankman, J. L.; Horne, E. A.; Thomazeau, A.; Lin, Y. H.; Coy, J.; Bodor, A. L.; Muccioli, G. G.; Hu, S. S.-J.; Woodruff, G.; Fung, S.; Lafourcade, M.; Alexander, J. P.; Long, J. Z.; Li, W.; Xu, C.; Moller, T.; Mackie, K.; Manzoni, O. J.; Cravatt, B. F.; Stella, N., The serine hydrolase ABHD6 controls the accumulation and efficacy of 2-AG at cannabinoid receptors. *Nat Neurosci* **2010,** 13, (8), 951-957.
122. Blankman, J. L.; Simon, G. M.; Cravatt, B. F., A comprehensive profile of brain enzymes that hydrolyze the endocannabinoid 2-arachidonoylglycerol. *Chemistry & Biology* **2007,** 14, (12), 1347-1356.
123. Reggio, P. H.; Traore, H., Conformational requirements for endocannabinoid interaction with the cannabinoid receptors, the anandamide transporter and fatty acid amidohydrolase. *Chem Phys Lipids* **2000,** 108, (1-2), 15-35.
124. Lopez-Rodriguez, M. L.; Viso, A.; Ortega-Gutierrez, S.; Lastres-Becker, I.; Gonzalez, S.; Fernandez-Ruiz, J.; Ramos, J. A., Design, synthesis and biological evaluation of novel arachidonic acid derivatives as highly potent and selective endocannabinoid transporter inhibitors. *J Med Chem* **2001,** 44, (26), 4505-8.
125. Glaser, S. T.; Kaczocha, M.; Deutsch, D. G., Anandamide transport: A critical review. *Life Sciences* **2005,** 77, (14), 1584-1604.
126. Wu, X.; Han, L.; Zhang, X.; Li, L.; Jiang, C.; Qiu, Y.; Huang, R.; Xie, B.; Lin, Z.; Ren, J.; Fu, J., Alteration of endocannabinoid system in human gliomas. *J Neurochem* **2012,** 120, (5), 842-9.
127. Basavarajappa, B. S., Neuropharmacology of the endocannabinoid signaling system-molecular mechanisms, biological actions and synaptic plasticity. *Current Neuropharmacology* **2007,** 5, (2), 81-97.
128. Varga, E. V.; Georgieva, T.; Tumati, S.; Alves, I.; Salamon, Z.; Tollin, G.; Yamamura, H. I.; Roeske, W. R., Functional selectivity in cannabinoid signaling. *Curr Mol Pharmacol* **2008,** 1, (3), 273-84.
129. Berg, K. A.; Maayani, S.; Goldfarb, J.; Scaramellini, C.; Leff, P.; Clarke, W. P., Effector pathway-dependent relative efficacy at serotonin type 2A and 2C receptors: Evidence for agonist-directed trafficking of receptor stimulus. *Molecular Pharmacology* **1998,** 54, (1), 94-104.
130. Kenakin, T., Inverse, protean, and ligand-selective agonism: matters of receptor conformation. *FASEB J* **2001,** 15, (3), 598-611.
131. Kenakin, T., Agonist-receptor efficacy. II. Agonist trafficking of receptor signals. *Trends Pharmacol Sci* **1995,** 16, (7), 232-8.
132. Howlett, A. C., Cannabinoid receptor signaling. *Handb Exp Pharmacol* **2005**, (168), 53-79.
133. Demuth, D. G.; Molleman, A., Cannabinoid signalling. *Life Sciences* **2006,** 78, (6), 549-563.
134. Di Marzo, V.; De Petrocellis, L., Plant, synthetic, and endogenous cannabinoids in medicine. *Annual Review of Medicine* **2006,** 57, 553-574.
135. Wilson, R. I.; Nicoll, R. A., Endocannabinoid signaling in the brain. *Science* **2002,** 296, (5568), 678-82.
136. Chevaleyre, V.; Takahashi, K. A.; Castillo, P. E., Endocannabinoid-mediated synaptic plasticity in the CNS. *Annu Rev Neurosci* **2006,** 29, 37-76.

137. Lovinger, D. M., Presynaptic modulation by endocannabinoids. *Handb Exp Pharmacol* **2008**, (184), 435-77.
138. Dalton, G. D.; Bass, C. E.; Van Horn, C. G.; Howlett, A. C., Signal transduction via cannabinoid receptors. *CNS Neurol Disord Drug Targets* **2009,** 8, (6), 422-31.
139. Glass, M.; Felder, C. C., Concurrent stimulation of cannabinoid CB1 and dopamine D2 receptors augments cAMP accumulation in striatal neurons: evidence for a Gs linkage to the CB1 receptor. *J Neurosci* **1997,** 17, (14), 5327-33.
140. Kearn, C. S.; Blake-Palmer, K.; Daniel, E.; Mackie, K.; Glass, M., Concurrent stimulation of cannabinoid CB1 and dopamine D2 receptors enhances heterodimer formation: a mechanism for receptor cross-talk? *Mol Pharmacol* **2005,** 67, (5), 1697-704.
141. Shoemaker, J. L.; Ruckle, M. B.; Mayeux, P. R.; Prather, P. L., Agonist-directed trafficking of response by endocannabinoids acting at CB2 receptors. *Journal of Pharmacology and Experimental Therapeutics* **2005,** 315, (2), 828-838.
142. Hudson, B. D.; Hébert, T. E.; M. Kelly, M. E., Ligand- and Heterodimer-Directed Signaling of the CB1 Cannabinoid Receptor. *Molecular Pharmacology* **2010,** 77, (1), 1-9.
143. Marinelli, S.; Di Marzo, V.; Berretta, N.; Matias, I.; Maccarrone, M.; Bernardi, G.; Mercuri, N. B., Presynaptic facilitation of glutamatergic synapses to dopaminergic neurons of the rat substantia nigra by endogenous stimulation of vanilloid receptors. *Journal of Neuroscience* **2003,** 23, (8), 3136-3144.
144. Premkumar, L. S.; Sikand, P., TRPV1: A target for next generation analgesics. *Current Neuropharmacology* **2008,** 6, (2), 151-163.
145. Park, C. K.; Lu, N.; Xu, Z. Z.; Liu, T.; Serhan, C. N.; Ji, R. R., Resolving TRPV1- and TNF-alpha-Mediated Spinal Cord Synaptic Plasticity and Inflammatory Pain with Neuroprotectin D1. *Journal of Neuroscience* **2011,** 31, (42), 15072-15085.
146. Fu, M.; Xie, Z.; Zuo, H., TRPV1: A potential target for antiepileptogenesis. *Medical Hypotheses* **2009,** 73, (1), 100-102.
147. Sawzdargo, M.; Nguyen, T.; Lee, D. K.; Lynch, K. R.; Cheng, R.; Heng, H. H. Q.; George, S. R.; O'Dowd, B. F., Identification and cloning of three novel human G protein-coupled receptor genes GPR52, ΨGPR53 and GPR55: GPR55 is extensively expressed in human brain. *Mol Brain Res* **1999,** 64, (2), 193-198.
148. Baker, D.; Pryce, G.; Davies, W. L.; Hiley, C. R., In silico patent searching reveals a new cannabinoid receptor. *Trends in Pharmacological Sciences* **2006,** 27, (1), 1-4.
149. Drmota, E.; Greasley, P.; Groblewski, T. Screening assays for cannabinoid-ligand type modulators. 2004.
150. Johns, D. G.; Behm, D. J.; Ao, Z. H.; Walker, D.; Parsons, M.; Senadhi, S.; T Goserud, M.; Daniels, D. A.; Riddick, M.; Staton, P. C.; Green, P.; Bao, W.; Aiyar, N.; Yue, T. L.; Brown, A. J.; Morrison, A. D.; Douglas, S. A., The novel cannabinoid receptor GPR55 binds atypical cannabinoids but does not mediate their vasodilatory effects. *Hypertension* **2006,** 48, (4), E86-E86.
151. Ryberg, E.; Larsson, N.; Sjogren, S.; Hjorth, S.; Hermansson, N. O.; Leonova, J.; Elebring, T.; Nilsson, K.; Drmota, T.; Geasley, P. J., The orphan receptor GPR55 is a novel cannabinoid receptor. *British Journal of Pharmacology* **2007,** 152, (7), 1092-1101.

152. Lauckner, J. E.; Jensen, J. B.; Chen, H. Y.; Lu, H. C.; Hille, B.; Mackie, K., GPR55 is a cannabinoid receptor that increases intracellular calcium and inhibits M current. *P Natl Acad Sci USA* **2008,** 105, (7), 2699-2704.
153. Ross, R. A., The enigmatic pharmacology of GPR55. *Trends Pharmacol Sci* **2009,** 30, (3), 156-63.
154. Whyte, L. S.; Ryberg, E.; Sims, N. A.; Ridge, S. A.; Mackie, K.; Greasley, P. J.; Ross, R. A.; Rogers, M. J., The putative cannabinoid receptor GPR55 affects osteoclast function in vitro and bone mass in vivo. *Proceedings of the National Academy of Sciences* **2009,** 106, (38), 16511-16516.
155. Oka, S.; Nakajima, K.; Yamashita, A.; Kishimoto, S.; Sugiura, T., Identification of GPR55 as a lysophosphatidylinositol receptor. *Biochem Bioph Res Co* **2007,** 362, (4), 928-934.
156. Staton, P. C.; Hatcher, J. P.; Walker, D. J.; Morrison, A. D.; Shapland, E. M.; Hughes, J. P.; Chong, E.; Mander, P. K.; Green, P. J.; Billinton, A.; Fulleylove, M.; Lancaster, H. C.; Smith, J. C.; Bailey, L. T.; Wise, A.; Brown, A. J.; Richardson, J. C.; Chessell, I. P., The putative cannabinoid receptor GPR55 plays a role in mechanical hyperalgesia associated with inflammatory and neuropathic pain. *Pain* **2008,** 139, (1), 225-236.
157. Pietr, M.; Kozela, E.; Levy, R.; Rimmerman, N.; Lin, Y. H.; Stella, N.; Vogel, Z.; Juknat, A., Differential changes in GPR55 during microglial cell activation. *FEBS Letters* **2009,** 583, (12), 2071-2076.
158. Moreno-Navarrete, J. M.; Catalan, V.; Whyte, L.; Diaz-Arteaga, A.; Vazquez-Martinez, R.; Rotellar, F.; Guzman, R.; Gomez-Ambrosi, J.; Pulido, M. R.; Russell, W. R.; Imbernon, M.; Ross, R. A.; Malagon, M. M.; Dieguez, C.; Fernandez-Real, J. M.; Fruhbeck, G.; Nogueiras, R., The L-alpha-Lysophosphatidylinositol/GPR55 System and Its Potential Role in Human Obesity. *Diabetes* **2011**.
159. Ford, L. A.; Roelofs, A. J.; Anavi-Goffer, S.; Mowat, L.; Simpson, D. G.; Irving, A. J.; Rogers, M. J.; Rajnicek, A. M.; Ross, R. A., A role for L-alpha-lysophosphatidylinositol and GPR55 in the modulation of migration, orientation and polarization of human breast cancer cells. *Br J Pharmacol* **2010,** 160, (3), 762-71.
160. Jay, M. A.; Ren, J., Peroxisome proliferator-activated receptor (PPAR) in metabolic syndrome and type 2 diabetes mellitus. *Curr Diabetes Rev* **2007,** 3, (1), 33-9.
161. Clark, R. B., The role of PPARs in inflammation and immunity. *Journal of Leukocyte Biology* **2002,** 71, (3), 388-400.
162. Stella, N., Cannabinoid and cannabinoid-like receptors in microglia, astrocytes, and astrocytomas. *Glia* **2010,** 58, (9), 1017-30.
163. McHugh, D.; Hu, S. S. J.; Rimmerman, N.; Juknat, A.; Vogel, Z.; Walker, J. M.; Bradshaw, H. B., N-arachidonoyl glycine, an abundant endogenous lipid, potently drives directed cellular migration through GPR18, the putative abnormal cannabidiol receptor. *Bmc Neuroscience* **2010,** 11.
164. Overton, H. A.; Fyfe, M. C. T.; Reynet, C., GPR119, a novel G protein-coupled receptor target for the treatment of type 2 diabetes and obesity. *British Journal of Pharmacology* **2008,** 153, S76-S81.
165. Perez-Reyes, E., Molecular physiology of low-voltage-activated T-type calcium channels. *Physiol Rev* **2003,** 83, (1), 117-161.

166. Anderson, M. P.; Mochizuki, T.; Xie, J.; Fischler, W.; Manger, J. P.; Talley, E. M.; Scammell, T. E.; Tonegawa, S., Thalamic Cav3.1 T-type Ca2+ channel plays a crucial role in stabilizing sleep. *Proc Natl Acad Sci U S A* **2005,** 102, (5), 1743-8.
167. Kim, D., Thalamic control of visceral nociception mediated by T-type Ca2+ channels (vol 302, pg 117, 2003). *Science* **2004,** 303, (5664), 1612-1612.
168. Tsakiridou, E.; Bertollini, L.; Decurtis, M.; Avanzini, G.; Pape, H. C., Selective Increase in T-Type Calcium Conductance of Reticular Thalamic Neurons in a Rat Model of Absence Epilepsy. *Journal of Neuroscience* **1995,** 15, (4), 3110-3117.
169. Vitko, I.; Chen, Y. C.; Arias, J. M.; Shen, Y.; Wu, X. R.; Perez-Reyes, E., Functional characterization and neuronal modeling of the effects of childhood absence epilepsy variants of CACNA1H, a T-type calcium channel. *Journal of Neuroscience* **2005,** 25, (19), 4844-4855.
170. Barbara, G.; Alloui, A.; Nargeot, J.; Lory, P.; Eschalier, A.; Bourinet, E.; Chemin, J., T-Type Calcium Channel Inhibition Underlies the Analgesic Effects of the Endogenous Lipoamino Acids. *Journal of Neuroscience* **2009,** 29, (42), 13106-13114.
171. You, H.; Gadotti, V. M.; Petrov, R. R.; Zamponi, G. W.; Diaz, P., Functional characterization and analgesic effects of mixed cannabinoid receptor/T-type channel ligands. *Mol Pain* **2011,** 7, 89.
172. McCallum, J. B.; Kwok, W. M.; Mynlieff, M.; Bosnjak, Z. J.; Hogan, Q. H., Loss of T-type calcium current in sensory neurons of rats with neuropathic pain. *Anesthesiology* **2003,** 98, (1), 209-216.
173. Flatters, S. J. L., T-type calcium channels: a potential target for the treatment of chronic pain. *Drug Future* **2005,** 30, (6), 573-580.
174. Chemin, J.; Monteil, A.; Perez-Reyes, E.; Nargeot, J.; Lory, P., Direct inhibition of T-type calcium channels by the endogenous cannabinoid anandamide. *EMBO J* **2001,** 20, (24), 7033-7040.
175. Ross, H. R.; Napier, I.; Connor, M., Inhibition of Recombinant Human T-type Calcium Channels by Δ9-Tetrahydrocannabinol and Cannabidiol. *Journal of Biological Chemistry* **2008,** 283, (23), 16124-16134.
176. Fan, P., Cannabinoid agonists inhibit the activation of 5-HT3 receptors in rat nodose ganglion neurons. *J Neurophysiol* **1995,** 73, (2), 907-10.
177. Barann, M.; Molderings, G.; Brüss, M.; Bönisch, H.; Urban, B. W.; Göthert, M., Direct inhibition by cannabinoids of human 5-HT3A receptors: probable involvement of an allosteric modulatory site. *British Journal of Pharmacology* **2002,** 137, (5), 589-596.
178. Oz, M.; Zhang, L.; Ravindran, A.; Morales, M.; Lupica, C. R., Differential Effects of Endogenous and Synthetic Cannabinoids on α7-Nicotinic Acetylcholine Receptor-Mediated Responses in Xenopus Oocytes. *Journal of Pharmacology and Experimental Therapeutics* **2004,** 310, (3), 1152-1160.
179. Hampson, A. J.; Bornheim, L. M.; Scanziani, M.; Yost, C. S.; Gray, A. T.; Hansen, B. M.; Leonoudakis, D. J.; Bickler, P. E., Dual effects of anandamide on NMDA receptor-mediated responses and neurotransmission. *J Neurochem* **1998,** 70, (2), 671-6.
180. Maingret, F.; Patel, A. J.; Lazdunski, M.; Honore, E., The endocannabinoid anandamide is a direct and selective blocker of the background K(+) channel TASK-1. *EMBO J* **2001,** 20, (1-2), 47-54.

181. Nicholson, R. A.; Liao, C.; Zheng, J.; David, L. S.; Coyne, L.; Errington, A. C.; Singh, G.; Lees, G., Sodium channel inhibition by anandamide and synthetic cannabimimetics in brain. *Brain Research* **2003,** 978, (1–2), 194-204.
182. Ameri, A., The effects of cannabinoids on the brain. *Prog Neurobiol* **1999,** 58, (4), 315-48.
183. Grant, J. E.; Chamberlain, S. R.; Schreiber, L.; Odlaug, B. L., Neuropsychological deficits associated with cannabis use in young adults. *Drug Alcohol Depend* **2012,** 121, (1-2), 159-62.
184. Arseneault, L.; Cannon, M.; Witton, J.; Murray, R. M., Causal association between cannabis and psychosis: examination of the evidence. *Brit J Psychiat* **2004,** 184, 110-117.
185. D'Souza, D. C.; Perry, E.; MacDougall, L.; Ammerman, Y.; Cooper, T.; Wu, Y. T.; Braley, G.; Gueorguieva, R.; Krystal, J. H., The psychotomimetic effects of intravenous delta-9-tetrahydrocannabinol in healthy individuals: implications for psychosis. *Neuropsychopharmacology* **2004,** 29, (8), 1558-72.
186. Hall, W.; Degnhardt, L., Cannabis use and the risk of developing a psychotic disorder. *World Psychiatry* **2008,** 7, (2), 68-71.
187. Caspi, A.; Moffitt, T. E.; Cannon, M.; McClay, J.; Murray, R.; Harrington, H.; Taylor, A.; Arseneault, L.; Williams, B.; Braithwaite, A.; Poulton, R.; Craig, I. W., Moderation of the effect of adolescent-onset cannabis use on adult psychosis by a functional polymorphism in the catechol-O-methyltransferase gene: Longitudinal evidence of a gene X environment interaction. *Biol Psychiat* **2005,** 57, (10), 1117-1127.
188. Fernandez-Espejo, E.; Viveros, M. P.; Nunez, L.; Ellenbroek, B. A.; Rodriguez de Fonseca, F., Role of cannabis and endocannabinoids in the genesis of schizophrenia. *Psychopharmacology (Berl)* **2009,** 206, (4), 531-49.
189. Aung, M. M.; Griffin, G.; Huffman, J. W.; Wu, M.-J.; Keel, C.; Yang, B.; Showalter, V. M.; Abood, M. E.; Martin, B. R., Influence of the N-1 alkyl chain length of cannabimimetic indoles upon CB1 and CB2 receptor binding. *Drug and Alcohol Dependence* **2000,** 60, (2), 133-140.
190. Huffman, J. W.; Dai, D.; Martin, B. R.; Compton, D. R., Design, Synthesis and Pharmacology of Cannabimimetic Indoles. *Bioorganic & Medicinal Chemistry Letters* **1994,** 4, (4), 563-566.
191. Every-Palmer, S., Synthetic cannabinoid JWH-018 and psychosis: an explorative study. *Drug Alcohol Depend* **2011,** 117, (2-3), 152-7.
192. Ginsburg, B. C.; Schulze, D. R.; Hruba, L.; McMahon, L. R., JWH-018 and JWH-073: Delta-tetrahydrocannabinol-like discriminative stimulus effects in monkeys. *J Pharmacol Exp Ther* **2012,** 340, (1), 37-45.
193. Bornheim, L. M.; Grillo, M. P., Characterization of cytochrome P450 3A inactivation by cannabidiol: possible involvement of cannabidiol-hydroxyquinone as a P450 inactivator. *Chem Res Toxicol* **1998,** 11, (10), 1209-16.
194. Russo, E.; Guy, G. W., A tale of two cannabinoids: the therapeutic rationale for combining tetrahydrocannabinol and cannabidiol. *Med Hypotheses* **2006,** 66, (2), 234-46.
195. Vann, R. E.; Gamage, T. F.; Warner, J. A.; Marshall, E. M.; Taylor, N. L.; Martin, B. R.; Wiley, J. L., Divergent effects of cannabidiol on the discriminative stimulus and place conditioning effects of Delta(9)-tetrahydrocannabinol. *Drug Alcohol Depend* **2008,** 94, (1-3), 191-8.

196. Bhattacharyya, S.; Morrison, P. D.; Fusar-Poli, P.; Martin-Santos, R.; Borgwardt, S.; Winton-Brown, T.; Nosarti, C.; CM, O. C.; Seal, M.; Allen, P.; Mehta, M. A.; Stone, J. M.; Tunstall, N.; Giampietro, V.; Kapur, S.; Murray, R. M.; Zuardi, A. W.; Crippa, J. A.; Atakan, Z.; McGuire, P. K., Opposite effects of delta-9-tetrahydrocannabinol and cannabidiol on human brain function and psychopathology. *Neuropsychopharmacology* **2010,** 35, (3), 764-74.
197. Zuardi, A. W.; Hallak, J. E.; Crippa, J. A., Interaction between cannabidiol (CBD) and (9)-tetrahydrocannabinol (THC): influence of administration interval and dose ratio between the cannabinoids. *Psychopharmacology (Berl)* **2012,** 219, (1), 247-9.
198. Klein, C.; Karanges, E.; Spiro, A.; Wong, A.; Spencer, J.; Huynh, T.; Gunasekaran, N.; Karl, T.; Long, L. E.; Huang, X. F.; Liu, K.; Arnold, J. C.; McGregor, I. S., Cannabidiol potentiates Delta-tetrahydrocannabinol (THC) behavioural effects and alters THC pharmacokinetics during acute and chronic treatment in adolescent rats. *Psychopharmacology (Berl)* **2011,** 218, (2), 443-57.
199. Mohamed, B. A., Cannabinoids in medicine: A review of their therapeutic potential. *Journal of Ethnopharmacology* **2006,** 105, (1–2), 1-25.
200. Sink, K. S.; Segovia, K. N.; Sink, J.; Randall, P. A.; Collins, L. E.; Correa, M.; Markus, E. J.; Vemuri, V. K.; Makriyannis, A.; Salamone, J. D., Potential anxiogenic effects of cannabinoid CB1 receptor antagonists/inverse agonists in rats: Comparisons between AM4113, AM251, and the benzodiazepine inverse agonist FG-7142. *Eur Neuropsychopharm* **2010,** 20, (2), 112-122.
201. Christensen, R.; Kristensen, P. K.; Bartels, E. M.; Bliddal, H.; Astrup, A., Efficacy and safety of the weight-loss drug rimonabant: a meta-analysis of randomised trials. *Lancet* **2007,** 370, (9600), 1706-13.
202. Hill, A. J.; Williams, C. M.; Whalley, B. J.; Stephens, G. J., Phytocannabinoids as novel therapeutic agents in CNS disorders. *Pharmacology & Therapeutics* **2012,** 133, (1), 79-97.
203. Russo, E. B., Taming THC: potential cannabis synergy and phytocannabinoid-terpenoid entourage effects. *British Journal of Pharmacology* **2011,** 163, (7), 1344-1364.
204. Gertsch, J.; Pertwee, R. G.; Di Marzo, V., Phytocannabinoids beyond the Cannabis plant - do they exist? *Br J Pharmacol* **2010,** 160, (3), 523-9.
205. Woelkart, K.; Salo-Ahen, O. M. H.; Bauer, R., CB receptor ligands from plants. *Curr Top Med Chem* **2008,** 8, (3), 173-186.
206. Pertwee, R. G.; Thomas, A.; Stevenson, L. A.; Ross, R. A.; Varvel, S. A.; Lichtman, A. H.; Martin, B. R.; Razdan, R. K., The psychoactive plant cannabinoid, Delta9-tetrahydrocannabinol, is antagonized by Delta8- and Delta9-tetrahydrocannabivarin in mice in vivo. *Br J Pharmacol* **2007,** 150, (5), 586-94.
207. Izzo, A. A.; Borrelli, F.; Capasso, R.; Di Marzo, V.; Mechoulam, R., Non-psychotropic plant cannabinoids: new therapeutic opportunities from an ancient herb. *Trends Pharmacol Sci* **2009,** 30, (10), 515-27.
208. De Petrocellis, L.; Di Marzo, V., Non-CB1, Non-CB2 Receptors for Endocannabinoids, Plant Cannabinoids, and Synthetic Cannabimimetics: Focus on G-protein-coupled Receptors and Transient Receptor Potential Channels. *Journal of Neuroimmune Pharmacology* **2010,** 5, (1), 103-121.
209. Gertsch, J.; Raduner, S.; Altmann, K. H., Review - New natural noncannabinoid ligands for cannabinoid type-2 (CB2) receptors. *J Recept Sig Transd* **2006,** 26, (5-6), 709-730.

210. Raduner, S.; Majewska, A.; Chen, J. Z.; Xie, X. Q.; Hamon, J.; Faller, B.; Altmann, K. H.; Gertsch, J., Alkylamides from Echinacea are a new class of cannabinomimetics - Cannabinoid type 2 receptor-dependent and -independent immunomodulatory effects. *Journal of Biological Chemistry* **2006,** 281, (20), 14192-14206.
211. Ghelardini, C.; Galeotti, N.; Di Cesare Mannelli, L.; Mazzanti, G.; Bartolini, A., Local anaesthetic activity of beta-caryophyllene. *Farmaco* **2001,** 56, (5-7), 387-9.
212. Fournier, G.; Lenicque, P. M.; Paris, M. R., [Toxic effects of essential oil of Cannabis sativa L. and main constituents on planarian (Dugesia tigrina) (author's transl)]. *Toxicol Eur Res* **1978,** 1, (6), 385-9.
213. Politeo, O.; Jukic, M.; Milos, M., Chemical composition and antioxidant activity of essential oils of twelve spice plants. *Croat Chem Acta* **2006,** 79, (4), 545-552.
214. FDA, Everything Added to Food in the United States (EAFUS). In 2012.
215. Gertsch, J.; Leonti, M.; Raduner, S.; Racz, I.; Chen, J. Z.; Xie, X. Q.; Altmann, K. H.; Karsak, M.; Zimmer, A., Beta-caryophyllene is a dietary cannabinoid. *P Natl Acad Sci USA* **2008,** 105, (26), 9099-9104.
216. Bento, A. F.; Marcon, R.; Dutra, R. C.; Claudino, R. F.; Cola, M.; Pereira Leite, D. F.; Calixto, J. B., β-Caryophyllene Inhibits Dextran Sulfate Sodium-Induced Colitis in Mice through CB2 Receptor Activation and PPARγ Pathway. *The American Journal of Pathology* **2011,** 178, (3), 1153-1166.
217. Cho, J. Y.; Chang, H. J.; Lee, S. K.; Kim, H. J.; Hwang, J. K.; Chun, H. S., Amelioration of dextran sulfate sodium-induced colitis in mice by oral administration of beta-caryophyllene, a sesquiterpene. *Life Sci* **2007,** 80, (10), 932-9.
218. Legault, J.; Pichette, A., Potentiating effect of beta-caryophyllene on anticancer activity of alpha-humulene, isocaryophyllene and paclitaxel. *Journal of Pharmacy and Pharmacology* **2007,** 59, (12), 1643-1647.
219. Lima, S. R. M.; Veiga, V. F.; Christo, H. B.; Pinto, A. C.; Fernandes, P. D., In vivo and in vitro studies on the anticancer activity of Copaifera multijuga Hayne and its fractions. *Phytotherapy Research* **2003,** 17, (9), 1048-1053.
220. Di Sotto, A.; Evandri, M. G.; Mazzanti, G., Antimutagenic and mutagenic activities of some terpenes in the bacterial reverse mutation assay. *Mutation Research/Genetic Toxicology and Environmental Mutagenesis* **2008,** 653, (1-2), 130-133.
221. Gertsch, J.; Pertwee, R. G.; Di Marzo, V., Phytocannabinoids beyond the Cannabis plant – do they exist? *British Journal of Pharmacology* **2010,** 160, (3), 523-529.
222. Mechoulam, R., Interview with Prof. Raphael Mechoulam, codiscoverer of THC.. Interview by Stanley Einstein. *Int J Addict* **1986,** 21, (4-5), 579-87.
223. Pertwee, R. G., Cannabinoid pharmacology: the first 66 years. *British Journal of Pharmacology* **2006,** 147, (S1), S163-S171.
224. Raduner, S.; Majewska, A.; Chen, J.-Z.; Xie, X.-Q.; Hamon, J.; Faller, B.; Altmann, K.-H.; Gertsch, J., Alkylamides from Echinacea Are a New Class of Cannabinomimetics. *Journal of Biological Chemistry* **2006,** 281, (20), 14192-14206.
225. Chicca, A.; Raduner, S.; Pellati, F.; Strompen, T.; Altmann, K.-H.; Schoop, R.; Gertsch, J., Synergistic immunomopharmacological effects of N-alkylamides in Echinacea purpurea herbal extracts. *International Immunopharmacology* **2009,** 9, (7–8), 850-858.

226. Zimmerman, C., Life without pain unites friends from afar. *The Daily News* **2010**.
227. Woolf, C. J.; Salter, M. W., Neuronal Plasticity: Increasing the Gain in Pain. *Science* **2000,** 288, (5472), 1765-1768.
228. Stewart, W. F.; Ricci, J. A.; Chee, E.; Morganstein, D.; Lipton, R., Lost Productive Time and Cost Due to Common Pain Conditions in the US Workforce. *JAMA: The Journal of the American Medical Association* **2003,** 290, (18), 2443-2454.
229. Stokowski, L. A. Managing Relentless Pain in Cancer Survivors. http://www.medscape.com/viewarticle/737345
230. Finnerup, N. B.; Sindrup, S. r. H.; Jensen, T. S., The evidence for pharmacological treatment of neuropathic pain. *Pain* **2010,** 150, (3), 573-581.
231. Turk, D. C.; Audette, J.; Levy, R. M.; Mackey, S. C.; Stanos, S., Assessment and Treatment of Psychosocial Comorbidities in Patients With Neuropathic Pain. *Mayo Clinic proceedings. Mayo Clinic* **2010,** 85, (3), S42-S50.
232. Ren, K.; Dubner, R., Interactions between the immune and nervous systems in pain. *Nat Med* **2010,** 16, (11), 1267-1276.
233. von Hehn, Christian A.; Baron, R.; Woolf, Clifford J., Deconstructing the Neuropathic Pain Phenotype to Reveal Neural Mechanisms. *Neuron* **2012,** 73, (4), 638-652.
234. Gracely, R. H.; Lynch, S. A.; Bennett, G. J., Painful neuropathy: altered central processing maintained dynamically by peripheral input. *Pain* **1992,** 51, (2), 175-194.
235. Devor, M., Ectopic discharge in Aβ afferents as a source of neuropathic pain. *Experimental Brain Research* **2009,** 196, (1), 115-128.
236. Xiao, W. H.; Bennett, G. J., Chemotherapy-evoked neuropathic pain: Abnormal spontaneous discharge in A-fiber and C-fiber primary afferent neurons and its suppression by acetyl-l-carnitine. *Pain* **2008,** 135, (3), 262-270.
237. Burchiel, K. J.; Russell, L. C.; Lee, R. P.; Sima, A. A., Spontaneous activity of primary afferent neurons in diabetic BB/Wistar rats. A possible mechanism of chronic diabetic neuropathic pain. *Diabetes* **1985,** 34, (11), 1210-1213.
238. King, T.; Qu, C.; Okun, A.; Mercado, R.; Ren, J.; Brion, T.; Lai, J.; Porreca, F., Contribution of afferent pathways to nerve injury-induced spontaneous pain and evoked hypersensitivity. *Pain* **2011,** 152, (9), 1997-2005.
239. Amir, R.; Kocsis, J. D.; Devor, M., Multiple Interacting Sites of Ectopic Spike Electrogenesis in Primary Sensory Neurons. *The Journal of Neuroscience* **2005,** 25, (10), 2576-2585.
240. Løseth, S.; Mellgren, S. I.; Jorde, R.; Lindal, S.; Stålberg, E., Polyneuropathy in type 1 and type 2 diabetes: comparison of nerve conduction studies, thermal perception thresholds and intraepidermal nerve fibre densities. *Diabetes/Metabolism Research and Reviews* **2010,** 26, (2), 100-106.
241. Siau, C.; Xiao, W.; Bennett, G. J., Paclitaxel- and vincristine-evoked painful peripheral neuropathies: Loss of epidermal innervation and activation of Langerhans cells. *Experimental Neurology* **2006,** 201, (2), 507-514.
242. Boyette-Davis, J.; Xin, W.; Zhang, H.; Dougherty, P. M., Intraepidermal nerve fiber loss corresponds to the development of Taxol-induced hyperalgesia and can be prevented by treatment with minocycline. *Pain* **2011,** 152, (2), 308-313.
243. Danbolt, N. C., Glutamate uptake. *Prog Neurobiol* **2001,** 65, (1), 1-105.
244. Sung, B.; Lim, G.; Mao, J., Altered expression and uptake activity of spinal glutamate transporters after nerve injury contribute to the pathogenesis of neuropathic pain in rats. *J Neurosci* **2003,** 23, (7), 2899-910.

245. Yaster, M.; Guan, X.; Petralia, R. S.; Rothstein, J. D.; Lu, W.; Tao, Y.-X., Effect of Inhibition of Spinal Cord Glutamate Transporters on Inflammatory Pain Induced by Formalin and Complete Freund's Adjuvant. *Anesthesiology* **2011,** 114, (2), 412-423 10.1097/ALN.0b013e318205df50.
246. Niederberger, E.; Schmidtko, A.; Rothstein, J. D.; Geisslinger, G.; Tegeder, I., Modulation of spinal nociceptive processing through the glutamate transporter GLT-1. *Neuroscience* **2003,** 116, (1), 81-87.
247. Olechowski, C. J.; Parmar, A.; Miller, B.; Stephan, J.; Tenorio, G.; Tran, K.; Leighton, J.; Kerr, B. J., A diminished response to formalin stimulation reveals a role for the glutamate transporters in the altered pain sensitivity of mice with experimental autoimmune encephalomyelitis (EAE). *Pain* **2010,** 149, (3), 565-72.
248. Tao, Y.-X.; Gu, J.; Stephens, R., Role of spinal cord glutamate transporter during normal sensory transmission and pathological pain states. *Mol Pain* **2005,** 1, (1), 30.
249. Gao, Y.-J.; Ji, R.-R., Chemokines, neuronalâ€“glial interactions, and central processing of neuropathic pain. *Pharmacology & Therapeutics* **2010,** 126, (1), 56-68.
250. Brownjohn, P. W.; Ashton, J. C., Novel targets in pain research: The case for CB2 receptors as a biorational pain target. *Current Anaesthesia & Critical Care* **2009,** 20, (5–6), 198-203.
251. Bridges, D.; Ahmad, K.; Rice, A. S., The synthetic cannabinoid WIN55,212-2 attenuates hyperalgesia and allodynia in a rat model of neuropathic pain. *Br J Pharmacol* **2001,** 133, (4), 586-94.
252. Scott, D. A.; Wright, C. E.; Angus, J. A., Evidence that CB-1 and CB-2 cannabinoid receptors mediate antinociception in neuropathic pain in the rat. *Pain* **2004,** 109, (1-2), 124-31.
253. Whiteside, G. T.; Lee, G. P.; Valenzano, K. J., The role of the cannabinoid CB2 receptor in pain transmission and therapeutic potential of small molecule CB2 receptor agonists. *Curr Med Chem* **2007,** 14, (8), 917-36.
254. Anand, P.; Whiteside, G.; Fowler, C. J.; Hohmann, A. G., Targeting CB2 receptors and the endocannabinoid system for the treatment of pain. *Brain Res Rev* **2009,** 60, (1), 255-66.
255. Galiègue, S.; Mary, S.; Marchand, J.; Dussossoy, D.; Carrière, D.; Carayon, P.; Bouaboula, M.; Shire, D.; Le Fur, G.; Casellas, P., Expression of Central and Peripheral Cannabinoid Receptors in Human Immune Tissues and Leukocyte Subpopulations. *European Journal of Biochemistry* **1995,** 232, (1), 54-61.
256. Carlisle, S. J.; Marciano-Cabral, F.; Staab, A.; Ludwick, C.; Cabral, G. A., Differential expression of the CB2 cannabinoid receptor by rodent macrophages and macrophage-like cells in relation to cell activation. *International Immunopharmacology* **2002,** 2, (1), 69-82.
257. Atwood, B. K.; Wager-Miller, J.; Haskins, C.; Straiker, A.; Mackie, K., Functional Selectivity in CB2 Cannabinoid Receptor Signaling and Regulation: Implications for the Therapeutic Potential of CB2 Ligands. *Mol Pharmacol* **2012,** 81, (2), 250-63.
258. Malan Jr, T. P.; Ibrahim, M. M.; Lai, J.; Vanderah, T. W.; Makriyannis, A.; Porreca, F., CB2 cannabinoid receptor agonists: pain relief without psychoactive effects? *Current Opinion in Pharmacology* **2003,** 3, (1), 62-67.
259. Gin C Hsieh, M. P., Prasant Chandran, Bradley A Hooker, Chang Z Zhu, Anita K Salyers, Erica J Wensink, CenChen Zhan, William A Carroll, Michael J Dart, Betty

B Yao, Prisca Honore, and Michael D Meyer, Central and peripheral sites of action for CB2 receptor mediated analgesic activity in chronic inflammatory and neuropathic pain models in rats. *British Journal of Pharmacology* **2010,** 162, (2), 428-440.

260. Walter, L.; Franklin, A.; Witting, A.; Wade, C.; Xie, Y.; Kunos, G.; Mackie, K.; Stella, N., Nonpsychotropic Cannabinoid Receptors Regulate Microglial Cell Migration. *The Journal of Neuroscience* **2003,** 23, (4), 1398-1405.
261. Bingham, B.; Jones, P. G.; Uveges, A. J.; Kotnis, S.; Lu, P.; Smith, V. A.; Sun, S. C.; Resnick, L.; Chlenov, M.; He, Y.; Strassle, B. W.; Cummons, T. A.; Piesla, M. J.; Harrison, J. E.; Whiteside, G. T.; Kennedy, J. D., Species-specific in vitro pharmacological effects of the cannabinoid receptor 2 (CB2) selective ligand AM1241 and its resolved enantiomers. *Br J Pharmacol* **2007,** 151, (7), 1061-70.
262. Urban, J. D.; Clarke, W. P.; von Zastrow, M.; Nichols, D. E.; Kobilka, B.; Weinstein, H.; Javitch, J. A.; Roth, B. L.; Christopoulos, A.; Sexton, P. M.; Miller, K. J.; Spedding, M.; Mailman, R. B., Functional Selectivity and Classical Concepts of Quantitative Pharmacology. *Journal of Pharmacology and Experimental Therapeutics* **2007,** 320, (1), 1-13.
263. Trotter, B. W.; Nanda, K. K.; Burgey, C. S.; Potteiger, C. M.; Deng, J. Z.; Green, A. I.; Hartnett, J. C.; Kett, N. R.; Wu, Z.; Henze, D. A.; Della Penna, K.; Desai, R.; Leitl, M. D.; Lemaire, W.; White, R. B.; Yeh, S.; Urban, M. O.; Kane, S. A.; Hartman, G. D.; Bilodeau, M. T., Imidazopyridine CB2 agonists: optimization of CB2/CB1 selectivity and implications for in vivo analgesic efficacy. *Bioorg Med Chem Lett* **2011,** 21, (8), 2354-8.
264. Sain, N. M.; Liang, A.; Kane, S. A.; Urban, M. O., Antinociceptive effects of the non-selective cannabinoid receptor agonist CP 55,940 are absent in CB1(-/-) and not CB2(-/-) mice in models of acute and persistent pain. *Neuropharmacology* **2009,** 57, (3), 235-41.

CHAPTER II EARLY FORMULATION AND ENABLING DRUG DELIVERY SYSTEMS DESIGN

1 Introduction.

Recent progress in parallel chemistry and high-throughput screening has resulted in an increase of poorly soluble drug candidates. New Chemical Entities (NCE) characteristics differ dramatically in term of physicochemical properties [e.g. chemical structure (planarity, chirality), polymorphism form, particle size, hydrophilicity/lipophilicity balance, (logD), pKa, polar surface area (PSA)] and potency. The pharmacological activity of a drug is the result of affinity and interaction with the biological target but also optimum exposure at the target site. It is therefore necessary for the drug to reach the site of action following administration (i.e. oral, intravenous, transdermal etc.) at sufficient concentrations. In addition, accurate and reproducible dosing is a prerequisite to study dose-response activity. The pharmaceutical area dealing with these challenges is the early formulation. Early formulation is an integral part of drug discovery and drug development. Design of a stable drug delivery system (DDS) during the early formulation stage should allow drug escalation studies in different animal models using different routes of administration. Early formulation has mainly the following aim: "*to deliver the drug at the right place, at the right concentration for the right period of time*"[18]. Formulation of sparingly water- soluble drugs is a common issue for the formulators (i.e. solubilization and/or particle engineering) especially when a controlled-release drug profile is required for an optimum therapeutic index or to compensate a poor stability. In addition, the search for suitable DDS often takes place under little compound availability, incomplete physicochemical property characterization and time constraints. Enabling formulation approaches may allow the selection of NCE showing not ideal drug-like profile to be evaluated for *in vitro/in vivo* testing to validate a target and/or a therapeutic strategy at the early phase of drug discovery. For these drugs, the absorption and bioavailability could be influenced by their intrinsic solubility and dissolution rate in

biological fluids. There are many DDS development strategies to enhance the solubility of lipophilic drugs and subsequently the delivery of these drugs. The commonly used strategies in marketed products include salt formation (i.e. pH adjustment), cosolvency (e.g. ethanol, propylene glycol, PEG400 etc.), micellization (e.g. polysorbate 80, cremophor ELP etc.), (nano)- (micro)- emulsification, complexation (e.g. cyclodextrins), encapsulation in lipid-based formulation (e.g. liposomes) or nanoparticles (NPs) DDS[20-23]. Combination of two or more of these techniques may produce synergistic effect in solubilization[24-26]. In addition to the solubility and the physicochemical stability of the drug in DDS and in biological fluids, the biodistribution and the pharmacokinetic/pharmacodynamic (PK/PD) properties of pharmacologically active drug candidate can also be altered. When nano- drug carriers are used, the following characteristics will be usually also requested: lack of long-term host accumulation, non-toxicity and immunoginecity along with acceptable encapsulation and targeting ability (passive or active), prolonged plasma circulation, and controlled release. Overall, the development and selection of a suitable DDS will aim to enhance the therapeutic effect (i.e. bioavailability) and tolerance of drugs, in a reproducible way and in a case-to-case manner to compensate for “non drug-like” properties of a drug candidate.

During this thesis, we set up an early formulation strategy (Fig. 8) for rapid evaluation of NCE on a broad range of *in vitro* and *in vivo* assays, such as pharmacodynamic, pharmacokinetic, toxicology or pharmacology studies. Despite the differences in objectives, sufficient exposure of the selected organism to the early-stage candidate as well as dose accuracy and tolerability, are necessary to obtain reliable results from these studies[27]. Starting from the orange box, the different excipients used for preformulation studies are selected according to the NCE solubility and permeability using the Biopharmaceutics Classification System BCS[28] and also according to the route of administration, the biological target and the animal species to be dosed. From a regulatory aspect, the excipients chosen are published in the official pharmacopeia of the United States (USP) or their safety ratio is listed in the Inactive Ingredient Guide (IIG) for FDA approved drugs (i.e. excipients used in marketed pharmaceutical products). At the least a Drug Master File (DMF) submitted to the FDA is required for the excipient to be retained and tested. Scientific articles and technical brochures from the suppliers are thoroughly consulted for information related to the material toxicity/safety. In addition, excipients are endowed with intrinsic properties i.e. absorption/dissolution enhancer,

solubilizing agents, antioxidant/preservative, P-gp inhibitor that may be useful to consider. After initial solubility/stability screening in pure excipients, a DDS based on mixture of the selected excipients in water is designed. If poor solubility compromises conventional strategies approaches (i.e. blue and green boxes), (micro)- and (nano)-suspension might be used.

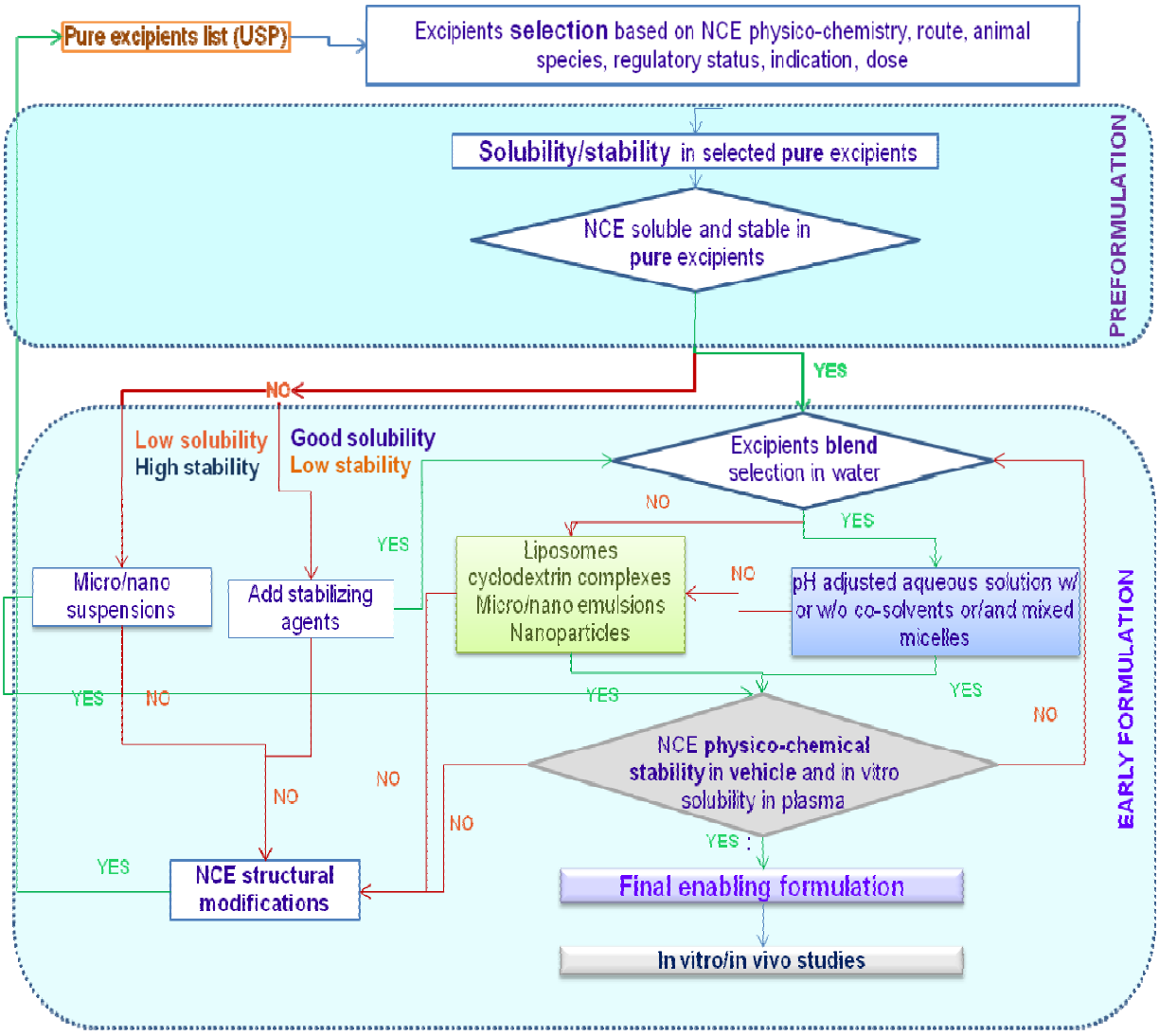

Figure 8 : Pre-formulation/Early formulation strategy suggested for the design of enabling Drug Delivery Systems (DDS) at the drug discovery stage.

Alternatively, stabilizing agents(e.g. antioxidants, preservatives) may allow increased physical/chemical stability of the new chemical entity (NCE). Colloidal systems (e.g. liposomes, nano- micro- particles) and inclusion complexes (e.g. cyclodextrins) could be designed to solve stability issue and/or poor solubility in excipients mixture and/or

bioavailability issues. A final enabling formulation is selected before *in vitro* or *in vivo* administration, after *in vitro* assessment of NCE physicochemical stability and solubility by macroscopic/microscopic observation and LC/MS dosing, and non precipitation when diluted in synthetic plasma. The data generated at these early stages allow anticipation and identification of potential development challenges from a biopharmaceutical perspective (i.e. solubility, stability, permeability) and thus selection and optimization of the best candidates for lead nomination. In case of high limitations arising in preformulation or early formulation studies regarding the NCE formulability, an alternative strategy could be adopted such as NCE structural modification or physiological parameters modification depending on the route of administration.

In this project, we designed different enabling DDS for synthetic cannabinoid compounds synthesized by our laboratory, to evaluate their pharmacological activity in *in vivo* models of neuropathic pain and to conduct a PK study with the lead compound selected. For reasons of low amount of drug supplied and according to the BCS class II (poor solubility/high permeability) of the hit compounds investigated, we pre-selected four formulation concepts to develop: (a) co-solvent/surfactant micelles solution, (b) self-emulsifying drug delivery system (SEDDS), (c) cyclodextrin inclusion complexes and (d) liposomal suspension.

1.2 Cyclodextrins.

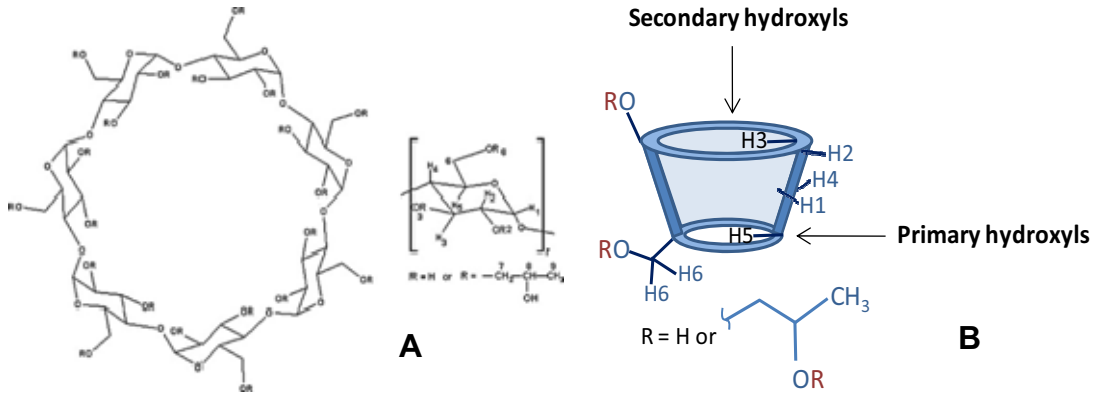

Figure 9: A) Hydroxypropyl-*beta*- cyclodextrin chemical structure (HPβCD) **B**) HPβCD torus-like molecular shape.

Cyclodextrins (CDs) are a group of cyclic oligosaccharides derived from the enzymatic degradation of the starch with a torus-like molecular shape (Fig. 9B). These cyclic oligosaccharides containing six, seven, eight, or more (α-1,4-)-linked d-glucopyranose units respectively α, β, γ cyclodextrins, consist of a relatively hydrophobic inner cavity and a hydrophilic outer surface. One of their interesting attributes is their ability to form host-guest inclusion complexes with a variety of lipophilic compounds which can be partially or totally included in the hydrophobic internal cavity, the hydrophilic outer surface being exposed to the solvent. In addition, CDs are not restricted to host-guest interactions and that more complex interactions like non-inclusion complexes or nanostructures formation do exist in aqueous cyclodextrin solutions[29-31]. These versatile nanocarriers are widely used to solve physicochemical and pharmaceutical issues of administered drugs to increase the aqueous solubility of poorly water-soluble drugs, to stabilize compounds to chemical and enzyme degradation and to enhance bioavailability[32-36]. CDs have also enabled improvement of drug bioavailability by affecting permeability through biological membrane[37-38] and by controlling the rate and/or time profile of drug release[39-41]. CDs are reported to be relatively well tolerated at low to moderate oral and intravenous doses[42-43] and have been used to reduce or prevent gastrointestinal or ocular irritation, for smells or tastes masking, to prevent drug-drug or drug-additive interactions, to lower compound volatility, or even to convert oils and liquid drugs into microcrystalline or amorphous powders[44-45]. The non functionalized natural α-, β-,γ- CDs (Table 3)[31] show limited aqueous solubility, especially for the β-CDs, ascribed to the intramolecular ring of hydrogen bonds form between the C2-OH and C3-OH group of glucopyranosides along with the secondary hydroxyls on the outside the CD. This complete secondary belt enhances the rigidity of β-CD[46]. By functionalizing the external hydroxyl groups of natural CDs, aggregates formation through hydrogen bond interaction are likely reduced increasing aqueous solubility. Water-soluble CDs derivatives of more pharmaceutical relevance have been developed with the aim to provide versatile delivery systems for hydrophilic and hydrophobic drugs. Among the most used functionalized CDs in the pharmaceutical field are found the hydroxypropyl derivatives of β-CD (HPβCD) and γ-CD (HPγCD), the randomly methylated β-cyclodextrin (RMβCD), and sulfobutylether β-cyclodextrin sodium salt (SBEβCD). CDs and derivatives have been investigated for oral, rectal, sublingual, ocular, nasal, pulmonary, and dermal delivery.

Nearly 30 marketed commercial drug products currently benefited from such CD technology (Table 4)[49]. Regarding their regulatory status, α-CD, β-CD and γ-CD are listed in the generally regarded as safe (GRAS) list of the FDA for use as a food additive, and α-CD, β-C are USP/NF and Ph.Eur. HPβCD, HPγCD, RMβCD and SBEβCD used in various pharmaceutical dosage forms are cited in the FDA's list of Inactive Pharmaceutical Ingredients.

Table 3[31]: Physicochemical properties of the natural α-CD, β-CD and γ-CD.

Property	**α-Cyclodextrin**	**β-Cyclodextrin**	**γ-Cyclodextrin**
Molecular weight of anhydrous compound (dalton):	973	1135	1297
Number of glucopyranose units:	6	7	8
Number of water molecules present in the stable hydrates of the CD lattices[47]:			
Total number:	6.4	9.6	14.2
Inside the cavity:	2	6	8.8
Approximate dimensions (nm)[48]:			
Height (H):	0.78	0.78	0.78
Inner diameter (di):	0.50	0.62	0.80
Outer diameter (do):	1.46	1.54	1.75
Solubility in water at 25 °C (mg/ml)[47]	129.5 ± 0.7	18.4 ± 0.2	249.2 ± 0.2

1.2.1 Cyclodextrins and complexation.

Understanding of the kinetics and thermodynamics of complexation and the need to optimize the CDs amount and drug-to-CDs ratios are critical success factors in the formulation of CD-based drug product. For optimal thermodynamic activity and subsequently delivery of the drug, sufficient quantity of CDs is needed to solubilize the drug whereas excess of CDs may impair the drug bioavailability. In term of kinetics of drug-complex formation and dissociation, no covalent bonds are generally formed or broken in aqueous solutions and the drug molecules in complex with CDs are in rapid

equilibrium with free molecules[50]. The phenomenon of CD inclusion complex formation is a complex process driven by many factors, mainly due to displacement of enthalpy-rich water molecules from the inside of the hydrophobic CD cavity (repulsive polar-non polar interactions)[32] by a "guest molecule" with appropriate geometry and physicochemical properties. The predominant interactions engaged in the drug-CD complex include van der Waals and hydrophobic interactions but other such as hydrogen bonding[51-52], release of ring strain in CD and change in solvent-surface tensions[53] are also involved.

In solution, a complexed compound is always in kinetic or thermodynamic equilibrium with its free components. This equilibrium can be expressed by the stability constant ($K_{m:n}$) of the drug-CD complex and is an index of change in physicochemical properties of a complexed compound:

$$m \text{ x D} + n \text{ x CD} \overset{(K_{m:n})}{\leftrightharpoons} D_m/CD_n \qquad (1)$$

where m free drug molecules (D) interact with n CD molecules (CD) to form a D_m/CD_n complex.

Therefore, at a given temperature, the stability constant $K_{m:n}$ is described as:

$$K_{m:n} = \frac{[D_m/CD_n]}{[D]^m\,[CD]^n} \qquad (2)$$

In practice, stability constants of 10 M^{-1} to $1x10^3$ M^{-1} are not uncommon, values of $1x10^4$ M^{-1} are seen occasionally, and values $>1x10^5$ M^{-1} are very rare. Practical drug solubility using CDs have been often reported to be increased by 10-fold to 1,000-fold and occasionally higher[54]. Most of small lipophilic molecules are forming guest-host complexes with a stoichiometry of 1:1 whereas higher order complexes are not unusual[55].

The stoichiometry of the complexes formed and the numerical value of their stability constants can be assessed by different methods described in literature and reviewed by Loftsson[32] and Chadha[53], observing the changes of the drug physicochemical properties such as aqueous solubility, chemical reactivity, molar absorptivity and other optical properties, NMR chemical shifts, pH-metric methods, calorimetric titration, freezing point depression and liquid chromatography retention times.

1.2.1.1 Stoichiometry of inclusion complexes and association constant.

1.2.1.1.1 Job's plot.

The study of supramolecular complexes to determine the stoichiometry of drug-CD complexes and their stability constant is commonly performed using the reliable method of continuous variation (Job's plot)[56]. A Job's graph is constructed by plotting an appropriate physicochemical parameter directly related to the concentration of the complex (e.g. absorbance, solubility, NMR chemical shift) varying molar fraction of drug (D) to cyclodextrin (CD) while the sum of their concentrations is kept constant. In a single stable complex, the plot has a triangle shape with the maximum concentration of drug-CD complex present in the sample where the molar ratio *R* corresponds to the complexation stoichiometry. For example, if a maximal value occurs at a molar ratio of 0.5, CD forms a 1:1 complex with the guest molecule. NMR chemical shift of an atom is directly related to its environment (anisotropy). Therefore, proton of a guest molecule interacting with CD will have different chemical shift compared to the same proton of the guest molecule not complexed. NMR spectroscopy chemical shifts of the anisotropically shielded atoms are sensitive to complex formation and are frequently used to determine the inclusion complexes stoichiometry and stability constant[57-61]. Since the association–dissociation process is rapid relative to the NMR time scale (microsecond to millisecond range)[62], the chemical shift δ_{obs} of protons involved in the host-guest interaction at each *R* (molar ratio) can be determined as follows[63]:

$$\delta_{obs} = f_D \delta_D + f_{D/CD} \delta_{D/CD} \qquad (3)$$

where δ_D and $\delta_{D/CD}$ are the chemical shifts of the free and complexed CD, and f_D and $f_{D/CD}$ are their molar fractions.

Chemical shift (δ) reported in ppm and chemical shift changes ($\Delta\delta$) are calculated by using the formula:

$$\Delta\delta = \delta_{obs} - \delta_D \qquad (4)$$

Where the variation of the chemical shift observed ($\Delta\delta$) is calculated as the difference in between the δ_{obs} (eq. 3), sum of the free drug and the drug complexed in a defined

system of solvent(s), and $\delta_{D,}$ the chemical shift of the free drug only in the same system of solvent(s), formula adapted from[64-65].

1.2.1.1.2 Mass spectrometry analysis.

Electrospray mass spectrometry (ESI-MS) has been used to investigate noncovalent complexes of different classes of compounds[66]. The ESI-MS allows detecting non-covalent interactions of the supramolecular inclusion host-guest complexes with various molecules in the gas phase. Electrospray provides a faithful image of the composition of the complex formed in solution and subsequently its stoichiometry in the range of concentrations used for *in vivo* studies[67], provided that all species are kinetically stable enough to reach the detector intact[66]. However it has been suggested that to avoid non specific aggregation occurring upon droplet evaporation, analyzed sample should be diluted and the electrospray flow rate decreased[66-68].
In this work we will focus on identifying stable noncovalent interactions formed between selected synthetic cannabinoids and HPβCD in the gas phase using ESI-MS, considering the parameters mentioned above, in concentrated and diluted solutions.

1.2.1.1.3 Phase solubility analysis.

The study of supramolecular complexes to determine the stoichiometry of drug-CD complexes and their stability constant is commonly performed using the reliable method of Phase solubility analysis which also allow the evaluation of the effect of CD complexation on the drug solubility.

Phase-solubility diagrams developed by Higuchi and Connors[16] (Fig. 10) are generated by plotting the total molar concentration of the drug against the molar concentration of the CD, and are more relevant to drug formulation conditions since performed in saturated solutions compared to highly dilute systems used in the Job's plot protocol. Phase diagrams are generally classified as either type A (a soluble complex is formed) or type B (a complex with definite solubility is formed). The type A can be further subclassified in types A_L, A_P, and A_N, where the guest solubility of the first type increases linearly with CD concentration while those of the second and third types deviate positively and negatively, respectively, from the straight line. The complex formation with a 1:1 stoichiometry gives the A_L type diagram, whereas the higher order complex formation in which more than one CD molecule are involved in the complexation gives the A_P type. The interaction mechanism for the A_N-type is complicated and may arise because of a significant contribution of solute−solvent interaction to the complexation or self-association of the ligand at high concentrations. In the case of the B_S type, the initial ascending portion of the solubility change is followed by a plateau region and then a decrease in the solubility at higher CD concentrations, accompanying a microcrystalline precipitation of the complex. The B_i-type diagram is indicative of the formation of insoluble complexes in water.

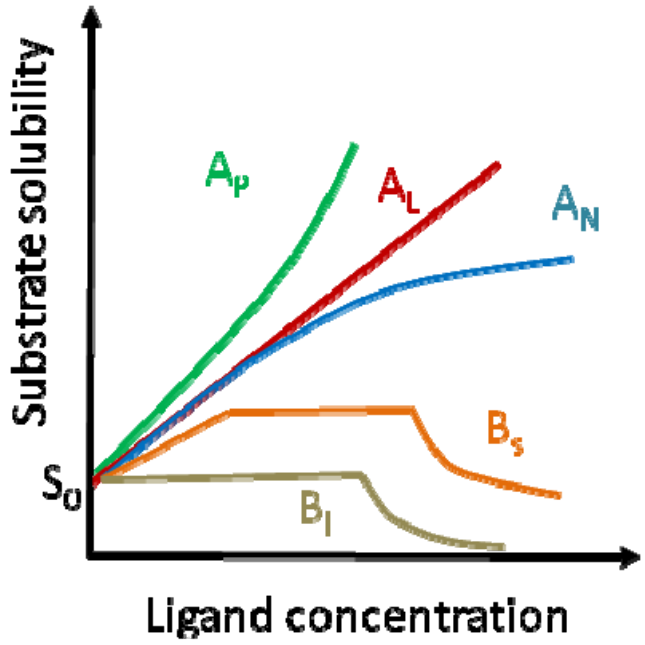

Figure 10: Phase-solubility profiles and classification of complexes according to Higuchi and Connors[16]. S_0 is the intrinsic solubility of the drug in the aqueous complexation media when no ligand (i.e. CD) is present.

Interestingly, the phase-solubility diagram allows not only quality assessment of the stoichiometry of the drug-CD complex but also the derivation of the stability constant ($K_{m:n}$). Under the conditions of A_L type linear phase solubility diagram when 1 molecule of drug interacts with 1 molecule of CD, the stability constant ($K_{1:1}$) with units of M^{-1} doesn't change over the range of CD studied and can be calculated from the slope and the intrinsic solubility (S_0) of the drug in the aqueous complexation medium.

$$K_{m:n} = \frac{[D_m/CD_n]}{[D]^m\,[CD]^n} \qquad (2)$$

In equation (2), given that: $[D]=S_0$ and $D_{tot}= S_0+m[D_m/CD_n]$ and $CD_{tot}= [CD]+ n[D_m/CD_n]$ With S_0 is the intrinsic solubility or equilibrium solubility of the drug i.e. in the absence of solubilizer, D_{tot} is the total concentration of the drug (D), free and complexed, and CD_{tot} is the total concentration of CD.

Then $$[D_m/CD_n]= \frac{[D_{tot} - S_0]}{m} \qquad (5)$$

And $$[CD]= [CD_{tot}] - n[D_m/CD_n] \qquad (6)$$

For phase-solubility system that are first order with respect to the CD (n=1), the following equation can be derived:

$$D_{tot}= \frac{mK\,S_0^{\,m}\,[CD_{tot}]}{1 + K\,S_0^{\,m}} + S_0 \qquad (7)$$

A plot of $[D_{tot}]$ in mM function of $[CD]_{tot}$ in mM should give a straight line with a slope less than the unity with y-intercept representing S_0 and the slope being:

$$\text{Slope}= \frac{mK\,S_0^{\,m}}{1 + K\,S_0^{\,m}} \qquad (8)$$

The stability constant ($K_{1:1}$) of the complex can be calculated from the slope and the intrinsic solubility (S_0) of the drug in the aqueous complexation medium.

$$K_{1:1} = \frac{slope}{S_0\,(1\text{-slope})} \qquad (9)$$

Stability constant of higher order drug-CD complex can be determined but it won't be the focus of this work (for review see[49]).

However the $K_{1:1}$ value determined by Eq. (9) is strongly affected by the S_0 value which is usually very inaccurate for compounds with S_0< 0.1 mg/mL[55] and K 1:1, obtained from phase-solubility diagrams is frequently used to compare the solubilizing effect of different CDs on a specific drug which is dependent on the composition of the complexation medium (i.e. presence of co-solvents or polymer). A more reliable method for evaluation of CDs and their solubilizing potentials for poorly water soluble compounds is to determine the Complexation Efficiency (*CE*), which is equal to the complex to free CD concentration ratio and can be obtained from the slope of their phase-solubility profile[69].

$$CE = S_0 . K_{1:1} = \frac{[D/CD]}{[CD]} = \frac{slope}{(1\text{-slope})} \qquad (10)$$

The *CE* may remain rather low to solubilise amount of lipophilic drug required for *in vivo* dosing and instead of increasing the amount of CDs, numerous pharmaceutical additives such as polymer, organic solvents, buffer salts, surfactants, preservatives have been investigated to enhance S_0 or/and *K* and subsequently *CE*[69]. One should take into account that although additives (e.g. surfactants, cosolvents) can be successfully used to increase S_0, they also may decrease *K* by competing with the drug for the CD, resulting in less complexation efficiency[69].

Overall, when selecting cyclodextrin complexation as an approach to increase the drug solubility in drug formulation design, solutions with high concentration of CDs (i.e. 20-30% w/w) are often investigated. This high CD concentration can promote aggregates and eventually higher than 1:1 drug-CD complex formation[30, 49, 70-71]. Recently, the

positive effect of CDs on physicochemical properties of drug has been ascribed to nanoparticulate aggregations (i.e. micelles-like structure) in addition to the formation of drug-CD inclusion complexes[31]. Self-aggregation of cyclodextrins (CDs) in water, frequently in the range of several hundred nanometers[31], is an aspect that is still not completely understood and which vary considerably with the type of CD involved[31, 72]. This phenomenon can be characterized by techniques such as Transmission Electron Miscroscopy (TEM), Scanning Electron microscopy (SEM) or Dynamic Light Scattering (DLS) and is also observed when phase-solubility diagram is linear and of $A_{(L)}$-type.

1.2.1.2 Preparation of inclusion complexes.

Several methods have been developed to prepare solid inclusion complexes[32, 73]. including spray-drying, co-precipitation, kneading, solid phase complexation, freeze-drying and recently by supercritical fluids (SCF)[74-76]. Generally, the drug and the CDs are combined in a varying proportion of water according to the method used prior to the solid complex obtention.

1.2.1.3 If drugs bind to cyclodextrins, how is the drug released in vivo?

After oral or parental administration, even the drugs with high range stability constant (i.e. 10^4 M^{-1}) appear to be rapidly and quantitatively released from CD inclusion complexes. Dilution in the biological fluids is the predominant mechanism involved in drug release from the drug-CD complex which continuously forms and dissociates with lifetimes in the range of milliseconds or less. Many others parameters may contribute to availability of the drug for target of interest such as competitive displacement, protein binding, change in ionic strength and temperature, drug uptake by tissues or cyclodextrin renal clearance[50, 77].

1.2.1.4 Cyclodextrins safety considerations.

We will mainly focus on reviewing HPβCD safety data since it has been selected to evaluate the *in vivo* effect of our synthetic cannabinoids on rat pain models. CDs due to their physicochemical properties do not cross biological membranes easily and cause only limited toxicity following oral administration, especially for HPβCD where the main adverse effect observed is diarrhoea[78]. The oral bioavailability of HPβCD in humans, due to passive diffusion, was estimated to be less than 1% following administration of HPβCD in an oral solution of itraconazole[79-80] whereas bioavailability of the guest is improved by increase of water solubility. When drugs are administered by injection CDs have very limited bioavailability and distribute among extracellular compartments on absorption[54]. Following i.v. administration, HPβCD, contained in Sporanox® (Itraconazole), undergoes rapid renal clearance (short half-life of 1 to 2 hours) and demonstrates no accumulation following successive daily doses[81].

Compared to the parent CDs, α- β- and δ-, which have shown renal toxicity, HPβCD and SBEβCD have been extensively studied with regard to their parenteral safety in several animal species and humans[78, 82-83] and are currently used in at least six Food and Drug Administration (FDA)-approved products (four for SBEβCD and two for HPβCD. See Table 4 with commercial products).

The lethal dose 50 (LD50) after single injection of HPβCD to rats has been determined to be 10 g/Kg[44] and no adverse clinical effect has been observed when a dose of 1 g/Kg/day was injected to rats[1, 82]. In addition, HPβCD does not cause irritation due to its low surface tension and is generally regarded as a safe excipient[84]. Based on the toxicity studies available in literature on natural CDs and derivatives, and since our cannabinoid compounds are non ionic, HPβCD had the best balance of enhanced aqueous solubility and capability to form stable complexes with a large range of structurally diverse analogues. In addition, HPBCD are very soluble in water, greater than 500 mg/ml at room temperature compared to 18 mg/ml for βCD and can be incorporated in DDS for clinical applications.

Table 4:[49] Some of the marketed pharmaceutical products that contain cyclodextrins.

Drug/cyclodextrin	Trade name	Formulation	Company (country)
α-Cyclodextrin (αCD)			
Alprostadil	Caverject Dual	Intravenous solution	Pfizer (Europe)
Cefotiam-hexetil HCl	Pansporin T	Tablet	Takeda (Japan)
Limaprost	Opalmon	Tablet	Ono (Japan)
PGE1	Prostavastin	Parenteral solution	Ono (Japan); Schwarz (Europe)
β-Cyclodextrin (βCD)			
Benexate HCl	Ulgut, Lonmiel	Capsule	Teikoku (Japan); Shionogi (Japan)
Cephalosporin	Meiact	Tablet	Meiji Seika (Japan)
Cetirzine	Cetrizin	Chewable tablet	Losan Pharma (Germany)
Chlordiazepoxide	Transillium	Tablet	Gador (Argentina)
Dexamethasone	Glymesason	Ointment, tablet	Fujinaga (Japan)
Dextromethorphan	Rynathisol	Synthelabo (Europe)	
Diphenhydramine and chlortheophylline	Stada-Travel	Chewable tablet	Stada (Europe)
Ethinylestradiol and drospirenone	Yaz	Tablet	Bayer (Europe, USA)
Iodine	Mena-Gargle	Solution	Kyushin (Japan)
Meloxicam	Mobitil	Tablet and suppository	Medical Union (Egypt)
Nicotine	Nicorette	Sublingual tablet	Pfizer (Europe)

Drug/cyclodextrin	Trade name	Formulation	Company (country)
Nimesulide	Nimedex	Tablets	Novartis (Europe)
Nitroglycerin	Nitropen	Sublingual tablet	Nihon Kayaku (Japan)
Omeprazole	Omebeta	Tablet	Betafarm (Europe)
PGE2	Prostarmon E	Sublingual tablet	Ono (Japan)
Piroxicam	Brexin, Flogene, Cicladon	Tablet, suppository	Chiesi (Europe); Aché (Brazil)
Tiaprofenic acid	Surgamyl	Tablet	Roussel-Maestrelli (Europe)
2-Hydroxypropyl-β-cyclodextrin (HPβCD)			
Cisapride	Propulsid	Suppository	Janssen (Europe)
Indometacin	Indocid	Eye drop solution	Chauvin (Europe)
Itraconazole	Sporanox	Oral and intravenous solution	Janssen (Europe, USA)
Mitomycin	MitoExtra, Mitozytrex	Intravenous infusion	Novartis (Europe)
Sulfobutylether β-cyclodextrin sodium salt (SBEβCD)			
Aripiprazole	Abilify	Intramuscular solution	Bristol-Myers Squibb (USA); Otsuka Pharm. (USA)
Maropitant	Cerenia	Parenteral solution	Pfizer Animal Health (USA)
Voriconazole	Vfend	Intravenous solution	Pfizer (USA, Europe, Japan)
Ziprasidone mesylate	Geodon, Zeldox	Intramuscular solution	Pfizer (USA, Europe)
Randomly methylated β-cyclodextrin (RMβCD)			
17*β*-Estradiol	Aerodiol	Nasal spray	Servier (Europe)
Chloramphenicol	Clorocil	Eye drop solution	Oftalder (Europe)

Drug/cyclodextrin	Trade name	Formulation	Company (country)
2-Hydroxypropyl-γ-cyclodextrin (HPγCD)			
Diclofenac sodium salt	Voltaren Ophtha	Eye drop solution	Novartis (Europe)
Tc-99 Teboroxime[a]	CardioTec	Intravenous solution	Bracco (USA)

1.3 Liposomes.

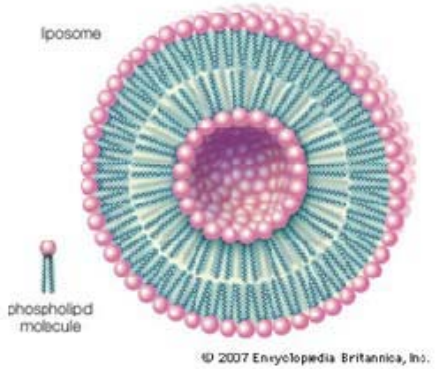

Figure 11: Schematic transversal representation of a liposome.

Liposomes are among the most applied technologies for drug encapsulation and delivery and were the first nanopharmaceuticals introduced in the market for the formulation of Doxorubicin with Doxil® PEGylated liposomal (1995). Liposomes are self-assembled vesicles with a size varying from nanometer to micrometer composed of a central aqueous cavity surrounded by a lipid membrane formed by concentric bilayer(s) (lamellas)[85], mainly composed of natural or synthetic phospholipids such as phosphatidylcholine (PC) or other constituents including cholesterol and/or lipid-conjugated hydrophilic polymer.

These versatile DDS can either encapsulate hydrophilic compounds (in the inner core) or hydrophobic compounds (in the lipid bilayers). Natural and synthetic phospholipids are amphiphilic structures which have the spontaneous ability to arrange as bilayers in an aqueous enviroement as a consequence of the interaction between the polar head group of the phospholipid and water. Many mechanisms have been proposed for the formation of liposomes[86], one of them theorizes the self-closing of a bilayer into a liposome resulting from a competition between two effects, the bending or curvature energy and the edge energy of a bilayer[87]. In hydrophilic environment, there is a high surface tension at the rim of the lamellar sheet. Bending can reduce this energy but implies an energy penalty caused by the induced curvature. A higher curvature is required to minimize the

edge energy and finally a closed sphere will be formed where the edge energy is reduced to zero[88]. Liposomes can be small or large and may be composed from one to several concentric bilayers. With respect to the size and the number of lamellae, liposomes are commonly classified as unilamellar, oligolamellar and multillamelar (Fig. 12 and Table 5)[19].

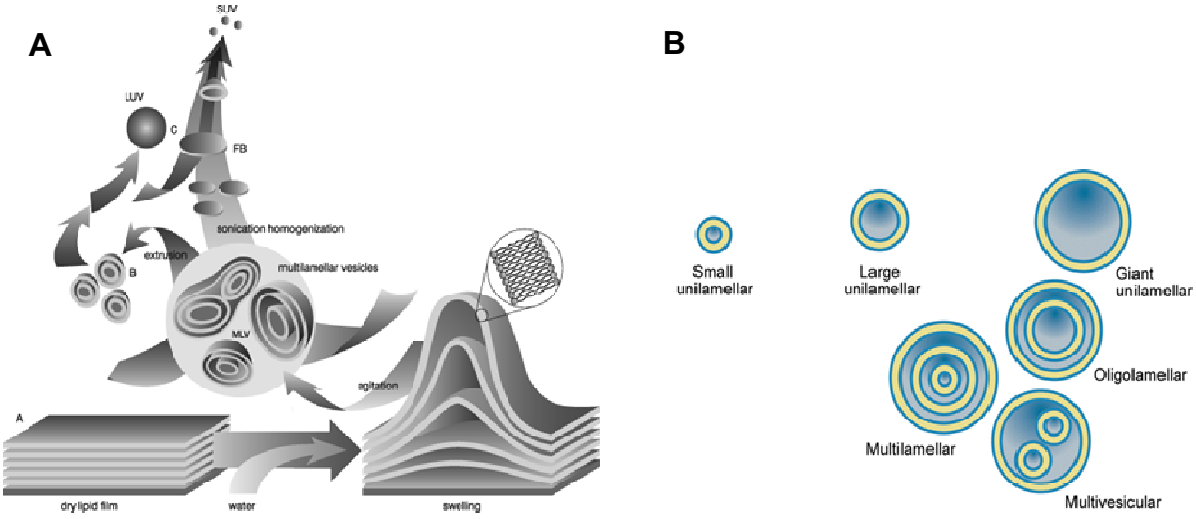

Figure 12: Schematic representation of **A)** Small Unilamellar Vesicles (SUV), Large Unilamellar Vesicles (LUV), Multi Lamellar Vesicles (MLV) formation following thin-film lipid hydration[15] and **B)** the commonly applied liposomes classification[19].

Table 5[86, 89]**:** Classification of liposomes by size and lamellarity.

Vesicle Type	Abbreviation	Diameter Size Range	Number of lipid bilayers
Small unilamellar vesicles	SUV	≈0.02-0.1 μm	One lipid bilayer
Large unilamellar vesicles	LUV	≈0.1-1 μm	One lipid bilayer
Giant unilamellar vesicles	GUV	>1 μm	One lipid bilayer
Multilamellar vesicles	MLV	>0.5 μm	Five to twenty lipid bilayers
Oligolamellar vesicles	OLV	≈0.1-1μm	Approximately five bilayers
Multivesicular vesicles	MMV	>1 μm	Multicompartmental structure

Retention of the encapsulated drug and subsequently its PK profile is affected by the liposomes size, surface charge, phase transition, hydrogen-bonding capacity, membrane rigidifying potential and functional groups of phospholipids[90-91]. Other components may be added such as cholesterol to reduce the bilayer fluidity, increasing stability against enzymatic degradation and thereby decreasing clearance rate[92-93], sometimes associated with sphingomyelin to reduce the membrane permeability and drug release[94-95]. The surface of the liposomes can also be modified by covalent binding of natural (e.g. proteins, polysaccharides, glycolipids, antibodies, enzymes) or synthetic molecules (e.g. PEG) to either achieve drug targeting or enhance blood residency time[17, 85]. As drugs are encapsulated in liposomes, the PK disposition of the liposomal drug is dependent on the liposome until the drug is released from the carrier[91]. Different mechanisms have been proposed for drug delivery upon liposome-cell interaction (Fig. 13)[17].

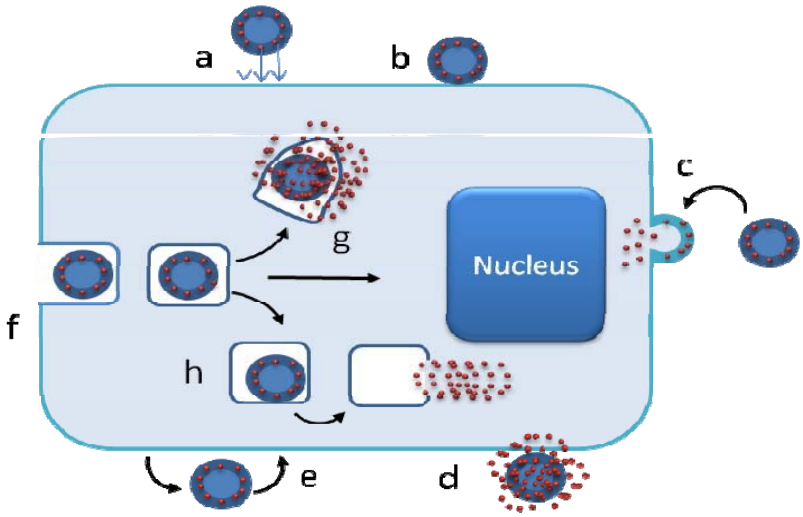

Figure 13[17]: Drug delivery mechanisms suggested upon liposome-cell interaction drug-loaded liposomes can specifically (a) or nonspecifically (b) adsorb onto the cell surface. Liposomes can also fuse with the cell membrane (c), and release their contents into the cell cytoplasm, or can be destabilized by certain cell membrane components when adsorbed on the surface (d) so that the released drug can enter cell via micropinocytosis. Liposome can undergo the direct or transfer-protein-mediated exchange of lipid components with the cell membrane (e) or be subjected to a specific or nonspecific endocytosis (f). In the case of endocytosis, a liposome can be delivered by the endosome into the lysosome (g) or, en route to the lysosome, the liposome can provoke endosome destabilization (h), which results in

Several physicochemical properties have been attributed to these lipidic nanocarriers including permeability of their membrane to different drugs of various polarities, enhancing their solubility and stability, and providing sustained delivery of entrapped drugs through biological membranes. Through encapsulation in liposomes, side effects can be minimized in result of targeting of specific cells, owing reduced off-target and change in the volume of biodistribution of the drug retained in the carrier, reducing the accumulation of otherwise toxic drugs in sensitive organs like heart, kidney, lung and muscle[96]. Conventional liposomes distribute preferentially to organ and tissues involved in the Mononuclear Phagocytic System (MPS) or ReticuloEndothelial System (RES)[17, 97-98] including spleen as well as tumors with impaired microvasculature due to the Enhanced Permeability and Retention (EPR) effect. When the target of interest is extra MPS-tissues/organ, designing coated surface liposomes is a more suitable strategy to enhance blood residency time and vesicles stability (e.g. PEGylated liposomes) and to achieve active targeting (e.g. growth factors, antibodies, proteins)[91]. All these factors have contributed to the increased therapeutic index observed with liposomal formulations of chemotherapeutic agents (e.g. doxorubicin)[90, 99] and triggered numerous pharmaceutical applications for the administration of chemotherapeutic agents, vaccines, radiopharmaceuticals and nucleic-acid based therapeutics (Table 6).

Liposomes can be prepared by various techniques, the most commonly used are thin-film, ultrasonication, detergent depletion, reverse-phase evaporation and ether/ethanol injection methods[100].

Liposome size can then be modified by several techniques such as dehydration-rehydration and freeze-thaw extrusion methods[101]. The liposomes may need to undergo purification procedure (e.g. column filtration, centrifugation) depending on the manufacturing process selected. Numerous analytical methods have been developed to characterize the resulting liposomes in term of size and/or morphology by freeze-fracture electron microscopy and negative staining electron microscopy (i.e. TEM, SEM), and Photon Correlation Spectroscopy (PCS). Lamellarity behaviors analysis by ^{31}P NMR and drug release have also been conducted[102]. For more detail Information on the composition, characterization, and production of liposomes the reader is directed to a review “Liposomes: a practical approach”[103].

Table 6: Some of the marketed liposomal drugs.

Drug	Product name	Indications	Company
Daunorubicin	DaunoXome®	Acute lymphocytic leukemia, acute non lymphocytic leukemia Kaposi's sarcoma	Gilead Scientific
Doxorubicin	Myocet®	Combinational therapy of recurrent breast cancer	Elan
PEG-liposomes Doxorubicin	Doxil® Caelyx®	Refractory Kaposi's sarcoma, ovarian cancer, recurrent breast cancer	Johnson&Johnson Janssen
Amphotericin B	AmBisome®	Fungal infections	Gilead Scientific/ Fujisawa Healthcare
Cytarabine	DepoCyt®	Lymphomatous meningitis	Enzon Pharmaceutiicals Inc.
Amphotericin B	Albecet®	Fungal infections	Enzon Pharmaceutiicals

1.4 Micelles.

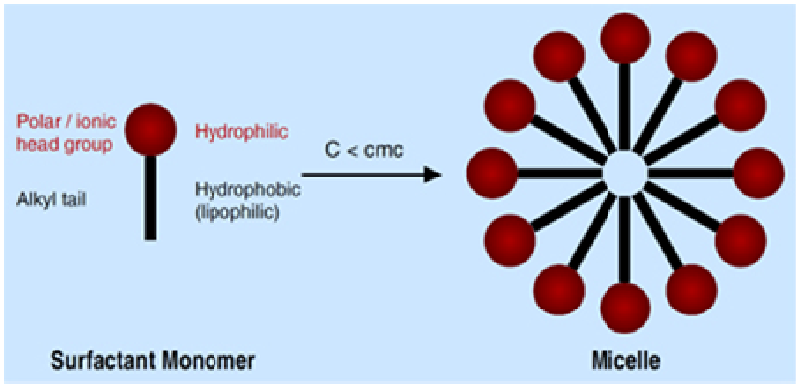

Figure 14[14]: Schematic representation of a monomer surfactant and micelle.

The use of certain micelle-forming amphiphilic compounds in formulations of sparingly soluble pharmaceuticals is a conventional approach especially at the early stage of the drug development to support the *in vitro* and *in vivo* studies. Micelles have many

advantageous characteristics as carriers of hydrophobic drugs including hydrophobic-core-hydrophilic-shell structure allowing water solubilization of poor-soluble drugs, hydrophilic shells minimizing uptake by RES or MPS, size that prevents renal excretion, accumulation of micelle-incorporated drugs in tumors because of the EPR effect[104-107]. Micelles are thermodynamically stable colloidal dispersions (with a particle size ranging normally within 5 to 100 nm) that form spontaneously, under certain concentration and temperature, from amphiphilic molecules or surface active agents (surfactants), molecules of which consist of two distinct regions, an hydrophobic "tail" and an hydrophilic "head", with opposite affinities toward a given solvent such as water[108]. At low concentrations, surfactants exist as monomers in the aqueous solution. As their concentration increase, amphiphilic molecules self-assemble above the so-called critical micelle concentration (CMC) into aggregates of well-defined shapes, such as spherical or cylindrical micelles, usually containing from 60 to 100 surfactants molecules (i.e. aggregation number)[109-111]. This average number of surfactant monomers in each micelle is approximately constant in range up to 100-fold the CMC, with the number of micelles varying[112]. The CMC can be detected as an inflection point when physicochemical properties such as surface tension, conductivity, particle size, fluorescence[113] are plotted as a function of concentration. The formation of micelles is driven by the decrease of free energy and the entropy increase in the system because of the removal of hydrophobic "tails" from the aqueous environment and the loss of the order structure of the water molecules around this region of the molecule. Then, the hydrophilic "heads" are exposed to the solvent and hydrogen bond network in water are re-established[108, 114]. Micelles formed in non aqueous solvent (reverse or inverted micelles) have a core composed of the hydrophilic groups surrounded by a layer composed of the hydrocarbon chains and are usually not of a common pharmaceutical interest since they are hydrophobic. Thermodynamic and structural features of the aggregation process depend on the chemical structure of the surfactant and its concentration, solvent type, presence of salt, pH and temperature[114-116].

Micelles have been characterized on their size, shape, aggregation number, polydispersity, enthalpy using various methods such as PCS, Small Angle Neutron Scattering (SANS), fluorescence quenching, FTIR, calorimetry, NMR[109]. However, micelles do not possess a well-defined structure (i.e. fluid) and no detailed high-resolution picture using TEM or SEM is available[109]. Micelles have been extensively

studied as DDS since lipophilic and poorly soluble drugs can be solubilized within the inner core of assembled hydrophobic “tails” while more polar compounds can be either adsorbed on the micelle surface or distributed along the surfactant molecules in intermediate positions[23]. Besides the increase of drug solubilization and prevention of precipitation through micellization, these nanostructures may improve the stability of labile drugs, reduce the toxicity caused by administration of neat drugs, and decrease the variability of absorption of poorly-soluble drugs[23]. Because of their small size, micelles can gradually and selectively accumulate (passive targeting) in areas such as tumors and infarcts with discontinuous endothelium through EPR effect[108]. Interestingly, some surfactants commonly used in micellar DDS such as Cremophor™ ELP (Polyoxyl-35 Castor Oil) or Tween™ 80 (polysorbate 80) can increase the absorption of drugs by either a direct inhibition of P-glycoprotein-mediated drug efflux[117-119] and/or by interfering with gastrointestinal epithelial membrane to enhance the permeability of drug[120-122]. There are four categories of conventional surfactants, anionic, cationic, zwitterionic and non ionic. Generally, nonionic surfactants have the least toxicity profile with very much lower CMC values and higher aggregation numbers than their ionic counterparts with similar hydrocarbon chains, and thus are the major class of surfactants used in pharmaceutical system through both oral and parenteral routes[123] (Table 7).

Table `7: Some of the marketed surfactant-micelles solutions.

Drug	Product name	Indications	Composition (for 1 mL)	Company
Paclitaxel	Taxol (i.v.)	Breast cancer	527 mg *Cremophor EL,* 49.7% *dehydrated alcohol.* (5-20-fold dilution before administration)	Bristol-Myers Squibb
Teniposide	Vumon (i.v.)	Refractory childhood acute lymphoblastic leukemia	30 mg *benzyl alcohol,* 60 mg *N,N dimethylacetamide,* 500 mg *Cremophor® EL,* 42.7% (v/v) *dehydrated alcohlo,* to be diluted	Bristol-Myers Squibb
Phytomenadione (Vitamin K_1)	Konakion MM (i.m., oral))	Prophylaxis of vitamin K deficiency bleeding (VKDB) in neonates and infants antidote to anticoagulant drugs of the coumarin type	*Glycocholic acid* *Sodium hydroxide* *Lecithin (phospholipon 100)* Hydrochloric acid Water for injection	Roche Products
Docetaxel	Taxotere (i.v.)	Breast, lung, prostate, stomach, and head and neck cancers	*Polysorbate 80* *Éthanol 95* % (v/v) in water (13/87 w/w)	Sanofi Aventis
Darbepoetin alfa	Aranesp® (i.v., s.c.)	Anemia due to chronic kidney desease	0.05 mg *Polysorbate 80* 8.18 mg sodium chloride 0.66 mg sodium phosphate dibasic anhydrous 2.12 mg sodium phosphate monobasic monohydrate Water for Injection	Amgen Inc.
Amprenavir	Agenerase® (oral) solution	Inhibitor of HIV-1 protease	*d-alpha tocopheryl polyethylene glycol 1000 succinate (TPGS)* 170 mg *Polyethylene glycol 400 (PEG 400)* 550 mg *Propylene glycol* Others:saccharin sodium, sodium chloride, sodium citrate (dihydrate), acesulfame potassium, artificial grape bubblegum flavor, citric acid (anhydrous), menthol, natural peppermint flavour.	Glaxo-SmithKline

i.v.: intravenous, i.m. : intramuscular, s.c. : subcutaneous.

From the pharmacological perspective, the lower CMC value of non ionic surfactants is beneficial in improving the physicochemical stability of the drug incorporated micelles. When injected intravenously, the large volume of blood causes dilution of the administered solution and only micelles of surfactants with very low CMC value can exist, while micelles of surfactants with high CMC value may dissociate into monomers and their content may precipitate in the blood[113]. Although well-tolerated, non ionic surfactants are not usually incorporated at concentration above 5-20 % (w/v)[23] in parenteral formulations because of their potential haemolytic activity and/or toxicity profile. In formulation design of sparingly soluble compounds, organic cosolvents are almost always added to micellar solutions to enhance drug solubilization and achieve therapeutic dose. This approach is particularly widespread during the screening of NCE where a library of potential drug candidates needs to be brought into solution to be tested for biological activity. Among the most frequently water-soluble cosolvents evaluated in oral and injectable formulations are propylene glycol, ethanol, polyethylene glycol (i.e.PEG 400), glycerol, N-methyl pyrrolidone (NMP), dimethyl sulfoxide (DMSO) and dimethylacetamide (DMA)[21]. The solubilizing effect of cosolvents can be expressed by the log-linear model established by Yalkowsky[124-125] or by the Jouyban-Acree[126] model. The solubilization capacity by surfactants has been described, in pure water-surfactant systems, by different authors using molar solubilization capacity and the micelle-water partition coefficient[127-128] and in a combination of water-surfactant-cosolvent system[26]. It remains however complicated to predict how cosolvents addition will affect surfactant micelles formation. Addition of cosolvents to the surfactant(s) solution may have a positive effect regarding the drug solubility enhancement while improving the intrinsic solubility of the drug or change in the solution properties (i.e. dielectric constant, surface tension), but may also compete with the drug for the inner core of the micelle or change its physicochemical properties resulting in a decrease in the solubilization capacity of the micelles[129-131]. In our project the solubilization capacity of different cosolvents and surfactant combinations over different cannabinoid compounds has been determined experimentally. The effect of dilution of the micellar preparation on the NCE precipitation was also investigated *in vitro* in order to prevent *in vivo* issues. The PK profile of drug delivered from micelles has been quite extensively studied. The kinetics of association and disassociation of surfactants forming a micelle are usually very rapid. The

characteristic time for the surfactant monomers moving in and out of micelle is typically in the range of 10^{-8} to 10^{-3}s[132]. This brings a practical issue of possible precipitation of solute among dilution of surfactants at a concentration below CMC that could affect drug performance. In the absence of drug carriers, drug molecules mostly enter cells by diffusion out of the micelle and through the cell membrane[133-134]. When micelles remain stable in the systemic circulation, the endocytic pathway is the mechanism suggested for the (polymeric) drug-loaded micelle entering the cell[104, 135] and advantageously bypassing efflux pumps.

1.5 Oral Self-Emulsifying Drug Delivery System (SEDDS).

The efficiency of drug absorption from the gastrointestinal (GI) tract (GIT) is affected by many factors. These include physicochemical factors (e.g., pKa, solubility, stability, lipophilicity, polar surface area, hydrogen bonding, crystalline form and size), physiological factors (e.g., GI pH, blood flow and transit time, gastric emptying, absorption mechanisms), and factors related to the dosage form (e.g., tablet, capsule, solution, suspension, emulsion)[136]. Otherwise complex, Amidon et al.[3] demonstrated that rate and extent of oral drug absorption are strongly influenced and correlated to the drug solubility/dissolution in GIT and permeability through the GIT. The oral absorption of poorly water soluble compounds when presented in the crystalline state to the GIT is typically dissolution rate-limited. Some proposed mechanisms of enhancing oral bioavailability include to increase the dissolution rate and/or to maintain the drug in solution through the GIT in a supersaturated state[137-140]. The rate and extent of absorption of such compounds is then highly dependent on the performance of the formulated product[141-142]. Among many such delivery options, like incorporation of drugs in oils, surfactant dispersion, emulsions and liposomes, one of the most popular approaches are the Self-Emulsifying Drug Delivery Systems (SEDDSs)[143]. The preclinical and clinical usefulness of the SEDDS have gained considerable interest for their ability to increase solubility and oral bioavailability of poorly soluble drugs after the commercial success of Sandimmune® Neoral (Cyclosporin A), Fortovase® (Saquinavir) and Norvir® (Ritonavir)[144]. SEDDSs are isotropic mixtures of naturals or synthetic oils and surfactants, sometimes containing cosolvents, and can be used for the design of

formulations in order to improve the oral absorption of highly lipophilic compounds. SEDDSs emulsify spontaneously to produce fine oil-in-water emulsions or microemulsions when introduced into an aqueous phase (i.e. GI fluids) under gentle agitation[145]. Self-emulsifying formulations spread readily in the GIT, and the digestive motility of the stomach and the intestine provide the agitation necessary for self-emulsification. The spontaneous formation of emulsion advantageously presents the drug in a dissolved form, and the resultant small droplets size provides a large interfacial surface area for the drug absorption. SEDDSs typically produce dispersion with an optically clear-to-turbid appearance depending on the droplet size, generally between 100–300 nm[146]. According to Reiss[147], self-emulsification occurs when the entropy change that favors dispersion is greater than the energy required to increase the surface area of the dispersion. The efficiency of self-emulsification is usually estimated by determining the rate of emulsification and droplet size distribution. Turbidity measurements can be performed to determine the rapid equilibrium reached by the dispersion and the reproducibility of this phenomenon[146, 148]. Additionally, the components used in SEDDS such as surfactants (e.g. Labrasol®, Cremophor ELP, Polysorbate 80) and oils (e.g. Labrafil 1944 CS®, long chain triglycerides) have been reported to improve lipophilic drug oral bioavailability by mechanisms including membrane fluidity to facilitate transcellular absorption, opening tight junction to allow paracellular transport, inhibiting P-gp and/or Cytochrome P450 (CYP450) enzymes to increase intracellular concentration and residence time, stimulating lipoprotein/chylomicron production by lipid and promotion of intestinal lymphatic transport (i.e. reduction of first pass metabolism) or alterations in gastric transit time[149-152, 153].

2 Development of enabling Drug Delivery Systems for the *in vivo* administration of a series of lipophilic synthetic cannabinoids.

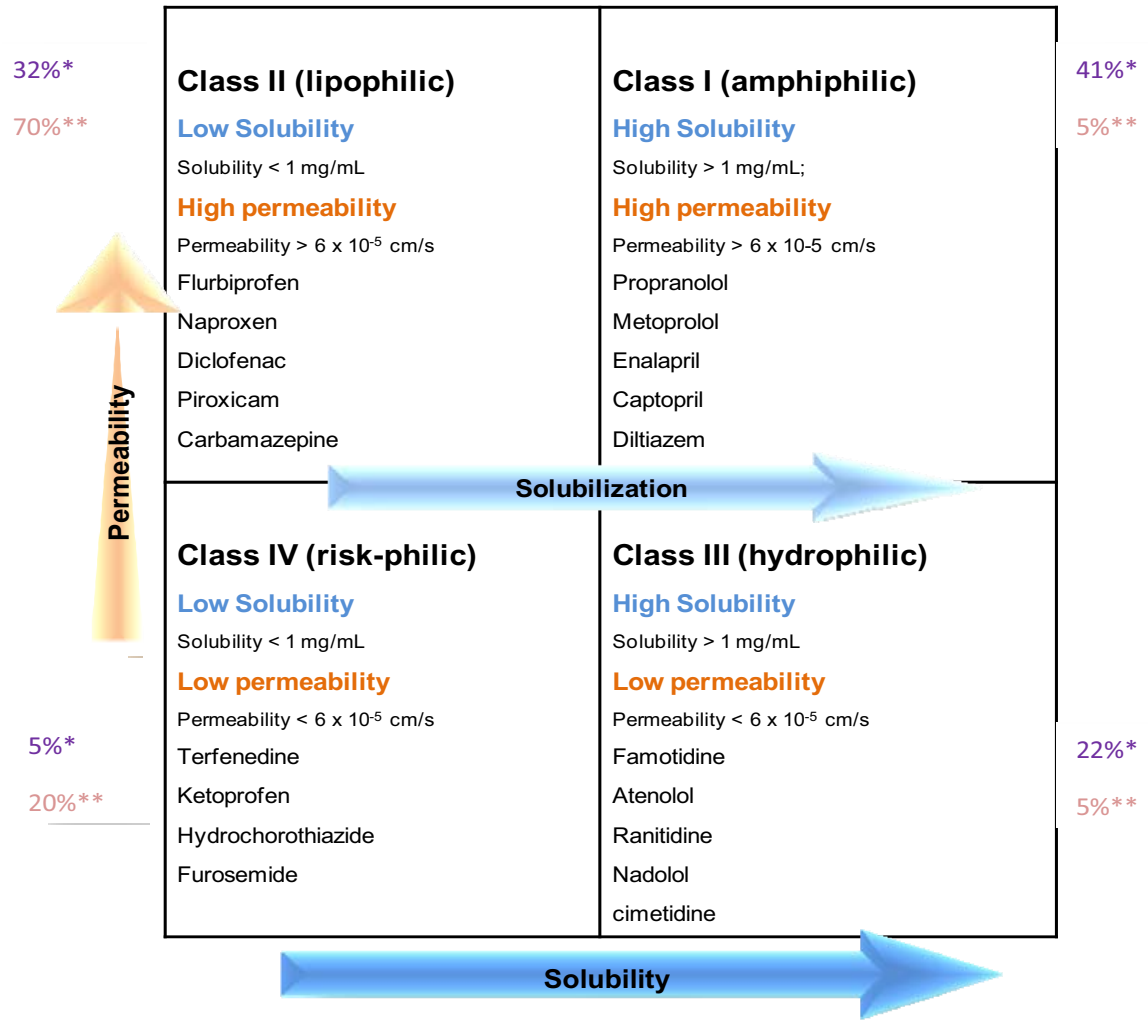

* Marketed drugs
** NCE

Figure 15: Schematic representation of the BCS (adapted from Amidon[3-5]). Solubilization could shift BCS class II drug candidates to class I drug region.

The first aim of this project was to design DDS for parenteral and oral administration of a series of novel synthetic cannabinoids at the early stage of drug discovery. The compounds selected to be tested *in vivo* in PD/PK studies share structural similarities but differ in term of physico-chemical and water solubility properties, selectivity and potency. Paton et al.[154] was one of the first groups of investigators to emphasize the importance of cannabinoid lipophilicity for potentializing its pharmacological activity. The cannabinoids

we synthesized and evaluated for their therapeutic activity are hydrophobic in nature. Solubility plays an essential role in drug disposition, since the maximum rate of passive drug transport across a biological membrane, the main pathway for drug absorption, is the product of permeability and solubility. A Biopharmaceutics Classification System (BCS) provided by the FDA and established by Amidon[3] has been developed to categorize compounds based on their aqueous solubility and gastrointestinal permeability, ascribed to be the most important parameters affecting drug bioavailability[155]. A large number of poorly water-soluble drugs belong to classes II and IV of the BCS and only 8% of the NCE have high permeability and solubility[156].

According to the FDA, in the BCS, a drug substance is considered “highly permeable” when the extent of absorption in humans is determined to be 90% or more of an administered dose, and a drug substance is considered “highly soluble” when the highest dose strength is soluble in 250 mL or less of aqueous media over the pH range of 1–7.5 at 37 °C[157].

Poor solubility has been identified as the cause of numerous drug development failures[158]. The delivery of this poor-water soluble compound has always been challenging for formulators since inadequate aqueous solubility can affect *in vitro* screening assays and the ability to achieve optimum, reproducible and reliable exposure in animals. Various formulation techniques are applied for solubilization of poorly soluble drugs and the selection of a DDS depends on the physicochemical properties and the stability of the drug, the biocompatibility of the vehicle/excipients for a given delivery route and animal species (or the biological system tested) and the frequency of dosage (i.e. acute, chronic). In addition to the ability of enhancing solubilization of drugs, suitable DDS may also alter the physicochemical stability of the drug in the vehicle and in biological fluids (i.e. metabolic stability), the biodistribution and the tolerance of the drug, and deliver the drug at a controlled rate to its site of action. Overall, DDS are used to improve the PK/PD properties of drug with the aim of increasing its therapeutic efficacy.

2.1 MDA7.

The first compound selected for *in vivo* testing was the CB2 selective agonist MDA7 (BCS class II).

2.2 MDA7 physico-chemical properties.

Figure 16: MDA7 chemical structure.

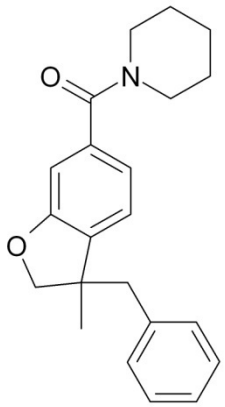

Table 8: MDA7 physicochemical properties calculated *in silico* using ACD PhysChem sofware.

Name	Value
Log P	4.54 +/- 0.37
MW	335.44 $g.mol^{-1}$
PSA	29.54 $Å^3$
FRB	3
HDonors	0
HAcceptors	3
Violation of Rule of 5	0

Log P: partition coefficient, MW: molecular weight, PSA: polar surface area, FRB: free rotatable bounds, HDonors: hydrogen donors, HAcceptors: hydrogen acceptors.

Solubility in Pure water at pH=7: 5.69 10^{-3} mg/mL

MDA7 purity was determined by LCUV-MS and >99.0% based on the ratio of peak area at 7.03 minutes retention time and the structure and purity confirmed by NMR.

2.3 *In vitro* characterization of MDA7[159].

In the competitive binding assays performed in membranes of CHO-K1 cells selectively expressing the human CB2 receptor, MDA7 potently displaced the ligand [^{3}H]CP55,940 from human receptors (Table 9).

In the competitive binding assays performed in membranes of CHO-K1 cells selectively expressing human CB1 receptors, MDA7 (up to 3 μM) did not demonstrate detectable radioligand displacement (Table 9). Corresponding K_i values at CHO-K1 cells selectively expressing the rat CB1 and CB2 receptors were about 10-fold higher for the CB1 than for the CB2 receptor (Table 9).

Table 9: Radioligand competitive binding assays.

Ligand	Mean K_i (nM)			
	Human CB_1	**Human CB_2**	**Rat CB_1**	**Rat CB_2**
MDA7	>10,000	422±123	2565±695	238±143
CP55,940	3.4	1.8±1.1	ND	1.1±0.02
AM251	ND	ND	0.58±0.06	ND

Abbreviations: CB_1, cannabinoid receptor type 1; CB_2, cannabinoid receptor type 2; ND, not determined.

In GTPγ[^{35}S] functional assays, MDA7 gave measurable EC_{50} values (Table 10) at human and rat CB2 receptors, but was without any activity at human or rat CB1 receptors, up to 1 μM.

Table 10: GTPγ[^{35}S] functional assays .

Ligands	Agonist EC_{50} (nM) (mean±s.e. mean) relative to CP55,940 (%)			
	GTPγ[^{35}S] functional assays		GTPγ[^{35}S] functional assays	
	Human CB_1	Human CB_2	Rat CB_1	Rat CB_2
MDA7	NA	128±32	NA	67.4±4.9
CP55,940	9±1.3	6.5±2.1		

Abbreviations: CB_1, cannabinoid receptor type 1; CB_2, cannabinoid receptor type 2; NA, not active at 1 μM.

Weak CB1 partial agonist activity was detected at a concentration of more than 1 μM (Fig. 17). MDA7 showed good affinity and excellent selectivity for CB_2 receptors and low affinity and efficacy at CB_1 receptors. In this study, MDA7 exhibited specificity for human CB2 receptors, indeed CB1 receptor mediated functional activity for MDA7 was so low that we were not able to calculate the crorresponding EC_{50} for MDA7 at human CB1 receptors.

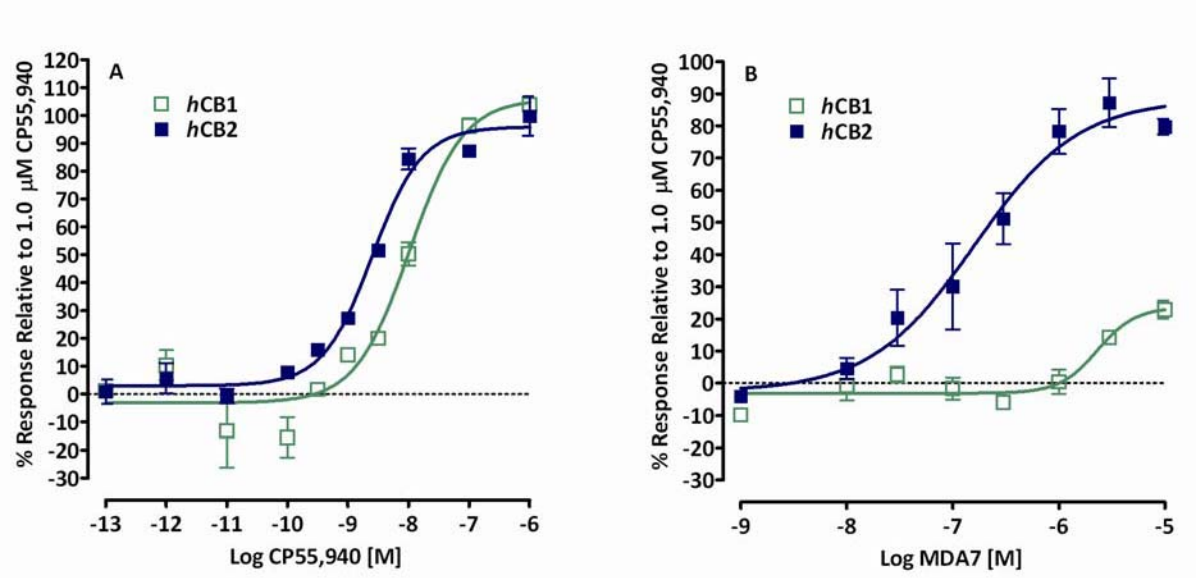

Figure 17: Characterization of CP55,940 **a)** and MDA7 **b)** in recombinant human cannabinoid types 1 and 2 (CB_1 and CB_2) (hCB1 and hCB2) GTPγ[^{35}S] assay systems. The levels of receptor activation were calculated and were expressed as a percentage relative to the response to 1.0 µM CP55,940.

2.4 Enabling Drug Delivery System design and development.

The aim of this project was to develop enabling DDS for the *in vivo* administration of MDA7 to rats (average weight: 150g-350g) to assess its pharmacological efficacy in three models of neuropathic pain and its PK profile in rats. The requirements for these pre-clinical studies were different in terms of the dose of MDA7 to administer ranging from 5 mg/Kg to 30 mg/Kg, route of administration: intraperitoneal (i.p.) and intravenous (i.v.) for the activity/efficacy pharmacological studies and oral versus i.v. for the PK study, and finally the frequency of dosing: single injection versus chronic injection over a period up to 14 days. Developing a DDS able to be administered both orally and parenterally for lipophilic drugs, ensuring reproducible animal exposure, remained a challenge as enhancement of solubility and minimization of chemical degradation in both the DDS and biological fluids (i.e. plasma, GI) needed to be addressed. We have developed and compared the therapeutic benefit of a same dose of MDA7 (10 mg/Kg) formulated in three different DDS for parenteral administration namely, micellar solution, inclusion

complexes and liposomes. A PK study was also conducted with the micellar solution after i.v. administration and compared to SEDDS after oral administration. In order to bypass potential issues of inconsistent drug absorption related to solubility (i.e. non-ideal NCE: variable crystallinity and purity) and limited dissolution rate, preformulation and early formulation studies were conducted with dissolved NCE.

2.4.1 Preformulation studies.

Before the formulation of a drug substance into a dosage form, it must be chemically and physically characterized. Preformulation studies supply the information needed to define the physicochemical properties of the drug substance, its solubility and stability in selected and compendial solvents. This information is then used as the framework for the drug's combination with pharmaceutical ingredients in the design of DDS.

2.4.1.1 MDA7 kinetic solubility and stability in pure excipients.

Kinetic solubility provides useful information even though it is not as robust as thermodynamic solubility (i.e. equilibrium solubility). The measurement is rapid (e.g. a few hours), involves no use of high performance liquid chromatography (HPLC) or other instrumentation and provides much-needed solubility data in a variety of solvents/excipients and vehicles with small amount of drug. Kinetic solubility can be broadly used in developing formulations containing cosolvents, surfactants, cyclodextrins, lipids, and polymer. The kinetic solubility of MDA7 was studied following a detailed procedure described by Li et al.[22] in hydrophilic, amphiphilic and lipophilic excipients for the selection of a suitable enabling formulation (Table 11). The solubility of the drug was assessed by serial addition of a known amount of solvent to a known amount of drug.

Table 11: MDA7 kinetic solubility in various solvents/excipients at 25°C.

Solvents/Excipients INCI Name	**MDA7 Solubility (w / w)**	
	mg MDA7/**g** Excipient	**mg** MDA7/**100mg** Excipient (%)
Propylene glycol (PG)	<10.1	<1.0
Ethanol 95% (EtOH)	68.0<S<152.7	6.8<S<15.2
Polyethylene Glycol 400 (PEG 400)	11.6<S<17.9	1.2<S<1.8
Dimethylsulfoxide (DMSO)	>166.6	>17.0
N-Methyl-2-pyrrolidone (NMP)	>197.6	> 19.8
PEG-8 capric/caprylic triglycerides (Labrasol®)	<9.9	< 0.9
Macrogol 15-hydroxystearate (Solutol® HS 15)	12.3<S <19.2	1.2<S< 1.9

S: solubility

Solubilization was observed visually. Degradation of MDA7 in the different solvents was monitored using Thin Layer Chromatography (TLC) by comparing the Retention Factors (R_f) at specific time *t* and at initial time ($t = 0$). MDA7 R_f is of 0.509 in a solvent mixture Ethyl acetate-heptane (30/70).

Table 12: MDA7 chemical stability in various excipients/solvents stored at 25°C determined by TLC.

Solvents/Excipients INCI Name	**MDA7 stability**		
	t 24H	*t* 1 week	*t 3 months*
Ethanol (EtOH)	Stable	Stable	Stable
Dimethylsulfoxide (DMSO)	Stable	Stable	ND
N-Methyl-2-pyrrolidone (NMP)	Stable	Stable	Stable
PEG-8 capric/caprylic triglycerides (Labrasol®)	Stable	ND	ND
Macrogol 15-hydroxystearate (Solutol® HS 15)	Unstable (2 spots)	ND	ND

ND, not done

The solvents/excipients ranked in order of decreasing solubilization capacity for MDA7 were NMP>DMSO>EtOH>Solutol® HS15≈ PEG400>Labrasol®≈PG. MDA7 chemical stability was evaluated in the three most relevant solvents i.e. NMP, DMSO and EtOH as well as the two amphiphilic agents susceptible to form micelles i.e. Labrasol and Solutol® HS 15. MDA7 chemical stability was satisfactory in all the excipients evaluated except the Solutol® HS 15 which led to MDA7 degradation as fast as 24h after preparation of the solution (2 spots on the TLC plate, R_f of 0.466 and R_f of 0.416).

2.4.2 MDA7 enabling DDS design and development

MDA7 is a preclinical lead. The doses selected to be tested in rats in pre-clinical studies ranged from 5 mg/Kg to 30 mg/Kg. However, the age of the animal and the corresponding weight varied in the different studies. According to our own experience, the volume administered i.v., i.p., oral, to rats should be lower than 1.66 mL/Kg (e.g. 250µL for 150g rat) of the animal to prevent any animal discomfort. Ideally, the dosing formulation should afford concentration of MDA7 up to 18 mg/mL. Since MDA7 solubility was lower than 1% (w/w) or <10 mg/ml in water, it was necessary to further evaluate

solubility in pharmaceutical excipients and vehicles[22] to design a suitable formulation for *in vivo* testing.

2.4.2.1 i.v./ i.p. cosolvents-surfactant micelles solution.

2.4.2.1.1 Design and development.

According to the results shown in Table 11, the cosolvents approach was seemingly promising since about approximately 10% (w/w) or 166 mg/Kg (e.g. 250µL for 150g rat) of the major excipient, NMP or DMSO, would allow solubilizing 18 mg/mL of MDA7, with EtOH possibly used as a cosolvent. This dose of excipient (i.e. NMP or DMSO) is acceptable in term of tolerability (see Table 13). Indeed 166 mg/Kg of NMP represents 15-fold safety factor compared to its LD_{50} reported to be of 2.4 g/Kg, and more than 30-fold safety factor for DMSO compared to its LD_{50} of 5.2 g/Kg. Animals tolerate single administration of high concentration of cosolvents but it is recommended to keep this concentration lower than 60% (w/w) in the dosing solution[160].

Should we have to increase the dose of MDA7 to support toxicological studies and subsequently the solubilizing agent, we didn't select DMSO first since a solution of higher than 15% (w/v) DMSO injected to rats in a volume of 5 mL/kg showed behavior or neurotoxical effects[161] and putative analgesic properties[162]. NMP was selected as the main excipient based on the good solubility of MDA7. PEG400 and PG were used as cosolvent to decrease a potential toxic effect induced by NMP.

Addition of surfactants and cosurfactant was then evaluated for the use in the cosolvent(s) formulation in order to form micelles resulting in a decrease of potential *in vivo* drug precipitation. The *in vitro* static serial dilution method described by Ping Li et al.[22] was used as a guiding tool for the screening process and select DDS showing the best potential to prevent drug crystallization. The rate and extent of NCE precipitation can vary, both of which are important indicators in predicting potential drug precipitation *in vivo* upon injection. If the precipitation is not to occur within a short time period (e.g. a few minutes), the formulation is considered less likely to precipitate *in vivo* due to rapid physiological dilution by blood flow.

Table 13: Review of data available in literature regarding median lethal dose (LD_{50}) and tolerated use level of some excipients used in MDA7 DDS development, determined upon administration to rats.

Excipients INCI Name	**DL_{50} g/Kg**			**Ref.**	**Maximum tolerated use level (study period)[1-2] g/Kg**		
	Oral	*i.v.*	*i.p.*		*Oral*	*i.v.*	i.p.
Ethanol (EtOH)	3.6-13.7	0.96-1.15	3.8	6-8	10 (1 week)	-	-
Dimethylsulfoxide (DMSO)	14.5	5.2-8.1	8.2	1, 11-12	5	0.2	5
N-Methyl-2-pyrrolidone (NMP)	4.2	2.4	2.4	9-11			
Polyethylene Glycol (PEG400)	-	7.3	-	8, 11	5	0.5	5
Propylene Glycol (PG)	20	-	-	8	2.5	-	-
PEG-8 capric/caprylic triglycerides (Labrasol®)	22	-	-	1, 8	3 (6 months)	0.01	
Hydroxypropyl-β-cyclodextrin (HPβCD)	18.8	-	0.33	8	10 (10 doses)	10 (1 month)	-
Polysorbate 80 (P80)	34.5	-	-	8	5	0.1	-
Polyoxyl 35 hydrogenated castor oil (Cremophor™ ELP)	6.4	-	-	8	0.1	-	-
Macrogol 15-hydroxystearate (Solutol® HS 15)	>0.02	-	-		-	-	-

i.v.: intravenous, i.p.: intraperitoneal, Ref: references.

Li et al. had compared the *in vitro* static serial dilution with other *in vitro* precipitation methods (i.e. dynamic injection method, dropwise addition method) and it is the most effective in quantifying the amount of precipitation and more descriptive of the formation and dissolution of the precipitate methods[163].

To begin the DDS design, we arbitrary fixed the maximum concentration of the major solubilizing agent to 40% w/w or 400 mg/mL for safety concern. This amount of NMP enabled to solubilize MDA7 in concentration up to 11.3 mg/mL but as expected with a lipophilic compound, even a concentration of MDA7 at 6 mg/mL triggered a massive crystallization upon dilution with Phosphate Buffer Saline (PBS) (entries A, B in Table 14). Nevertheless NMP was the best solubilizing agent and this system was identified for further testing with surfactants. Use of surfactant can induce formation of micelles containing MDA7 solubilized in the excipients resulting in increased water solubility. P80 one of the most commonly used surfactant for parenteral pharmaceuticals (Table 7), was the first evaluated (entries C, D, E in Table 14) in the above system but concentration up to 100 mg/mL did not prevent MDA7 crystallization. A cosolvent, PEG400 was then added for potential synergistic interactions with NMP to increase drug solubility and decrease excipient-related toxicity. Amount of cosolvents (NMP/PEG400) was then increased to 60% (w/w) or 600 mg/mL, affording solubilization up to 25 mg/mL of MDA7 (entries G, H in Table 14). No precipitation of the drug was observed (microscopic observation: no crystal) in DDS containing P80 but the solution was opalescent due to a poor cosolvents miscibility (the vehicle was opalescent even without MDA7 incorporated: data not shown). We then evaluated, another widely used surfactant (Table 7), Cremophor™ ELP (CrELP) since it had a better solubilization capacity with a lower CMC value (0.032mM) compared to P80 (0.05mM)[164] (entry I Table 14). Only slight improvement was observed about keeping MDA7 into solution. PG was then evaluated as a cosolvent, even though it showed a poor solubilizing capacity as a pure excipient, it had a better miscibility with NMP. The system NMP/PG/CrELP (25%/25%/10% w/w) led to a transparent solution physically stable (t=48h), longer than over the study period (i.e. few hours), with MDA7 being “less likely to precipitate” according to *in vitro* testing for drug precipitation (entry J in Table 14). Increasing MDA7 dose in the previous DDS (entries K, L in Table 14) provided limited physical stability with crystallization occurring 1h and 3h after preparation. MDA7 showed a good solubility in pure EtOH. However, EtOH cannot be used at high concentration because of toxicity and potential neurological

effects. EtOH was evaluated as a cosolvent/cosurfactant on the MDA7 solubilization and stabilization in the DDS developed (NMP/PG/CrELP/EtOH: 25%/25%/10%/10% w/w). EtOH is considered as a cosurfactant since it can intercalate in between the surfactant hydrophilic moieties at the surface of the micelles. EtOH afforded a clear solution containing MDA7 at concentration of 18 mg/mL (entry M in Table 14) physically stable for more than 1 month (microscopic observation: no crystal), "unlikely to precipitate" upon administration to animals according to *in vitro* serial dilution results. After >10 rounds of testing using different cosolvents, surfactants, and different concentrations, the final composition (entry N in Table 14), in the formulation selected for *in vivo* studies (i.e. pharmacological and PK, see section 2.5) was 30% NMP+ 30%PG + 10% CrELP + 10% EtOH in quantum satis (QS) 100% PBS (w/w). This vehicle allows MDA7 to be administered at doses up to 30 mg/Kg (e.g. 250µL for 150g rat) that did not precipitate upon mixing with PBS containing 1% (w/v) Bovine Serum Albumin (BSA), the buffer mimicking blood physiological dilution in the *in vitro* serial dilution model. The pH of the formulation is 7.4. The chemical stability of the final enabling DDS was determined by LC-MS (Table 15) and by ^{1}H-NMR (Table 16). MDA7 formulated in the former system is physically (no crystallization, Table 14) and chemically (no degradation, Tables 15 and 16) stable stored at room temperature, for at least 1 month. Entries J and M in Table 14 were also compliant with the specifications since no crystallization of the drug in the vehicle at least for 1H after preparation and in the *in vitro* serial dilution testing, was observed. However, we decided to select one versatile DDS enabling the administration of a series of structurally diverse synthetic cannabinoids (i.e. MDA19[165], MDA42 Compound 19 in[166] *in vivo* to obviate any "vehicle effect". Indeed, animal systemic exposure can be erratically affected by the solvents and DDS used[167] and can pose significant problems for the liquid chromatography/tandem mass spectrometric (LC/MS/MS) analysis of incurred samples[168].

Table 14: MDA7 i.v./i.p. cosolvent/surfactant micelles DDS design and development summary.

Entry	A	B	C	D	E	F	G	H	I	J	K	L	M	N
Dose*(mg/Kg)	15	10	10	10	10	10	10	10	10	15	30	15	15	30
Volume**(µL)	200	250	250	250	250	250	250	100	250	250	250	250	250	250
Weight# (g)	150	150	150	150	150	150	150	250	150	250	250	300	300	150
Ingredients	**Amount mg/mL**													
MDA7	11.3	6	6	6	6	6	6	25	6	15	30	18	18	18
NMP	400	400	400	400		300	300	300		250	250	250	250	300
PEG400						400	400	400						
PG										250	250	250	250	300
EtOH													100	100
P80			30	100	100		100	100						
CrELP									100	100	100	100	100	100
PBS qs. 1 mL	588.7	594	564	494	894	294	194	175	894	385	370	382	282	182
Macroscopic appearance	Cryst.	Cryst.	Cryst.	Cryst.	Cryst.	Cryst.	Opal.	Opal.	Troub.	Trans.	Trans.	Trans.	Trans.	Trans.
Microscopic appearance	NA	NA	NA	NA	Cryst.	NA	No Cryst.	No Cryst.	Cryst.	ND	NA	NA	No Cryst. t=1 mth	No Cryst. t=1 mth
***In vitro* serial dilution**	NA	NA	NA	NA	NA	NA	ND	ND	NA	Trans. 10 tub. >5 min.	ND	Troub. <5 min.	Trans. 10 tub. >10 min	Trans. 10 tub. >10 min
Physical stability	NA	NA	NA	NA	NA	NA	ND	ND	ND	Cryst. t=48H	Troub. t=1H	Troub. t=3H	Trans. t=1 mth.	Trans. t=1 mth

* Dose to be administered to rat, ** volume to be administered to rat, # rat weight, NMP: N-methyl-2-pyrrolidone, PEG400: Polyethylene Glycol, PG: propylene Glycol, EtOH; Ethanol 95%, P80: Polysorbate 80, CrELP; Cremophor^{TM} ELP, PBS: Phosphate Buffer Saline, Cryst.: Crystals, Opal.:Opalescent, Troub.: Trouble, Trans.:Transparent, NA: Not Applied, ND: Not Done, tub.: tubes.

2.4.2.1.2 Characterization.

2.4.2.1.2.1 Physical stability.

The stabilities of formula M and N tested in the *in vivo* models (section 2.5) were followed over 1 month and no macroscopic or microscopic crystallization of MDA7 was observed. *In vitro* static serial dilution testing do not show any precipitation of the drug even after dilution of the DDS up to 1024-folds. This is well above the dilution ratio the drug would undergo *in vivo*. Since the total blood volume is 64 mL/Kg for rats[169], i.v. injection of 250 µL to a rat (250g) would lead to a dilution ratio about 1:100. Entries M and N were likely to prevent forming crystals which could produce severe pain and phlebitis, as well as altering bioavailability[163].

2.4.2.1.2.2 Dynamic Light Scattering (DLS).

Dynamic light Scattering (DLS) also referred to as Photon Correlation Spectroscopy (PCS) or Quasi-Elastic Light Scattering (QELS), is a non-invasive technique used for measuring the size of sub micron particles by measuring fluctuations in intensity due to particles in suspension undergoing Brownian motion. Brownian motion is the random movement of particles induced by the bombardment by solvent molecules that themselves are moving due to their thermal energy (Figure 18A). If the particles or molecules are illuminated with a monochromatic light beam such as a laser, the intensity ***I*** of the scattered light fluctuates at a rate that is dependent upon the size of the particles, namely, smaller particles move more rapidly (Figure 18B). By analyzing the time dependence of these intensity fluctuations of the scattered light and computing (Malvern DTS Nano ZS software) the intensity correlation function $g^2(t)$, the translational diffusion coefficient ***D*** of the particle can be determined. The second order correlation function is given by the following equation[13],

$$g^{(2)}(\tau) = \frac{[I(t)\, I\,(t+\tau)]}{[I(t)]^{2}}$$

where ***I(t)*** is the intensity of the scattered light at time ***t***, and the brackets indicate averaging over all ***t*** where ***τ*** is the delay time . The correlation function depends on the delay ***t***, that is, the amount that a duplicate intensity trace is shifted from the original before the averaging is performed. A typical correlation function for a monodisperse sample is shown in (Figure 18C).

The correlation function for a monodisperse sample can be analyzed by the equation:

$$g^{(2)}(\tau) = B + \beta \exp(-2\,\Gamma\,\tau)$$

where ***B*** is the baseline of the correlation function at infinite delay, ***β*** is the correlation function amplitude at zero delay, and ***Γ*** is the decay rate.

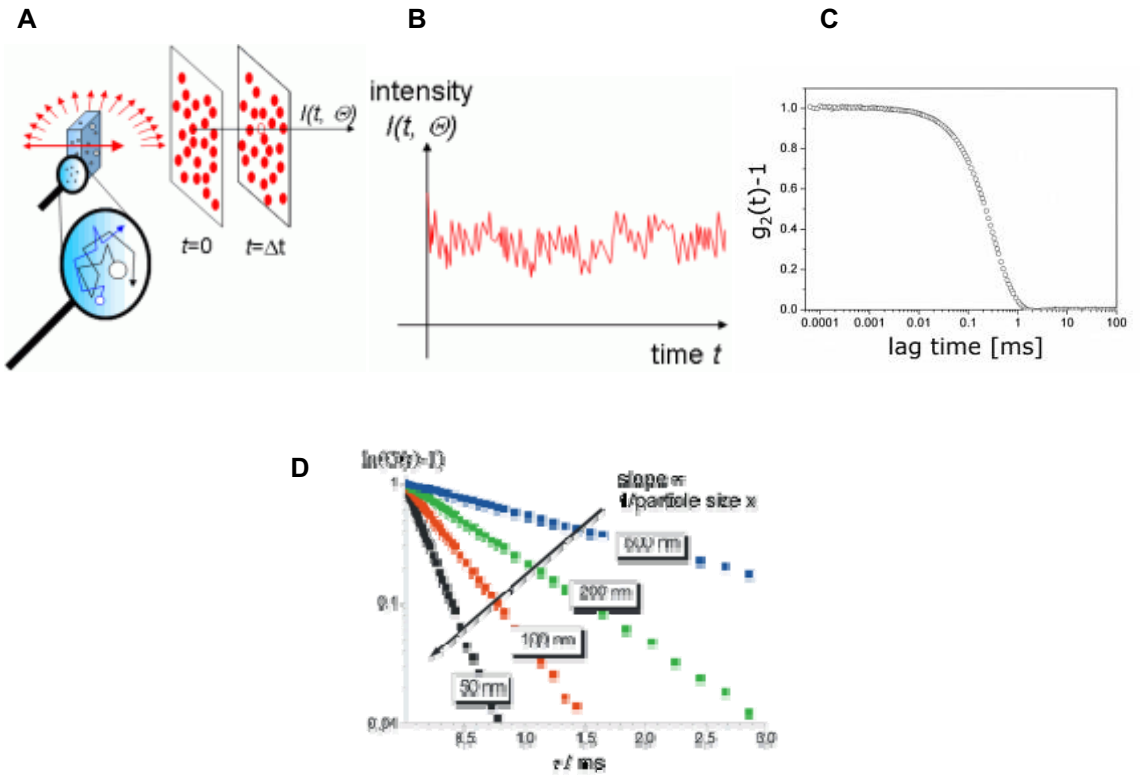

Figure 18: DLS measurement principle[13].
A) The Brownian motion results from impacts of the thermal movement of the molecules of the suspending fluid on the particles. **B)** The intensity in the diffraction pattern observed under a scattering angle Θ fluctuates with time ***t***. **C)** Correlation function ***g2(t)*** of intensity fluctuations in function of time. **D)** As the near-order of fine particles dissolves faster than the near-order of coarse particles, the particle size can be deducted e. g. from the slope of the auto-correlation function G (with known viscosity ***η*** and temperature ***T***).

A nonlinear least squares fitting algorithm can be used to fit the measured correlation function to the previous equation to retrieve the correlation function decay rate ***Γ***. From this point, ***Γ*** can be converted to the diffusion constant ***D*** for the particle via the relation:

$$D = \frac{\Gamma}{q^2}$$

Here, ***q*** is the magnitude of the scattering vector, and is given by,

$$q = \frac{4 \pi n_0}{\lambda_0} \sin(\theta/2)$$

where n_0 is the solvent index of refraction, λ_0 is the vacuum laser wavelength of the incident light, and θ is the scattering angle.
The diffusion coefficient D is then related to the hydrodynamic radius R for a spherical particle by means of the Stokes-Einstein equation in (Figure 18D).

$$D = \frac{k\,T}{6\,\pi\,R\,\eta}$$

where R is the hydrodynamic diameter, D is the translational diffusion coefficient, K is Boltzmann's constant, T is thermodynamic temperature, η is dynamic viscosity.
An accurately known and constant temperature is necessary since knowledge of the viscosity η of the suspending fluid for the estimation of the average particle size and its distribution function (and for volume fractions the refractive index n) is required. For a given particle the lower the solvent viscosity (or the temperature higher), the greater the Brownian motion will be.
PCS yields the mean diameter of the bulk population (*z*-average, measuring range: 3 nm – 10 µm) and a polydispersity index (PDI) as measure for the width of the size distribution. The PI ranges from zero (monodisperse particles) to 0.5 (broad distribution), values above 0.5 do not allow allocation of a logarithmic normal distribution to the PI.
The average mean diameter of the micelles bulk population formed in the cosolvents/surfactant DDS entry N in Table 14 was assessed using a Malvern Nano ZS. Monodisperse micelles exhibited an average size of 15 nm (PDI 0.11).

2.4.2.1.2.3 MDA7 chemical stability by ^{1}H-NMR

Lin et al.[170] have described a simple and reliable ^{1}H-NMR-based method for determining a suitable formulation (i.e. drug solubility, stability) for discovery compounds in support of early *in vivo* studies. NMR is a powerful technique for solution sample analysis. It provides detailed information of each component in the solution and can also be used for quantitative analysis. Quantitation can be carried out using an external standard without a calibration curve, which makes using NMR for quantitation convenient and provides a time saving over the HPLC-UV method. In this study, Maleic Acid (MA) was used as the

external standard. The two germinal protons of the MA are observed as a singlet at δ 6.26 ppm[171] in D_2O. MA was selected since it does not show overlaps with the aromatic protons of the drug studied (e.g. MDA7) but the signal at 6.40 ppm is relatively close to the signal of aromatic protons to reduce any effects resulting from baseline deviation. MA is non volatile and can be prepared in bulk D_2O facilitating the process. In order to avoid any contamination of the analyte by the chosen standard, we placed a 0.16 M solution of MA in a capillary filled with the dissolved MA in D_2O inside the analyte NMR tube[172]. Since the NMR method is non-destructive, samples can be reanalyzed over time to yield information on the chemical stability of the compound in any formulation. The analyte was dissolved in the same solvent, D_2O, when formulated.

The assay of the analyte $\boldsymbol{P_d}$ was calculated directly from the NMR standard of known assay $\boldsymbol{P_{std}}$:

$$P_d = I_d/I_{std} * N_{std}/N_d * M_d/M_{std} * m_{std}/m * P_{std}$$

Where $\boldsymbol{M_d}$ and $\boldsymbol{M_{std}}$ are the molar mass of respectively the analyte and standard, $\boldsymbol{m}$ and $\boldsymbol{m_{std}}$ are the weights of the sample and standard, $\boldsymbol{P_d}$ and $\boldsymbol{P_{std}}$ the assays of analyte and standard respectively, $\boldsymbol{I_d}$ and $\boldsymbol{I_{std}}$ are the integrated signal of analyte and standard[173].

MDA7 formulated in the cosolvents/surfactant micelles DDS (Batch#1 in Table 15) was chemically stable stored at room temperature for 1 month (≈100% of the initial amount of MDA7 was recovered) as determined by NMR.

Table 15: MDA7 chemical stability assessed by ^{1}H-NMR.

Entry N	**MDA7 concentration mg/mL / % recovery (w/w)**		
Batch#1	*Nominal amount*	t_{initial}	$t_{\text{1 month}}$
	11.6	11.4	12.5 / 109.4

% recovery = ([MDA7]t_{1month} / [MDA7]$t_{initial}$) 100*

2.4.2.1.2.4 MDA7 chemical stability by UPLC-MS.

A different batch of the entry N manufactured to supply the PK study and assayed by UPLC-MS after storage at room temperature for 15 days confirmed the chemical stability

of MDA7 in entry N aqueous micellar system (97.3% of the initial amount of MDA7 was recovered) (Batch#2 in Table 16).

Table 16: MDA7 chemical stability assessed by UPLC-MS.

Entry N	**MDA7 concentration mg/mL / % recovery (w/w)**		
Batch#2	*Nominal amount*	$t_{initial}$	$t_{15\ days}$
	11.2	11.3	11 / 97.3

% recovery = ([MDA7]t_{15days} / [MDA7]$t_{initial}$) 100*

2.4.2.2 Oral Self-Emulsifying Drug Delivery System (SEDDS).

The absolute bioavailability of MDA7 (15mg/Kg) was determined in a PK study to obtain a plasma drug concentration versus time plot, for the drug after both intravenous (i.v.) and extravascular (non-intravenous, i.e. oral) administration, in rats. Compared to aqueous solutions (e.g. surfactants-based micellar solution), lipid based formulations such as SEDDS offer a potential platform for improving solubility and oral bioavailability of drugs especially those belonging to the BCS class II, poorly water soluble and with a high permeability coefficient (P_{app} >1× 10^{-6}cm/s)[174] such as MDA7. The objective of the present investigation was to design a SEDDS for MDA7 and to evaluate its potential to enable sufficient drug loading and oral bioavailability. The physical stability of MDA7 in the developed SEDDS has been investigated by macroscopic and microscopic observation. The rate and the capacity of self-emulsification have also been evaluated by *in vitro* testing. The SEDDS droplets size was measured using PCS. MDA7 chemical stability was assessed by UPLC-MS over 4 days to cover the time of the study (from dosing DDS preparation to *in vivo* administration).

2.4.2.2.1 Design and development.

In addition to the advantages mentioned above, an anhydrous system such as SEDDS would prevent crystallization of MDA7 in the DDS, increasing its physical stability over time. The system Labrasol®/Labrafil® 1944 CS has been safely used by Delongeas et

al.[175] as a non clinical vehicle for poorly water soluble compounds for 4-weeks oral toxicity study in rats. This same system in a ratio of 65% v/v Labrasol, 25% v/v Labrafil M 1944 CS has been successfully described by Balakrishnan et al.[149] for improving the oral bioavailability of the lipophilic Coenzyme Q10. Labrasol® (PEG-8 Caprylic/Capric Glycerides) and Labrafil® (Apricot Kernel oil PEG-6 esters) are used respectively as solubilizer and surfactant, Labrasol® playing an additional role of absorption promoter. According to the solubility study performed in Table 11, NMP with a solubility capacity higher than 197.6 mg/g was selected as primary solvent of MDA7 at a concentration of 10% w/w. Labrafil® 1944CS (HLB=4) was selected as oil at a concentration of 64 % w/w and Labrasol® (HLB=14) as surfactant at a concentration of 25% w/w, in the same ratio used by Balakrishnan et al. From a safety point of view, we ascertained that the doses of each excipient orally administered in 0.5 mL of the selected SEDD to rat (150 g) would be well tolerated and below the safety ratio either reported in literature or by toxicological studies carried out by the supplier (Table 13). In SEDDS, the primary self-emulsification assessment is done by visual evaluation[176]. The efficiency of self-emulsification could be estimated by determining the rate of emulsification, and droplet size distribution. The droplet size of the emulsion is a crucial factor in self-emulsification performance because it determines the rate and extent of drug release as well as absorption. Since the fed and fasted rat gastrointestinal water volume has been reported to be respectively about 44.6+/-8.5 ml/Kg and 18.3+/-10.3 mL/Kg[177], 0.5 mL of the entry O SEDDS in Table 17 had been introduced into 7 mL of water in a glass beaker at 37 °C and the contents were mixed gently with a magnetic stir bar. The tendency and the time to emulsify spontaneously and also the progress of emulsion droplets were observed and recorded. The tendency to form an emulsion was judged as satisfactory when droplets spread easily in water and formed a fine milky emulsion[149]. The emulsification time was assessed visually as reported by Bachynski et al.[178] and the average mean diameter of emulsion droplets were measured on an aliquot of the same dispersion by PCS.

The SEDDS entry O in Table 17 had permitted to administer a dose up to 15 mg/Kg (e.g. 500µL for 150g rat) MDA7 that did not precipitate upon mixing with water when tested for self-emulsification performance and followed over the course of 1 month.

Table 17: MDA7 oral Self-Emulsifying Drug Delivery System.

	Entry O		
Dose*(mg/Kg)	15		
Volume(µL)**	500		
Rat Weight# (g)	150		
Ingredients	**(mg/mL)**	**Dose administered** (mg/Kg)	**Safety ratio**
MDA7	4.5	15	ND
NMP	100	333	LD_{50} 4.2 G/KG[9-11]
Labrasol®	250	833	NOAEL 3.0 G/KG/DAY (TOX AND SAFETY OVERVIEW GATTEFOSSE)
Labrafil 1944® CS	645.5 (650.0 in placebo)	2166	LD0>20ML/KG (TOX AND SAFETY OVERVIEW GATTEFOSSE)
Macroscopic appearance	Transparent viscous solution		
Microscopic appearance	No crystal		
Self emulsification	Spontaneous and immediate		
Physical stability	Transparent *t*=1 month		

2.4.2.2.2 Characterization.

2.4.2.2.2.1 Physical stability.

As shown in Table 17 the physical stability of the enabling SEDDS entry O tested in *in vivo* (see section 2.5) was followed over 1 month at room temperature and no macroscopic or microscopic crystallization of MDA7 was observed. The results in the *in vitro* self-emulsification testing didn't show any precipitation of the drug nor emulsion droplets coalescence when subjected to aqueous dilution ratio mimicking the *in vivo* dilution undergone by MDA7 in GI juice (fed) after oral administration to rat. The emulsification time study showed that the formulation used in the PK study could spontaneously emulsify in time lower than 20 s. in aqueous environment which is in accordance with previous results reported by several authors[149, 179-180] which have used

SEDDS. In the process of spontaneous emulsification, surfactants form a layer around the emulsion droplets and reduce the interfacial energy as well as providing a mechanical barrier to coalescence[179]. The referred SEDDS didn't show any demixion nor crystallization of MDA7 when stored at room temperature and observed macroscopically over 1 month.

2.4.2.2.2.2 DLS

The average mean diameter of the emulsion droplets formed in the SEDDS entry O was assessed using a Malvern Nano ZS. Since the SEDDS droplets distribution was polydisperse (PDI>0.5) the instrument was not able to give reliable Z-average value by the method of Cumulants. However, the Nano ZS is routinely used to describe individual peaks in particle size distributions derived from multi-modal correlogram fitting algorithms such as CONTIN and NNLS (non negative least squares)[181]. As verified by the distribution results derived from the NNLS analysis of the correlogram, the sample is composed of a mixture of approximately 260 nm and 30 nm size droplets representing respectively around 93% and 7% of the total droplets distribution, with low dispersity for both droplets families (PDI<0.02). SEDDS typically produce emulsions with a droplet size between 100 and 300 nm[146]. The droplet size of the emulsion is a crucial factor in self-emulsification performance because it determines the rate and extent of drug release and absorption[146, 182-183]. For example in the two formulations containing the immunosuppressive agent Cyclosporine A, Neoral® was shown to elicit increased bioavailability compared to Sandimmune®[184]. The more efficient SEDDS, Neoral® is characterized by droplets size ranging from 100 nm to 250 nm whereas Sandimmune® have droplets ranging from few nanometers to several micrometers[185]. Our results indicate the ability of the SEDDS developed to produce a nanoemulsion (droplets size <300 nm) that offers larger interfacial surface area required for drug absorption[146, 148-149].

2.4.2.2.2.3 MDA7 chemical stability by UPLC-MS.

MDA7 chemical stability was investigated on two batches (see Table 18) of entry P. Batch#1 was manufactured to generate preliminary stability results and Batch#2 was

manufactured to supply the PK study. Both samples were assayed by UPLC-MS on samples stored at room temperature over a period of 15 days, showing chemical stability of MDA7 (an average of 95.3% of MDA7 initial amount was recovered).

Table 18: MDA7 chemical stability assessed by UPLC-MS.

Entry O	**MDA7 concentration mg/mL / % recovery (w/w)**		
	Nominal amount	$t_{initial}$	$t_{15\ days}$
Batch#1	4.0	3.9	3.9 / 100.0
Batch#2	4.1	4.2	3.8 / 90.5

% recovery = ($[MDA7]t_{15days}$ / $[MDA7]t_{initial}$) 100*

Solvent ratio in the i.p./i.v. DDS developed was relatively high (≈60%). High solvent ratio can limit the pertinent safety assessment of lead compounds, especially during long-term exposure studies where the drug is required to be dosed at several multiples of the projected human doses. This suggests that conventional technologies such as synergistic combinations of cosolvents and surfactants are not sufficient to develop toxicological pre-clinical and clinical viable formulations for poorly soluble drugs. Encapsulation using lipids (i.e. liposomes) and complexation using cyclodextrins were also adopted as alternative strategies for the administration of MDA7 for future pre-clinical and clinical studies.

2.4.2.3 Liposomes.

2.4.2.3.1 Design and development.

In this work, MDA7 liposomes have been prepared in order to enhance MDA7 blood residency and thereby to prolong its activity *in vivo* during the time of encapsulation. The composition and the manufacturing were adapted from a procedure described by Lopez-Berestein[186] and Zou et al.[187] to successfully form MLVs or oligolamellar liposomes with respectively both lipophilic (N-(4-hydroxyphenyl)retinamide) and hydrophilic (annamycin) drugs (Fig. 19).

The lipid used was dimyristoylphosphatidyl choline (DMPC) with a molar lipid:drug ratio of 10:1. The formulation developed was a liposomal lyophilized powder containing DMPC, MDA7, DMSO and Polysorbate 20 as described in the composition below, for the i.v. administration of 10 mg/Kg of MDA7 (i.e. 250 µL for 150g rat):

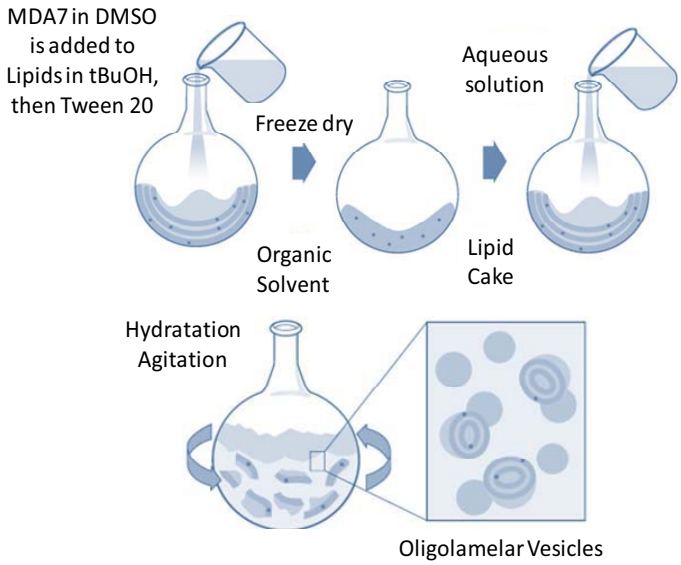

Figure 19: Freeze-drying process for preparation of MLVs liposomal dispersion, adapted from[15]

Entry P: 1.5 mg MDA7
37.5 mg DMSO
30.3 mg DMPC
1.59 mg polysorbate 20

The liposome suspension was obtained on the day of use by adding PBS at 30°C to the lyophilized powder. Temperature of 30°C was chosen to stay above the phase transition temperature of DMPC that is 23°C. This temperature is required to induce a change in the lipid state, from ordered gel phase where the hydrocarbon chains are fully extended and closely packed, to the disordered liquid crystalline phase, where the hydrocarbon chains are randomly oriented and fluid[188]. According to the results of a study realized by Zou et al.[187] with liposomes of similar composition, Polysorbate 20 has been added to shorten the reconstitution step (from>2h to about 1 min.), avoiding the early formation of free drug crystals, and reducing the median particle size by 10-fold (from 1.5 µm to 0.15 µm) without destroying the liposome vesicles. MDA7 containing-liposomes were then characterized with respect to particle size (PCS) and morphology (TEM). The drug loading and the chemical stability of the lyophilized powder/cake stored at room temperature over 1 month were determined using ^{1}H-NMR spectroscopy. The physical stability (no crystallization) was assessed over 1 month for the lyophilized powder/cake and over 1 hour for the reconstituted liposomal suspension in PBS.

MDA7 liposomal lyophilized powder entry P above, had permitted to administer 10 mg/Kg MDA7 (e.g. 250µL for 150g rat) that did not precipitate upon mixing with PBS when reconstituted to afford physiological aqueous suspension at 6 mg/mL of MDA7. MDA7 formulated in this system is physically (no crystallization see Fig. 20) and chemically (no degradation see Table 19) stable stored at room temperature, for at least 1 month.

2.4.2.3.2 Characterization.

2.4.2.3.2.1 Morphology and size.

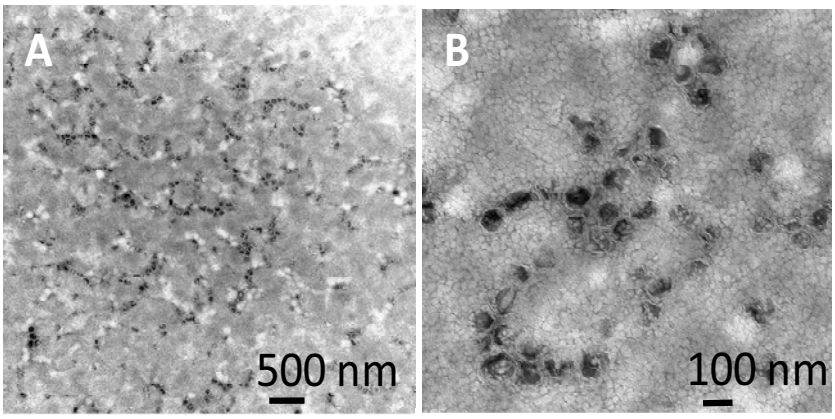

Figure 20: TEM images of MDA7 liposomal dispersions. **A**) magnifying X25,000. **B)** magnifying X100,000.

Morphology and size of MDA7 liposomal lyophilized powder was investigated by TEM 24H after manufacturing (Fig. 20) and shows the presence of an homogenous population of closed round-shaped oligolamellar (OLVs) MDA7 containing-liposomes, with an average size of approximately 100 nm. No MDA7 crystallization occurred in the liposomal powder.

2.4.2.3.2.2 Physical stability.

Extemporaneously reconstituted MDA7 liposomal suspension in PBS ([MDA7]= 6 mg/mL) from liposomal powder ([MDA7]= 21.16 mg/g), tested in the *in vivo* spinal nerve ligation neuropathic pain model see section 2.5, was followed over 1 hour and no crystallization (see Fig. 21 A) of MDA7 was observed, which is conform to the specification of physical stability expected. Physical stability of MDA7 liposomal powder/cake ([MDA7]= 21.16 mg/g), stored at 4°C over 1 month, was evaluated after

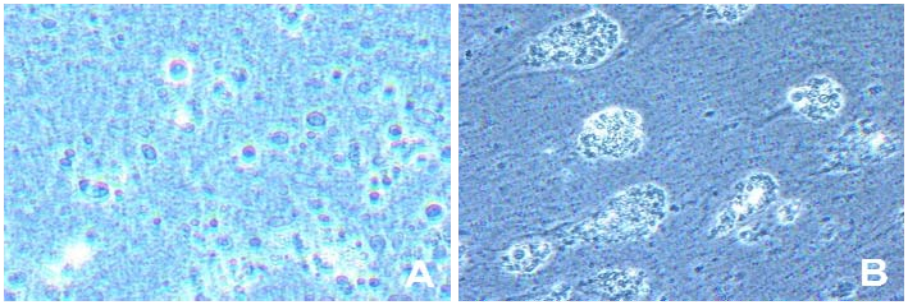

Figure 21: MDA7 (6 mg/mL) liposomal suspension microscopic observation (IX70 Olympus). **A)** $t_{initial}$ and 1 hour after reconstitution in PBS, magnifying X100. **B)** $t_{1\ month}$ and 5 min. after reconstitution in PBS, magnifying X40.

reconstitution of MDA7 liposomal suspension in PBS ([MDA7]= 6 mg/mL). No crystallization of MDA7 occurred (see Fig. 21 B)

2.4.2.3.2.3 MDA7 chemical stability by ^{1}H-NMR.

^{1}H-NMR method has been used to determine the chemical stability of MDA7 ([MDA7]=21.16 mg/g) in the lyophilized powder. MDA7 liposomes were dissolved in methanol-d_4 at a concentration of 1.31 mg/mL of MDA7. MDA7 was chemically stable stored as a lyophilized powder at 4°C for 1 month and extemporaneously reconstituted before injection (100% of the initial MDA7 amount was recovered).

Table 19: MDA7 chemical stability assessed by ^{1}H-NMR.

Entry P	**MDA7 concentration mg/mL / % recovery (w/w)**		
	Nominal amount	$t_{\ initial}$	$t_{\ 1\ month}$
	1.3	1.2	1.2 / 100.0

% recovery = ($[MDA7]t_{1month}$ / $[MDA7]t_{initial}$) 100*

2.4.2.3.2.4 DLS.

MDA7 liposomal composition entry P obtained by freeze-drying process and reconstituted in PBS, yielded to a monodisperse distribution of OLVs with an average mean diameter of 117 nm (PDI <0.1) corroborating the TEM results. Several studies have reported the marked influence of liposome size on the PK profile and biodistribution of the carrier and the encapsulated drug, on the drug loading capacity, aggregation and

sedimentation[189-190] after i.v. administration. It is generally known that liposomes with a size in the range of 100-200 nm show better physical stability and a longer circulating time compared to smaller (e.g. 50 nm) or larger (e.g.>300nm) which respectively undergo reduced interaction with plasma protein and higher recognition/uptake by macrophages of the ReticuloEndothelial System (RES)[189, 191]. Studies examining i.v. injected liposomes demonstrate a diameter of about 100 nm as the optimal size for accumulation because of the enhanced permeability retention (EPR) found in tumor[90, 190]. In tumor tissue, the vasculature is discontinuous, and pore sizes vary from 100 to 780 nm. By comparison pore size in normal vascular endothelium is <2 nm in most tissues, 6 nm in postcapillary venules, 40–60 nm for the kidney glomerulus, and up to 150 nm for sinusoidal epithelium of the liver and spleen[192]. The size of liposomes for Doxil® drug is between 80-100 nm and the size of liposomes for Myocet® is around 150 nm[193]. The liposomal forms of Doxorubicin Doxil® and Myocet® are both very effective drugs. Besides, peripheral nerve permeability change may occur after Spinal Nerve Ligation (SNL)[194-195] as well as disruption of the blood-spinal cord barrier (BSCB), associated with breakdown of microvascular permeability[196-197]. Since we were going to test the developed MDA7 liposomes in an *in vivo* model of SNL, we hypothesized that the same size of liposomes that have been shown to be efficient in tumors models with discontinuous vasculature may be suitable for this particular *in vivo* neuropathic pain model.

2.4.2.4 Cyclodextrins.

Cyclodextrins (CDs) are one of the most used drug-carriers because they are able to form inclusion complexes (host-guest complexes) with a wide variety of small lipophilic molecules. Inclusion complexes are water soluble and furthermore complexation can increase the stability (e.g. metabolic) of the guest molecule. The FDA-approved and chemically modified cyclodextrins, 2-hydroxypropyl-β-cyclodextrins (HPβCD) have attracted growing interest based on their low toxicity, water solubility and complexation potential. Considering the advantages of HPβCD and in the aim of developing a formulation appropriate for further human use, we prepared MDA7 inclusion complexes to increase its aqueous solubility and metabolic stability. We tested i.v. administration of MDA7 inclusion complexes at 10 mg/Kg dose (i.e. 250 µL for 150g rat) using a rat model

of neuropathic pain and compared MDA7 antinociceptive efficacy formulated in CDs, micellar solution and liposomal preparation. In addition HPβCD are versatile DDS for MDA7 since they can advantageously be administered orally and intraveneously, hence a solely DDS may be used to support additional PK study avoiding any vehicle effect. MDA7-HPβCD inclusion complexes were characterized by phase-solubility diagram, Job's plots and differential scanning calorimetry. Association mode in solution was determined by NMR spectroscopy and ESI-mass spectrometry. HPβCD aggregates were characterized by TEM and DLS. Complexed MDA7 chemical stability was also evaluated using UPLC-MS.

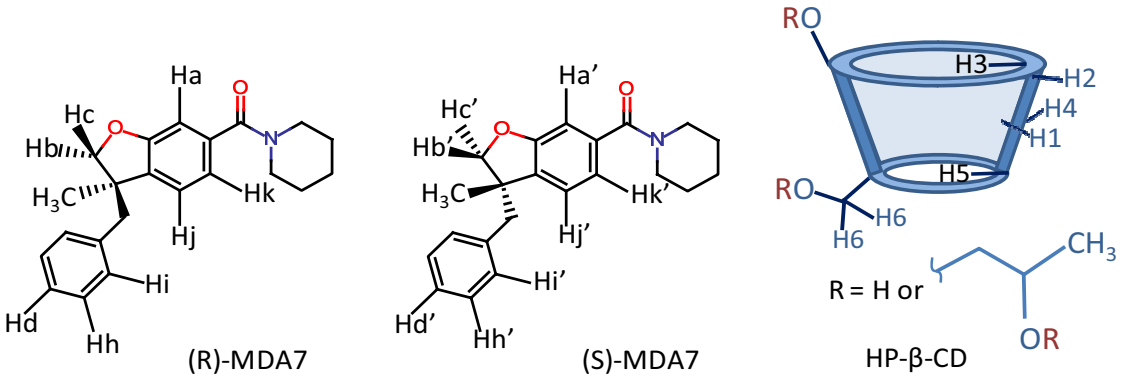

Figure 22: Numbered chemical structures of the two enantiomers of MDA7 and of HP-β-CD.

2.4.2.4.1 Phase solubility studies

The phase solubility method was carried out according to Higuchi and Connors[198] method to study the effect of complexation on MDA7 solubility in water. Complexes were prepared as described in experimental section 4.6.1.

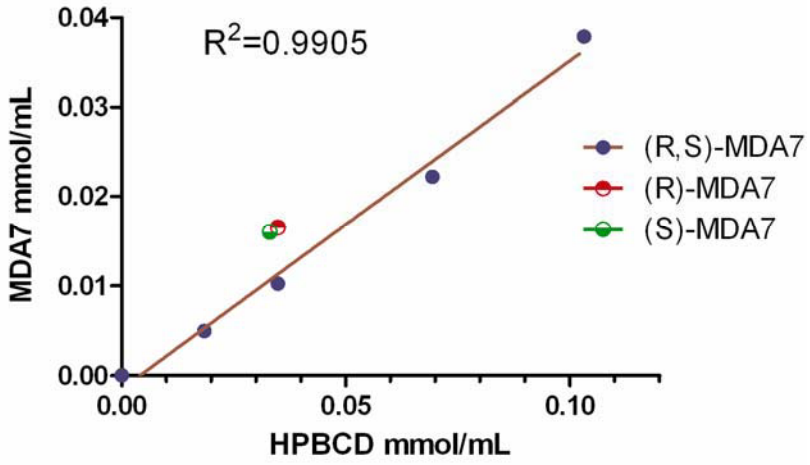

Figure 23: Phase-solubility diagram for (R,S)-MDA7 at increasing HPβCD concentrations and (R)-MDA7 and (S)-MDA7 solubility values at a MDA7:HPβCD molar ratio of 1:1.

The determination of $K_{1:1}$ between MDA7 and HPβCD was based on the quantification of the concentration of soluble MDA7 determined by NMR upon inclusion. The increase on MDA7 solubility occurred as a linear function of HPβCD concentration (Fig. 23) corresponding to an A_L-type profile defined by Higuchi and Connors. This relationship confirmed a first order kinetics on the complex formation between MDA7 and HPβCD and confirmed the formation of a 1:1 complex.

A stability constant ($K_{1:1}$) of 18 200 M^{-1} was calculated from the slope and the intrinsic solubility (S_0) of the drug in the aqueous complexation medium according to Eq. 1[49] with intrinsic water solubility of MDA7 = 31.8 µM and slope = 0.367.

$$K_{1:1} = \frac{[\text{MDA7/HP}\beta\text{CD}]}{[\text{MDA7}] \times [\text{HP}\beta\text{CD}]} = \frac{\text{Slope}}{S_0\,(1\text{-Slope})} \qquad (1)$$

Where [MDA7/HPβCD] is the concentration of dissolved complex, [HPβCD] is the concentration of dissolved free HPβCD assuming that [MDA7] is the intrinsic solubility of MDA7 and Slope is the slope of the phase-solubility plot.

Intrinsic solubility (S_0) of a drug is expected to be determined by the intercept with Y axis. In the case of MDA7 the Y-intercept is -0.001475 mol/mL. However, MDA7 is a highly lipophilic molecule which is poorly water soluble. An intrinsic solubility of 31.8 µM was previously determined using the shake flask method[199]. In this case a more accurate method to determine the solubilizing effect of HPβCD is to determine the complexation efficiency (*CE*). *CE* is the concentration ratio between free HPβCD and HPβCD complexing MDA7. *CE* is independent of both S_0 and the intercept and is more reliable for poorly soluble guest. A *CE* of 0.58 was determined according to Eq. 2[200].

$$CE = S_0 \times K_{1:1} = \frac{[MDA7/HP\beta CD]}{[HP\beta CD]} = \frac{Slope}{(1-Slope)} \quad (2)$$

The drug:cyclodextrin molar ratio in water saturated with MDA7 can be determined according to Eq. 3.

$$MDA7:\ HP\beta CD\ molar\ ratio = \frac{(CE + 1)}{CE} \quad (3)$$

MDA7:HPβCD ratio has a value of 1:2.7 indicating that, on a 1:1 MDA7:HPβCD complexation, just one out of approximately 3 HPβCD molecules is forming an inclusion complex with MDA7. Since HPβCD is a mixture of randomly hydroxypropylated CDs with different molecular weights, MDA7:HPβCD ratio is similar to the experimental MDA7:HPβCD ratio determined to solubilized MDA7 with a value between 3 and 4. In addition we compared the solubilisation of (R)-MDA7 and (S)-MDA7 with (R,S)-MDA7 at MDA7:HPβCD molar ratio of 1:1. Both enantiomers exhibited a comparable water solubility value after complexation with HPβCD with the racemic mixture (Fig. 23).

2.4.2.4.2 Differential scanning calorimetry.

DSC curves (Fig. 24) of the inclusion complexes were compared with physical mixture. MDA7 showed an endothermic peak at 108°C corresponding to melting point. HPβCD exhibited two broad endothermic peaks in the range of 50-150°C and 300-350°C[201]. The first endothermic event assigned to loss of water and the second one to thermal decomposition[202]. The DSC curve of MDA7/HPβCD physical mixture showed the endoterms corresponding to HPβCD (50-150°C and 300-350°C) and the melting peak of

MDA7 at 108°C. The absence of MDA7 melting peak in the inclusion complexes with MDA7:HPβCD molar ratio of 1:1, 1:4 and 1:6.7 is a strong indication of inclusion complex formation[203]. The broad endotherm at 50-150°C due to loss of water molecules absorbed and bonded to HPβCD is dramatically decreased with 1:1 molar ratio and increased with MDA7:HPβCD molar ratio. This effect reflects that higher active substance content of the complex means less water content. This effect of complexation on the loss of water indicates that inclusion complex formation results in displacement of water molecules.

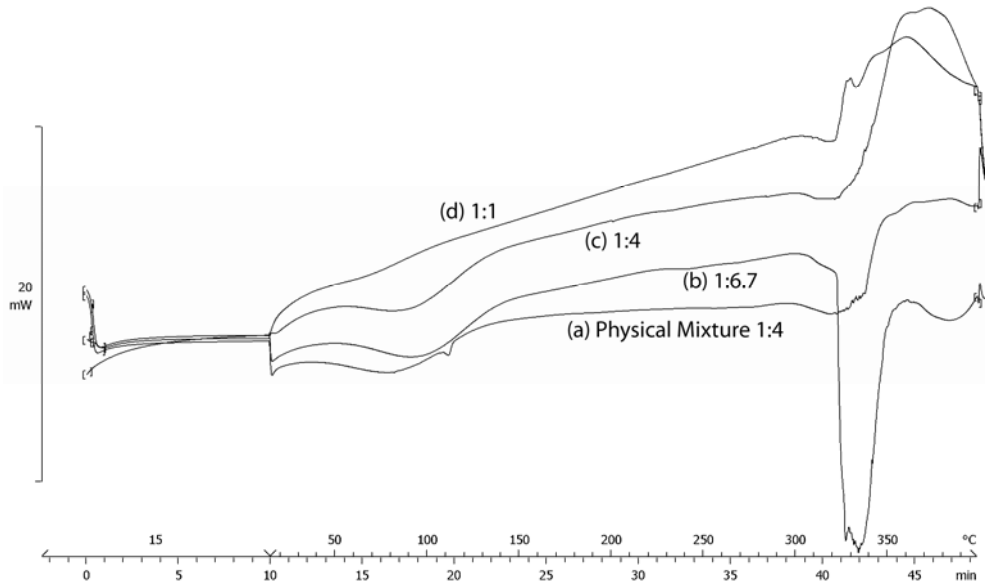

Figure 24: DSC thermograms of **a** HPβCD /MDA7 physical mixture molar ratio of 1:4; **b)** HPβCD /MDA7 inclusion complex molar ratio 1:6.7; **c)** HPβCD /MDA7 inclusion complex molar ratio 1:4 and **d)** HPβCD /MDA7 inclusion complex molar ratio 1:1.

2.4.2.4.3 ESI-MS analysis.

Electrospray mass spectrometry (ESI-MS) has been used to investigate noncovalent complexes of different classes of compounds[66]. ESI-MS allows detecting non-covalent interactions of supramolecular inclusion “host-guest” complexes with various molecules in the gas phase. Electrospray provides a faithful image of the composition of the complex formed in solution and subsequently its stoichiometry in the range of concentrations used for *in vivo* studies[67], provided that all species are kinetically stable enough to reach the detector intact[66]. However it has been suggested that to avoid non specific aggregation occurring upon droplet evaporation, analyzed sample should be

diluted and electrospray flow rate decrease[66-68]. The ESI mass spectra were observed for mixtures of uncomplexed HPβCDs and the supramolecular complexes with MDA7 (Fig. 25). HPβCD is a mixture of several hydroxylpropylated CD with a degree of substitution ranging from 1 to 8, which corresponds to the m/z peak distribution from 1193 to 1600. The ions ranging from m/z 1645 to 1820 correspond to $[HP\beta CDs+MDA7+H]^+$ with a degree of hydroxylpropyl substitution ranging from 3 to 6: 1309+335+1, 1368+335+1, 1426+335+1, 1484+335+1. Fig. 25 shows the presence of MDA7:HPβCD complex at a ratio of 1:1 confirming the results obtained by the method of continuous variation (Job's analysis). No signal of higher order drug:HPβCD have been detected in the range of m/z studied (1900-5000).

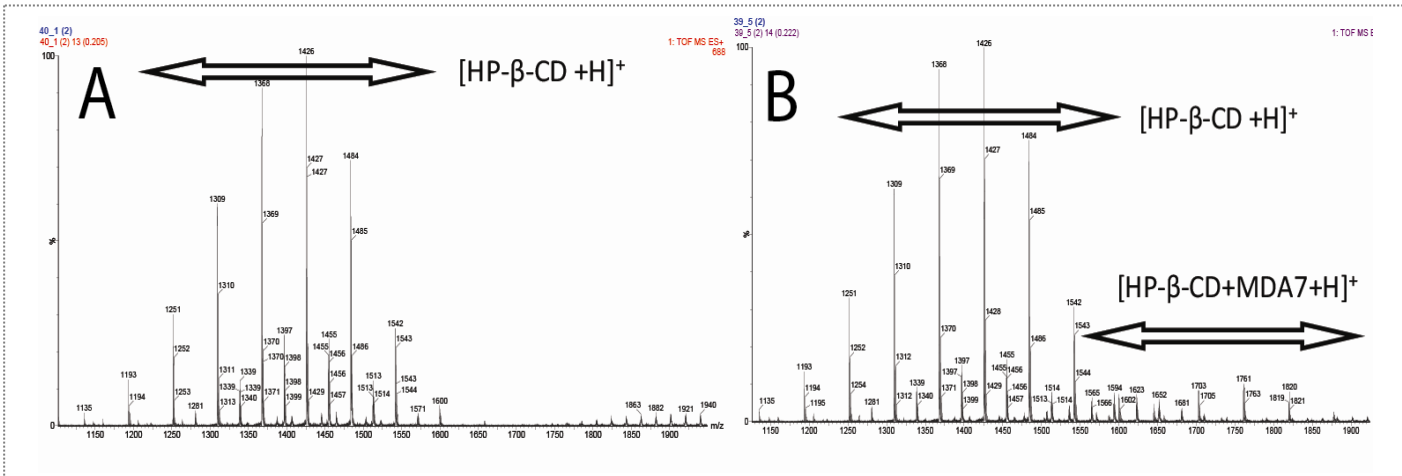

Figure 25: Electrospray mass spectra of (A) empty HPβCDs and (B) MDA7/ HPβCD 1:1 complexes.

2.4.2.4.4 Continuous variation method (Job's plots).

Stoichiometry of the inclusion complex was determined by continuous variation plot (Job's plot) studying ^1H NMR spectra. Continuous variation curves were obtained by monitoring chemical shifts of the outer proton H1, the internal cavity proton H5 and $CH3_{HP\beta CD}$ protons located in the hydroxypropyl moieties of the host (HPβCD) which were well separated from those of MDA7. HPβCD is not a single compound but rather a mixture of randomly hydroxypropylated molecules of β-CD resulting in complexe NMR spectra.

Table 20: ^{1}H NMR chemical shifts (δ in ppm) and changes ($\Delta\delta$ in ppm) of HPβCD protons upon complexation of MDA7 at 0.5 molar ratio in an equimolar solution of D_2O and methanol-d_4 at 300 K.

HPβCD protons	δ free (ppm)	δ complex (ppm)	$\Delta\delta$ (ppm)	MDA7 protons	δ free (ppm)	δ complex (ppm)	$\Delta\delta$ (ppm)
H1	5.024	5.014	-0.01	Ha	6.5745	6.6370	0.0625
H5	3.846	3.805	-0.041	Ha'	6.5745	6.6540	0.0795
$CH_{3\ HP\text{-}\beta\text{-}CD}$	1.144	1.141	-0.003	Hc	4.1700	4.1270	-0.0430
				Hc'	4.1700	4.1060	-0.0640
				Hb	4.6175	4.6285	0.0110
				Hb'	4.6175	4.6230	0.0055
				CH_3	1.439	1.430	-0.009

No new peaks were observed in NMR spectra indicating that free and complexed forms of MDA7 were in a rapid exchange relative to NMR timescale. The plots obtained for H5 reach a minimum at an *R* value of 0.5 on the abscissa axis indicating formation of exclusively 1:1 adduct (Fig. 26). As expected, the largest chemical shift variation was obtained for H5 compared to H1 and CH3 $_{HP\beta CD}$ of HPβCD with an up-field of $\Delta\delta$ 0.041 ppm. Since H5 is located in the cavity of HPβCD the chemical shift observed clearly suggests the presence of MDA7 in the cavity. The upfield shielding effect probably results from a diamagnetic anisotropy effect due to the inclusion of π-electrons belonging to MDA7 into the hydrophobic central cavity of the HPβCD[204-205]. Chemical shift variations of H1 and CH3 $_{HP\beta CD}$ of HPβCD upon MDA7 complexation are moderate compared to H5. H1 which is located on the outer rim of HPβCD, and the CH3 $_{HP\beta CD}$ moiety which is at the outer surface of cyclodextrin showed minor changes of their chemical shifts. In addition, the effects of HPβCD on the ^{1}H NMR chemical shift of MDA7 were investigated. Continuous variation curves were obtained by recording chemical shifts of protons located in different regions of the guest, MDA7: Ha,a'; Hb,b'; Hc,c' and CH_3. These protons were selected because no peak overlaps were observed.

^{1}H NMR chemical shifts of MDA7 protons upon complexation by HPβCD are summarized in Table 20. Proton Ha,a'; Hb,b' are probably located close to an oxygen of HPβCD since a downfield displacement of the host protons indicates that they are close to an electronegative atom such as oxygen.

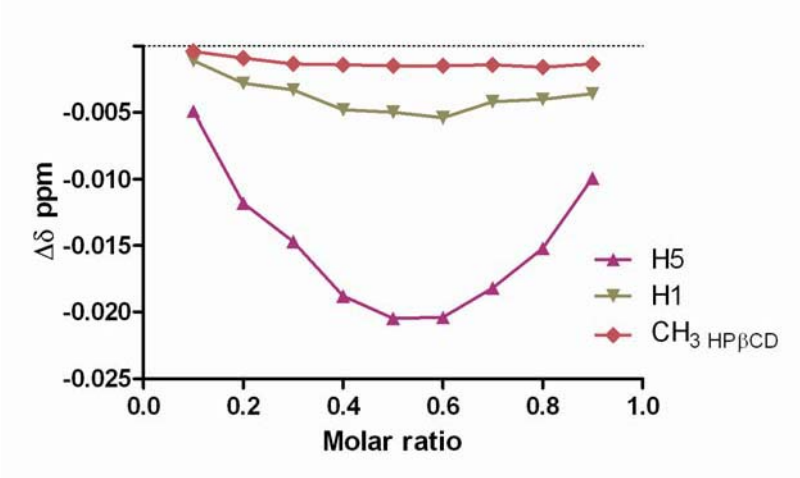

Figure 26: Continuous variation plot corresponding to the chemical shift induced displacement of HPβCD protons, H5, H1 and $CH_{3\ HP\text{-}\beta\text{-}CD}$ in an equimolar solution of D_2O and methanol-d_4 at 300 K.

In contrast, protons Hc,c' and from the CH_3 are probably located close to an hydrogen atom as indicated by an upfield displacement due to changes in the local polarity due to the inclusion of the drug into the lipophilic central cavity or Van der Waals interactions between MDA7 and hydrogen atoms of HPβCD cavity[206]. Magnitude of the shift difference for protons of the guest molecule is dependent on the relative strength of the two types of interaction with oxygen or hydrogen atoms with the HPβCD cavity. Shielding effects for Ha,a'; Hb,b' were the most intense compared to Hc,c' and CH_3 indicating that the phenyl ring of the benzofuran moiety is deeply located in the HPβCD cavity .

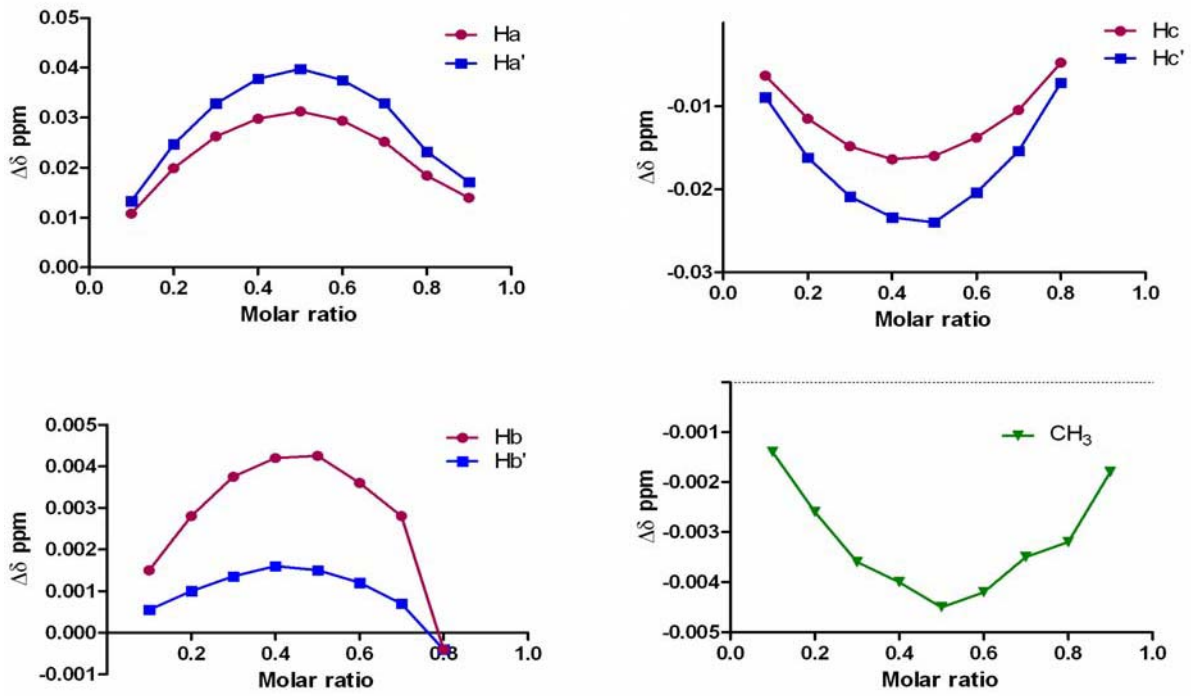

Figure 27: Continuous variation plot corresponding to the chemical shift induced displacement of MDA7 protons, Ha,a'; Hb,b'; Hc,c' and CH_3 in an equimolar solution of D_2O and methanol-d_4 at 300 K.

2.4.2.4.4.1 Enantiomeric recognition.

Many drugs such as the popular selective serotonin reuptake inhibitors, fluoxetine are currently marketed as racemic mixtures. We decided to formulate and test the racemic mixture *in vivo* even though the eutomer of MDA7 has been isolated and identified as being (S)-MDA7[199]. Enantiomeric recognition by CDs has been used as an analytical tool. It was reasonable to expect that HPβCD will form diasteriomeric inclusion complexes with racemic mixture of MDA7. Enantiomeric recognition was observed in equimolar solution of D_2O and methanol-d_4 at the low concentrations which were used for Job's plots studies as shown in Fig. 27 and in the system used for *in vivo* studies in D_2O (Fig. 28). ^1H NMR spectra of enantiomerically pure (R)-MDA7 and (S)-MDA7 were compared to MDA7 racemic mixture to infer the ^1H NMR chemical shifts for each enantiomer. The Job plots showed a marked difference between the two enantiomers. Chemical shift differences do not vary in the same manner for each enantiomer (e.g.

Ha,a'; Hb,b' and Hc,c'). (S)-MDA7/ HPβCD complex appears to have larger *Δδ* for Ha' and Hc' than that of (R)-MDA7/ HPβCD complex (Ha and Hc). On the other hand, *Δδ* for Hb from (R)-MDA7/ HPβCD complex is larger than that of Hb' from (S)-MDA7/ HPβCD complex. It is difficult to conclude which enantiomer has the higher affinity for HPβCD since the positioning of the two enantiomers in HPβCD is different according to chemical shift differences but the ^{1}H NMR study is possible only for protons well resolved and not overlapping. The *Δδ* of the CH_3 of MDA7 is small and no appreciable discrimination between the enentiomers was observed in the Job's plot study where a mixture of methanol-D_4 and D_2O was used as solvent. On the other hand chiral recognition was observed in D_2O (Fig. 28). As expected, chiral recognition was reduced when the concentration of HPβCD was reduced in methanol-d_4 and D_2O. Chiral recognition for the aromatic and furanic protons decreases when 0.5 to 4 equivalents of HPβCD were used in D_2O while no discrimination was observed for 4 and 5 equivalents. Surprisingly, enantiomeric recognition was observed for aromatic protons when 6.7 equivalent of HPβCD were used. On the other hand, Chiral recognition was observed for the methyl moiety of the benzofuran scaffold at 0.5 to 6.7 equivalents of HPβCD were used in D_2O.

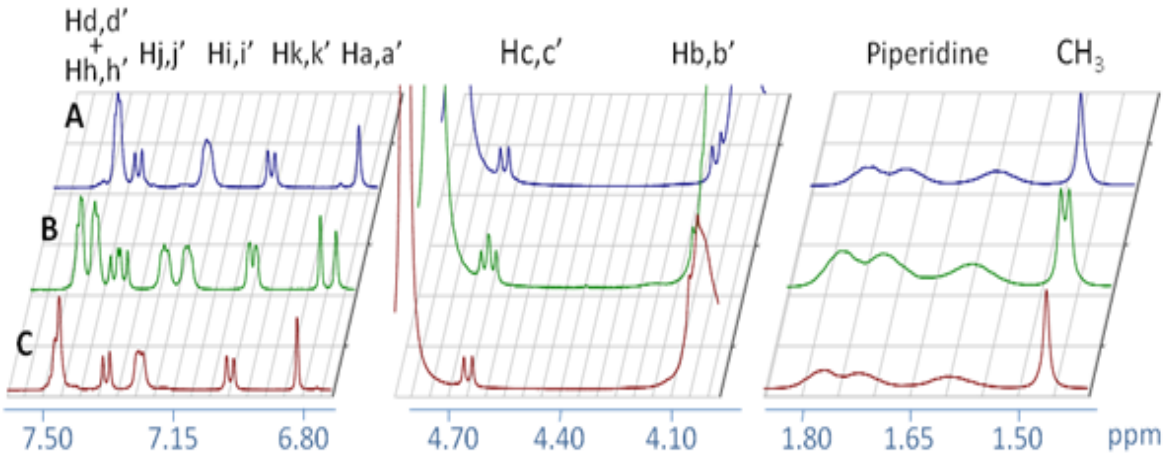

Figure 28: Portions of NMR spectra of an equimolar mixture of (A) (R)-MDA7, of (B) (R,S)-MDA7 and of (C) (S)-MDA7 upon complexation by HPβCD at a concentration of 33 mM in D_2O at 300 K.

2.4.2.4.5 2D NMR spectroscopy.

Two-dimensional rotating-frame NOE spectroscopy (ROESY) has been used widely for the characterization of CD inclusion complex. NOE cross-peaks resulting from dipolar

coupling after complexation indicate a distance smaller than 5 Å between two protons of the host and the guest molecules. As mentioned above, HPβCD is a mixture of randomly hydroxypropylated molecules of β-CD and in addition just one out of 3 HPβCD molecules is forming an inclusion complex with MDA7. These parameters are adding complexity on the interpretation of ROESY experiments. The spatial environment of MDA7 within HPβCD cavity was determined according to NOE cross-peaks.

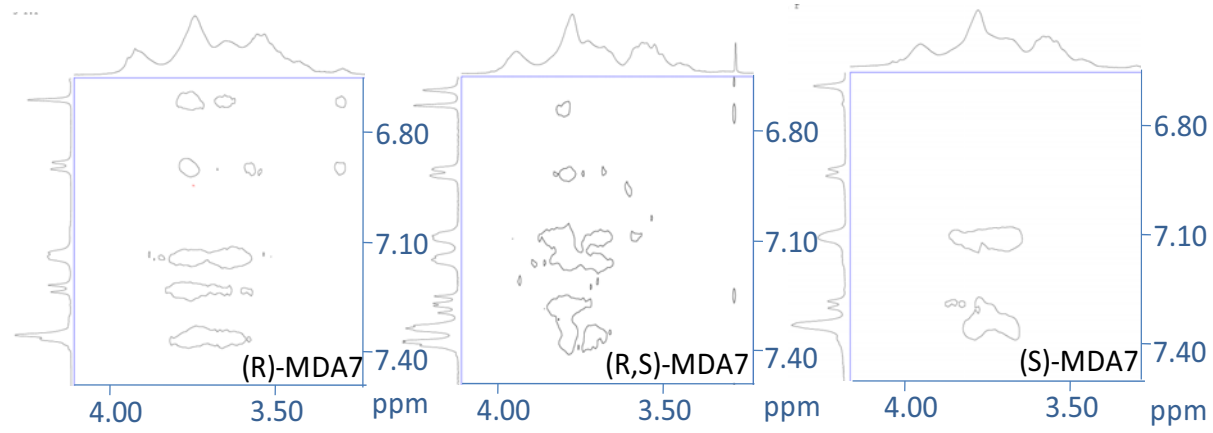

Figure 29: Partial contour plots of 2D ROESY spectrum of MDA7:HPβCD inclusion complexes in D_2O at 300 K upon complexation by HPβCD at a concentration of 33 mM in D_2O at 300 K. For the proton labeling see Fig. 22.

The 2D ROESY spectra of the complex MDA7:HPβCD were acquired at different molar ratio in pure D_2O. Aromatic protons Hi,i', Hd,d' and Hh,h' of MDA7 at 1:1 molar ratio exhibited intermolecular cross-peaks with the NMR signals including H5 and H6 of HPβCD. These observations suggest that the benzyl moiety of MDA7 is positioned deeply inside the cavity. In this case, cross-peak between MDA7 and H3 should confirm the hypothesis. It was difficult to conclude about possible interactions between CH_3 and the benzylic CH_2 of MDA7 with H3 of HPβCD since H3 is overlapping with Hb,b' protons. (R)-MDA7 protons Ha, Hj and Hk had additional cross-peaks with NMR region including H5 and H6 of HPβCD compared to (S)-MDA7. A dynamic equilibrium between two different complexes in the NMR timescale can explain these additional interactions. Benzofuran moiety of (R)-MDA7 could interact with HPβCD in addition to the benzyl moiety. These two complexes could coexist in solution. (R,S)-MDA7 ROESY studies at 1:1 molar ratio confirm the data obtained with pure enantiomers. (R,S)-MDA7 ROESY studies at 1:4 molar ratio did not show big differences compared to 1:1 ratio. Hk,k' cross-

peaks were weak in both spectra. Interaction between NMR region including H5 and H6 of HPβCD and Ha,a' indicates that at higher concentration of HPβCD, (R)-MDA7 is forming the 2 complexes.

2.4.2.4.1 Molecular modeling.

To further explore the mode of complexation of MDA7 by HPβCD we performed molecular modeling studies (Fig. 30). We observed that the complexes with the highest score were with the benzyl ring inserted into the HPβCD cavity ($E_{S\text{-}MDA7}$ = -537.0 kcal mol^{-1}, $E_{R\text{-}MDA7\ pink}$ = -627.0 kcal mol^{-1}, $E_{R\text{-}MDA7\ cyan}$ = -579.0 kcal mol^{-1}) which is in agreement with the results obtained by NMR spectroscopy. In addition the complex with the benzofuran ring into the HPβCD cavity for (R)-MDA7 was among the complexes with the highest score ($E_{R\text{-}MDA7\ purple}$ = -614.0 kcal mol^{-1}), confirming that the two mode of complexation can coexist.

.

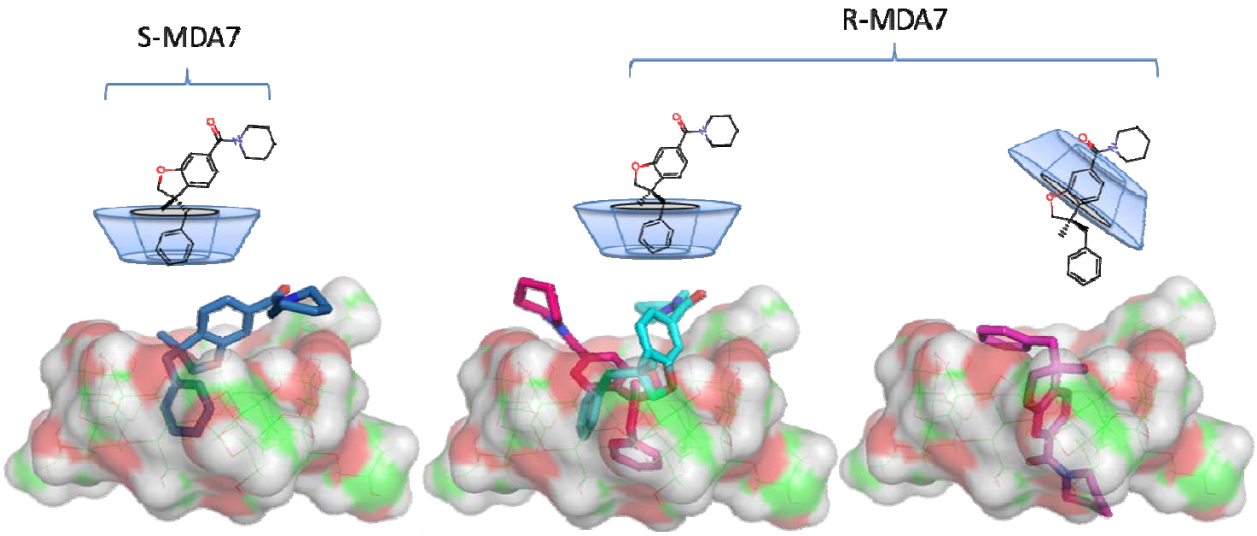

Figure 30: Schematic structures and lowest energy inclusion complexes of (S)-MDA7 and (R)-MDA7 in HPβCD. In Blue (S)-MDA7:HPβCD complex with the benzyl ring inserted into the cavity of HPβCD, in cyan and pink two conformation of (R)-MDA7:HPβCD complexes with the benzyl ring inserted into the cavity of HP-β-C and, in purple (R)-MDA7:HPβCD complex with benzofuran ring inserted into the cavity of HPβCD.

2.4.2.4.2 Morphology and size

Hydrodynamic radii of samples containing HPβCD at 130 mM, and mixture of MDA7 and HPβCD at 1:1, 1:4 and 1:6.7 molar ratio with a concentration of respectively 30 mM, 130 mM and 230 mM were determined by DLS. The Z-average and the PDI results given by the single mode cumulant couldn't be exploited since different populations of particles are present in the dispersion. However pure HPβCD solution is composed of a mixture of discrete populations with an average diameter of approximately 2 nm (PDI <0.1) and 340 nm (PDI <0.1). A hydrodynamic radius of approximately 2 nm is in reasonable agreement with the size expected for a single HPβCD[71].

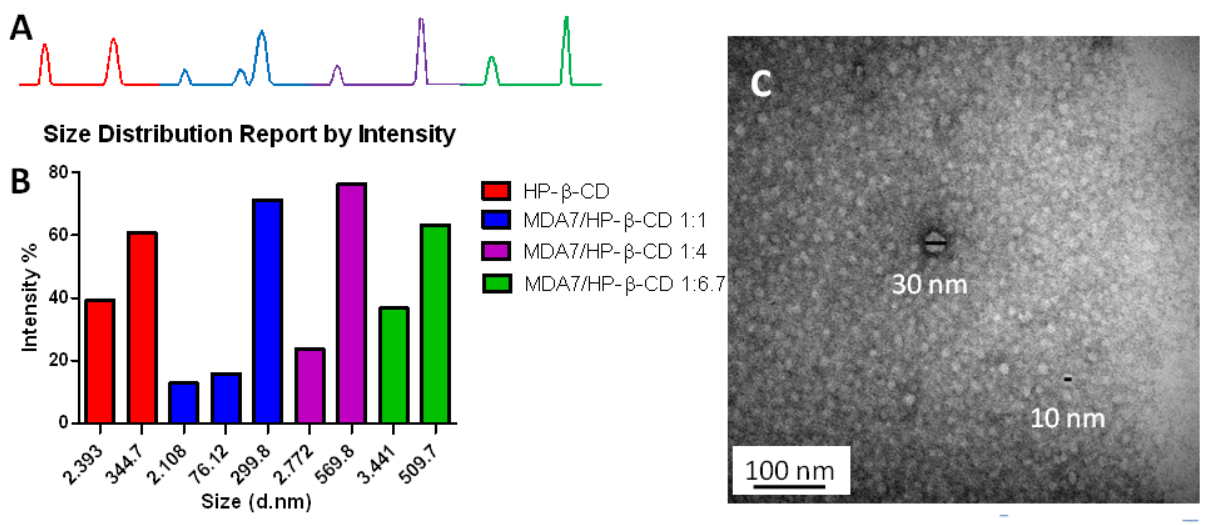

Figure 31: A) DLS results showing size distribution by intensity of the aqueous solutions of HPβCD and MDA7/ HPβCD at 1:1, 1:4 and 1:6.7 molar ratio; **B**) Flow charts corresponding to the size distribution by intensity; **C**) TEM images of aggregated 230 mM 1:6.7 MDA7/ HPβCD magnifying X 150,000.

This population was found in all the samples containing MDA7 and HPβCD at different molar ratio. Complexation of HPβCD with MDA7 is not expected to dramatically change the hydrodynamic radius of single MDA7/HPβCD complex compared to a single HP-β-CD. The second population was composed by particles with a mean hydrodynamic radius of approximately 340 nm (PDI <0.1) corresponding probably of self-aggregated HPβCD forming nanoparticles. We observed the same bimodal distribution for the samples containing MDA7 and HPβCD at 1:4 and 1:6.7 molar ratios. However, the mean

hydrodynamic radii corresponding to self-aggregated HPβCD were larger for samples containing MDA7 and HPβCD than in the sample containing pure HP-β-CD. MDA7 can affect the size of the self-aggregated HPβCD inducing formation of larger aggregates[200]. Surprisingly, a third population with a mean hydrodynamic radius of approximately 76 nm (PDI <0.1) was identified in the sample with MDA7/HPβCD at a molar ratio of 1:1.

Furthermore the mean diameter of the larger population was similar than for pure HP-β-CD. The lower concentration of HPβCD in the former sample compared to the sample with pure HPβCD could explain the differences in term of distribution and diameter. The aggregation and the size of the aggregates increase with increasing cyclodextrin concentration[200]. The morphology and the size of self-aggregates of HPβCD were also analyzed by TEM. Two populations of spherical aggregates of HPβCD with diameter of 5-10 nm and 30 nm were observed (Fig. 31C). These results were not in agreement with DLS experiments but sample preparation can affect the size of the aggregates observed by TEM. Nevertheless, TEM results confirm that spherical aggregates of different sizes are present in aqueous MDA7/HPβCD solutions as previously shown with other host molecules[207].

2.4.2.4.3 Physicochemical stability

We evaluated the physicochemical stability of the MDA7:HPβCD inclusion complex used *in vivo* with a molar ratio 1:6.7 ([MDA7]= 6 mg/mL) respectively over a period of 15 days and 1 month, to correlate with the *in vivo* model testing of spinal nerve ligation see section 2.5. This DDS has been selected for *in vivo* studies with a concentration in CDs above the solubility determined (between molar ratio 1:3 and 1:4) as to prevent *in vivo* crystallization with a safety margin. In addition, this DDS brings some flexibility if higher concentration of MDA7 has to be tested *in vivo*. We ascertained that the dose of CDs (30% w/v or 500 mg/Kg) is safe for i.v. and oral administration to rats. Excellent reviews of toxicological data concerning HPβCD are published and concentration up to 10g/Kg delivered acute or subchronic, oral or i.v., to rats have been reported to be not toxic[1-2]. Sporanox® a marketed product for i.v. administration of itraconazole contains this excipient at concentrations of up to 40%[21].

2.4.2.4.3.1 Physical stability.

No macroscopic crystallization of MDA7 formulated at concentrations ranging from 6 to 11.3 mg/mL had been observed in the MDA7:HPβCD solution stored at room temperature over 1 month.

2.4.2.4.3.2 MDA7 chemical stability by UPLC-MS.

No degradation occurred for MDA7 in PBS formulated in MDA7:HPβCD DDS (molar ratio 1:6.7), Entry Q in Table 21, Batch #1, assayed by UPLC-MS after storage at room temperature for 15 days (98.4% of the initial amount of MDA7 was recovered).

Table 21: MDA7 chemical stability assessed by UPLC-MS.

Entry Q	**MDA7 concentration mg/mL / % recovery (w/w)**		
Batch #1	*Nominal amount*	t_{initial}	$t_{\text{15 days}}$
		12.7	12.5 / 98.4

% recovery = ([MDA7]t_{15days} / [MDA7]$t_{initial}$) 100*

2.4.2.4.3.3 MDA7 chemical stability by ^{1}H NMR.

A different batch #2, entry Q was assayed by ^{1}H NMR after storage at room temperature for 1 month and confirmed the chemical stability of MDA7 in PBS formulated in MDA7:HPβCD DDS (102.5 % of the initial amount of MDA7 was recovered) (Batch#2 in Table 22).

Table 22: MDA7 chemical stability assessed by ^{1}H NMR.

Entry Q	**MDA7 concentration mg/mL / % recovery (w/w)**		
Batch#2	*Nominal amount*	$t_{initial}$	$t_{1\ month}$
	11.8	12.0	12.1 / 102.5

% recovery = ([MDA7]$t_{1\ month}$ / [MDA7]$t_{initial}$) 100*

2.5 *In vivo* characterization of MDA7.

2.5.1 Pharmacokinetic study.

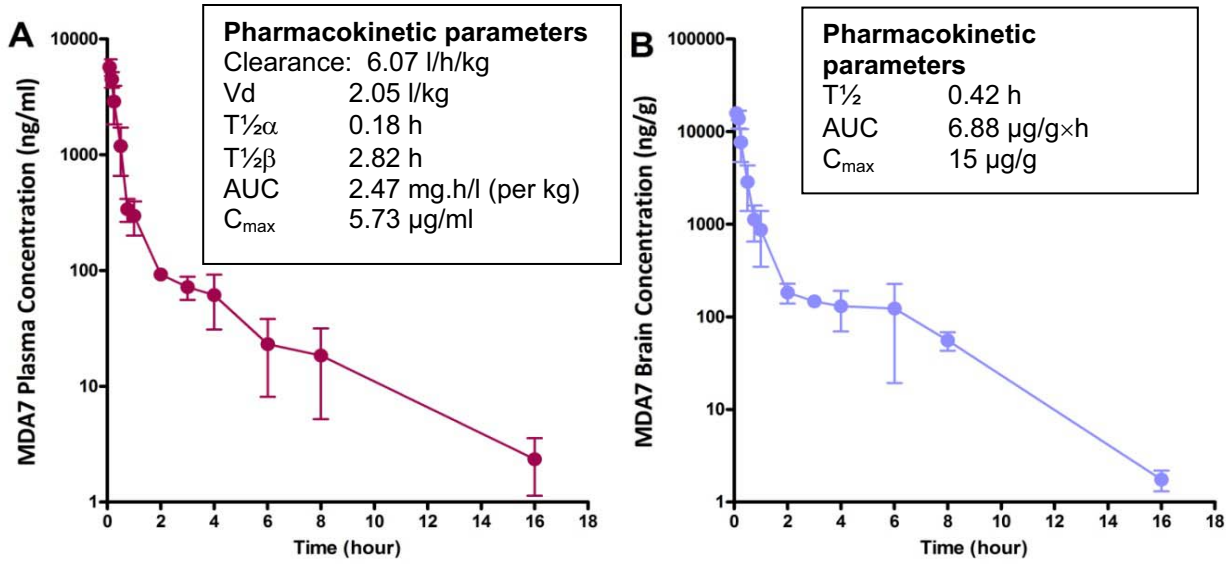

Figure 32: Pharmacokinetic parameters after intravenous administration of MDA7 in rats. Intravenous administration of 15 mg/kg MDA7 achieved a plasma concentration (C_{max} 5.73 µg/ml) **(A)** that was approximately 3-fold less than that simultaneously measured in the central nervous system **(B)**.

A pilot pharmacokinetic study of MDA7 in rats was conducted following single administration of 15 mg/kg dose of MDA7 either intravenously (250 µL for 150g rat) or

orally (500 µL for 150g rat), respectively incorporated in micellar solution and SEDDS (Table 23).

Table 23: Composition of the two DDS administered by oral and i.v. route respectively micellar solution and SEDDS.

Micellar solution	
Entry	**N**
Ingredients	**mg/mL**
MDA7	9.0
NMP	300.0
PG	300.0
EtOH	100.0
CrELP	100.0
PBS qs. 1 mL	191.0

SEDDS	
Entry	**O**
Ingredients	**mg/mL**
MDA7	4.5
NMP	150.0
Labrasol®	150.0
Labrafil® 1944 Cs	121.2

By comparison to intravenous (Fig. 32) and oral systemic exposure (AUC) (data not shown), the calculated oral bioavailability was <5%. Both dosage forms achieved brain tissue concentrations higher than simultaneously measured plasma drug concentrations, demonstrating some degree of MDA7 sequestration in the CNS. The intravenous dosage form achieved a peak CNS concentration 3-fold greater than the simultaneously measured plasma concentration, which declined to concentrations < 0.1 µg/mL within 4 hours. Plasma drug concentrations were maintained above 0.1 µg/ml for approximately 2 hours. The intravenous dose form may be considered suitable for administration as it maintains concentrations above 10 ng/ml for > 10 hours. The considerably lower bioavailability of the oral dosage form suggests intra-luminal GI metabolism may be responsible for what appears to be a rapid 1st pass metabolism, since drug permeability doesn't seem to be a limiting factor[166]. The intravenous dosage form has a bioavailability advantage, and with a half-life of almost 3 hours in a rodent species, is the preferred dosage form over the current oral formulation. Taking in account these findings we decided to perform *in vivo* evaluation of MDA7 using DDS for i.v. administration.

2.5.2 Influence of the DDS selected on MDA7 *in vivo* efficacy.

In vivo experiments were carried out to study the influence of three different DDS, HP-β-CD, liposomes and micellar preparation of the CB2 agonist MDA7, to modify its efficacy *in vivo* at therapeutic dose. Formulation concepts based on micellar solution, liposomes and inclusion complexes were selected because of their common use in intravenous formulations and their high solubilizing ability for lipophilic drugs such as MDA7. Using the compositions described in Table 24, MDA7 was administered to rats by intravenous injection at a dose of 10 mg/kg (250 µL for 150g rat). In the spinal nerve ligation neuropathic pain model, MDA7 in the three different DDS attenuated tactile allodynia (Fig. 33). MDA7 formulated in HPβCD produced a significantly greater antiallodynic effect than that noted with liposomes or with the vehicle. A similar or slightly reduced antiallodynic effect was obtained with MDA7 formulated in micellar preparation (Fig. 33).

Table 24: Composition of the different DDS injected, micellar solution, liposomal preparation and HPβCD inclusion complexes .

Micellar solution	
Entry	**N**
Ingredients	**mg/mL**
MDA7	6.0
NMP	300.0
PG	300.0
EtOH	100.0
CrELP	100.0
PBS qs. 1 mL	194.0

Liposomal preparation	
Entry	**P**
Ingredients	**mg/mL**
MDA7	6.0
DMSO	150.0
DMPC	121.2
Polysorbate 20	6.4
PBS qs. 1 mL	716.4

HPβCD inclusion complexes	
Entry	**Q**
Ingredients	**mg/mL**
MDA7	6.0
HPβCD	156.8
PBS qs. 1 mL	837.2

Significant solubility enhancement was obtained for MDA7 owing to suitable solubilizing properties of the three DDS developed for MDA7 dose of 10 mg/Kg. Although the solubilizing system shouldn't influence the intrinsic PK of the drug, evidences have been reported on the impact of DDS on drugs PK profile by affecting transporters, metabolic enzymes, proteins binding, possibly cytochrome-mediated metabolism and biodistribution[208-210]. MDA7 is lipophilic with a Log P value of 4.54, poorly water soluble (31.8 µM) and moderately protein bound (82.8%)[199]. Excipients modulate protein binding

and cellular partitioning of compounds in blood which is expected to impact the overall drug disposition. The half time life of MDA7 in the plasma is short (0.18 h)[211] and the effect of drug-DDS interactions on unbound fraction may result in better antinociceptive effect.

Cremophor™ELP has been shown to reduce protein binding in plasma, thereby increasing the free drug fraction available to exert its efficacy. However, the micelle component could be expected to disappear because of simple dilution in the plasma below the CMC of the surfactant and the fast release of MDA7. Theoretically, micelles may reform as more dosing product is infused unless surfactant monomer is exposed to metabolic clearance by plasma enzymes as well as interactions with proteins. Considering the equilibrium between monomers and micelles, a combination of the above phenomena may lead to accelerated loss of micelles integrity and release of “free” drug[212]. Micelles represent versatile, easy to prepare and characterize DDS for enabling formulations of lipophilic cannabinoids but may suffer from drug precipitation in addition to significant toxicity after parenteral administration with high solvents concentration, when chronic administration is required.

Lipid excipients such as phosphatydilcholine used to prepare the liposomes are generally considered as safe and have proven to be minimally toxic even in applications where they have been employed at very high concentrations. Liposomal DDS are usually more stable to dilution in contrast to cosolvents-micelles approaches and have a good potential for preventing *in vivo* drug precipitation. Liposomes used for this study were not sterically stabilized and quite rapidly elimination by the immune system (i.e. MPS) was expected[90]. They may not have been circulating long enough for the drug to exert its therapeutic effect and explain the reduced effect of MDA7 prepared in liposomes compared to the two other DDS. Steric stabilization of conventional liposomes using inert hydrophilic polymer (often referred as “stealth” liposomes) has been reported to increase their colloidal stability as well as circumventing MPS uptake and clearance. However, some other authors have reported that conventional liposomes could be more efficient than the pegylated ones[213] or cyclodextrin[214] and address the issue of accelerated clearance of sterically stabilized liposomes upon repeated injection[215].

Complexation by HPβCD can protect MDA7 from metabolism thereby increasing MDA7 plasma concentration.

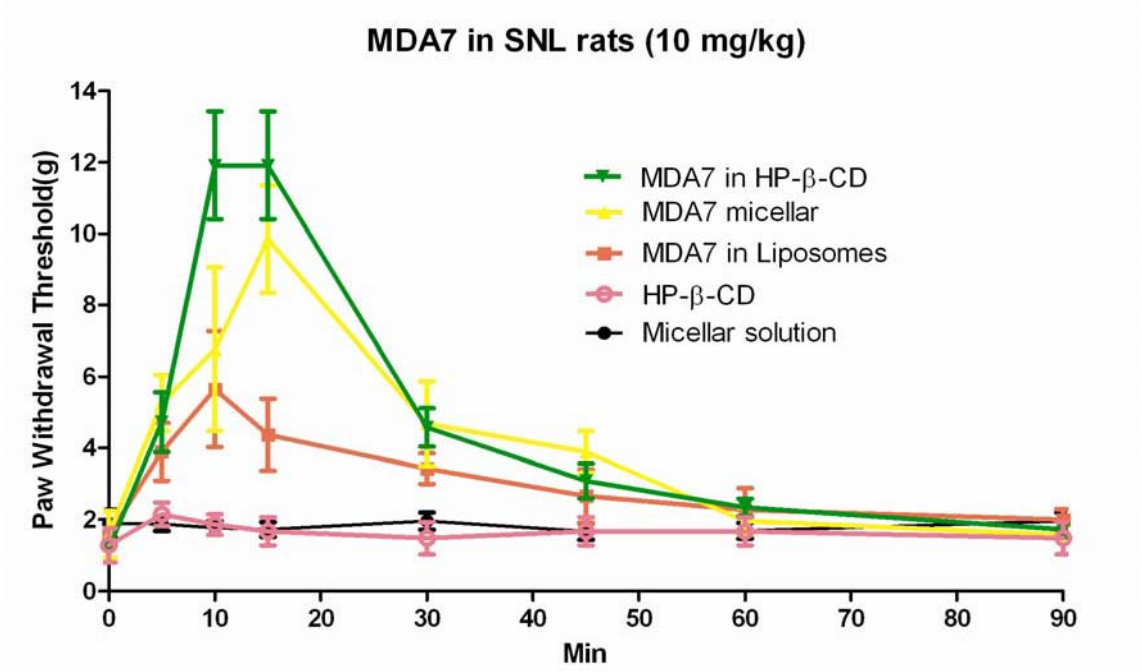

Figure 33: Effects of MDA7 formulated in HPβCD, liposomes and micellar preparation administered by i.v. injection on tactile allodynia in a spinal nerve ligation neuropathic pain model at a dose of 10 mg/kg. MDA7 effects were greatest in HPβCD>liposomes>micellar preparations at increasing the paw withdrawal threshold of the nerve-injured paw. **P<0.01, *P<0.05 versus corresponding vehicle. +P<0.05 versus MDA7 in HPβCD or in micellar preparations (two-way analysis of variance followed by Student-Newman-Keuls multiple comparisons test).

MDA7 exhibited a high affinity constant ($K_{1:1}$= 18 200 M^{-1}) for HPβCD. After parental administration, drugs appear to be rapidly and quantitatively released from CDs inclusion complexes, particularly for *K* value < 10^5 M^{-1} and dilution in the biological fluids. This is a predominant mechanism involved in drug release from the drug-CD complex that continuously forms and dissociates with lifetimes in the range of milliseconds or less[50].

Complexation by HPβCD and aggregates formation, can decrease MDA7 metabolism and renal excretion of the complexes, thereby increasing MDA7 plasma concentration.

Our study has shown that through inclusion complexation and possibly formation of aggregates, HPβCD can enhance the aqueous solubility of lipophilic drugs without compromising their intrinsic ability to permeate biological membranes. Enabling formulation using HPβCD improved antiallodynic effect of the CB2 agonist MDA7 in comparison to incorporation in micellar preparation or liposomes. Biopharmaceutics Classification System (BCS) Class II preclinical drug candidates to treat neuropathic pain such as MDA7 could behave as BCS Class I drug candidates by using HPβCD based

DDS as an early formulation strategy, which would result in an improved bioavailability and an increased *in vivo* efficacy.

2.5.3 Effect of MDA7 administered intraperitoneally on models of nociception in rats.

These studies were conducted following administration to rats (250 µL, average weight: 150 g) of 1-15 mg/kg dose of MDA7 intraperitoneally (i.p.), incorporated in micellar solution composed of 25% w/w PG, 25% w/w NMP, 10% w/w CrELP, qs 1 mL PBS (entry L in Table 14).

2.5.3.1 Effects of MDA7 on thermal nociception in naive rats.

Administration of 1 or 3 mg kg^{-1} of MDA7 i.p. did not block the nociceptive effect of a thermal stimulus applied to the hind paws of naive rats. Increasing the dose of MDA7 to 10 mg kg^{-1} i.p. resulted in a short-lasting antinociceptive effect (Fig. 34).

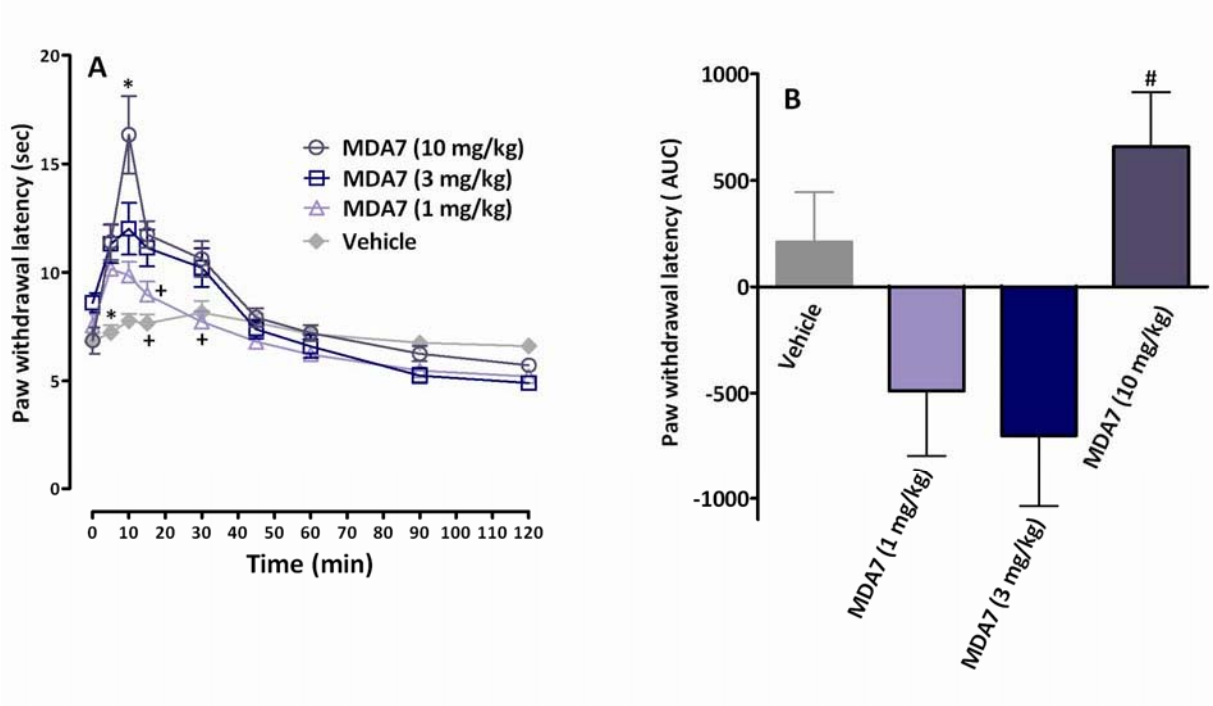

Figure 34: Effects of i.p. administration of MDA7 on the hind paw withdrawal latency in response to noxious heat in naive rats (n=10 per group). (A) The time course of percent maximal possible effect (%MPE) and (B) the area under the curve (AUC) of 1.0, 3.0 and 10 mg kg^{-1} of MDA7 and the vehicle. *P<0.05 compared with other groups. ^{+}P<0.05 compared with 3.0 or 10 mg kg^{-1} of MDA7 and the vehicle (ANOVA followed by Tukey–Kramer test for multiple group comparison). $^{\#}P$<0.05 compared with 1.0 and 3.0 mg kg^{-1} of MDA7 (ANOVA followed by Tukey–Kramer test for multiple group comparison). Each point represents the mean±s.e.mean.

2.5.4 Effects of MDA7 on tactile allodynia in the spinal nerve ligation model of neuropathic pain.

In rats, spinal nerve ligation produced tactile allodynia one week after surgery, as demonstrated by a marked reduction in paw withdrawal threshold to mechanical stimulation with Von Frey filaments (Fig. 35A).

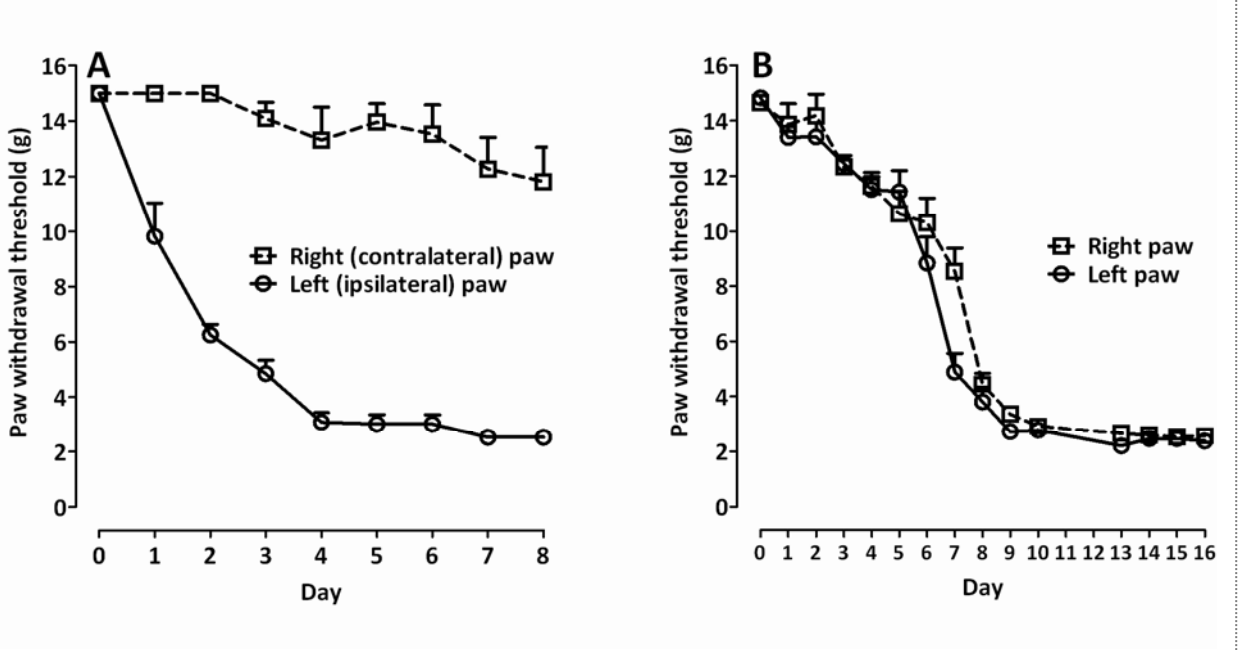

Figure 35. Development of tactile allodynia **A)** after spinal nerve ligation and **B)** after intraperitoneal administration of paclitaxel for 4 days (n = 10 per group). Each point represents the mean ± s.e. mean.

MDA7 (i.p.) attenuated tactile allodynia in a dose-related manner; the ED_{50} was 7.5 $mg.kg^{-1}$ i.p. (95% CI = 5.6–9.9 $mg.kg^{-1}$). The higher doses of MDA7 (10 and 15 $mg.kg^{-1}$) produced a significantly greater antiallodynic effect than that noted with a dose of 5 $mg.kg^{-1}$ (Fig. 36).

The receptor specificity of MDA7 was investigated in this spinal nerve ligation model using receptor-selective antagonists (Fig. 36C). Pretreatment with AM630 (5 $mg.kg^{-1}$ i.p.), a selective CB2 receptor antagonist[216-217] significantly reversed the antiallodynic effects induced by MDA7 (10 $mg.kg^{-1}$ i.p.) ($P<0.001$).

In contrast, pretreatment with AM251 (5 $mg.kg^{-1}$ i.p.), a selective CB1 receptor antagonist[218], did not affect the antiallodynic effects induced by MDA7. The rats treated with CB1 or CB2 receptor antagonists alone at the doses used in these studies exhibited no significant change in paw withdrawal threshold compared with results from the vehicle-treated animals (Fig. 36c). Administration of AM1241 (15 $mg.kg^{-1}$ i.p.), a CB2 ligand (Ibrahim et al., 2003), produced antiallodynic effects that were significantly different ($P<0.001$) from those of the vehicle (Fig. 37).

However, the antiallodynic effects of 10 $mg.kg^{-1}$ of MDA7 i.p. were significantly greater ($P<0.001$) than those that were observed with AM1241.

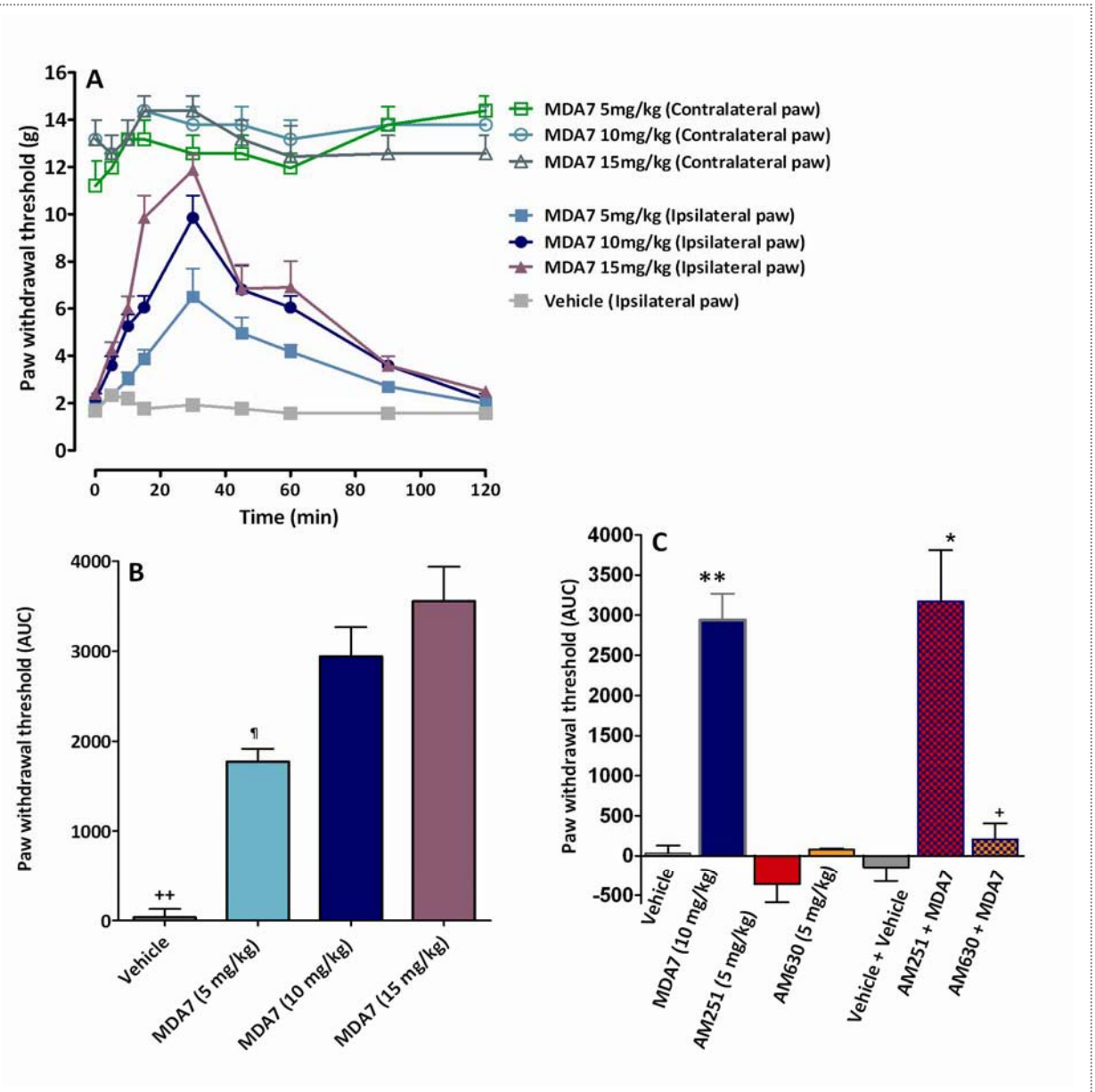

Figure 36. Effects of intraperitoneal administration of MDA7 on hind paw withdrawal latency in response to noxious heat in naïve rats (n = 10 per group). (A) The time course of percent maximal possible effect (%MPE) and (B) the area under the curve (AUC) of 1.0, 3.0, and 10 mg/kg of MDA7 and the vehicle. c) Effects of selective antagonists for CB1 and CB2 receptors on the antiallodynic effects of 10 $mgkg^{-1}$ of MDA7, shown as AUC (n=6 per group). *P<0.05 compared with other groups. +P<0.05 compared with 3.0 or 10 mg/kg of MDA7 and the vehicle (ANOVA). #P<0.05 compared with 1.0 and 3.0 mg/kg of MDA7. Each point represents the mean ± s.e. mean.

The antinociceptive effects of AM1241 have been shown to involve the μ-opioid receptor system and β-endorphin, and to be blocked by administration of the opioid receptor antagonist naloxone or antiserum to b-endorphin[219]. In this study, rats subjected to spinal

nerve ligation were treated with naloxone (10 mg.kg^{-1} i.p.) 15 min before the administration of MDA7. Naloxone pretreatment had no effect on the antiallodynic activity of MDA7 (Fig. 37). However, pretreatment with naloxone significantly reversed the antiallodynic activity of AM1241 (Fig. 37, P<0.01), confirming that the antiallodynic effects of MDA7 were not mediated by μ-opioid receptor-dependent activity.

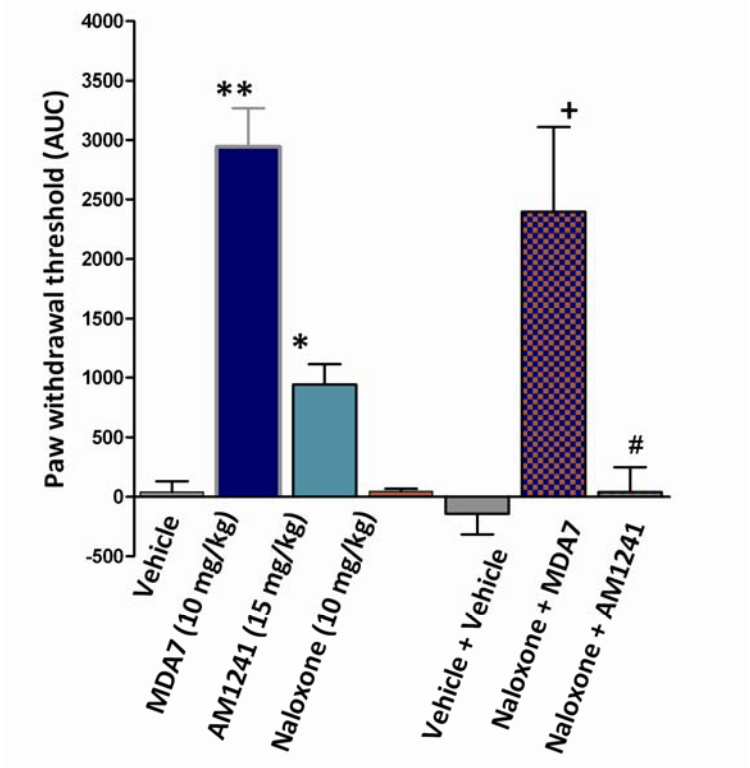

Figure 37. Effects of the opioid receptor antagonist naloxone on MDA7- and AM1241-induced antiallodynic effects in a spinal nerve ligation neuropathic pain model in rats (n = 6 per group). All drugs were administered by intraperitoneal injection. The antiallodynic effects of MDA7 (10 mg/kg) were significantly greater than were those of a CB_2-selective agonist, AM1241 (15 mg/kg). Administration of the opioid antagonist naloxone (10 mg/kg) did not affect the paw withdrawal threshold. Pretreatment with naloxone (10 mg/kg) followed 15 min later by MDA7 (10 mg/kg) (naloxone + MDA7) did not affect the antiallodynic effects of MDA7. In contrast, pretreatment with naloxone (10 mg/kg) followed 15 min later by AM1241 (15 mg/kg) (naloxone + AM1241) reversed the antiallodynic effects of AM1241. $^{**}P<0.001$ compared with vehicle, AM1241, and naloxone. $^{*}P<0.001$ compared with vehicle and naloxone. $^{+}P<0.01$ compared with vehicle + vehicle and naloxone. $^{\#}P<0.01$ compared with AM1241.

2.5.5 Effects of MDA7 on tactile allodynia in a paclitaxel-induced neuropathic pain model.

Tactile allodynia developed in 100% of rats 10 days after the start of paclitaxel administration, as demonstrated by a reduction in paw withdrawal threshold to mechanical stimulation with Von Frey filaments to 2.9±0.19 and 2.8±0.15 g for the right and left paws, respectively (Fig. 35B).

In paclitaxel-treated rats, i.p. administration of MDA7 suppressed mechanical allodynia (Fig. 38) in a dose-dependent manner, as indicated by an increase in %MPE withdrawal threshold AUC and an ED_{50} of 24 $mg.kg^{-1}$. The %MPE for reversing mechanical allodynia, observed at 30 min with 15 $mg.kg^{-1}$ of MDA7, was 42±8.8%.

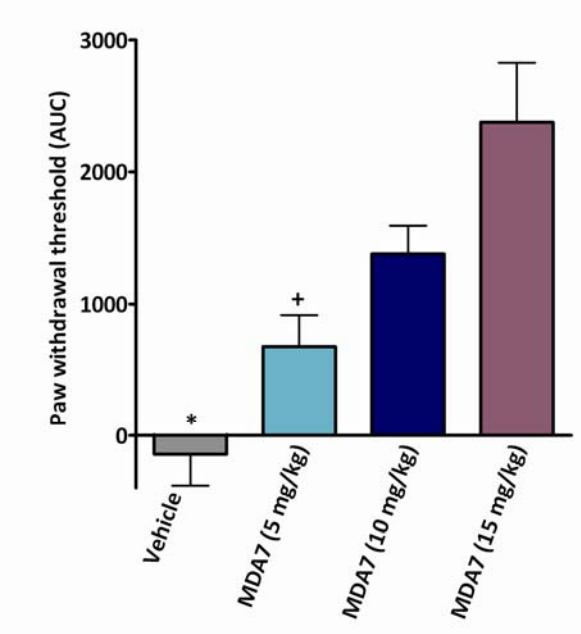

Figure 38: Effects of MDA7 administered by intraperitoneal injection (i.p.) on tactile allodynia in a paclitaxel-induced neuropathic pain model in rats (n = 8 per group). MDA7 dose-dependently attenuated tactile allodynia in this model, as evidence by an increase in the %MPE withdrawal threshold area under the curve (AUC). *$P \leq 0.05$ compared with 10 mg/kg and 15 mg/kg of MDA7. $^{+}P \leq 0.05$ compared with 15 mg/kg of MDA7.

2.5.6 Open-field chamber testing

In contrast to administration of MDA7 (15 mg/kg i.p.), administration of WIN 55,212-2 (7 mg/kg i.p.) and haloperidol (1 mg/kg i.p.) significantly ($P<0.05$) decreased exploratory behavior in rats, as evidenced by a reduction in the total distance traveled (Fig. 39), time spent ambulating (Fig.39B), vertical movements (Fig. 39C), and zone entries (Fig. 39D).

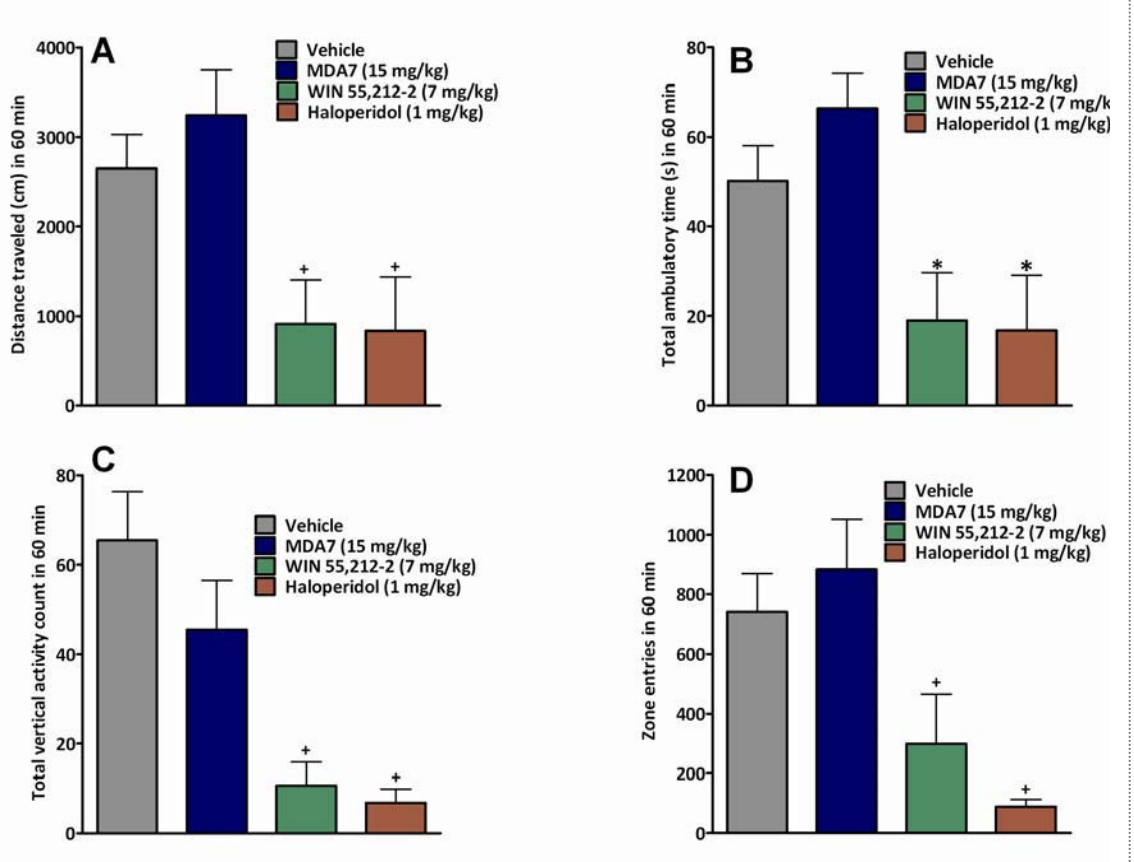

Figure 39: Effect of MDA7 on locomotor activity in rats. Exploratory behaviour was tested in an open-field chamber following i.p. administration of vehicle, MDA7, WIN 55,212-2 or haloperidol (n= 6 per group). The following parameters were scored for 60 min: distance travelled (a), ambulatory time (b), vertical activity (c) and number of zone entries (d). $^{+}$P<0.05 versus vehicle and MDA7 (ANOVA followed by Tukey–Kramer test for multiple group comparison). *P<0.05 versus MDA7 (ANOVA followed by Tukey–Kramer test for multiple group comparison).

2.6 Other cannabinoids evaluated *in vivo*

The same was used to study the effect of other cannabinoids *in vivo*. Studies were conducted following administration to rats (250 µL, average weight: 150 g) of 1-15 mg/kg dose of MDA19 and MDA42 i.p., incorporated in micellar solution composed of 25% w/w PG, 25% w/w NMP, 10% w/w CrELP, qs 1 mL PBS (Entry L in Table 14).

MDA19

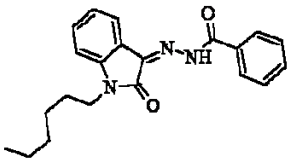

Name	Value	Error
LogP	4.99	0.66
MW	349.43	-
PSA	61.77	-
FRB	7	-
HDonors	1	-
HAcceptors	5	
Rule Of 5	0	-
Calculated intrinsic solubility	1.73 µg/mL	

MDA42

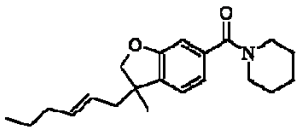

Name	Value	Error
LogP	5.12	0.5
MW	327.46	-
PSA	29.54	-
FRB	5	-
HDonors	0	-
HAcceptors	3	
Rule Of 5	1	-
Calculated intrinsic solubility	7.10 µg/mL	

Figure 40: MDA19 and MDA42 physicochemical properties calculated *in silico* using ACD PhysChem software.

.

In the spinal nerve ligation neuropathic pain model, MDA19 (i.p.) attenuated tactile allodynia in a dose-related manner; the ED50 was 9.1 mg/kg i.p. (95% CI = 6.9-11.8 mg/kg) at 30 min (Fig. 41A and 41B). Analyses of AUCs revealed that the highest doses of MDA19 (15 mg/kg) produced a significantly ($p < 0.01$) greater antiallodynic effect than that noted with a dose of 5 mg/kg or with the vehicle (data not shown). Pretreatment with AM630 (5 mg/kg i.p.), a CB2 receptor–selective antagonist, significantly reversed the antiallodynic effects induced by MDA19 (10 mg/kg i.p.) ($p < 0.05$) (Fig. 41C). The rats treated with CB2 receptor antagonists alone exhibited no significant change in paw withdrawal threshold compared with results in the vehicle-treated animals (Fig. 41C).

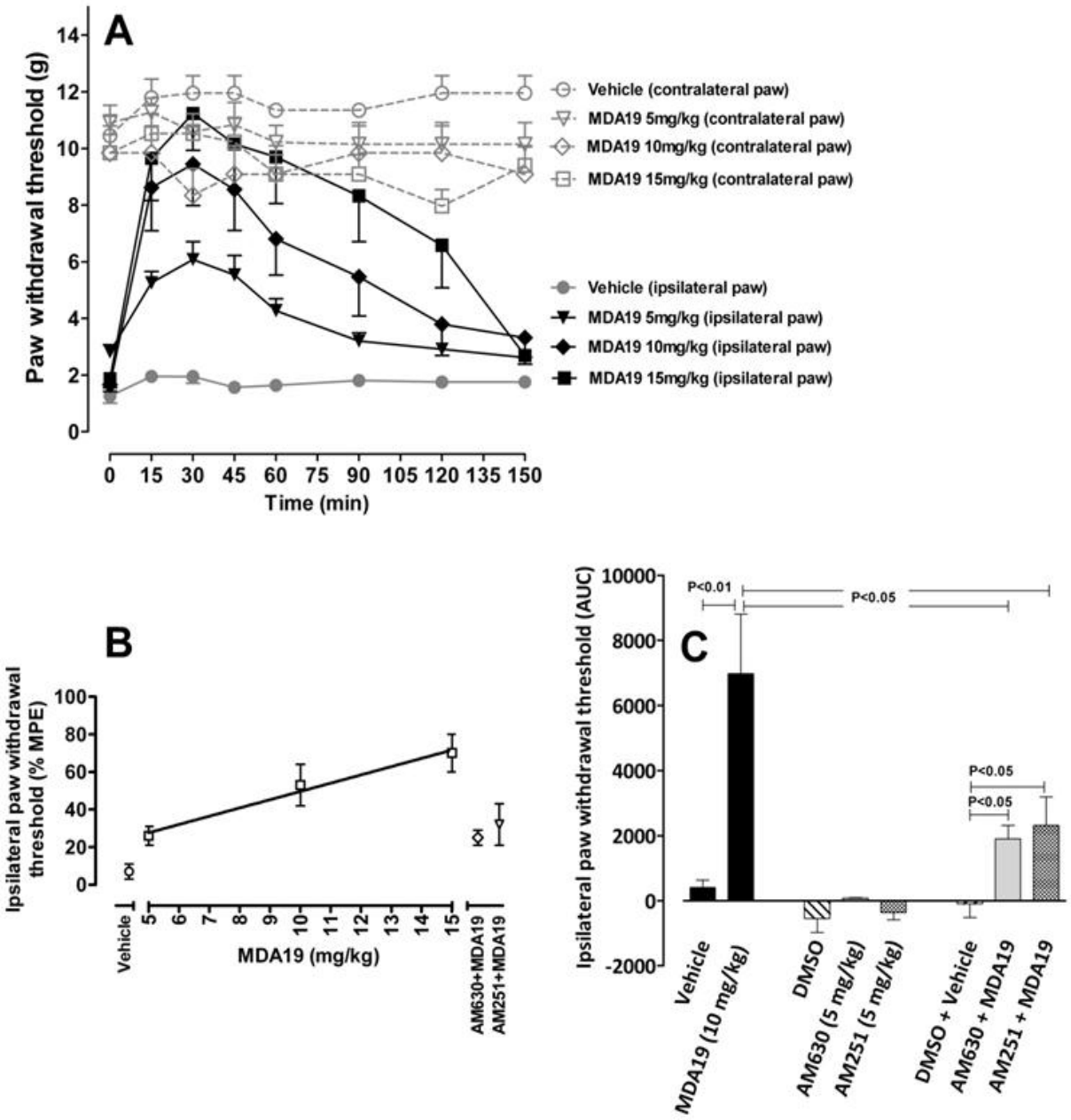

Figure 41. Effects of MDA19 administered by intraperitoneal (i.p.) injection on tactile allodynia in a spinal nerve ligation neuropathic pain model. (A) MDA19 increased the paw withdrawal threshold of the nerve-injured paw in a dose-dependent manner (n = 12 per group). (B) MDA19 attenuated tactile allodynia in a dose-dependent manner (at 30 min, ED50 = 9.1; 95% confidence interval = 6.9-11.8 mg/kg i.p.; n = 12 per group). Data are expressed as mean ± s.e. mean. Vehicle = vehicle used for MDA19. DMSO was the solvent used for other compounds. (C) Effects of CB_2 selective antagonists on the antiallodynic effects of 10 mg/kg of MDA19 in a spinal nerve ligation neuropathic pain model in rats (n = 6 per group). All drugs were administered by i.p. injection. Administration of 5 mg/kg of AM630, a selective CB2 antagonist, had no effect. Administration of 5 mg/kg of AM630 15 min before administration of MDA19 (AM630 + MDA19) reversed the antiallodynic effects of MDA19 ($p < 0.05$). Data are expressed as mean ± s.e. mean. Vehicle = vehicle used for MDA19. DMSO was the solvent used for other compounds.

In paclitaxel-treated rats, intraperitoneal administration of MDA42 (Fig. 42) suppressed mechanical allodynia in a dose-dependent manner.

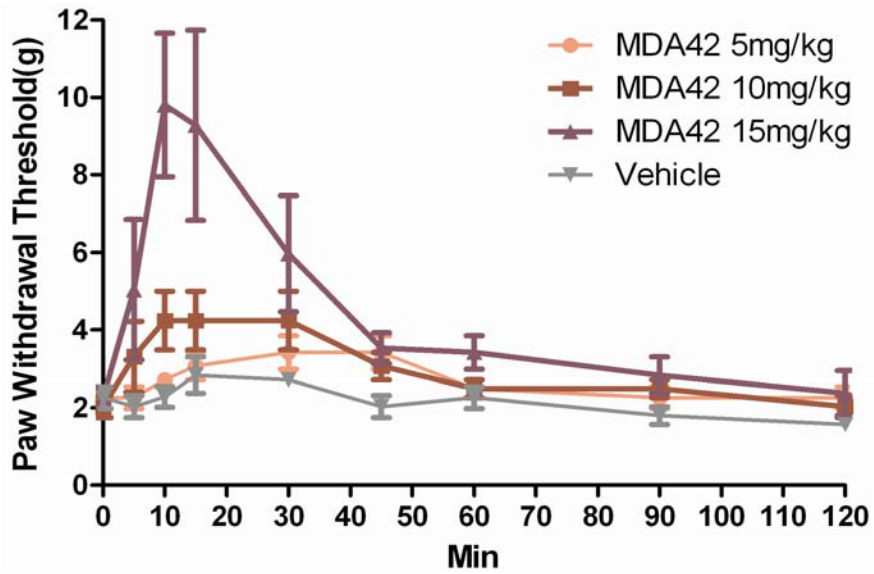

Figure 42. Effects of MDA42 administered by intraperitoneal injection on tactile allodynia in a paclitaxel-induced neuropathic pain model in rats (n = 5-6 per group). MDA42 dose-dependently attenuated tactile allodynia in this model.

3 Summary and Conclusion.

In summary we found that MDA7 formulated in micellar solution was effective in treating various models of neuropathic pain in rats in a dose dependent fashion by activating CB2 receptors without affecting the locomotor behavior of the animals. PK profile study revealed that this novel CB2 agonist was suffering from poor oral bioavailability probably due to low metabolic stability and validated i.v. administration as a preferred route of administration. Despite a short half life, MDA7 accumulates preferentially into the CNS which could be a major advantage to treat neuropathic pain.

Significant solubility enhancement was obtained for MDA7 owing to suitable solubilizing properties of the four DDS developed, namely micellar solution, SEDDS, liposomes and HPβCD and sufficient exposure achieved for MDA7 exerting its *in vivo* activity.

In our specific study comparing the influence of the DDS used on the drug efficacy, we evidenced that DDS alter not only the physicochemical properties of the drug (e.g. solubility, stability) but also its pharmacokinetics (e.g. elimination, metabolic stability). Concepts of enabling formulation and the excipients themselves participate to this effect and their selection should be considered on case by case basis during the process of NCE development. Through inclusion complexation and possibly formation of aggregates, HPβCD improved greatly antiallodynic effect of the CB2 agonist in comparison to incorporation in micellar preparation or liposomes. Biopharmaceutics Classification System (BCS) Class II preclinical drug candidates to treat neuropathic pain such as MDA7 could behave as BCS Class I drug candidates by using HPβCD based DDS as an early formulation strategy, which will results in an improved bioavailability and an increased *in vivo* efficacy. In addition HPβCD DDS are transformable into clinical formulations. Further studies with fluorescent dyes incorporated in the nanocarriers may help evaluating their *in vivo* fate (e.g. integrity, elimination) and subsequently address and overcome *in vivo* delivery of the drug.

In addition, the DDS based on micellar preparation allow us to test different molecules MDA19 and MDA42 *in vivo* with high lipophilicity (>4). They both showed efficacy in *in vivo* model of neuropathic pain confirming the versatility of this vehicle for lipophilic molecules such as cannabinoid ligands. Even though MDA19 and MDA42 exhibit a high lipophilicity, their corresponding PSA values are significantly different. In addition, MDA19 is a planar molecule and MDA42 has a quaternary carbon resulting in a non planar structure. Thus this micellar preparation can be used with molecules exhibiting different chemical architecture.

4 REFERENCES

1. Gad, S. C.; Cassidy, C. D.; Aubert, N.; Spainhour, B.; Robbe, H., Nonclinical vehicle use in studies by multiple routes in multiple species. *International Journal of Toxicology* 2006, 25, (6), 499-521.
2. Gad, S. Vehicles for animal studies. http://www.gadconsulting.com/vehicles.htm
3. Amidon, G. L.; Lennernäs, H.; Shah, V. P.; Crison, J. R., A Theoretical Basis for a Biopharmaceutic Drug Classification: The Correlation of *in vitro* Drug Product Dissolution and *in vivo* Bioavailability. *Pharmaceutical Research* 1995, 12, (3), 413-420.
4. Altan, S. *Issues in Non-Clinical Statistics*; Rutgers university: New Jersey, 2009.
5. Kerns, L. D. a. E. H. *Optimizing the Physicochemical Properties of Clinical Candidates During Drug Discovery*; 2009.
6. Ash, M. a. I., *Handbook of preservatives*. Synapse Information Resources, Inc: NY, 2004.
7. FDA, APPENDIX 6. TOXICOLOGICAL DATA FOR CLASS 3 SOLVENTS. In.
8. Shah, A. K.; Agnihotri, S. A., Recent advances and novel strategies in pre-clinical formulation development: an overview. *J Control Release* 2011, 156, (3), 281-96.
9. ISP *Pharmasolve (N-Methyl-2-Pyrrolidone)*; International Specialty Products: 2000.
10. WHO, W. H. O.-. *N-methyl-2-pyrrolidone - Concise International Chemical Assessment Document 35*; Geneva, 2001.
11. Mottu, F.; Laurent, A.; Rufenacht, D. A.; Doelker, E., Organic solvents for pharmaceutical parenterals and embolic liquids: a review of toxicity data. *PDA J Pharm Sci Technol* 2000, 54, (6), 456-69.
12. Pestel, S.; Martin, H.-J.; Maier, G.-M.; Guth, B., Effect of commonly used vehicles on gastrointestinal, renal, and liver function in rats. *Journal of pharmacological and toxicological methods* 2006, 54, (2), 200-14.
13. GmbH, S. Photon Correlation Spectroscopy. http://www.sympatec.com/EN/PCCS/PCS.html
14. University_Waterloo Research overview - Surfactants. http://science.uwaterloo.ca/~wettig/Research/overview.html
15. Lasic, D. D., *Liposomes in Gene delivery*. Boca Raton, 1997.
16. Higuchi, I., Phase-Solubility Techniques. *Advances in analytical chemistry and instrumentation* 1965, 4, (117).
17. Torchilin, V. P., Recent advances with liposomes as pharmaceutical carriers. *Nature Reviews Drug Discovery* 2005, 4, (2), 145-160.
18. Sattler, K. D., *Handbook of Nanophysics: Nanomedicine and Nanorobotics*. CRC Press: Boca Raton, 2011.
19. Jesorka, A.; Orwar, O., Liposomes: technologies and analytical applications. *Annu Rev Anal Chem (Palo Alto Calif)* 2008, 1, 801-32.
20. Yalkowsky, S. H., *Solubility and Solubilization in Aqueous Media*. Oxford University Press: New York 1999.
21. Strickley, R. G., Solubilizing excipients in oral and injectable formulations. *Pharm Res* 2004, 21, (2), 201-30.
22. Li, P.; Zhao, L., Developing early formulations: Practice and perspective. *International Journal of Pharmaceutics* 2007, 341, (1–2), 1-19.
23. Liu, R., *Water-insoluble drug formulation*. Second edition ed.; CRC Press: Boca Raton, 2008.

24. Li, P.; Zhao, L.; Yalkowsky, S. H., Combined effect of cosolvent and cyclodextrin on solubilization of nonpolar drugs. *J Pharm Sci* 1999, 88, (11), 1107-11.
25. Chang, R. K.; Shojaei, A. H., Effect of hydroxypropyl beta-cyclodextrin on drug solubility in water-propylene glycol mixtures. *Drug Dev Ind Pharm* 2004, 30, (3), 297-302.
26. Kawakami, K.; Miyoshi, K.; Ida, Y., Solubilization behavior of poorly soluble drugs with combined use of Gelucire 44/14 and cosolvent. *Journal of Pharmaceutical Sciences* 2004, 93, (6), 1471-1479.
27. Maas, J.; Kamm, W.; Hauck, G., An integrated early formulation strategy--from hit evaluation to preclinical candidate profiling. *Eur J Pharm Biopharm* 2007, 66, (1), 1-10.
28. Sun, D. X.; Yu, L. X.; Hussain, M. A.; Wall, D. A.; Smith, R. L.; Amidon, G. L., In vitro testing of drug absorption for drug 'developability' assessment: Forming an interface between in vitro preclinical data and clinical outcome. *Curr Opin Drug Disc* 2004, 7, (1), 75-85.
29. Loftsson, T.; Magnusdottir, A.; Masson, M.; Sigurjonsdottir, J. F., Self-association and cyclodextrin solubilization of drugs. *J Pharm Sci* 2002, 91, (11), 2307-16.
30. Loftsson, T.; Masson, M.; Brewster, M. E., Self-association of cyclodextrins and cyclodextrin complexes. *J Pharm Sci* 2004, 93, (5), 1091-9.
31. Messner, M.; Kurkov, S. V.; Jansook, P.; Loftsson, T., Self-assembled cyclodextrin aggregates and nanoparticles. *Int J Pharm* 2010, 387, (1-2), 199-208.
32. Loftsson, T.; Brewster, M. E., Pharmaceutical applications of cyclodextrins. 1. Drug solubilization and stabilization. *J Pharm Sci* 1996, 85, (10), 1017-25.
33. Ozdemir, N.; Erkin, J., Enhancement of dissolution rate and bioavailability of sulfamethoxazole by complexation with beta-cyclodextrin. *Drug Dev Ind Pharm* 2012, 38, (3), 331-40.
34. Bouquet, W.; Ceelen, W.; Adriaens, E.; Almeida, A.; Quinten, T.; De Vos, F.; Pattyn, P.; Peeters, M.; Remon, J. P.; Vervaet, C., In vivo toxicity and bioavailability of Taxol and a paclitaxel/beta-cyclodextrin formulation in a rat model during HIPEC. *Ann Surg Oncol* 2010, 17, (9), 2510-7.
35. Abosehmah-Albidy, A. Z.; York, P.; Wong, V.; Losowsky, M. S.; Chrystyn, H., Improved bioavailability and clinical response in patients with chronic liver disease following the administration of a spironolactone: beta-cyclodextrin complex. *Br J Clin Pharmacol* 1997, 44, (1), 35-9.
36. Ricevuti, G.; Mazzone, A.; Pasotti, D.; Uccelli, E.; Pasquali, F.; Gazzani, G.; Fregnan, G. B., Pharmacokinetics of dipyridamole-beta-cyclodextrin complex in healthy volunteers after single and multiple doses. *Eur J Drug Metab Pharmacokinet* 1991, 16, (3), 197-201.
37. Shulman, M.; Cohen, M.; Soto-Gutierrez, A.; Yagi, H.; Wang, H.; Goldwasser, J.; Lee-Parsons, C. W.; Benny-Ratsaby, O.; Yarmush, M. L.; Nahmias, Y., Enhancement of naringenin bioavailability by complexation with hydroxypropoyl-beta-cyclodextrin. *PLoS One* 2011, 6, (4), e18033.
38. Loftsson, T.; Brewster, M. E., Pharmaceutical applications of cyclodextrins: effects on drug permeation through biological membranes. *J Pharm Pharmacol* 2011, 63, (9), 1119-35.
39. Nakanishi, K.; Masukawa, T.; Nadai, T.; Yoshii, K.; Okada, S.; Miyajima, K., Sustained release of flufenamic acid from a drug-triacetyl-beta-cyclodextrin complex. *Biological & Pharmaceutical Bulletin* 1997, 20, (1), 66-70.

40. Palem, C. R.; Battu, S. K.; Gannu, R.; Yamsani, V. V.; Repka, M. A.; Yamsani, M. R., Role of cyclodextrin complexation in felodipine-sustained release matrix tablets intended for oral transmucosal delivery: In vitro and ex vivo characterization. *Pharm Dev Technol* 2011.
41. Hirayama, F.; Hirashima, N.; Abe, K.; Uekama, K.; Ijitsu, T.; Ueno, M., Utilization of diethyl-beta-cyclodextrin as a sustained-release carrier for isosorbide dinitrate. *J Pharm Sci* 1988, 77, (3), 233-6.
42. Park, J. H.; Choi, K. H.; Kwak, H. S., Single- and 14-Day Repeat-Dose Toxicity of Cross-Linked beta-Cyclodextrin in Rats. *Int J Toxicol* 2011, 30, (6), 700-6.
43. Lina, B. A.; Bar, A., Subchronic oral toxicity studies with alpha-cyclodextrin in rats. *Regul Toxicol Pharmacol* 2004, 39 Suppl 1, S14-26.
44. Brewster, M. E.; Loftsson, T., Cyclodextrins as pharmaceutical solubilizers. *Advanced Drug Delivery Reviews* 2007, 59, (7), 645-66.
45. Ribeiro-Rama, A. C.; Figueiredo, I. V.; Veiga, F.; Castel-Branco, M. M.; Cabrita, A. M.; Caramona, M. M., Evaluation of gastric toxicity of indomethacin acid, salt form and complexed forms with hydroxypropyl-beta-cyclodextrin on Wistar rats: histopathologic analysis. *Fundam Clin Pharmacol* 2009, 23, (6), 747-55.
46. Szejtli, J., Medicinal applications of cyclodextrins. *Med Res Rev* 1994, 14, (3), 353-86.
47. Sabadini, E.; Cosgrove, T.; Egidio Fdo, C., Solubility of cyclomaltooligosaccharides (cyclodextrins) in H2O and D2O: a comparative study. *Carbohydr Res* 2006, 341, (2), 270-4.
48. Dodziuk, H., *Cyclodextrins and their complexes: chemistry, analytical methods, applications*. Wiley-VCH: 2006.
49. Loftsson, T.; Brewster, M. E., Pharmaceutical applications of cyclodextrins: basic science and product development. *Journal of Pharmacy and Pharmacology* 2010, 62, (11), 1607-1621.
50. Stella, V. J.; Rao, V. M.; Zannou, E. A.; Zia, V., Mechanisms of drug release from cyclodextrin complexes. *Advanced Drug Delivery Reviews* 1999, 36, (1), 3-16.
51. Tabushi, I., Cyclodextrin Catalysis as a Model for Enzyme Action. *Accounts Chem Res* 1982, 15, (3), 66-72.
52. Szejtli, J., *Cyclodextrin Technology*. Kluwer: Dordrecht, 1988.
53. Chadha, R.; Kashid, N.; Saini, A., Account of analytical techniques employed for the determination of thermodynamics of inclusion complexation of drugs with cyclodextrins. *J Sci Ind Res India* 2004, 63, (3), 211-229.
54. Stella, V. J.; He, Q., Cyclodextrins. *Toxicologic Pathology* 2008, 36, (1), 30-42.
55. Loftsson, T.; Hreinsdóttir, D.; Másson, M., Evaluation of cyclodextrin solubilization of drugs. *International Journal of Pharmaceutics* 2005, 302, (1–2), 18-28.
56. Job, P., Formation and stability of inorganic complexes in solution. *Annali di Chimica Applicata* 1928, (9), 113-203
57. Cabrer, P. R.; Azvarez-Parrilla, E.; Meijide, F.; Seijas, J. A.; Nunez, E. R.; Tato, J. V., Complexation of sodium cholate and sodium deoxycholate by beta-cyclodextrin and derivatives. *Langmuir* 1999, 15, (17), 5489-5495.
58. Ramstad, T.; Hadden, C. E.; Martin, G. E.; Speaker, S. M.; Teagarden, D. L.; Thamann, T. J., Determination by NMR of the binding constant for the molecular complex between alprostadil and alpha-cyclodextrin. Implications for a freeze-dried formulation. *Int J Pharm* 2005, 296, (1-2), 55-63.

59. Steffan, B.; Fischer, W.; Cordes, G.; Habon, I.; Muller, R., 1H-nuclear magnetic resonance (NMR) studies on the inclusion complex of prostaglandin E1 (PGE1) with alpha-cyclodextrin. *Pharmaceutical Research* 1992, 9, (4), 575-7.
60. Fielding, L.; McKellar, S. C.; Florence, A. J., Precision studies in supramolecular chemistry: a 1H NMR study of hydroxymethoxyacetophenone/beta-cyclodextrin complexes. *Magn Reson Chem* 2011, 49, (7), 405-12.
61. Bernini, A.; Spiga, O.; Ciutti, A.; Scarselli, M.; Bottoni, G.; Mascagni, P.; Niccolai, N., NMR studies of the inclusion complex between beta-cyclodextrin and paroxetine. *Eur J Pharm Sci* 2004, 22, (5), 445-50.
62. Cramer, F.; Saenger, W.; Spatz, H. C., Inclusion Compounds. XIX.1a The Formation of Inclusion Compounds of α-Cyclodextrin in Aqueous Solutions. Thermodynamics and Kinetics. *Journal of the American Chemical Society* 1967, 89, (1), 14-20.
63. Connors, K. A., *Binding Constants. The Measurements of Molecular Complex stability*. Wiley: New York, 1987; p 189-192.
64. Figueiras, A.; Sarraguça, J.; Carvalho, R.; Pais, A.; Veiga, F., Interaction of Omeprazole with a Methylated Derivative of β-Cyclodextrin: Phase Solubility, NMR Spectroscopy and Molecular Simulation. *Pharmaceutical Research* 2007, 24, (2), 377-389.
65. Hazekamp, A.; Verpoorte, R., Structure elucidation of the tetrahydrocannabinol complex with randomly methylated β-cyclodextrin. *European Journal of Pharmaceutical Sciences* 2006, 29, (5), 340-347.
66. Gabelica, V.; Galic, N.; De Pauw, E., On the specificity of cyclodextrin complexes detected by electrospray mass spectrometry. *J Am Soc Mass Spectrom* 2002, 13, (8), 946-53.
67. Smith, R. D.; Light-Wahl, K. J., The observation of non-covalent interactions in solution by electrospray ionization mass spectrometry: Promise, pitfalls and prognosis. *Biological Mass Spectrometry* 1993, 22, (9), 493-501.
68. Schalley, C. A., Supramolecular chemistry goes gas phase: the mass spectrometric examination of noncovalent interactions in host–guest chemistry and molecular recognition. *International Journal of Mass Spectrometry* 2000, 194, (1), 11-39.
69. Loftsson, T.; Masson, M.; Sigurjonsdottir, J. F., Methods to enhance the complexation efficiency of cyclodextrins. *Stp Pharma Sci* 1999, 9, (3), 237-242.
70. Jansook, P.; Kurkov, S. V.; Loftsson, T., Cyclodextrins as solubilizers: Formation of complex aggregates. *Journal of Pharmaceutical Sciences* 2010, 99, (2), 719-729.
71. He, Y.; Fu, P.; Shen, X.; Gao, H., Cyclodextrin-based aggregates and characterization by microscopy. *Micron* 2008, 39, (5), 495-516.
72. Ghosh, P.; Maity, A.; Das, T.; Dash, J.; Purkayastha, P., Modulation of Small Molecule Induced Architecture of Cyclodextrin Aggregation by Guest Structure and Host Size. *The Journal of Physical Chemistry C* 2011, 115, (43), 20970-20977.
73. Ghosh, A.; Biswas, S.; Ghosh, T., Preparation and Evaluation of Silymarin beta-cyclodextrin Molecular Inclusion Complexes. *J Young Pharm* 2011, 3, (3), 205-10.
74. Van Hees, T.; Piel, G.; Evrard, B.; Otte, X.; Thunus, L.; Delattre, L., Application of supercritical carbon dioxide for the preparation of a piroxicam-beta-cyclodextrin inclusion compound. *Pharm Res* 1999, 16, (12), 1864-70.
75. Charoenchaitrakool, M.; Dehghani, F.; Foster, N. R., Utilization of supercritical carbon dioxide for complex formation of ibuprofen and methyl-beta-cyclodextrin. *Int J Pharm* 2002, 239, (1-2), 103-12.

76. Hussein, K.; Turk, M.; Wahl, M. A., Comparative evaluation of ibuprofen/beta-cyclodextrin complexes obtained by supercritical carbon dioxide and other conventional methods. *Pharmaceutical Research* 2007, 24, (3), 585-592.
77. Shimpi, S.; Chauhan, B.; Shimpi, P., Cyclodextrins: application in different routes of drug administration. *Acta Pharm* 2005, 55, (2), 139-56.
78. Gould, S.; Scott, R. C., 2-hydroxypropyl-beta-cyclodextrin (HP-beta-CD): A toxicology review. *Food and Chemical Toxicology* 2005, 43, (10), 1451-1459.
79. de Repentigny, L.; Ratelle, J.; Leclerc, J.-M.; Cornu, G.; Sokal, É. M.; Jacqmin, P.; de Beule, K., Repeated-Dose Pharmacokinetics of an Oral Solution of Itraconazole in Infants and Children. *Antimicrobial Agents and Chemotherapy* 1998, 42, (2), 404-408.
80. Stevens, D. A., Itraconazole in cyclodextrin solution. *Pharmacotherapy* 1999, 19, (5), 603-611.
81. Janssen-Cilag Sporanox I.V. 10 mg/ml concentrate and solvent for solution for infusion.
82. Irie, T.; Uekama, K., Pharmaceutical applications of cyclodextrins .3. Toxicological issues and safety evaluation. *Journal of Pharmaceutical Sciences* 1997, 86, (2), 147-162.
83. Thompson, D. O., Cyclodextrins--enabling excipients: their present and future use in pharmaceuticals. *Crit Rev Ther Drug Carrier Syst* 1997, 14, (1), 1-104.
84. Challa, R.; Ahuja, A.; Ali, J.; Khar, R. K., Cyclodextrins in drug delivery: an updated review. *Aaps Pharmscitech* 2005, 6, (2), E329-57.
85. Irache, J. M.; Esparza, I.; Gamazo, C.; Agueros, M.; Espuelas, S., Nanomedicine: novel approaches in human and veterinary therapeutics. *Vet Parasitol* 2011, 180, (1-2), 47-71.
86. Lasic, D. D., The mechanism of vesicle formation. *Biochem J* 1988, 256, (1), 1-11.
87. Lasic, D. D., A General-Model of Vesicle Formation. *Journal of Theoretical Biology* 1987, 124, (1), 35-41.
88. Fromherz, P., Lipid-Vesicle Structure - Size Control by Edge-Active Agents. *Chem Phys Lett* 1983, 94, (3), 259-266.
89. Hickey, H. D. C. S. A. J., Controlled Pulmonary Delivery. In Controlled Release Society: 2011.
90. Drummond, D. C.; Meyer, O.; Hong, K.; Kirpotin, D. B.; Papahadjopoulos, D., Optimizing liposomes for delivery of chemotherapeutic agents to solid tumors. *Pharmacol Rev* 1999, 51, (4), 691-743.
91. Song, G.; Wu, H.; Yoshino, K.; Zamboni, W. C., Factors affecting the pharmacokinetics and pharmacodynamics of liposomal drugs. *Journal of Liposome Research* 2012, 0, (0), 1-16.
92. Vemuri, S.; Rhodes, C. T., Preparation and characterization of liposomes as therapeutic delivery systems: a review. *Pharmaceutica acta Helvetiae* 1995, 70, (2), 95-111.
93. Weiner, N.; Martin, F.; Riaz, M., Liposomes as a Drug Delivery System. *Drug Development and Industrial Pharmacy* 1989, 15, (10), 1523-1554.
94. Saito, H.; Shinoda, W., Cholesterol Effect on Water Permeability through DPPC and PSM Lipid Bilayers: A Molecular Dynamics Study. *The Journal of Physical Chemistry B* 2011, 115, (51), 15241-15250.
95. Webb, M. S.; Harasym, T. O.; Masin, D.; Bally, M. B.; Mayer, L. D., Sphingomyelin-cholesterol liposomes significantly enhance the pharmacokinetic and therapeutic

properties of vincristine in murine and human tumour models. *Br J Cancer* 1995, 72, (4), 896-904.
96. Bista, R. K.; Bruch, R. F., Near-infrared spectroscopy of newly developed PEGylated lipids. *Spectrochim Acta A Mol Biomol Spectrosc* 2008, 71, (2), 410-6.
97. Maeda, H.; Bharate, G. Y.; Daruwalla, J., Polymeric drugs for efficient tumor-targeted drug delivery based on EPR-effect. *Eur J Pharm Biopharm* 2009, 71, (3), 409-19.
98. Gabizon, A. A., Pegylated liposomal doxorubicin: Metamorphosis of an old drug into a new form of chemotherapy. *Cancer Investigation* 2001, 19, (4), 424-436.
99. Gabizon, A.; Catane, R.; Uziely, B.; Kaufman, B.; Safra, T.; Cohen, R.; Martin, F.; Huang, A.; Barenholz, Y., Prolonged circulation time and enhanced accumulation in malignant exudates of doxorubicin encapsulated in polyethylene-glycol coated liposomes. *Cancer Res* 1994, 54, (4), 987-92.
100. Meure, L. A.; Foster, N. R.; Dehghani, F., Conventional and dense gas techniques for the production of liposomes: a review. *Aaps Pharmscitech* 2008, 9, (3), 798-809.
101. Samad, A.; Sultana, Y.; Aqil, M., Liposomal drug delivery systems: an update review. *Curr Drug Deliv* 2007, 4, (4), 297-305.
102. Berger, N.; Sachse, A.; Bender, J.; Schubert, R.; Brandl, M., Filter extrusion of liposomes using different devices: comparison of liposome size, encapsulation efficiency, and process characteristics. *International Journal of Pharmaceutics* 2001, 223, (1-2), 55-68.
103. Torchilin, V. P., *Liposomes : a practical approach*. Oxford University Press: Oxford, 2003.
104. Jones, M. C.; Leroux, J. C., Polymeric micelles - a new generation of colloidal drug carriers. *Eur J Pharm Biopharm* 1999, 48, (2), 101-111.
105. Matsumura, Y., Micelle carrier system in clinical trial. *Nihon Rinsho* 2006, 64, (2), 316-21.
106. Kim, S.; Shi, Y.; Kim, J. Y.; Park, K.; Cheng, J. X., Overcoming the barriers in micellar drug delivery: loading efficiency, in vivo stability, and micelle-cell interaction. *Expert Opin Drug Deliv* 2010, 7, (1), 49-62.
107. Sakai, H.; Aikawa, S.; Matsuda, W.; Ohmori, T.; Fukukita, Y.; Tezuka, Y.; Matsumura, A.; Torigoe, K.; Tsuchiya, K.; Arimitsu, K.; Sakamoto, K.; Sakai, K.; Abe, M., A cinnamic acid-type photo-cleavable surfactant. *J Colloid Interface Sci* 2012, 376, (1), 160-4.
108. Torchilin, V. P., Micellar nanocarriers: pharmaceutical perspectives. *Pharm Res* 2007, 24, (1), 1-16.
109. Lazaridis, T.; Mallik, B.; Chen, Y., Implicit solvent simulations of DPC micelle formation. *J Phys Chem B* 2005, 109, (31), 15098-106.
110. Moroi, Y.; Matuura, R., Thermodynamics of Solubilization into Surfactant Micelles - Effect of Hydrophobicity of Both Solubilizate and Surfactant Molecules. *J Colloid Interf Sci* 1988, 125, (2), 456-462.
111. Velinova, M.; Sengupta, D.; Tadjer, A. V.; Marrink, S. J., Sphere-to-rod transitions of nonionic surfactant micelles in aqueous solution modeled by molecular dynamics simulations. *Langmuir* 2011, 27, (23), 14071-7.
112. Rangel-Yagui, C. O.; Pessoa, A., Jr.; Tavares, L. C., Micellar solubilization of drugs. *J Pharm Pharm Sci* 2005, 8, (2), 147-65.
113. Vladimir P, T., Structure and design of polymeric surfactant-based drug delivery systems. *Journal of Controlled Release* 2001, 73, (2–3), 137-172.

114. Jusufi, A.; Sanders, S.; Klein, M. L.; Panagiotopoulos, A. Z., Implicit-Solvent Models for Micellization: Nonionic Surfactants and Temperature-Dependent Properties. *The Journal of Physical Chemistry B* 2011, 115, (5), 990-1001.
115. Schick, M. J., Effect of temperature on the critical micelle concentration of nonionic detergents. Thermodynamic of micelle formation 1. *The Journal of Physical Chemistry* 1963, 67, (9), 1796-1799.
116. Becher, P.; Trifiletti, S. E., Nonionic surface-active agents: XII. The effect of solvent on the thermodynamics of micellization. *J Colloid Interf Sci* 1973, 43, (2), 485-490.
117. Shono, Y.; Nishihara, H.; Matsuda, Y.; Furukawa, S.; Okada, N.; Fujita, T.; Yamamoto, A., Modulation of intestinal P-glycoprotein function by cremophor EL and other surfactants by an in vitro diffusion chamber method using the isolated rat intestinal membranes. *Journal of Pharmaceutical Sciences* 2004, 93, (4), 877-885.
118. Webster, L. K.; Cosson, E. J.; Stokes, K. H.; Millward, M. J., Effect of the paclitaxel vehicle, Cremophor EL, on the pharmacokinetics of doxorubicin and doxorubicinol in mice. *Br J Cancer* 1996, 73, (4), 522-4.
119. Hugger, E. D.; Novak, B. L.; Burton, P. S.; Audus, K. L.; Borchardt, R. T., A comparison of commonly used polyethoxylated pharmaceutical excipients on their ability to inhibit P-glycoprotein activity in vitro. *Journal of Pharmaceutical Sciences* 2002, 91, (9), 1991-2002.
120. Sinicrope, F. A.; Dudeja, P. K.; Bissonnette, B. M.; Safa, A. R.; Brasitus, T. A., Modulation of P-Glycoprotein-Mediated Drug Transport by Alterations in Lipid Fluidity of Rat-Liver Canalicular Membrane-Vesicles. *Journal of Biological Chemistry* 1992, 267, (35), 24995-25002.
121. Chervinsky, D. S.; Brecher, M. L.; Baker, R. M.; Hoelcle, M. J.; Tebbi, C. K., Reversal of C1300 murine neuroblastoma multidrug resistance by cremophorEL, a solvent for cyclosporin A. *Cancer Biother* 1993, 8, (1), 67-75.
122. Whitehead, K.; Mitragotri, S., Mechanistic analysis of chemical permeation enhancers for oral drug delivery. *Pharmaceutical Research* 2008, 25, (6), 1412-1419.
123. Narang, A. S.; Delmarre, D.; Gao, D., Stable drug encapsulation in micelles and microemulsions. *Int J Pharm* 2007, 345, (1-2), 9-25.
124. Li, A.; Yalkowsky, S. H., Predicting cosolvency based on the log-linear module. *Abstr Pap Am Chem S* 1998, 216, U805-U805.
125. Miyako, Y.; Khalef, N.; Matsuzaki, K.; Pinal, R., Solubility enhancement of hydrophobic compounds by cosolvents: role of solute hydrophobicity on the solubilization effect. *Int J Pharm* 2010, 393, (1-2), 48-54.
126. Jouyban, A., Review of the cosolvency models for predicting solubility of drugs in water-cosolvent mixtures. *J Pharm Pharm Sci* 2008, 11, (1), 32-58.
127. Alvarez-Nunez, F. A.; Yalkowsky, S. H., Relationship between Polysorbate 80 solubilization descriptors and octanol-water partition coefficients of drugs. *International Journal of Pharmaceutics* 2000, 200, (2), 217-222.
128. Atwood D., F. A. T., *Surfactants systems: Their chemistry, pharmacy and biology.* Chapman and Hall: New York, 1983.
129. Kawakami, K.; Oda, N.; Miyoshi, K.; Funaki, T.; Ida, Y., Solubilization behavior of a poorly soluble drug under combined use of surfactants and cosolvents. *European Journal of Pharmaceutical Sciences* 2006, 28, (1–2), 7-14.
130. Sarkar, B.; Lam, S.; Alexandridis, P., Micellization of Alkyl-Propoxy-Ethoxylate Surfactants in Water−Polar Organic Solvent Mixtures. *Langmuir* 2010, 26, (13), 10532-10540.

131. D'Errico, G.; Ciccarelli, D.; Ortona, O., Effect of glycerol on micelle formation by ionic and nonionic surfactants at 25 °C. *J Colloid Interf Sci* 2005, 286, (2), 747-754.
132. Lindman, W., Micelles, amphiphile aggregation in aqueous solution. *Topics in Current Chemistry.* 1980, 87, 1-83.
133. Christie, R. J.; Grainger, D. W., Design strategies to improve soluble macromolecular delivery constructs. *Adv Drug Deliv Rev* 2003, 55, (3), 421-37.
134. Hubbell, J. A., Materials science. Enhancing drug function. *Science* 2003, 300, (5619), 595-6.
135. Hillaireau, H.; Couvreur, P., Nanocarriers' entry into the cell: relevance to drug delivery. *Cellular and Molecular Life Sciences* 2009, 66, (17), 2873-2896.
136. Dahan, A.; Miller, J. M.; Amidon, G. L., Prediction of Solubility and Permeability Class Membership: Provisional BCS Classification of the World's Top Oral Drugs. *Aaps Journal* 2009, 11, (4), 740-746.
137. Wang, Y.; Sun, J.; Zhang, T.; Liu, H.; He, F.; He, Z., Enhanced oral bioavailability of tacrolimus in rats by self-microemulsifying drug delivery systems. *Drug Dev Ind Pharm* 2011, 37, (10), 1225-30.
138. Mohsin, K.; Long, M. A.; Pouton, C. W., Design of Lipid-Based Formulations for Oral Administration of Poorly Water-Soluble Drugs: Precipitation of Drug after Dispersion of Formulations in Aqueous Solution. *Journal of Pharmaceutical Sciences* 2009, 98, (10), 3582-3595.
139. Patel, J.; Patel, A.; Raval, M.; Sheth, N., Formulation and development of a self-nanoemulsifying drug delivery system of irbesartan. *J Adv Pharm Technol Res* 2011, 2, (1), 9-16.
140. Venkatesh, G.; Majid, M. I.; Mansor, S. M.; Nair, N. K.; Croft, S. L.; Navaratnam, V., In vitro and in vivo evaluation of self-microemulsifying drug delivery system of buparvaquone. *Drug Dev Ind Pharm* 2010, 36, (6), 735-45.
141. Pouton, C. W., Formulation of poorly water-soluble drugs for oral administration: Physicochemical and physiological issues and the lipid formulation classification system. *European Journal of Pharmaceutical Sciences* 2006, 29, (3–4), 278-287.
142. Pouton, C. W.; Porter, C. J. H., Formulation of lipid-based delivery systems for oral administration: Materials, methods and strategies. *Advanced Drug Delivery Reviews* 2008, 60, (6), 625-637.
143. Ritesh B. Patel, R. P. P., Madhabhai M. Patel, Self-Emulsifying Drug Delivery Systems. In *Pharmaceutical Technology*, Advanstar Communications, Inc. : 2008.
144. Pouton, C. W., Lipid formulations for oral administration of drugs: non-emulsifying, self-emulsifying and 'self-microemulsifying' drug delivery systems. *European Journal of Pharmaceutical Sciences* 2000, 11, Supplement 2, (0), S93-S98.
145. Hetal, K. V.; Vasant, K. D., A review on self emulsifying drug delivery system. *International Journal of Pharmaceutical and Chemical Sciences* 2012, 1, (1), 353-359.
146. Gursoy, R. N.; Benita, S., Self-emulsifying drug delivery systems (SEDDS) for improved oral delivery of lipophilic drugs. *Biomed Pharmacother* 2004, 58, (3), 173-82.
147. Reiss, H., Entropy-Induced Dispersion of Bulk Liquids. *J Colloid Interf Sci* 1975, 53, (1), 61-70.
148. Ajay, K.; Surabhi, S.; Ravindra, K., Self emulsifying drug delivery system (SEDDS): Future aspects. *International Journal of Pharmacy and Pharmaceutical Sciences* 2010, 2, (4).

149. Balakrishnan, P.; Lee, B. J.; Oh, D. H.; Kim, J. O.; Lee, Y. I.; Kim, D. D.; Jee, J. P.; Lee, Y. B.; Woo, J. S.; Yong, C. S.; Choi, H. G., Enhanced oral bioavailability of Coenzyme Q10 by self-emulsifying drug delivery systems. *Int J Pharm* 2009, 374, (1-2), 66-72.
150. Fatouros, D. G.; Karpf, D. M.; Nielsen, F. S.; Mullertz, A., Clinical studies with oral lipid based formulations of poorly soluble compounds. *Ther Clin Risk Manag* 2007, 3, (4), 591-604.
151. Sha, X.; Yan, G.; Wu, Y.; Li, J.; Fang, X., Effect of self-microemulsifying drug delivery systems containing Labrasol on tight junctions in Caco-2 cells. *European Journal of Pharmaceutical Sciences* 2005, 24, (5), 477-486.
152. Cornaire, G.; Woodley, J.; Hermann, P.; Cloarec, A.; Arellano, C.; Houin, G., Impact of excipients on the absorption of P-glycoprotein substrates in vitro and in vivo. *International Journal of Pharmaceutics* 2004, 278, (1), 119-131.
153. Kale, A. A.; Patravale, V. B., Design and evaluation of self-emulsifying drug delivery systems (SEDDS) of nimodipine. *Aaps Pharmscitech* 2008, 9, (1), 191-6.
154. Paton, R. G. P. D. T. W. D. M., *The general pharmacology of cannabinoids*. Oxford University Press: London, 1972; p 50-75.
155. Faller, B.; Ertl, P., Computational approaches to determine drug solubility. *Advanced Drug Delivery Reviews* 2007, 59, (7), 533-545.
156. Basavaraj K. Nanjwade*, G. K. D., Hiren M. Bechra, Veerendra K. Nanjwade and F.V. Manvi, Design and Characterization of Nanocrystals of Lovastatin for Solubility and Dissolution Enhancement. *J Nanomedic Nanotechnol* 2011, 2, (107).
157. FDA, Guidance for Industry, Waiver of in vivo bioavailability and bioequivalence studies for immediate-release solid oral dosage forms based on a biopharmaceutics classification system. In 2000.
158. Yan, B., *Analysis and Purification Methods in Combinatorial Chemistry*. Wiley-Intersciences: New Jersey, 2004.
159. Diaz, P.; Phatak, S. S.; Xu, J. J.; Fronczek, F. R.; Astruc-Diaz, F.; Thompson, C. M.; Cavasotto, C. N.; Naguib, M., 2,3-Dihydro-1-Benzofuran Derivatives as a Series of Potent Selective Cannabinoid Receptor 2 Agonists: Design, Synthesis, and Binding Mode Prediction through Ligand-Steered Modeling. *ChemMedChem* 2009, 4, (10), 1615-1629.
160. Lee, Y.-C.; Zocharski, P. D.; Samas, B., An intravenous formulation decision tree for discovery compound formulation development. *International Journal of Pharmaceutics* 2003, 253, (1–2), 111-119.
161. Cavas, M.; Beltran, D.; Navarro, J. F., Behavioural effects of dimethyl sulfoxide (DMSO): changes in sleep architecture in rats. *Toxicol Lett* 2005, 157, (3), 221-32.
162. M. Steven Evans, a., Kenneth H. Reid,b, and James B. Sharp Jr.c, Dimethyl Sulfoxide (DMSO) Blocks Conduction in Peripheral Nerve C Fibers: a Possible Mechanism of Analgesia *Neuroscience Letters* 1993, 150, 145-148.
163. Li, P.; Vishnuvajjala, R.; Tabibi, S. E.; Yalkowsky, S. H., Evaluation of in vitro precipitation methods. *Journal of Pharmaceutical Sciences* 1998, 87, (2), 196-199.
164. Balakrishnan, A.; Rege, B. D.; Amidon, G. L.; Polli, J. E., Surfactant-mediated dissolution: Contributions of solubility enhancement and relatively low micelle diffusivity. *Journal of Pharmaceutical Sciences* 2004, 93, (8), 2064-2075.
165. Xu, J. J.; Diaz, P.; Astruc-Diaz, F.; Craig, S.; Munoz, E.; Naguib, M., Pharmacological characterization of a novel cannabinoid ligand, MDA19, for treatment of neuropathic pain. *Anesth Analg* 2010, 111, (1), 99-109.

166. Diaz, P.; Phatak, S. S.; Xu, J.; Fronczek, F. R.; Astruc-Diaz, F.; Thompson, C. M.; Cavasotto, C. N.; Naguib, M., 2,3-Dihydro-1-Benzofuran Derivatives as a Series of Potent Selective Cannabinoid Receptor 2 Agonists: Design, Synthesis, and Binding Mode Prediction through Ligand-Steered Modeling. *ChemMedChem* 2009, 4, (10), 1615-1629.
167. Marty, M. S.; Domoradzki, J. Y.; Hansen, S. C.; Timchalk, C.; Bartels, M. J.; Mattsson, J. L., The Effect of Route, Vehicle, and Divided Doses on the Pharmacokinetics of Chlorpyrifos and Its Metabolite Trichloropyridinol in Neonatal Sprague-Dawley Rats. *Toxicological Sciences* 2007, 100, (2), 360-373.
168. Shou, W. Z.; Naidong, W., Post-column infusion study of the 'dosing vehicle effect' in the liquid chromatography/tandem mass spectrometric analysis of discovery pharmacokinetic samples. *Rapid Commun Mass Spectrom* 2003, 17, (6), 589-97.
169. Heiser, A., Rat Jugular Vein and Carotid Artery Catheterization for Acute Survival Studies. In Springer: West Roxbury, 2007.
170. Lin, M.; Tesconi, M.; Tischler, M., Use of ^{1}H NMR to facilitate solubility measurement for drug discovery compounds. *International Journal of Pharmaceutics* 2009, 369, (1–2), 47-52.
171. Walker, G. S.; Ryder, T. F.; Sharma, R.; Smith, E. B.; Freund, A., Validation of Isolated Metabolites from Drug Metabolism Studies as Analytical Standards by Quantitative NMR. *Drug Metabolism and Disposition* 2011, 39, (3), 433-440.
172. Holzgrabe, U.; Wawer, I.; Diehl, B., *NMR Spectroscopy in Pharmaceutical Analysis*. Elsevier B. V.: Oxford (UK), 2008.
173. Diehl, B. W. K. M., Frank; Holzgrabe, Ulrike Quantitative NMR spectroscopy in the quality evaluation of active pharmaceutical ingredients and excipients. . *Spectroscopy Europe* 2007, 19, (5).
174. Le Ferrec, E.; Chesne, C.; Artusson, P.; Brayden, D.; Fabre, G.; Gires, P.; Guillou, F.; Rousset, M.; Rubas, W.; Scarino, M. L., In vitro models of the intestinal barrier. The report and recommendations of ECVAM Workshop 46. European Centre for the Validation of Alternative methods. *Altern Lab Anim* 2001, 29, (6), 649-68.
175. Delongeas, J. L.; de Conchard, G. V.; Beamonte, A.; Bertheux, H.; Spire, C.; Maisonneuve, C.; Becourt-Lhote, N.; Goldfain-Blanc, F.; Claude, N., Assessment of Labrasol®/Labrafil®/Transcutol® (4/4/2, v/v/v) as a non-clinical vehicle for poorly water-soluble compounds after 4-week oral toxicity study in Wistar rats. *Regul Toxicol Pharm* 2010, 57, (2–3), 284-290.
176. Shah, N. H.; Carvajal, M. T.; Patel, C. I.; Infeld, M. H.; Malick, A. W., Self-Emulsifying Drug-Delivery Systems (Sedds) with Polyglycolyzed Glycerides for Improving in-Vitro Dissolution and Oral Absorption of Lipophilic Drugs. *International Journal of Pharmaceutics* 1994, 106, (1), 15-23.
177. McConnell, E. L.; Basit, A. W.; Murdan, S., Measurements of rat and mouse gastrointestinal pH, fluid and lymphoid tissue, and implications for in-vivo experiments. *J Pharm Pharmacol* 2008, 60, (1), 63-70.
178. Bachynsky, M. O.; Shah, N. H.; Patel, C. I.; Malick, A. W., Factors affecting the efficiency of a self-emulsifying oral delivery system. *Drug Development and Industrial Pharmacy* 1997, 23, (8), 809-816.
179. Craig, D. Q. M.; Barker, S. A.; Banning, D.; Booth, S. W., An Investigation into the Mechanisms of Self-Emulsification Using Particle-Size Analysis and Low-Frequency Dielectric-Spectroscopy. *International Journal of Pharmaceutics* 1995, 114, (1), 103-110.

180. Rahman, M. A.; Hussain, A.; Hussain, M. S.; Mirza, M. A.; Iqbal, Z., Role of excipients in successful development of self-emulsifying/microemulsifying drug delivery system (SEDDS/SMEDDS). *Drug Development and Industrial Pharmacy* 2012, 0, (0), 1-19.
181. Malvern *What does polydispersity mean?*; 2011.
182. Constantinides, P. P.; Scalart, J. P.; Lancaster, C.; Marcello, J.; Marks, G.; Ellens, H.; Smith, P. L., Formulation and intestinal absorption enhancement evaluation of water-in-oil microemulsions incorporating medium-chain glycerides. *Pharm Res* 1994, 11, (10), 1385-90.
183. Gershanik, T.; Benita, S., Self-dispersing lipid formulations for improving oral absorption of lipophilic drugs. *Eur J Pharm Biopharm* 2000, 50, (1), 179-188.
184. Rossi, G.; Reggiani, P.; Regazzi, M. B.; Gatti, S.; Ceccherelli, F.; Prato, P.; Galmarini, D.; Fassati, L. R., Neoral increases bioavailability versus oral sandimmune after porcine small bowel transplantation. *Transplant P* 1998, 30, (6), 2654-2656.
185. Taher Boukhris, M. L-S., Mohamed Skiba, Novel oral formulation of cyclosporine-spray-dried dispersion using cyclodextrin copolymer. *Digest Journal of Nanomaterials and Biostructures* 2012, 7, (1), 143-154.
186. Gabriel Lopez-Berestein, A. M. T., Soo-Jeong Lim Method to incorporate N-(4-hydroxyphenyl) retinamide in liposomes. 2002.
187. Zou, Y.; Priebe, W.; Perez-Soler, R., Lyophilized preliposomal formulation of the non-cross-resistant anthracycline annamycin: effect of surfactant on liposome formation, stability and size. *Cancer Chemother Pharmacol* 1996, 39, (1-2), 103-8.
188. Small, D. M., *Handbook of Lipid Research: The Physical Chemistry of Lipids, From Alkanes to Phospholipid*. Plenum Press: New York, 1986.
189. Litzinger, D. C.; Buiting, A. M. J.; van Rooijen, N.; Huang, L., Effect of liposome size on the circulation time and intraorgan distribution of amphipathic poly(ethylene glycol)-containing liposomes. *Biochimica et Biophysica Acta (BBA) - Biomembranes* 1994, 1190, (1), 99-107.
190. Uchiyama, K.; Nagayasu, A.; Yamagiwa, Y.; Nishida, T.; Harashima, H.; Kiwada, H., Effects of the size and fluidity of liposomes on their accumulation in tumors: A presumption of their interaction with tumors. *International Journal of Pharmaceutics* 1995, 121, (2), 195-203.
191. Nagayasu, A.; Uchiyama, K.; Kiwada, H., The size of liposomes: a factor which affects their targeting efficiency to tumors and therapeutic activity of liposomal antitumor drugs. *Advanced Drug Delivery Reviews* 1999, 40, (1–2), 75-87.
192. Siwak, D. R.; Tari, A. M.; Lopez-Berestein, G., The Potential of Drug-carrying Immunoliposomes as Anticancer Agents. *Clinical Cancer Research* 2002, 8, (4), 955-956.
193. Zhigaltsev, I. V.; Belliveau, N.; Hafez, I.; Leung, A. K.; Huft, J.; Hansen, C.; Cullis, P. R., Bottom-up design and synthesis of limit size lipid nanoparticle systems with aqueous and triglyceride cores using millisecond microfluidic mixing. *Langmuir* 2012, 28, (7), 3633-40.
194. Abram, S. E.; Yi, J.; Fuchs, A.; Hogan, Q. H., Permeability of injured and intact peripheral nerves and dorsal root ganglia. *Anesthesiology* 2006, 105, (1), 146-53.
195. Stein, C.; Machelska, H., Modulation of Peripheral Sensory Neurons by the Immune System: Implications for Pain Therapy. *Pharmacol Rev* 2011, 63, (4), 860-881.

196. Gordh, T.; Sharma, H. S., Chronic spinal nerve ligation induces microvascular permeability disturbances, astrocytic reaction, and structural changes in the rat spinal cord. *Acta Neurochir Suppl* 2006, 96, 335-40.
197. Echeverry, S.; Shi, X. Q.; Rivest, S.; Zhang, J., Peripheral Nerve Injury Alters Blood-Spinal Cord Barrier Functional and Molecular Integrity through a Selective Inflammatory Pathway. *Journal of Neuroscience* 2011, 31, (30), 10819-10828.
198. Higuchi, T.; Connors, K. A., Advances in Analytical Chemistry and Instrumentation. *Chapter 4. Phase Solubility Studies* 1965, 117-212.
199. Diaz, P.; Phatak, S. S.; Xu, J.; Astruc-Diaz, F.; Cavasotto, C. N.; Naguib, M., 6-Methoxy-N-alkyl isatin acylhydrazone derivatives as a novel series of potent selective cannabinoid receptor 2 inverse agonists: design, synthesis, and binding mode prediction. *J Med Chem* 2009, 52, (2), 433-44.
200. Loftsson, T.; Brewster, M. E., Cyclodextrins as functional excipients: Methods to enhance complexation efficiency. *Journal of Pharmaceutical Sciences* 2012, Epub ahead of print.
201. Veiga, M. D.; Merino, M.; Fernandez, D.; Lozano, R., Characterization of some cyclodextrin derivatives by thermal analysis. *J. Therm. Anal. Calorim.* 2002, 68, 511-516.
202. de Araújo, M. r. V. G.; Vieira, E. K. B.; Lázaro, G. S.; de Souza Conegero, L.; Ferreira, O. P.; Almeida, L. E.; Barreto, L. S.; da Costa Jr, N. B.; Gimenez, I. F., Inclusion complexes of pyrimethamine in 2-hydroxypropyl-β-cyclodextrin: Characterization, phase solubility and molecular modelling. *Bioorganic & Medicinal Chemistry* 2007, 15, (17), 5752-5759.
203. Orgoványi, J.; Pöppl, L.; H-Otta, K.; Lovas, G. A., Characterization of some cyclodextrin derivatives by thermal analysis. *J Therm Anal Calorim* 2005, 81, 261-266.
204. Djedaïni, F.; Lin, S. Z.; Perly, B.; Wouessidjewe, D., High-field nuclear magnetic resonance techniques for the investigation of a β-cyclodextrin:indomethacin inclusion complex. *Journal of Pharmaceutical Sciences* 1990, 79, (7), 643-646.
205. Loftsson, T.; Olafsdottir, B. J.; Frioriksdottir, H.; Jonsdottir, S., Cyclodextrin complexation of NSAIDSs: physicochemical characteristics. *European Journal of Pharmaceutical Sciences* 1993, 1, (2), 95-101.
206. Zornoza, A.; Martin, C.; Sanchez, M.; Velaz, I.; Piquer, A., Inclusion complexation of glisentide with α-, β- and γ-cyclodextrins. *International Journal of Pharmaceutics* 1998, 169, (2), 239-244.
207. Messner, M.; Kurkov, S. V.; Brewster, M. E.; Jansook, P.; Loftsson, T., Self-assembly of cyclodextrin complexes: Aggregation of hydrocortisone/cyclodextrin complexes. *International Journal of Pharmaceutics* 2011, 407, (1-2), 174-183.
208. Bittner, B.; Mountfield, R. J., Intravenous administration of poorly soluble new drug entities in early drug discovery: the potential impact of formulation on pharmacokinetic parameters. *Curr Opin Drug Discov Devel* 2002, 5, (1), 59-71.
209. Egger-Heigold, B. The effect of excipients on pharmacokinetic parameters of parenteral drugs. Basel University, Basel, 2005.
210. Dhanikula, A. B.; Singh, D. R.; Panchagnula, R., In vivo pharmacokinetic and tissue distribution studies in mice of alternative formulations for local and systemic delivery of Paclitaxel: gel, film, prodrug, liposomes and micelles. *Curr Drug Deliv* 2005, 2, (1), 35-44.
211. Naguib, M.; Xu, J. J.; Diaz, P.; Brown, D. L.; Cogdell, D.; Bie, B.; Hu, J.; Craig, S.; Hittelman, W. N., Prevention of Paclitaxel-Induced Neuropathy Through Activation

of the Central Cannabinoid Type 2 Receptor System. *Anesthesia & Analgesia* 2012, 114, (5), 1104-1120.
212. Agency, E. M. Reflection paper on the pharmaceutical development of intravenous medicinal products containing active substances solubilised in micellar systems. http://www.ema.europa.eu/docs/en_GB/document_library/Scientific_guideline/2012/03/WC500124410.pdf
213. Rouf, M. A. Development of Rapamycin drug delivery systems, their characterization and investigaqtion of the antiproliferative effect on cell cultures. Hacettepe University, Ankara, 2007.
214. Bruzell, E. M.; Morisbak, E.; Tonnesen, H. H., Studies on curcumin and curcuminoids. XXIX. Photoinduced cytotoxicity of curcumin in selected aqueous preparations. *Photoch Photobio Sci* 2005, 4, (7), 523-530.
215. Ishida, T.; Harashima, H.; Kiwada, H., Liposome clearance. *Biosci Rep* 2002, 22, (2), 197-224.
216. Hosohata, Y.; Quock, R. M.; Hosohata, K.; Makriyannis, A.; Consroe, P.; Roeske, W. R.; Yamamura, H. I., AM630 antagonism of cannabinoid-stimulated [35S]GTP gamma S binding in the mouse brain. *Eur J Pharmacol* 1997, 321, (1), R1-3.
217. Ross, R. A.; Brockie, H. C.; Stevenson, L. A.; Murphy, V. L.; Templeton, F.; Makriyannis, A.; Pertwee, R. G., Agonist-inverse agonist characterization at CB1 and CB2 cannabinoid receptors of L759633, L759656, and AM630. *Br J Pharmacol* 1999, 126, (3), 665-72.
218. Gatley, S. J.; Gifford, A. N.; Volkow, N. D.; Lan, R.; Makriyannis, A., 123I-labeled AM251: a radioiodinated ligand which binds in vivo to mouse brain cannabinoid CB1 receptors. *Eur J Pharmacol* 1996, 307, (3), 331-8.
219. Ibrahim, M. M.; Porreca, F.; Lai, J.; Albrecht, P. J.; Rice, F. L.; Khodorova, A.; Davar, G.; Makriyannis, A.; Vanderah, T. W.; Mata, H. P.; Malan, T. P., Jr., CB2 cannabinoid receptor activation produces antinociception by stimulating peripheral release of endogenous opioids. *Proc Natl Acad Sci U S A* 2005, 102, (8), 3093-8.

CHAPTER III CATIONIC POLYMERIC NANOCAPSULES.

1 Review.

1.1 Structure of drug-loaded nanoparticles.

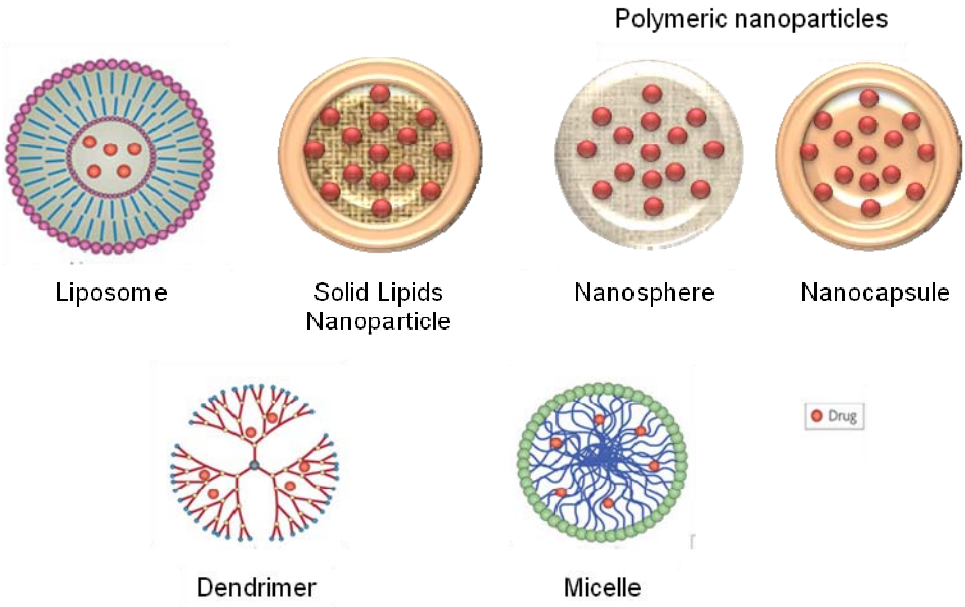

Figure 43: Schematic representation of different nanoparticulate-based drug-delivery systems adapted from Orive et al.[3]. Liposomes are spherical vesicles that comprise one or more lipid bilayer structures enclosing an aqueous core. Polymeric NPs are polymeric colloidal particles with a therapeutic agent either dispersed in the polymer matrix (nanosphere) or encapsulated in a liquid core surrounded by a polymeric shell (nanocapsule). Solid lipid NPs are made from solid lipids matrix stabilized by surfactants. Dendrimers are highly branched polymer with a controlled three-dimensional structure around a central core surrounded by a large number of reactive end groups. Micelles are aggregate of surfactants, which assemble in aqueous solution as outer hydrophilic layer and inner hydrophobic core.

Nanoparticles (NPs) are defined by the Encyclopedia of Pharmaceutical Technology[2] as solid colloidal particles ranging in size from 10 to 1000 nm. NPs (see Fig. 43) consist of

macromolecular materials and can be used therapeutically as drug carriers, in which the active principle is dissolved, entrapped, encapsulated or to which the drug is adsorbed or covalently conjugated.

2 Applications of drug-loaded polymeric nanoparticles.

NPs have been explored in various applications including biological markers, imaging, pharmaceuticals and diagnosis[6-11] and to deliver lipophilic drugs, proteins, peptides and genes through parenteral but also per oral/mucosal route of administration for local diseases treatment or systemic absorption[6, 12-14]. Polymeric NPs are divided into two categories: nanocapsules and nanospheres. The former are vesicular systems with a polymeric shell and an inner core (hydrophobic or hydrophilic) in which the drug is confined. The latter consist in continuous polymeric matrix inside which the drug is generally uniformly dispersed[15-16]. Depending on nanocapsules and nanospheres physicochemical properties and composition, the drug may also adsorb onto the surface[17]. Compared with conventional DDS, polymeric NPs present the advantages of high stability in biological fluids, high drug loading capacity, small number and amount of excipients, easy-to-manufacture process, and ability of incorporation of hydrophilic and lipophilic active compounds achieving controlled (sustained) drug release[6] which may be more suitable to treat chronic diseases[15]. NPs are considered as effective tools for the intracellular (i.e. nanometric size) delivery of practically insoluble and sensitive drugs to degradation, metabolism, plasma binding and multiple drug resistance. NPs properties can alter the incorporated drug pharmacokinetics, biodistribution and bioavailability promoting absorption through biological barrier[17-22]. Their surface physicochemical properties modification by altering their composition and/or charge and/or by addition of targeting moieties (e.g. antibodies, peptides, nucleic acids or receptor ligands) can allow selective and controlled delivery of therapeutic agents and offer interesting imaging/diagnosis additive properties[6-7, 23] with generally reduced toxicity[24]. In the past two decades, there has been a progressive increase in the number of commercially available nanoparticulate-based therapeutic products with two dominant classes, liposomes and polymer-drug conjugates. Despite the number of patents for nano drug delivery, commercialization is still at its early stage. This is probably due to the fact that

most of the research studies in nanocarriers are carried out by researchers in academia, the lack of regulatory guidelines, the challenges of scaling up and the fate of NPs in the body that still needs to be addressed. However, it is envisioned that with the expiration of more patents and market loss, as well as the undeniable ability of these versatile colloidal systems to increase therapeutic index, more pharmaceutical industries will take up the production of nanocarriers to compete favorably[25]. Drug-loaded polymeric NPs at the preclinical stages have been shown to greatly increase therapeutic effects of anticancer drugs i.e. doxorubicin[26-28], genistein[29] and paclitaxel[32], antiparasitic agent i.e. quinine[30], viral antigen i.e. rotavirus[31]. Fluorescent tagged NPs have also demonstrated their efficacy in cell imaging using rhodamine B[33].

3 Nanoparticles uptake in cells.

As it has been reviewed by Mailander et al.[34], NPs are taken up by a variety of cells. For particles in the range of a few to several hundred nanometers, mechanisms of uptake involve several possible mechanisms like pinocytosis, nonspecific endocytosis, receptor-mediated endocytosis, and, for larger particles, phagocytosis. Uptake process of NPs can be influenced and enhanced by several factors like size i.e. optimal in the range of 50−200 nm, surface properties i.e. positive or negative charge, nature of the polymer i.e. increased with polymer hydrophobicity, surface groups e.g. amphiphilic polymer physically adsorbed on NPs surface as transfection agent[35].

4 Drug-loaded nanoparticles composition and bioadhesion.

Polymeric NPs are generally composed of natural or synthetic, and biodegradable or biocompatible polymer. The nature of the polymer influences the size and the release profile of encapsulated drugs, natural polymer generally trigger immediate drug release while synthetic polymer enable more extended drug release[36]. Polymer used for the formulation of NPs include synthetic (poly(lactic acids) (PLA), poly(lactic-co-glycolic acids) (PLGA), poly(ε-caprolactone) (PCL), poly(methyl methacrylates), and poly(alkyl

cyanoacrylates)) or natural polymer (albumin, gelatin, alginate, collagen or chitosan). Biodegradable and biocompatible polyesters polymer, PLGA[37-43] and PLA are the most commonly used for the formulation of NPs. Interestingly, bioadhesive nanoparticles have been shown to be very advantageous over others carriers by providing prolonged retention at the site of application and a controlled rate of drug release for improved therapeutic outcome[21, 36, 44-46]. The presence of cationic polymer on the surface of NPs (i.e. chitosan, quaternary ammonium-containing polymethacrylates Eudragit®)[36, 47-50] can promote mucoadhesion by electrostatic interaction of their amino groups with the sialic groups of mucin, and increase internalization by epithelial cells which are also negatively charged at physiological pH[51-52]. These polymer are also known to increase transcellular and paracellular transport through interactions between the negatively-charged cell membrane and the positive charges of the polymer, or by complexing Ca^{2+} involved in the structure of tight junctions across mucosal epithelium, which is further indicative of their potential in oral delivery[36, 46, 52-58]. In addition to mucoadhesive properties, unlike particles with hydrophobic surface properties are rapidly removed from blood circulation by macrophages, cationic nanoparticles are less recognized by macrophages and remain in the circulation for a longer time[59].

5 Methods of preparation of polymeric drug-loaded nanoparticles.

Polymeric NPs can be obtained by polymerization *in situ* from monomers or preformed polymer. Six different methods are generally described for the preparation of nanocapsules from preformed polymer: nanoprecipitation, emulsion-diffusion, double emulsification, emulsion-coacervation, polymer-coating and layer-by-layer[4] (see Fig. 44).

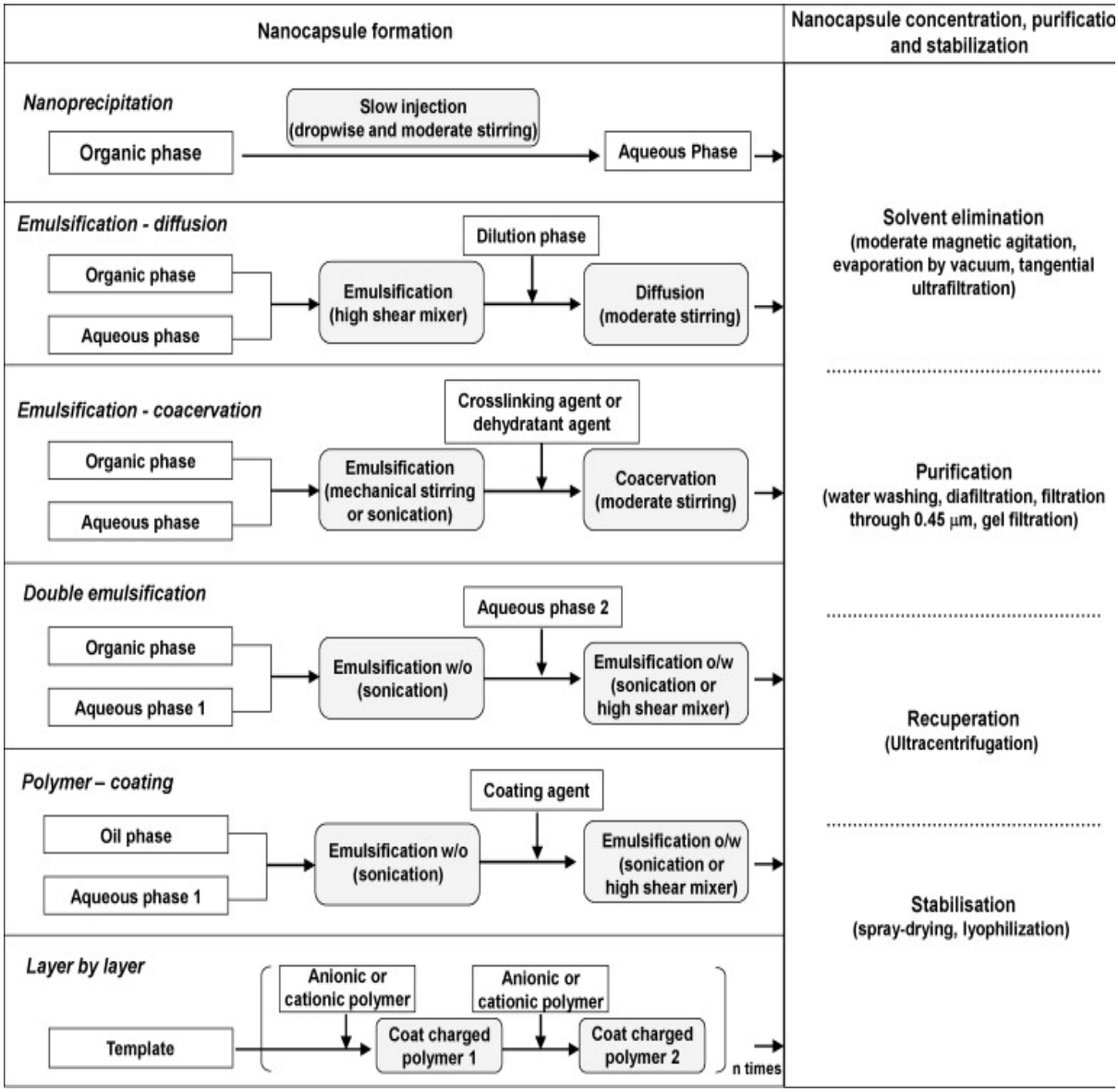

Figure 44[4]**:** General procedure of the different methods for the preparation of nanocapsules**.**

6 Nanoprecipitation of preformed polymer.

The nanoprecipitation method patented by Fessi et al.[60] is the most common encountered for obtaining lipophilic drug-loaded NPs and valued for the simplicity and robustness of manufacturing procedure, low cost, reproducible particle size and high encapsulation efficiency[4, 61-63] Based on this advantages, we decided to use this approach for the formation of cationic polymeric NPs. The nanoprecipitation method is also called solvent displacement or interfacial deposition. NCs are obtained as a

colloidal suspension when a solution of polymer, drug and oil in a semi-polar and water miscible organic phase (e.g. acetone, ethanol, methylene chloride) is injected slowly and with moderate stirring into an aqueous solution (being a non-solvent or antisolvent for drug and polymer) possibly containing an hydrophilic stabilizer (e.g. Poloxamer 188). NCs are instantaneously formed by rapid diffusion of the solvent into the aqueous phase and simultaneous interfacial deposition of preformed polymer. The organic solvent phase is then removed under reduced pressure[4, 60, 64-65]. Disagreement exists regarding the molecular mechanism leading to the instantaneous formation of NCs. The first hypothesis referred to the Gibbs-Marangoni effect as the driving force of nanoprecipitation process caused by interfacial turbulences and thermal inequities between two liquid phases[66-70]. According to this theory, NCs formation is due to polymer aggregation in stabilized emulsion droplets[4]. In contrast, recent publications promoted the "ouzo effect"[66, 71-72] for the physical phenomenon of spontaneous emulsification, observed when water is added to Ouzo (Greek liquor) or Pastis (French liquor) forming a milky and highly stable oil-in-water microemulsion. The "ouzo effect" occurs when a hydrophobic solute (i.e. polymer) is rapidly brought into the metastable region ("ouzo effect") between the binodal (miscibility-limit curve) and spinodal (stability-limit curve) boundaries in a ternary phase diagram composed of hydrophobic solute, solvent, and non-solvent. Local supersaturation of hydrophobic solute molecules leads to spontaneous nucleation in the form of small nuclei, larger than a critical size, that grow with time by capturing other solute molecules due to Ostwald ripening (i.e. nucleation and growth process)[66, 71]. In intimate contact with the non-solvent, the polymer precipitation is initiated and the final solidification is completed by a slow evaporation of the organic solvent.

7 Nanoparticles and oral delivery.

Oral route is the preferred route for the delivery of drugs. It is simple for self-administration, painless and it improves patient compliance particularly for chronic therapy such as neuropathic pain. However, oral absorption is limited by various physiological barriers (e.g. acidity, enzymes, mucus, and motility) and remains a scientific challenge. Nanometric-sized drug delivery systems including polymeric or lipid-based carriers (i.e. liposomes, micelles, dendrimers, nanoparticles) are being extensively

studied to enhance the bioavailability or the targeting of drug after oral administration[52]. As mentioned, polymeric nanoparticles offer significant advantages over other nanocarriers such as high drug loading and stability of encapsulated drug which can be protected from degradation along the gastro-intestinal tract (GIT) until the particles release their cargo (i.e. after erosion, degradation, swelling) and/or diffusion of the drug. The particles can be designed as site-specific delivery systems, with polymer dissolving at defined values of pH (corresponding to the pH of specific parts of the GIT) or at time-controlled delivery, with polymer swelling independently of the pH. The use of various polymeric materials enable the modulation of physicochemical characteristics (e.g. hydrophobicity, zeta potential), drug release properties (e.g. delayed, prolonged, triggered), and biological behavior (e.g. targeting, bioadhesion, permeation enhancing effect, inhibition of proteolytic enzymes) of nanoparticles[36, 46, 73-76]. Several mechanisms for gastrointestinal absorption of nanoparticles in their native structure and translocation from the intestinal mucosa to the systemic circulation have been reported, involving the M-cells in the Peyer's patches and the isolated follicles of the gut-associated lymphoid tissue (GALT), transcellular pathways through normal intestinal enterocytes and to a lesser extent paracellular pathways (also known as persorption)[77-87]. Factors affecting uptake include particle size, surface charge and hydrophobicity, the presence or absence of surface ligands, length of administration and the dose of particles and methods used to quantify particulate absorption[88-89]. Bioadhesive polymeric NPs have the potential to successfully address the issues related to oral drug delivery, retention and absorption and are considered potential candidates to carry drugs to the desired site of therapeutic action.

8 Concepts of the study.

8.1 Theragnostic drug-loaded polymeric nanocapsules.

The first aspect of this project was to design detectable polymeric NPs using cationic polymer in order to trace the particles *in vivo*[90-91]. Aqueous dispersion of cationic polymer have the unique property to yield a high proportion of counterionic condensation in the

presence of molecules bearing anionic groups[92] such as sulfobutylether-beta-cyclodextrin sodium salt (SBEβCD) (Fig. 46).

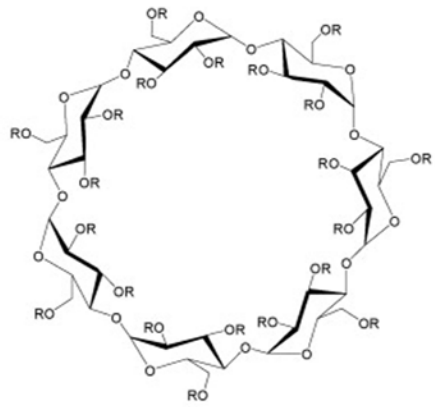

Figure 45: Sulfobutylether-beta-cyclodextrin (SBEβCD) chemical structure[5].

The resulting physicochemical properties of such nanostructures based on pair-ions interaction have been exploited in various purposes such as changes in solubility[93], stability[94-95] and drug-release pattern[96-97]. Recent approval in Europe of Sugammadex® (γ-cyclodextrin) for rapid reversal of rocuronium-induced neuromuscular blockade is also based on ion-pairing complexes formation. Sulfobutyl ether β-cyclodextrin (SBE-β-CD) is a chemically modified β-CD that is a cyclic hydrophilic oligosaccharide which is negatively charged in aqueous media. The solubility in water for SBEβCD is in excess of 70 g/100 ml at 25 °C)[5]. SBEβCD (Fig. 45) are safe for systemic administration and are currently used in marketed pharmaceutics such as Cerenia® or Vfen®.

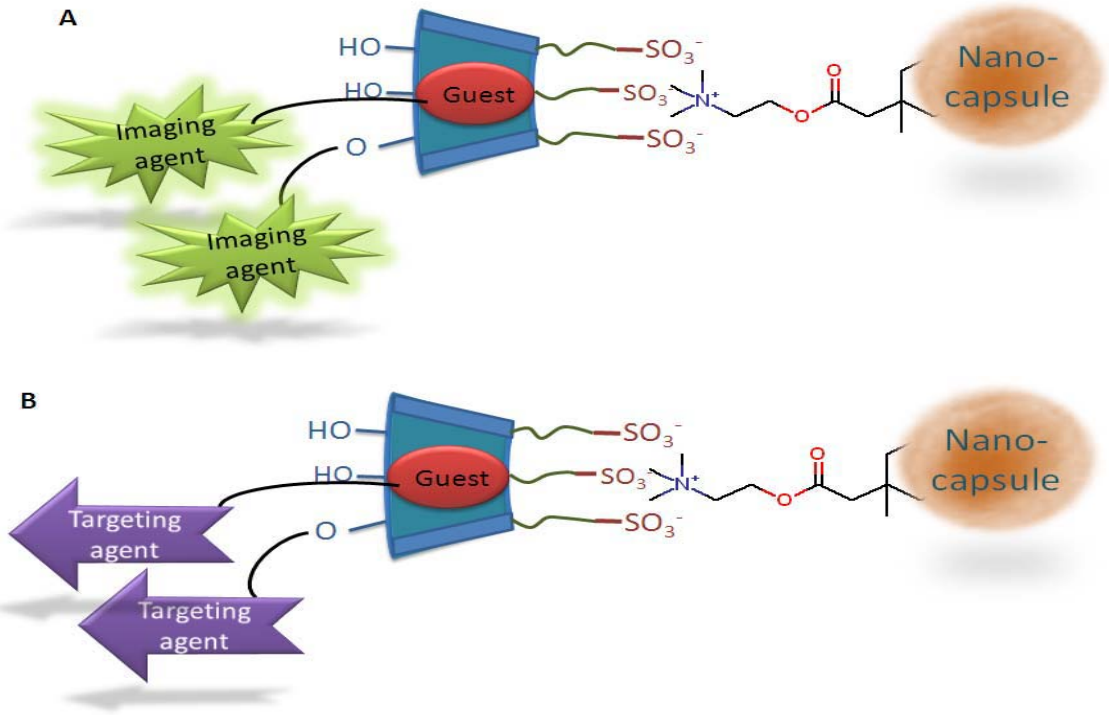

Figure 46: Schematic representation of a fluorescent and/or cell-specific targeting Ion-pair SBEβCD-NC supramolecular complex. **A)** The complex can be rendered fluorescent either by functionalizing the SBEβCD or the guest molecule using an imaging agent, or by encapsulating the imaging agent in the NC. **B)** The complex can be rendered cell-specific targeting either by functionalizing the SBEβCD or the guest molecule using a specific receptor targeting agent.

Polymer bearing quaternary ammonium moieties can also form supramolecular assembly through host-guest interaction or electrostatic interaction with macrocycles such as cucurbit[n]uril (CB[n])[98] (see Fig. 48) and more specifically functionalized CB[6] (Fig. 47). Cucurbiturils are macrocyclic molecules consisting of glycoluril repeat units. These compounds are particularly interesting because they are molecular containers that are

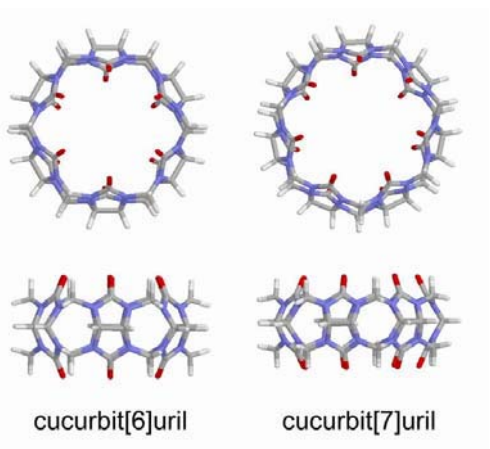

Figure 47[1]**:** Molecular structure of cucurbituril: top (top) and lateral (bottom) views.

capable of binding cationic molecules within their cavity. The name is actually derived from the resemblance of this molecule with a pumpkin of the family of Cucurbitaceae. The cavity of cucurbit[6]uril has nanoscale dimensions with an approximate height of 9.1 Å, outer diameter 5.8 Å and inner diameter 3.9 Å[99]. Cucurbiturils are efficient host molecules in molecular recognition and have a particularly high affinity for positively charged or cationic compounds. High association constants with positively charged molecules are attributed to the carbonyl groups that line each end of the cavity and can interact with cations in a similar fashion to crown ethers. For example the affinity equilibrium constant of cucurbit[7]uril with the positively charged derivatized adamantine is experimentally determined at 10^{12} M^{-1}[100]. Cucurbiturils host-guest properties have been explored for drug delivery vehicles. The potential of this application has been explored with cucurbit[7]uril that forms an inclusion compound with the important cancer fighting drug oxaliplatin[101]. The amine nitrogen atoms of oxaliplatin form hydrogen bonds with the oxygen atoms of the CB[7] portal, the oxalate group pointing away from the CB[7] portal. The synergistic effect of the hydrogen bonds and hydrophobic interactions of the cyclohexyl moiety of the guest with CB[7] cavity appear to be responsible for the remarkable stability of the complex in aqueous solution.

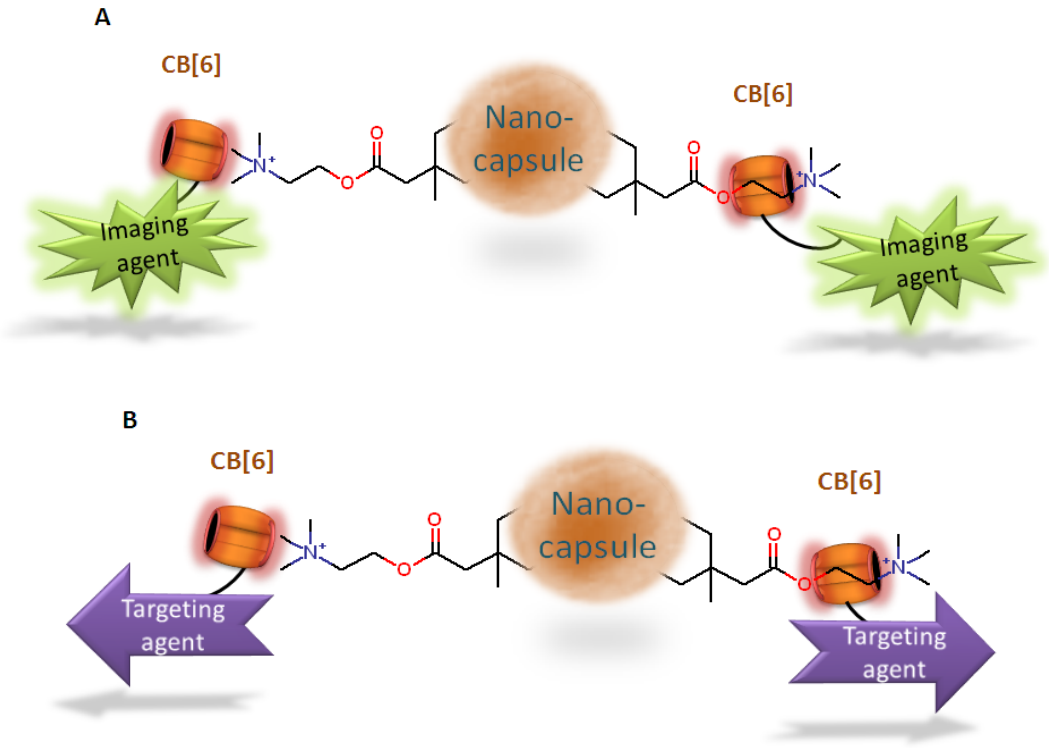

Figure 48: Schematic representation of a fluorescent and/or cell-specific targeting host-guest CB[6]-NC supramolecular complex. A) The complex can be rendered fluorescent either by functionalizing the CB[6] using an imaging agent, or by encapsulating the imaging agent in the NC. B) The complex can be rendered cell-specific targeting by functionalizing the CB[6] using a specific receptor targeting agent.

CB[n] derivatives exhibit a very low toxicity[102]. In this study we investigated interest to investigate the interaction of cationic polymeric nanoparticles (i.e. nanocapsules) and macrocycles such as SBEβCD or CB[6]. To render the NC detectable and allows monitoring after ingestion, a lipid specific fluorescent dye, e.g. Nile Red, can be encapsulated in the oily core of the NC along with a lipophilic drug e.g. β-caryophyllene [(E)-BCP], or be grafted either on the macrocycle hydroxyls groups or on the macrocycle guest molecule e.g. adamantyl wherewith β-cyclodextrin molecules are able to form high-affinity inclusion complexes with[103]. One of the common hydrophobic fluorescent dye described in the literature is the Nile Red[104-106] which the fluorescence is quenched in an aqueous environment, consequently ideal to detect the NCs inside the body and monitor drug delivery. Various fluorescent NPs, including colloidal inorganic semiconductor quantum dots (QDs) have also been developed[107-108] based on their extraordinary optical properties. Their cytotoxicity (e.g. hepatoxicity and nephrotoxicity of cadmium)

can be a critical concern upon *in vitro/in vivo* studies since QDs are complexes of heavy metals[9] and encapsulation in polymeric NCs may render them more biocompatible. The NCs we have developed may be of great interest for this purpose. Commercial contrast agents like Resovist® and Feridex® IV are available on the market but can be used as a dual efficient system for drug delivery and imaging[10]. In addition, the guest molecule complexed with SBEβCD or the macrocycles SBEβCD and CB[6] could be biofunctionalized on the hydroxyls groups with specific cell- targeting ligands offering the potential for delivery of therapeutic-loaded NPs to a particular site (e.g. brain, spinal cord) or specific cell type (e.g. tumor cells, immune cells) in the body[9, 109-110]. These cell/organ specific and/or fluorescent macrocycle-NCs based on counterionic condensation or host-guest complexion/electrostatic interaction, can be used as sensitive and highly-specific probes providing a unique concept of theragnostic combining diagnostic/imaging to assess the efficiency of drug delivery and possible mechanisms of NCs bioabsorption, and therapeutic activity.

8.2 Bioadhesive polymeric nanocapsules for oral delivery of a lipophilic drug.

The second aspect of this project was to investigate whether or not the sole cationic polymeric NPs developed (without macrocycle association) may serve as a suitable drug delivery system (DDS) for oral administration of lipophilic drug such as the natural dietary cannabinoid (E)-BCP. The GI sets a variety of morphological and physiological barriers that can limit intestinal absorption of the therapeutic agent, especially for (E)-BCP, a non drug-like compound for oral bioavailability, highly lipophilic and sensitive to oxidation and acidity. Strategy for oral administration of (E)-BCP with sufficient bioavailability (solubility, stability, intestinal targeting, blood residence, immunogenicity) would be its encapsulation in protective and mucoadhesive colloidal carriers, such as cationic NCs, which can also deliver it in a controlled manner.

9 Polymer materials selected.

We have selected the Eudragit® RS 100 (Eud RS100) and RL 100 (Eud RL100) since these polymer are already established for therapeutic use and regarded as non toxic, while providing high *in vivo* stability (maintaining long-lasting unaltered physicochemical properties) compared to chitosan rapidly degraded after oral administration[52], making them interesting for potential drug delivery and sensing applications[90]. Eud RS100 and RL100 are one type of high polymer material, widely used as film coating materials for oral dosage forms and appeared to be suitable inert nanocarriers for ophthalmic DDS[111-112]. Nanoparticles using Eudragit® polymer have already been developed to improve the stability and the availability of drug such as cloricromene[113] and ibuprofen[114] in ophthalmic delivery; indomethacin, propranolol[115] and cyclosporine[116] in oral delivery. Eudragit® are found in approved drug products[117] and listed in the Inactive Ingredient Guide list from the FDA[118]. Eudragit® RS and RL 100 (Fig. 49) are cationic copolymer of poly(ethylacrylate, methyl-methacrylate and chlorotrimethyl-ammonioethyl methacrylate), containing an amount of quaternary ammonium groups between 4.5–6.8% and 8.8–12% for RS and RL, respectively. Both are insoluble at physiological pH values but are permeable and capable of swelling, which means that drugs can be released by diffusion, ollowing pH independent time controlled drug release of encapsulated drugs.

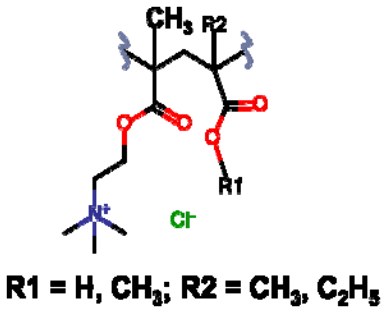

R1 = H, CH_3; R2 = CH_3, C_2H_5

Figure 49: Chemical structure of Eudragit® RS100 and Eudragit® RL100.

The degree of permeability depends on the relative proportion of functional quaternary ammonium groups in Eud RL100 and Eud RS100, respectively. By varying the ratio of Eud RL100 and Eud RS100, it is possible to adjust the drug release profile of the therapeutic agent[114].

10 Beta-caryophyllene as a model drug.

(E)-BCP has been selected as a model drug. Over the last years, (E)-BCP has gained great attention since it behaves as a selective and functional CB2 agonist phytocannabinoid (Ki = 155 =+/- 4 nM)[119] lacking psychoactivity. In addition, as a selective CB2 agonist, it has a good potential to treat or prevent neuropathic pain. (E)-BCP, used safely for decades as a food additive is a constituent of the essential oils of numerous spices and plants and a major component in Cannabis[120-124]. This dietary cannabinoid is a sesquiterpene insoluble in water, sensitive to acidity[125], that autoxidizes readily on air exposure to afford beta-caryophyllene oxide. Almost 50% of the original compound is consumed after 5 weeks[126] and oxidized.

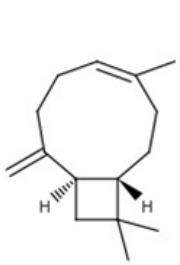

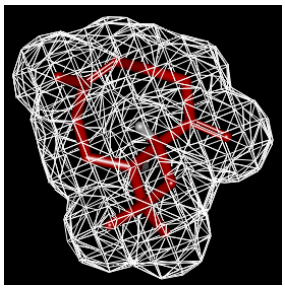

Name	Value
LogP	6.78
MW	204.35
PSA	0
FRB	0
HDonors	0
HAcceptors	0
Rule Of 5	1

Solubility in Pure Water at pH = 7, mg/ml 3.193e-6

Non Drug like molecule

Figure 50: (E)-BCP chemical structure and physicochemical properties.

The dissolution and bioavailability of (E)-BCP from oral preparations has been shown to be low due to its poor water solubility (Fig. 50) and possibly self-aggregation occurring in the GIT[119]. Pharmaceutical dosage forms comprising (E)-BCP described in the literature are micellar solutions[125, 127], olive oil[119] and DMSO[120]. These systems or excipients don't provide substantial protection of the drug against oxidation. This chemical instability increases low oral bioavailability. *In vitro* and *in vivo* decrease activities of (E)-BCP, increasing the doses, confirm this low oral bioavailability[119]. This phenomenon is probably due to coalescence of insoluble oil droplets. Besides, we[128] and other[129] recently demonstrated that CB2 agonists are effective in suppressing peripheral neuropathy evoked by paclitaxel administration in rats. In that context, a better

understanding of formulation of potential therapeutic agents could result in the development of better treatment for neuropathic pain and a good alternative for patients using medical marijuana, avoiding misuse and addiction issues. Fluorescent NCs may also allow the monitoring of (E)-BCP biodistribution providing new insight in regards with the peripheral or central target of neuropathic pain. The results from this research are expected to open a new area in the treatment of paclitaxel-induced neuropathic pain, which could possibly be extrapolated as a more general control mechanism of neuropathic pain. Altogether, (E)-BCP with its poor biopharmaceutical and pharmacokinetics properties represents an ideal drug as a model to investigate the efficiency of theragnostic polymeric NCs in controlled drug delivery and possible mechanisms of NCs bioabsorption.

11 Objectives of the study.

In the first stage of this project we focused our research on the preparation of bioadhesive polymeric NCs for the delivery of the lipophilic model drug (E)-BCP. A nanoprecipitation procedure was investigated for the preparation of NCs yielding to the following specifications:

- A loading capacity that can ensure therapeutic doses (10-20 mg/Kg, oral) for *in vivo* testing in rats.
- A monodisperse NCs population distribution with a nanometric size for a good drug bioavailability.
- An improved chemical stability of the encapsulated drug after storage 1 month at room temperature.
- A process allowing reproducibility in term of particle size and size distribution, drug loading/entrapment efficiency.

Studies were undertaken to evaluate the influence of different parameters on NCs formation prepared by nanoprecipitation: drug-to-polymer ratio, solvent phase-to-non solvent phase ratio, polymer-to-organic solvent ratio, nature and amount of surfactant, organic solvent nature, organic phase injection flow-rate, polymer (Eudragit® RS or RL) nature (Table 25). As preliminary data, we also investigated on a non optimized system

of particles the operating conditions (e.g. vacuum, temperature, duration) for solvent evaporation, and nature and concentration of cryoprotectants on NCs reconstitution after freeze-drying.

Table 25: Parameters and variations investigated on the standard nanosuspension entries 7 and 10 in the next sections.

Parameter	**Conditions studied (w/w)**	**Standard**
Polymer-to-organic solvent ratio	1.25 - 20.0%	10.0%
Drug-to-polymer ratio	1:4 – 1:26	1:13
Type of organic solvent(s)	acetone acetone/ethanol acetone/water	acetone
Solvent phase-to-NS ratio	6.0 – 10.0%	6.0%
Solvent-to-non solvent ratio	0.12 – 0.24	0.12
Type of stabilizer	Poloxamer 188 Oleic Macrogol-6 Glyceride	Poloxamer 188
Stabilizer-to-NC ratio	0 – 6.0%	1.5%
Type of polymer	Eudragit® RS100/RL100 (1:1) Eudragit® RS100 Eudragit® RL100	Eudragit® RS100/RL100 (1:1)
Solvent phase injection flow-rate	23.3 -1.4 – 0.7 mL.min^{-1}	1.4 mL. min-1

Particle size, distribution, and morphology of the prepared NCs were investigated using Photon Correlation Spectroscopy (PCS) and Transmission Electron Microscopy (TEM). Entrapment efficiency and drug loading were assessed by gas chromatography–mass spectrometry (GC-MS).

Once a reproducible process for the preparation of Eudragit®-based polymeric cationic NCs was obtained, we started investigating the feasibility of ion-pairing and host-guest or electrostatic interaction in between the developed NCs and macrocycles, using respectively SBEβCD and CB[7]. CB[7] exhibited a greater water solubility than CB[6] for the proof of concept studies. Functionalized CB[6] are expected to show a higher water solubility but introduction of functional groups will result in more complex behavior during

complexion. Particle size, distribution, and morphology of the prepared modified NCs were investigated using PCS and TEM. Finally, entrapment efficiency and drug loading were assessed by Gas chromatography–mass spectrometry (GC-MS) on the CB[7]-NCs developed.

12 Results and discussion.

12.1 (E)-BCP.

12.1.1 Purification

The purity of the (E)-BCP purchased from Sigma Aldrich was only 80%. In order to prevent any potential side effects due to unidentified impurities, we have developed a purification method using the Biotage (Medium pressure chromatography) for (E)-BCP to be incorporated in formulation studies. Analytical parameters such as Rf, solvent flow, column volume, injected volume, column equilibration have been optimized as described in the experimental section 6.2 with the aims of maximizing the purification yield and the resolution, and identifying the impurities. We collected very pure (assessed by NMR, GC/MS and TLC) (E)-BCP as compared with an analytical standard bought from Chromadex. TLC was used to follow the separation of (E)-BCP from the impurities. The solvent was removed using a rotary-evaporator and purity of the fraction containing (E)-BCP was assessed by ^{1}H-NMR. Besides, we have identified in the fractions containing the impurities α-humulene (also known as α-caryophyllene) and β-caryophyllene oxide in the commercial batch of (E)-BCP.

12.1.2 Stability.

(E)-BCP chemical stability was monitored by Gas Chromatography Mass Spectrometry (GC-MS) using the method described in the experimental part section 12.2 and section 6.3 (Experimental). Purified (E)-BCP and each of the impurities isolated from the commercial batch have been analyzed to enable further identification of degradation products/impurities over the course of the use of the compound. When entrapment

efficiency of NCs was evaluated, a standard curve with the purified (E)-BCP was freshly prepared, allowing in addition the monitoring of pure (E)-BCP chemical stability. (E)-BCP easily auto oxidizes affording 50% of (E)-BCP oxide after 5 weeks[126]. We have evidenced by qualitative TLC and NMR that a batch of (E)-BCP stored 7 months at 4°C under light protection had undergone some degradation to form (E)-BCP oxide and determined that packaging under nitrogen and in a air-tight container was required. Storage under appropriate conditions (N_2, air-tight container, 4°C), has extended the use of purified (E)-BCP batches to 18 months.

12.2 GC-MS method development for the determination of (E)-BCP entrapment efficiency and stability in drug-loaded nanocapsules.

The primary objective of this study was to develop a useful and accurate method for detection and identification of the volatile compound (E)-BCP and its possible degradation products in the cationic nanocapsules prepared. Gas chromatography/mass spectrometry (GC/MS) is a common sensitive analytical technique used to identify volatile analytes such as (E)-BCP[130-134]. Traditional methods often involve solvent extraction of the drug prior to direct injection into the GC[135]. GC-MS analyses were performed on an Agilent 6890N Gas Chromatograph with an Agilent 5973 Mass Spectrometer and analysis conditions are reported in experimental section 6.3.

12.2.1 Calibration and recovery.

For accuracy purposes, five calibration standards of pure (E)-BCP in the range of approximately 0-100 ppm were freshly prepared on each day of samples analysis. To limit the potential variations in instrument response (e.g. gas or liquid flow-rate, volume of sample solution injected) or in quantity of sample analyzed (e.g. sample loss occurring during sample preparation) that may be expected from run to run, a fixed concentration of α-pinene at a concentration of 100 ppm was incorporated as an internal standard. Standards curve samples were analyzed three times each to access the reproducibility of the method.

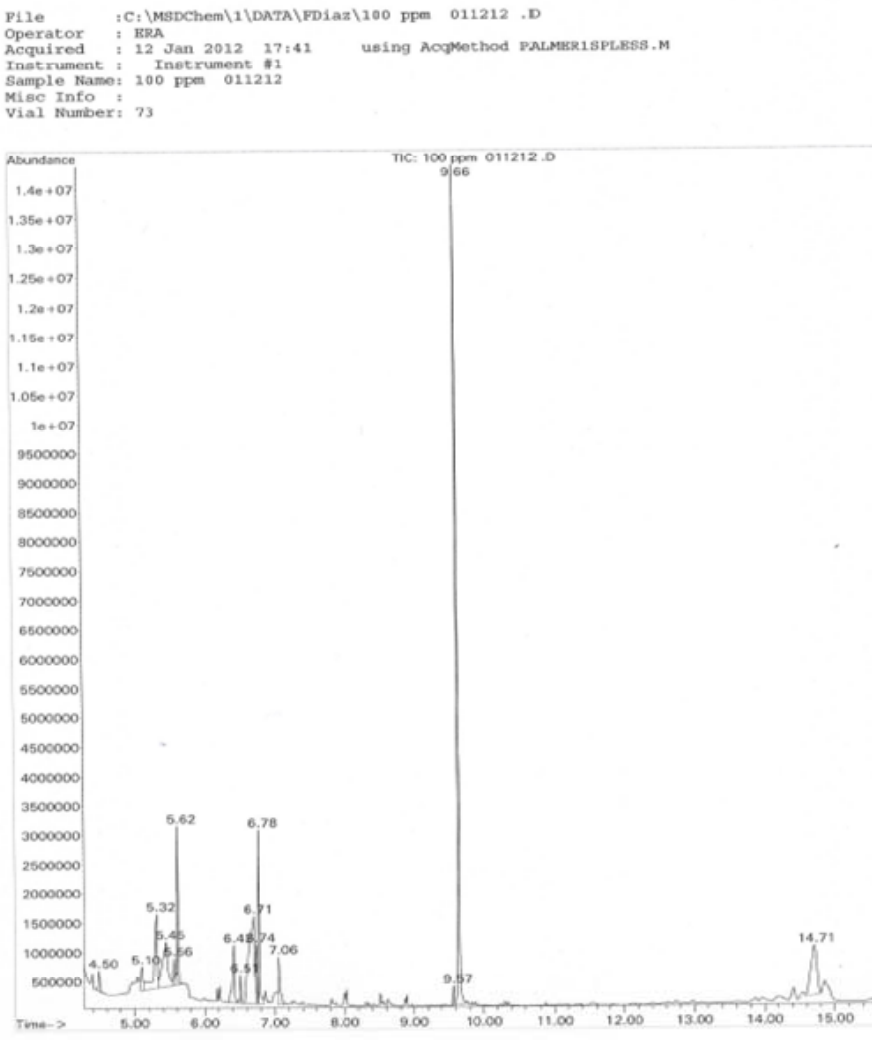

Figure 51: Total ion chromatogram: Pure (E)-BCP.

The drug eluted as single peak with retention times of 9.654 +/- 0.005 (Fig. 51 and 53). Specificity for (E)-BCP was detected using selective ion monitoring (SIM) for each substance. The full scan spectrum of (E)-BCP (Fig. 51) revealed the ionized product molecules to be in abundance with a mass-to-charge ratio of m/z= 91, m/z= 93 and m/z= 133 (Fig. 52). Compound peak identification was done by comparison to the spectrum in the National Institute of Standard and Technology (NIST) mass spectral library data. Representative single ions were extracted from total ion chromatogram and their area value integrated (Fig. 53).

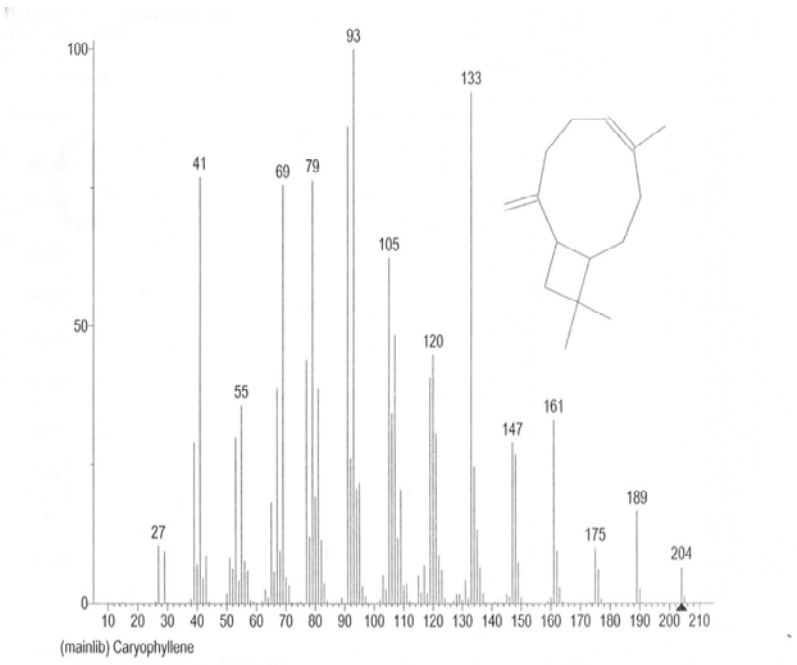

Figure 52: Full scan mass spectrum showing the monitored transitions of (E)-BCP, corresponding to the retention time at 9.66 min. on Fig.51.

The ratio of the peak area of the (E)-BCP to the peak area of the α-pinene internal standard was determined for each calibration standard.

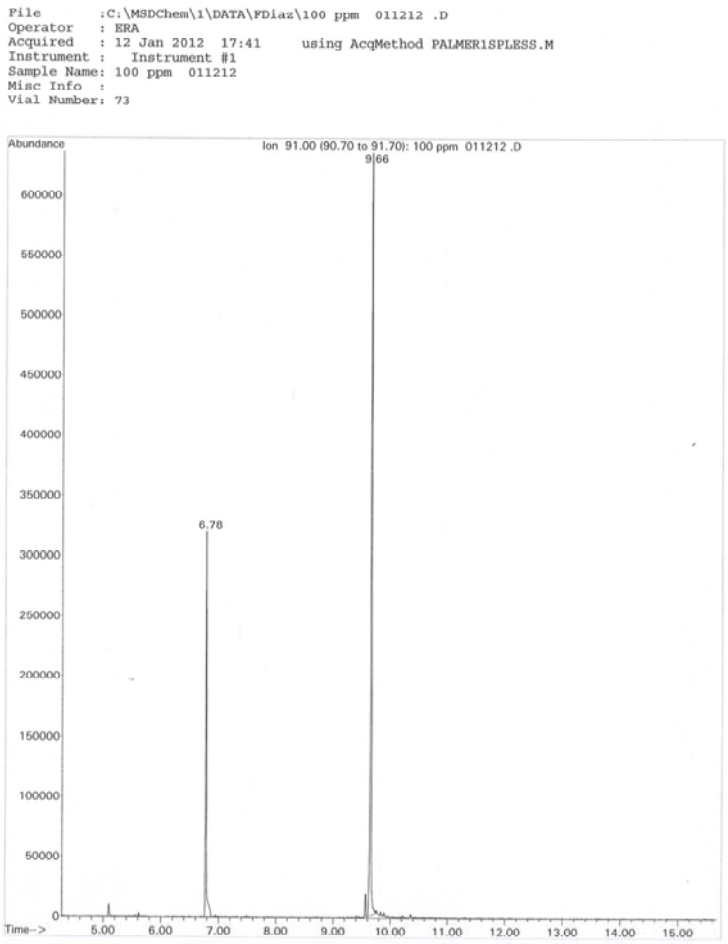

Figure 53: Representative (E)-BCP (Rt = 9.66) extracted ion (m/z=91) chromatogram and compared for quantitation to α-pinene (Rt = 6.78).

A calibration curve was prepared by plotting the ratio of the two peak areas versus the concentration of (E)-BCP. Linearity and reproducibility of calibration curves was determined using a second-degree polynomial regression and returned in acceptable results over the (E)-BCP range investigated. The correlation coefficient (r^2) for each curve was 0.9951 or better (see example Fig. 54).

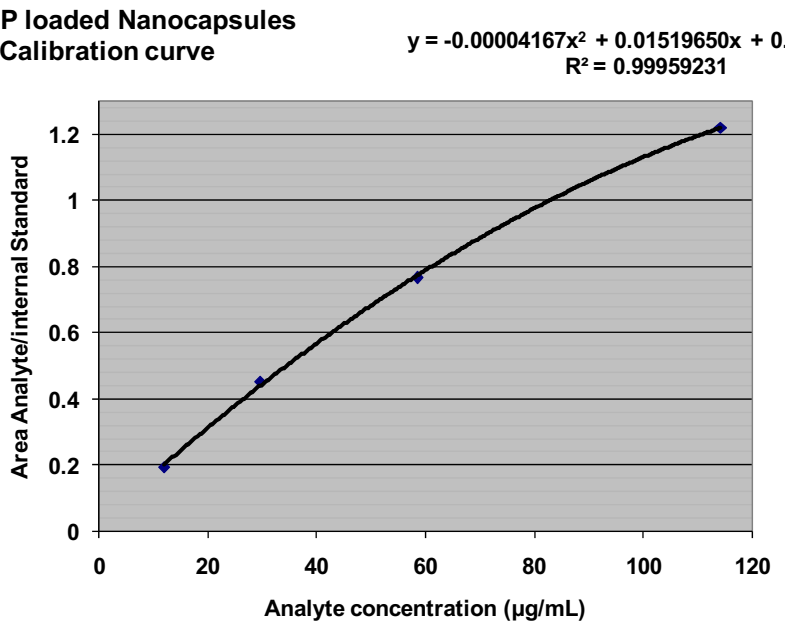

Figure 54: Example of calibration curve used to determine the (E)-BCP entrapment efficiency in NCs.

The concentration of extracted (E)-BCP from unknown samples was determined by measuring the ratio of the peak area for the analyte to that of the internal standard, and reading the concentration from the appropriate calibration curve. Recoveries were calculated as following:

$$\text{Drug entrapment efficiency \% w/w} = \frac{\text{Mass of drug recovered in NC}}{\text{Mass of drug incorporated in NS}} \text{ X } 100$$

Intra-day precision was determined for the (E)-BCP calibration curve by percentage of coefficient of variance (CV) according to the following formula:

$$\text{CV \% w/w} = \frac{\text{SD}}{\text{Mean}} \text{ X } 100$$

Where SD is the standard deviation.

The intra-day precision (CV) was very good. One example of calibration curve is given below with a CV as low as 0.6% (Table 26).

Table 26: Intra-day assay (calibration curve).

	Nominal (E)-BCP concentration (µg/ml)			
	11.9403	29.6296	58.5366	114.2857
	Recovered (E)-BCP concentration (µg/ml)			
	11.3477	30.3511	57.601	115.2041
	11.3509	30.4740	58.005	113.9264
	11.3886	30.6525	58.157	114.2366
Mean	11.36	30.49	57.92	114.46
SD	0.02	0.15	0.29	0.67
Precision - CV (%)	**0.20**	**0.50**	**0.50**	**0.58**

SD: standard deviation, CV: coefficient of variance

12.2.2 (E)-BCP extraction method.

Several attempts were performed to search for a suitable method for the extraction method of entrapped drug in NCs. Methanol, methylene chloride, tetrahydrofuran (THF), isopropanol, acetone and heptane were used as solvent to extract (E)-BCP from the freeze-dried NCs (containing 5% w/w of sucrose) and then diluted with heptane before injection into the GC-MS. Isopropanol didn't allow the solubilization of the NPs. According to the amount of (E)-BCP recovered (% w/w), the solvent extraction capacity ranked in descending order was tetrahydrofuran (63.4%) > methanol (62.4%) > acetone (48.5%), methylene chloride (35.8%) and heptane (2.1%). THF was the solvent selected for further (E)-BCP extraction.

13 Drug-loaded nanocapsules preparation.

The cationic NCs developed were successfully prepared by the nanoprecipitation technique patented by Fessi et al.[136] (Fig. 55 and Experimental section 6.4).

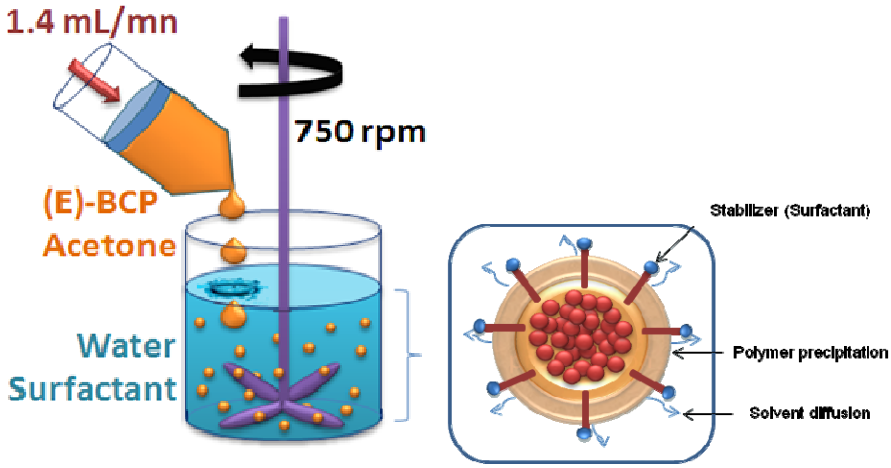

Figure 55: Set-up used for preparation of nanocapsules by nanoprecipitation method.

This simple and robust procedure allowed obtaining reproducible metastable NCs dispersions in term of entrapment efficiency, particle size, size distribution and morphology. The organic phase (i.e. acetone) containing beforehand dissolved polymer and (E)-BCP was injected at a constant flow-rate into stirred aqueous phase containing a hydrophilic stabilizer (i.e. Poloxamer 188), resulting into a colloidal NCs dispersion (see Fig. 56-1, -2, -3, -4) with a transparent to opalescent bluish aspect (i.e. Tyndall effect)[137-139]. This phenomenon is caused by the visible scattering of light along the path of a beam of light as it passes through a system containing discontinuities (i.e. colloidal particles). As particles were increasing in size in some of the experiments, the blue color of scattered light disappeared and the scattered radiation appeared white, with precipitation of the particles at the bottom of the beaker (see Fig. 56-5). The removal of the organic solvent from the swollen NCs by distillation at reduced pressure was monitored by FTIR (see Fig. 57), for safety concerns (i.e. toxicity) and to preserve NCs physicochemical properties (e.g. stability).

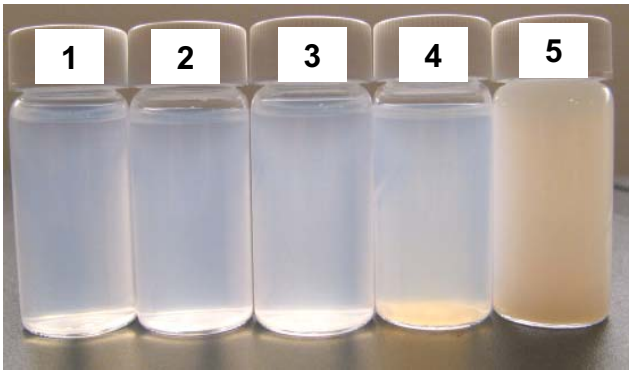

Figure 56: Picture of nanosuspensions prepared with increasing amount of polymer from left to right. 1, 2, 3, 4, are colloidal dispersions of polymeric NCs (Tyndall effect). 5, is opaque and composed of larger particles.

14 Selection of the organic solvent.

According to technical documents provided by Rohm and Haas Polymer[140], few semi-polar and water miscible solvents (e.g. methanol, ethanol, acetone, methylene chloride) were available to solubilize Eudragit® RS100 and RL100 in a time compatible with laboratory experiments (<2 hours). Unlike solvents such as dichloromethane or methanol classified “solvents in class 2” by the FDA, acetone and ethanol are classified “solvents in class 3” and may be regarded as less toxic in short-term toxicological studies, negative in genotoxicity studies and of lower risk to human health[141]. Amounts of these residual solvents of 50 mg per day would be acceptable without any justification. Copolymer solubility was then visually determined in ethanol and acetone to select the organic solvent to employ in the nanoprecipitation process to obtain polymeric NCs. 0.8 g of a mixture 1:1 Eudragit® RS 100 and RL100 stirred at room temperature didn’t dissolve in 6 g of ethanol after more than 2 hours while yielding to a transparent solution in less than 30 min when acetone was used. Acetone was selected for the organic solvent of phase.

15 Preliminary results.

At the beginning of this project, the available literature based on drug-loaded nanoparticles using Eudragit® RS 100 and RL100 polymer was sparse[112, 114, 116, 142-145]. To our knowledge, only two groups Ulbrich et al.[116] and Gargouri et al.[145] had used the nanoprecipitation method for respectively encapsulating cyclosporin and DNA in Eudragit® RS 100 and RL100 obtaining nanoparticles in the range of 50 nm to 350 nm. Recently, other authors[146-149] had developed drug-loaded Eudragit® RS 100 and/or RL100 nanoparticles but none of them provided detailed information with regard to solvent phase injection flow-rate or solvent evaporation conditions (e.g. reduced pressure value, duration and temperature). Prior to identifying a standard nanosuspension (NS) (entry 10 Table 31) and evaluate on that basis the relevant parameters and the mechanisms involved in nanoprecipitation technique, we proceeded by trial and error on non-optimized systems by visual observation and entrapment efficiency (EE) analysis. One of the preliminary system investigated contained 20% w/w polymer-to-solvent phase ratio and was proven to not be satisfactory in term of particle size range upon further particle sizing studies (entry 5 Table 29 and entry 11 Table 31). Despite many experiments involved, the results obtained are not always discussed if judged unreliable (e.g. non controlled conditions process) or are cited in support to results generated with the standard NS (entry 4 Table 29 and entry 10 Table 31) to confirm demonstrated trends. These preliminary results allowed us to address the essential need of controlled process parameters i.e. solvent phase injection flow-rate and monitoring of acetone removal during rotary evaporation as well as to support the set up of the GC-MS method developed. Also, the polymeric NCs presented in this work have been developed and often repeated in triplicate for particle analysis studies using a Coulter Sub Micron Particle Analyzer Model N4MD. Since this instrument is not equipped of software, no recorded raw data

Table 27: Composition of the NS entry A developed during the exploratory phase.

Entry	Drug loading (mg)	Eudragit® RS100/RL100 1:1 (mg)	Polymer:acetone ratio (% w/w)	Water volume (mL)
A	300	1200	20	50

could be retrieved. For that reason, and for accuracy purpose, experiments have all been repeated once in a host laboratory (Ateris^{TM}, Bozeman, USA) and analyzed using a Malvern Nano S.

15.1 Freeze-drying and cryoprotectants selection.

During this exploratory phase, the influence of several cryoprotectants (i.e. glycerol, sucrose, trehalose) has been determined on the stability of polymeric NCs (entry A Table 27) after freeze-drying. Lyophilization represents a useful methodology to ensure long-term conservation of drug-loaded NCs to obviate aggregation/particle fusion and/or chemical instability as well as drug leakage[150]. As the temperature decreases during freezing, the cryoprotectant forms a glassy/vitreous protective matrix surrounding the NP protecting it against mechanical stress of ice crystals and subsequent aggregation. Freeze-dried NCs resulted in white fluffy and sheet-like powder/cake whereas the appearance was more crystalline when sucrose or trehalose were added as cryoprotectants. All the cryoprotectants incorporated either at 0% or 5% w/w in the NCs preceding freezing at -80°C and lyophilization (Labconco FreeZone® 1), didn't preserve the NCs from physical degradation. Aggregation of NCs occurred, and redispersibility while stirring for 30 min. in a volume of water equivalent to the NS led to macroscopic aggregates and slight sedimentation, although less pronounced in the NS containing 5% w/w cryoprotectant. Nonetheless, concentration of 15-20% w/w of sucrose or trehalose were sufficient to prevent NCs fusion and/or destabilization[151] and redispersion was reached in less than 15 min.

15.2 Solvent removal conditions and monitoring.

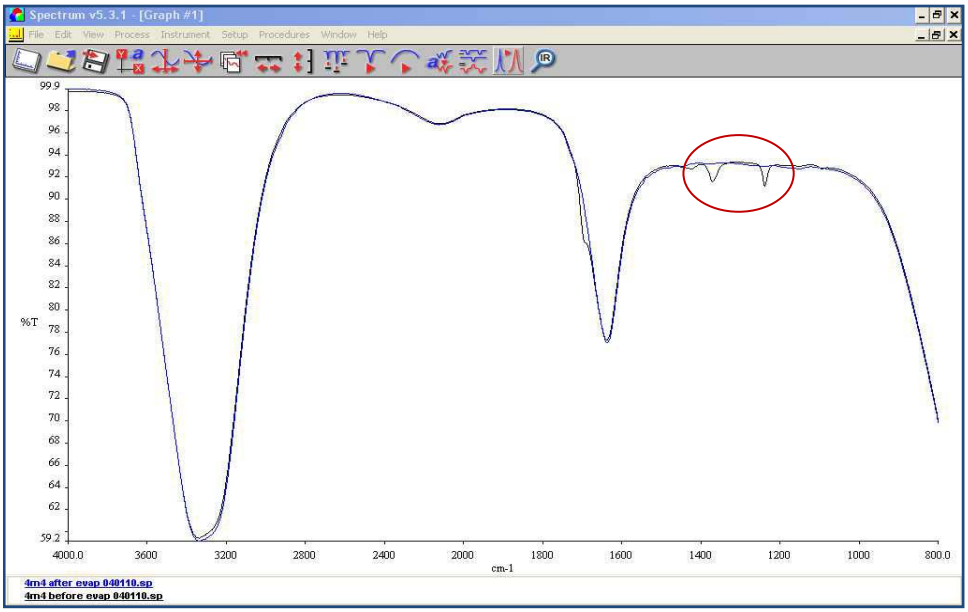

Figure 57 FTIR spectra of the NS entry 10. Superimposition of spectra obtained before and after rotary evaporation. The two characteristics peaks for acetone are at 1370.41 cm-1 and 1237.86 cm-1.

The residual acetone remaining in the polymer matrix after nanoparticles manufacturing can cause problems in the efficacy of the therapeutic, ranging from degradation of encapsulated drug and destabilization or deformation of the NPs to direct toxic biological effect[152-153] and other complications creating significant regulatory hurdles in the product development. In order to control the efficiency of solvent removal from the formed NCs, a sample of the NS was collected at regular time intervals and analyzed using FTIR (Fig. 57). The experiments conducted on preliminary NS batches were aimed at studying the characteristics of the extraction process namely the optimum time, temperature and reduced pressure required for complete solvent removal, NCs stability (assessed visually) and satisfactory (E)-BCP entrapment efficiency. All these parameters were essential in ensuring production of NS having (E)-BCP-loaded NCs with a narrow size distribution and minimum residual solvent. After optimization of the solvent removal process, only quality control testing was performed on NS after acetone evaporation. In the course of the development of the NCs particle size measurement of NS before rotary evaporation and after always led to a decrease in the NCs hydronamic radius. As an

example, these values were respectively and approximately 109 nm (PDI 0.18) before evaporation and 101 nm (PDI 0.15) after evaporation for the standard NS developed (entry 10 in Table 31).

In this set of experiments (Table 28), solvent-to-non solvent phase ratio was kept constant while impact of the solvent evaporation conditions was evaluated on the (E)-BCP EE of NS composed of various drug-to-polymer ratio. Visual observation of possible physical destabilization (i.e. particle coalescence) was also conducted. Composition of entries B, F, G, H and I in Table 28 are similar to the NS entry 10 Table 31 selected as our standard.

Table 28: Influence of solvent evaporation conditions on the entrapment efficiency of various NS taken as examples.

Entry	drug:polymer ratio (% w/w)	Drug loading (mg)	Polymer (mg)	Duration (min.)	Vacuum (mb)	Temperature (°C)	Entrapment Efficiency % w/w recovery +/- SD
A (n=2)	1:4	300	1200	60	70	40	82.2+/-0.9
B	1:13	45	600	60	70	40	48.3
C	1:13	23	300	60	70	40	35.3
D	1:6	45	300	60	70	40	13.5
E	1:6	23	150	60	70	40	5.2
F (n=2)	1:13	45	600	60	20	20	44.4+/-3.7
G	1:13	45	600	45	10	20	46.1
H (n=2)	1:13	45	600	60	10	20	0
I (n=5)	1:13	45	600	40 10	70 10	20	76.3+/-3.5

n=number of replicates, SD= standard deviation.

Entrapment efficiency was emphatically affected by the solvent removal process conditions. We evidenced (Table 28) that (E)-BCP was undergoing steam and vacuum co-distillation during the acetone and water rotary evaporation process. Steam distillation is a common technique used to purify temperature sensitive materials like natural aromatic compounds (i.e. essential oils)[133]. Sesquiterpenes such as (E)-BCP from clove

oil[123, 154] can be separated and isolated using this method. All the protocols reported in Table 28 allowed successful removal of acetone from the polymeric NCs as assessed by FTIR. For acetone evaporation, boiling point of 40°C is normally required at pressure condition of 556 mb. According to our results, conditions of 40 min/40°C/70 mb (entries A to E) or 40 min/20°C/70 mb followed by a second phase of 10 min/20°C/10 mb (entry I) were the minimal requirement to eliminate the acetone from our system. It is also necessary to take account of Raoult's law which states that the boiling temperature of a mixture (e.g acetone/water) rises as the concentration of its low-boiling component (e.g. acetone) decreases[155] in addition to the fact that the acetone distillation may be hampered by acetone-polymer interactions. Several attempts have been made to concentrate the (E)-BCP in the NS, evaporating water down to 1/10th of the initial NS volume (entries F, G and H). The aim was to facilitate *in vivo* administration of fresh NS (10-20 mg/Kg) with reduced "gavage" volume.

Among the NS prepared, only solvent removal conditions applied to entries A and I were satisfactory in term of EE (Entrapment Efficiency) with 82.2% and 76.3% of drug recovered respectively. It seems obvious than the composition of the NCs, and particularly the polymer content and the drug-to-polymer ratio, alter significantly the NCs drug loading. For NS manufactured following identical pressure conditions (entries A-E) i.e. 40 min/40°C/70 mb the trend observed was that the lower the polymer content, the lower the EE (entries E< C< D< B < A). Keeping the same ratio of drug-to-polymer, with decreased polymer content (e.g. entries E< D or C<B) confirmed this observation. According to different authors, the NC shell thickness could be increased with higher polymer concentration and may affect the drug release[156-159] or the propensity of (E)-BCP towards steam distillation. When vacuum was reaching values of 10 mb or 20 mb, the drug distillation was enhanced (entries F, G, H) since at 40 mb the water boiling point is lower (13.4°C) than the temperature we set up (20°C). Loss of the entire (E)-BCP entrapped was noticed under the conditions undergone by the NS entry H. The pressure conditions described for the entry I selected as a standard for further investigations were optimal considering the high and reproducible EE achieved (76.3%) over five replicated NS, allowing reliable acetone removal without any physical NCs destabilization i.e opalescent and bluish dispersions. In addition this EE was even improved upon formation of macrocycles-NCs complexes (see section 16.9).

15.3 Optimization of solvent phase addition flow-rate.

A programmable syringe pump was used to inject the organic solution into the aqueous phase through a syringe (10 mL) at a constant flow-rate of 1.4 mL.min^{-1} in order to ensure reproducibility of the process. Some authors reported that a preferred way to prepare NPs using nanoprecipitation method is to rapidly inject the organic phase into the aqueous phase[66, 136, 160] to reduce mean size of the resulting NCs. We investigated three different flow-rates of 0.7, 1.4 mL.min^{-1} and 23.3 mL.min^{-1} on one batch of the standard NS entry 10 Table 31. Flow-rate of 0.7 mL.min^{-1} didn't produce any colloidal system formation since precipitation of polymer occurred at the aperture of the syringe because of acetone evaporation before mixing with aqueous phase. With flow-rates of 1.4 mL.min^{-1} and 23.3 mL.min^{-1} the particles were not significantly different in mean diameter, respectively 105 (PDI 0.21) and 115 (PDI 0.41), although the NCs size was more homogeneous with slower rate. However the EE was fairly impacted and decreased by faster mixing of organic phase and aqueous phase, 65.6% w/w recovered, compared to 74.8% w/w recovered using a flow-rate of 1.4 mL.min^{-1}. As described by Beck-Broichsitter et al.[66], one of the critical parameter in NCs formation is the velocity of diffusion of the polymer containing-organic phase. Higher diffusion rates are usually thought to favour homogeneous dispersion of polymer/acetone/drug droplets in the aqueous phase, lower local acetone concentration and higher velocity diffusion, resulting in smaller particles. However the flow-rates reported are generally no greater than 10 mL.min^{-1}. Higher flow-rate may provoke too high local supersaturation in polymer/acetone/drug reducing solvent diffusion thereby yielding to polymer aggregation, increased NCs polydispersity and poor drug entrapment efficiency. An appropriate flow-rate needs to be set up in order to circumvent polymer aggregation and favour organic solute nucleation and growth owing to homogeneous high supersaturation. Flow-rates of 1.4 mL.min^{-1} yielded to relatively monodisperse NCs and satisfactory (E)-BCP loading.

16 Physicochemical parameters associated with NCs formation.

In order to design suitable nanocapsules with predictable performance and reliable process, understanding of the relationships between composition, process parameters,

and physicochemical properties of the final nanosuspension are essential. Despite the literature available in this area, there is still no ‘‘universal theory’’ for predicting NPs size, size distribution, and dispersion stability[61, 161-163]. Thus large numbers of samples are required to explore a particular nanoparticulate material, and the effect of parameters such as drug-to-polymer ratio, solvent phase-to-non solvent phase ratio, polymer-to-organic solvent ratio, nature and amount of surfactant, organic solvent nature, organic phase injection flow-rate, polymer (Eudragit® RS or RL) nature were evaluated on the NCs size and particle size distribution (PCS) and entrapment efficiency (GC-MS). The methods used for PCS and GC-MS are described respectively in the experimental section 4.3.4 and 6.3.

16.1 Influence of polymer to solvent phase ratio.

The drug release profile can be customized by combination of Eudragit® RL and RS in different ratio since Eudragit® RL is composed of more functional quaternary ammonium groups as previously mentioned and therefore is subsequently more permeable than Eudragit® RS. We arbitrarily selected a ratio of 1:1 Eud RL/RS and prepared different batches of empty NCs with an increased concentration of polymer amount (see Table 29). The objective was to define a range of polymer concentration wherein the polymer solution would be diluted enough to be metastable (“Ouzo” region) which would result in stable colloidal dispersion, while affording a drug loading capacity compatible with therapeutic oral dose.

Table 29: Mean particles diameter (Z-average) and size distribution of nanosuspensions prepared with varying polymer concentration.

Entry	Eudragit® RS100/RL100 1:1 (mg)	Polymer:acetone ratio (% w/w)	Z-average (nm) [PDI]	Aggregates % w/w in NCs (mg)
1	75.0	1.25	128 [0.33]	-
2	150.0	2.50	60 [0.26]	-
3	300.0	5.00	74 [0.24]	-
4	600.0	10.00	78 [0.22]	-
5	1200.0	20.00	131 [0.20]	0.95% (13.8mg)

NCs: nanocapsules, PDI: polydispersity

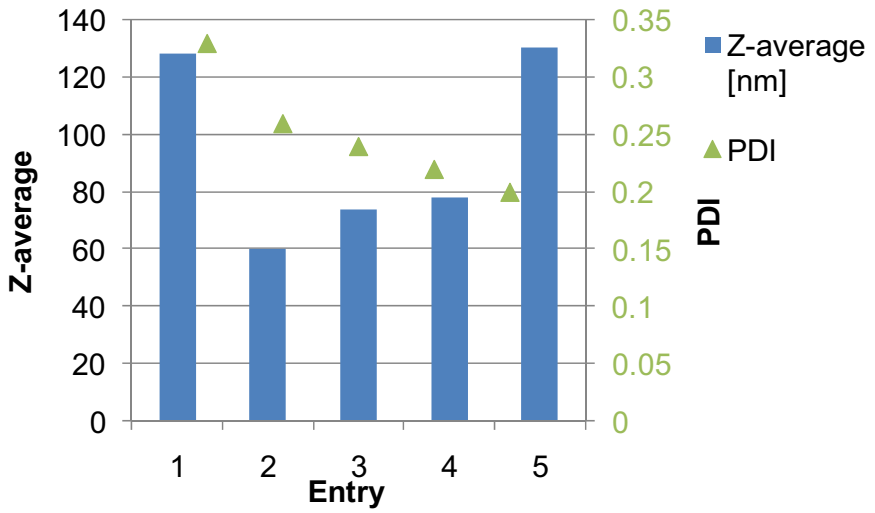

Figure 58: Representation of the Z-average size of nanosuspensions prepared with varying polymer concentration.

In a first set of experiments, the polymer to phase solvent (pol/$\Phi_{solv.}$) ratio was varied from 1.25% to 20.00% (w/w) (Figure 58 and Table 29) in a total volume of 6 mL acetone. At the lowest polymer concentration, a transparent to opalescent bluish dispersion was obtained. As the polymer concentration increased, the opalescence intensified (entries 1-4 in Figure 56 and entry 3 in Fig. 59). At the highest concentration (entry 5 in Figure 56 and 60), sedimentation of aggregates was obvious. According to the "Ouzo" theory[72, 164], nanosuspensions prepared with polymer concentration ranging from 1.25% to 10.0% (pol/$\Phi_{solv.}$) can correspond to the metastable region (i.e. "Ouzo" region) located between the binodal (miscibility limit curve) and spinodal (stability limit curve) of the phase diagram

Figure 59: Picture of entry 3 in Table 29.

Figure 60: Picture of entry 5 in Table 29.

composed by polymer/solvent and non solvent phase[164] where this nucleation-and-growth process produces dispersion of stable nanoparticles. Beyond the "Ouzo" boundary, when polymer concentrations are comprised somewhere in between 10.0% and 20.0% (pol/$\Phi_{solv.}$), the dispersion becomes unstable and macroscopic aggregates are triggered as observed for the entry 5.

Analyses of particle size for the nanosuspensions containing from 2.5% to 20.0% (pol/$\Phi_{solv.}$) i.e. entries 2-5 confirmed these observations. NPs Z-average increased as the polymer concentration increased, ranging from 60 nm to 131 nm (entries 2-4) while the polydispersity (PDI) decreased. However, it was noticed than in the entry 1 although composed of dilute polymer, the mean particle size was greater than for the entries 2-4. It is known that the resulting size of NPs yielded by nanoprecipitation technique is dramatically correlated to the polymer concentration[4, 65, 162, 165] and consequently to the viscosity of the polymer solution. Indeed, the viscosity of the organic phase should be low enough to circumvent entanglements between the polymer chains forming macroaggregates[165]. The theory of Lamer[139] describes the nucleation-and-growth of small nuclei in supersaturated solutions and is helpful in understanding how the polymer concentration influences the NCs size. When hydrophobic substances (i.e. polymer) are injected into hydrophilic substances (i.e. water), they become supersaturated resulting in the formation of small nuclei followed by growth by diffusion of molecularly dissolved solute (i.e. polymer) to nuclei (=Ostwald ripening), until the supersaturation is reduced and colloidal stability is reached. Above a certain concentration of solute, claimed to be >10^{-2}g S/l by Lamer[139] or 10.0% (pol/$\Phi_{solv.}$), the rate of production of nuclei is so rapid that both nucleation and growth occur rapidly. With such degree of saturation that rate of formation of nuclei can't become practically zero

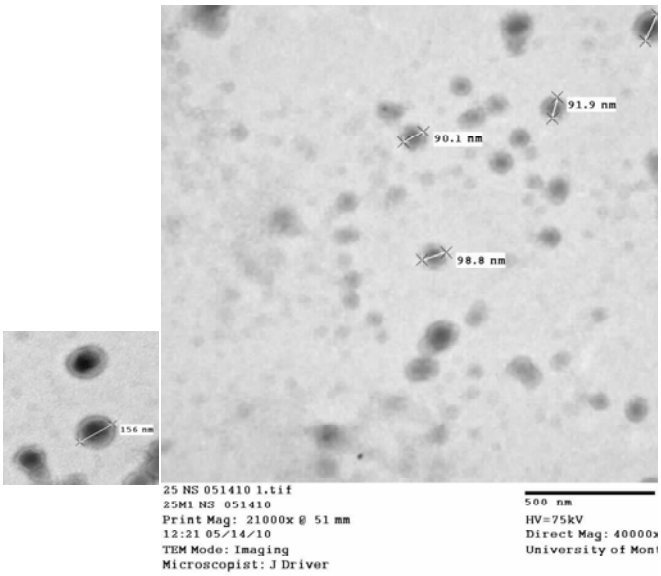

Figure 61: TEM imaging NS entry 7. Magnifying A) x50,000 B) x40,000.

being relieved by diffusion and repetitive nucleation[71-72] and/or nucleation-aggregation mechanism[166-167]. Either of the former events lead to macro aggregates or microparticles as observed for the entry 5 and formation of NCs located outside of the “Ouzo boundary”. Altogether, when the concentration of polymer solution is sufficiently dilute avoiding the entanglement of polymer chains and repetitive nucleation/nucleation-aggregation phenomena, the nucleation of polymer occurs in the metastable “Ouzo” region. In this region (solutions with small polymer-to-solvent ratio i.e. 1.25%-10.0%), so few polymer molecules are near each nucleus that only very small particles form. With increasing polymer-to-solvents ratio, more polymer are near each nucleus, so larger droplets are formed by Ostwald ripening[72] resulting in a more homogeneous population of nanoparticles (PDI decreasing as the polymer-to-solvent ratio is increased), preserving however their colloidal appearance (Fig. 56) and stability (unquantifiable macroaggregrates Table 29). According to Aubry et al.[65] in very low supersaturation conditions, heterogeneous nucleation and formation of a smaller number of nuclei (since the number of critical nuclei varies exponentially with the supersaturation[166]), yield to larger particles. This is in accordance with what was observed for the polydisperse nanosuspension entry 1 (Z-average 128 nm) wherein more than one species is present (PDI 0.33).

16.2 Influence of drug to polymer ratio.

The nanosuspension particle size and Entrapment Efficiency (EE) were investigated in formulations wherein the (E)-BCP content was varied in the range of drug-to-polymer ratio comprised in between 1:4 and 1:26 (22.5mg to 90mg of (E)-BCP) and the polymer content was kept constant (600mg).

Table 30: Mean particles diameter (Z-average), size distribution and entrapment efficiency of nanosuspensions prepared with varying drug-to-polymer ratio.

Entry	Drug:polymer ratio	Drug loading % w/w in NCs	Entrapment efficiency % (w/w) recovery	Z-average (nm) [PDI]
6	1:4	11.10	74.20	147 [0.34]
7	1:13	6.50	74.80	105 [0.21]
8	1:26	3.40	75.70	88 [0.24]

NCs: nanocapsules, PDI: polydispersity

(E)-BCP is an oil and this study confirms the high drug loading capacity of NCs compared to nanospheres[168]. When initial drug loading-to-polymer was decreased (from entries 6 to 8 in Table 30, Fig. 62), the NCs size decreased significantly while the EE didn't exhibit any change.

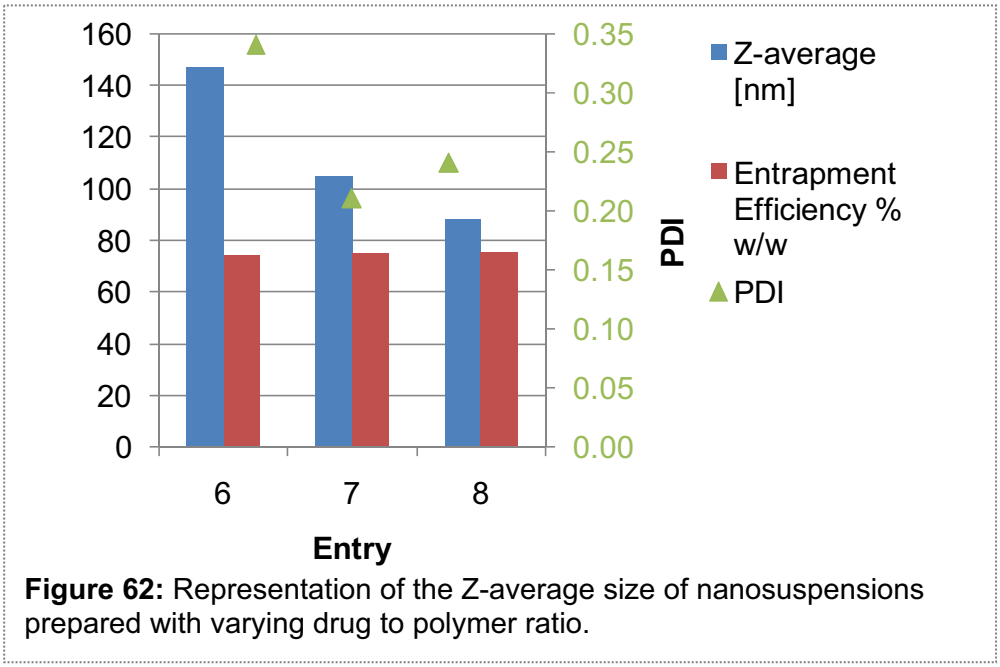

Figure 62: Representation of the Z-average size of nanosuspensions prepared with varying drug to polymer ratio.

These results were similar to that previously reported when different nature of oils have been incorporated in NCs (e.g. sunflower seed oil, soybean oil[4], castor oil, sesame oil and Labrafac® Hydro[169]). It is assumed that increasing the oil content triggers higher viscosity of the dispersed solvent phase and interface tension, and as a consequence a greater particle diameter and PDI. The entry 6, loading with 90 mg of (E)-BCP yielded to a non stable (i.e. slight sedimentation) and opaque dispersion. Entries 7 and 8 were both

stable and colloidal nanosuspensions. Entry 7 allowed higher drug loading (45mg) and morphology studies evidenced rounded-shape NCs with an oily core surrounded by a polymeric shell with a thickness of approximatively 25 nm (Fig. 61). Entry 7 composed of 1:13 drug-to-polymer ratio was selected as a standard for further characterization studies.

16.3 Influence of polymer-to-solvent phase ratio on drug-loaded NCs.

Table 31: Mean particles diameter (Z-average), size distribution and entrapment efficiency of drug-loaded nanosuspensions prepared with varying drug to polymer ratio.

Entry	Polymer (mg)	Polymer:acetone ratio % w/w	Entrapment efficiency % w/w recovery		Z-average (nm) [PDI]	
			NF	F	$t_{initial}$	t_{1day}
9	300.0	5.0	66.70	60.4	104 [0.20]	98 [0.19]
10	600.0	10.0	77.20	75.7	101 [0.15]	99 [0.16]
11	1200.0	20.0	94.40	NA	130 [0.23]	157 [0.36]

PDI: polydispersity, F: Nanosuspension filtered through 0.45µm syringe filter, NF: Non filtered, NA: Not Applied

In the objective of confirming the results obtained in the section 16.1 on empty NPs, with respect to the mean particle diameters of the dispersions formed by “Ouzo” effect as a function of polymer content, we conducted similar experiments with drug-loaded NCs. The polymer-to-phase solvent ratio was varied from 5.0% to 20.0% and the drug content was fixed at 45 mg or 1:13 polymer-to-drug ratio. Entries 9 and 10 were obtained as opalescent bluish dispersions whereas entry 11 was an opaque dispersion composed of microaggregates. As expected, (E)-BCP-loaded NCs (entries 9, 10, 11 in Table 31) had a mean diameter larger than the corresponding drug free particles (respectively around 74 nm, 78 nm and 131 nm for 5%, 10% and 20% w/w of polymer content) with a relatively narrow PDI. Similar characteristics in terms of particle size and macroscopic appearance were observed. The higher polymer concentration in the solvent phase led to an increase in particle size (Fig. 63). EE was also linearly affected by the polymer content. EE obtained for filtered and non filtered entries 9 and 10 NS were similar and corroborates

the hypothesis of metastable dispersions containing only nanoparticles. Filtration of entry 11 wasn't feasible because of immediate clogging of the filter (0.45µm), supporting the hypothesis of nano- and micro- particles or macroaggregates formation.

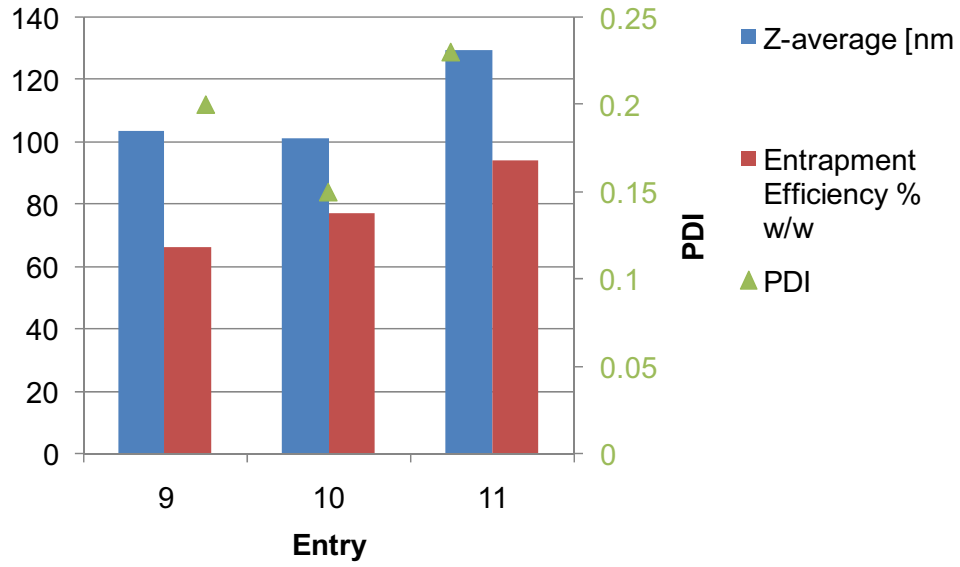

Figure 63: Representation of the Z-average size of nanosuspensions prepared with varying drug to polymer ratio.

PCS analysis performed at t_{1day} (entry 11) strengthened that aggregation/coalescence and destabilization mechanisms were taking place in the system resulting in enlargement of the NCs size and sedimentation in the vial. Although entries 9 and 10 were composed of different polymer amounts, these NS exhibited similar particle size distribution. As reported, the NC shell thickness could be increased with higher polymer concentration while the number and size of NCs is not necessarily affected[156-159]. In addition, we observed in other sets of experiments (see section 15.2) that (E)-BCP was undergoing steam distillation during the solvent evaporation phase using a rotary evaporator. It could be assumed that (E)-BCP steam distillation occurring during the solvent evaporation is inversely related to the NC shell thickness as observed for the entry 9 (5% polymer) compared to entry 10 (10% polymer). Overall, drug EE can be improved by increasing the polymer content but only NS formed in the "Ouzo" region will be relevant in drug delivery.

16.4 Influence of solvent phase nature and ratio on drug-loaded NCs.

The main prerequisite for the choice of the solvents was good solubility properties for the polymer, also miscible with water and low boiling point to facilitate its elimination by evaporation[162]. We investigated the effect of the nature and the ratio of different organic solvents on the nanosuspension particle size and EE where (E)-BCP and polymer content were kept constant at respectively 45 mg and 600 mg.

Table 32: Mean particles diameter (Z-average), size distribution and entrapment efficiency of drug-loaded nanosuspensions prepared with varying solvent phase nature and ratio.

Entry	Acetone (mg)	Ethanol (mg)	Water (mg)	Entrapment efficiency % (w/w) recovery	Z-average (nm) [PDI]
10	6.0	-	-	77.20	101 [0.15]
11	3.3	2.7	-	54.70	67 [0.38]
12	3.3	-	2.7	47.50	73 [0.45]
13	10.0	-	-	58.80	85 [0.41]

PDI: polydispersity

The organic solvent phase was modified using a total volume of binary liquids (acetone-ethanol entry 11 and acetone-water entries 12 Table 32) set to 6 mL whereas pure acetone was also tested at two different total volumes of 6mL (entry 10) and 10mL (entry 13). At a polymer concentration where aggregation was not apparent, the mean particle size and the drug EE were clearly dependent on the nature or the ratio of the solvents, and were both generally reduced compared to the entry NS 10. In the procedure of NCs formation by nanoprecipitation, when both solvent and non-solvent phases are in contact, it is assumed that the organic phase diffuses into water and carries some polymer chains and the liquid lipophilic oil which are still in solution. As the solvent diffuses further, oil repels the polymer at the oil/water interface, and the polymer aggregates, forming the NC[161]. The exact composition of the solvent/non-solvent system has been reported to strongly determine the particle size and size distribution[66, 164-165].

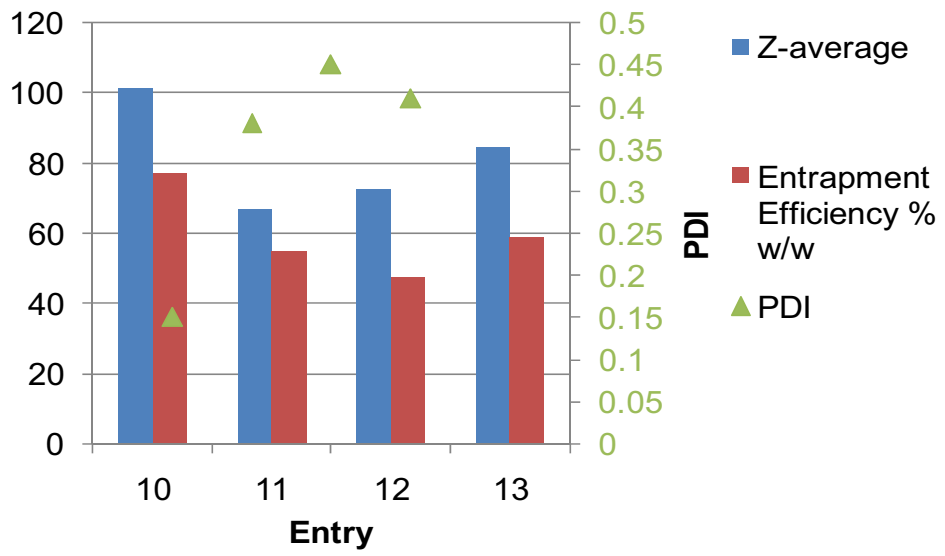

Figure 64: Representation of the Z-average size of drug-loaded nanosuspensions prepared with varying solvent phase nature and ratio.

Comparison of the results from the different preparation procedures in literature[66, 161, 170] indicates that the diffusion coefficient of the phase solvent into the non solvent phase is of great importance. Parameters such as dielectric constant ε (respectively 80.4, 24.6 and 21.0 for water, ethanol and acetone), Hildebrand solubility parameter δ (respectively 0.0, 27.0 and 34.4 for water, ethanol and acetone[162]), and the solvent/non-solvent (i.e. water) interaction parameter χ (respectively 11.0 and 23.7 for ethanol and acetone[161]) have been described to influence the solvent diffusion rate. One general rule is the higher the polarity of solvent (expressed as its ε) and the lower its χ, the higher its diffusion rate and the lower particle size[163, 171]. The viscosity of the organic phase[66, 172] and interactions between the polymer and the solvent[165] also need to be considered. It is claimed that high affinity in between polymer and solvent would lead to solvent remaining in the supersaturated polymer region and hinder the solvent motion. Depressing the viscosity could consist of including small quantity of non-solvent or less solvent (either water or ethanol) in the acetone prior to spontaneous emulsification. Both procedures are believed to suppress entanglements between polymer chains, which, when present, are enough to fail the emulsification process[71]. The results obtained for the entries 11 and 12 are in accordance with the literature, in respect with their particle size. However, these NS exhibit low EE. Most of the research in the area of the phenomena which

govern nanoprecipitation are mostly performed without drug incorporated in the nanosystems and few arguments are available in this regard. One should expect that smaller particles are yielded by higher number of nuclei generated by the supersaturation phenomenon[164] and subsequent thinner NCs shell thickness[159]. In addition, the polymer and (E)-BCP solubility has been dramatically reduced in entries 11 and 12 solvents binary systems, particularly for entry 12 where the organic phase appearance was turbid. Under these conditions, polymer chain entanglements may occur leading to the formation of microparticles or polymer macroaggregates, as supported by the large particle distribution (PDI>0.35). As mentioned in the previous paragraph, steam distillation of (E)-BCP has been evidenced upon solvent evaporation and should be expected to be greater with thinner NCs wall or entrapment of (E)-BCP in non discrete nanoparticles.

Otherwise, similar trend as for the above NS has been observed with the entry 13 (10mL of acetone) with regard to NCs size, size distribution and EE. The role of the polymer-polymer interactions may be involved since the polymer chains are independent and no overlapping of the coils may occur. Furthermore, in a more dilute regime than for the entry 10 (6mL of acetone), the solvent viscosity is reduced providing lower mass transfer resistance and increase of the organic phase diffusion rate, favoring an overall smaller NPs formation with potential higher polydispersity caused by heterogeneous nucleation[164]. The combination on the final NCs of decreased shell thickness (for the low range particle size) and higher polymer solvation may render it more porous and a greater amount of (E)-BCP could be lost during solvent evaporation. Also, with a higher amount of acetone, the supersaturation is less and (E)-BCP may lie longer in a solvated state, and propensity of polymer chains to aggregate in encapsulating (E)-BCP is less likely. Altogether, the solvent phase selected was 6 mL of acetone (entry 10), since a good EE and suitable particle size for oral delivery was reached.

16.5 Influence of solvent-to-non-solvent ratio on drug-loaded NCs by changing the volume of the continuous phase.

Table 33: Mean particles diameter (Z-average), size distribution and entrapment efficiency of drug-loaded nanosuspensions prepared with varying solvent-to-non solvent phase ratio.

Entry	Water (mL)	Solvent/non-solvent ratio =solvent mass fraction	Entrapment efficiency % (w/w) recovery	Z-average (nm) [PDI]	
				$t_{initial}$	t_{1day}
10	50.0	0.12	77.20	101 [0.15]	99 [0.16]
14	25.0	0.24	77.90	89 [0.17]	87 [0.14]
15	15.0	0.4	75.50	128 [0.02]	ND

ND: Not Done, PDI: polydispersity

As diffusion processes are predominantly gradient driven, the volume ratios of solvent and non-solvent were expected to contribute significantly to particle size[68, 170]. The aim of this study was to investigate the effect of the solvent-to-non-solvent ratio on the particle size and EE while drug-to-polymer ratio, polymer-to-solvent phase ratio were kept constant and similar to the entry 10, respectively 1:13 and 10.0% w/w.

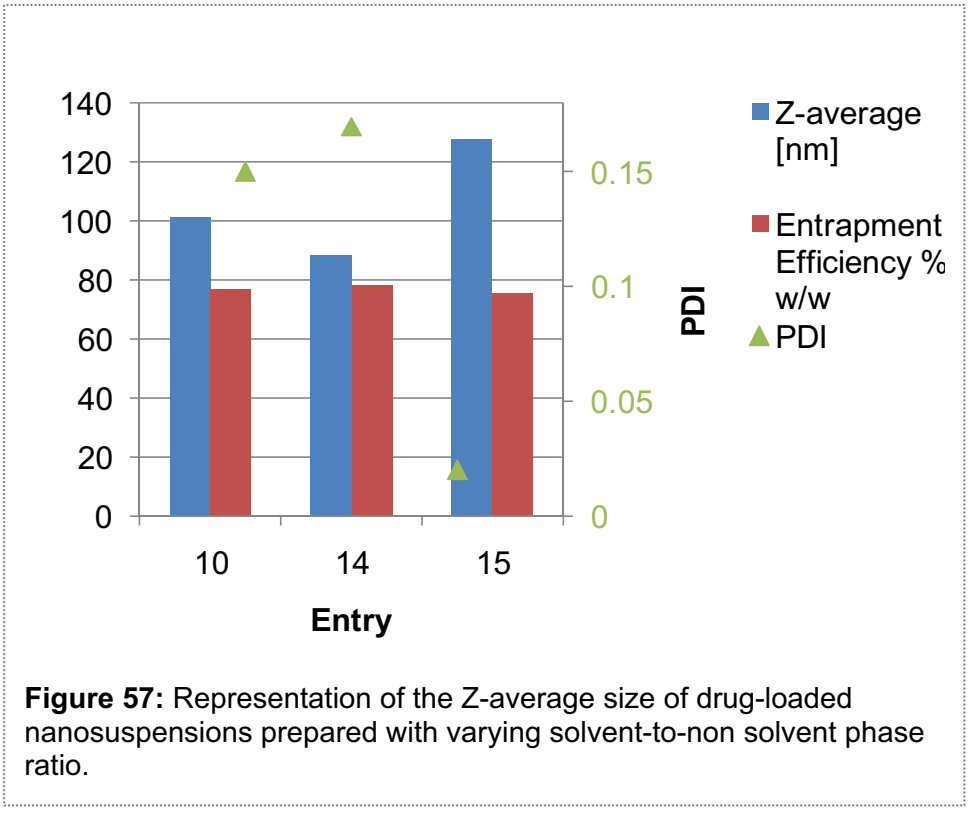

Figure 57: Representation of the Z-average size of drug-loaded nanosuspensions prepared with varying solvent-to-non solvent phase ratio.

Variations of the volume of water phase down to 15 mL didn't trigger any different behavior in terms of EE but was of significant influence for the NCs formed (i.e. size and size distribution) and appearance since the NS entry 15 (Table 33) was opaque whereas entries 10 and 14 were transparent to opalescent bluish dispersions. Aubry et al.[164] also showed that polymethylmethacrylate (PMMA) -based final dispersions size was predominantly affected by the solvent mass fraction in specific regions of the "Ouzo" boundary, when the solvent mass fraction was ≥ 0.25. For equivalent amount of polymer (entries 10, 14, 15) and small additions of water (acetone mass fraction ≥0.24), we observed the same trend as Aubry et al. since the variation of the mean NCs diameter was less impacted by the solvent mass fraction for values near 0.25 (entry 14) compared to mean NCs diameter and PDI obtained when the solvent mass fraction was dramatically increased up to 0.4 (entry 15). Considering the PDI values, the entries 10 and 14 don't exhibit fundamental dissimilarity. As discussed previously, during the nanoprecipitation procedure, a transient solvent concentration gradient is created across the non-solvent phase leading to further oil nanodroplets formation with aggregation of polymer on its surface. Smaller volume of continuous phase (i.e. water) may result in slower precipitation of the polymer chains and as suggested by Choi et al[172], larger nanoparticles will be formed by the solvent loss from the surface of the NC. Sirnikova et al.[173] demonstrated than the formation of nuclei (timescale in the range of milliseconds or faster)[174] is accompanied by further growth due to molecular diffusion known as Ostwald ripening (seconds or longer)[174]. This process occurs when the smallest droplets dissolve, since the polymer and oil concentration has dropped to below the supersaturation (i.e. nucleation ceased), and the larger ones grow by diffusion of oil and polymer into the already nucleated droplets, since their saturation is smaller and thermodynamically favored. Nucleation is a random process, so initially the droplets not uniformly distributed may tend to show an increased average size and a more evenly distribution. Ostwald ripening (OR) occurs slowly because dissolution rates are very small and the diffusion rates of the molecules are minimized as the droplets become fewer and thus farther from each other[174-175]. Combination of slow OR event and slow rigidification of the NC shell in the referred system (entry 15), may support the result incurred which is the production of large monodisperse NCs. In addition, some technical issues (i.e reproducible stirring) have been encountered because of low volume of continuous phase. Either the NS entry 10 or 14 could be selected from this batch of experiments in regards with the NCs size,

size distribution, EE and physical stability of the NCs after storage at room temperature for one day.

16.6 Influence of stabilizing agents on drug-loaded NCs.

Previous publications investigated the use of hydrophilic and polymeric surfactants in order to decrease the interfacial energy between water and polymer suggested to be involved when the Marangoni effect is claimed to be the driving force for NPs formation[66, 176]. Use of surfactants has been shown to improve oral absorption[177-179] and reduce uptake by the RES due to their steric barrier properties and subsequent longer systemic residency time[180]. Lipophilic stabilizers have also been incorporated to control drug release and reduce the interfacial tension in the system[181-182].

Table 34: Mean particles diameter (Z-average), size distribution and entrapment efficiency of drug-loaded nanosuspensions prepared with varying concentration in stabilizers.

Entry	Hydrophilic stabilizer %(w/w) in NS Poloxamer 188	Lipophilic stabilizer %(w/w) in NS Oleic Macrogol-6 Glyceride	Entrapment efficiency % (w/w) recovery	Z-average (nm) [PDI]	
				$t_{initial}$	t_{1day}
16	5.0	-	70.3	95 [0.18]	94 [0.18]
10	1.5	-	77.2	101 [0.15]	99 [0.16]
17	-	-	77.1	104 [0.18]	101 [0.15]
18	-	3.00	69.1	112 [0.16]	ND
19	1.5	6.00	45.7	ND(opaque)	ND

NS: nanosuspension, PDI: polidispersity, ND: not done.

The effect of non-ionic hydrophilic (i.e. poloxamer 188, HLB>29), and lipophilic (i.e. oleic macrogol-6 glycerides, HLB=4) surfactants have been evaluated, after being incorporated in the aqueous phase and the solvent phase (Table 34). The poloxamer 188 was selected as a standard, prior to any investigations and was added in proportion below the critical micelle concentration[179] at a concentration of 1.5% (w/w) of total NP weight or 0.02% (w/w) in NS. Variation in concentrations (0%-5% w/w) of this difunctional block copolymer surfactant terminating with primary hydroxyl groups didn't alter the particle size and size

distribution of the NS entries 16, 10 and 17. Only an increase up to a concentration of 5% seemed to tend to decrease the (E)-BCP EE (entry 16).

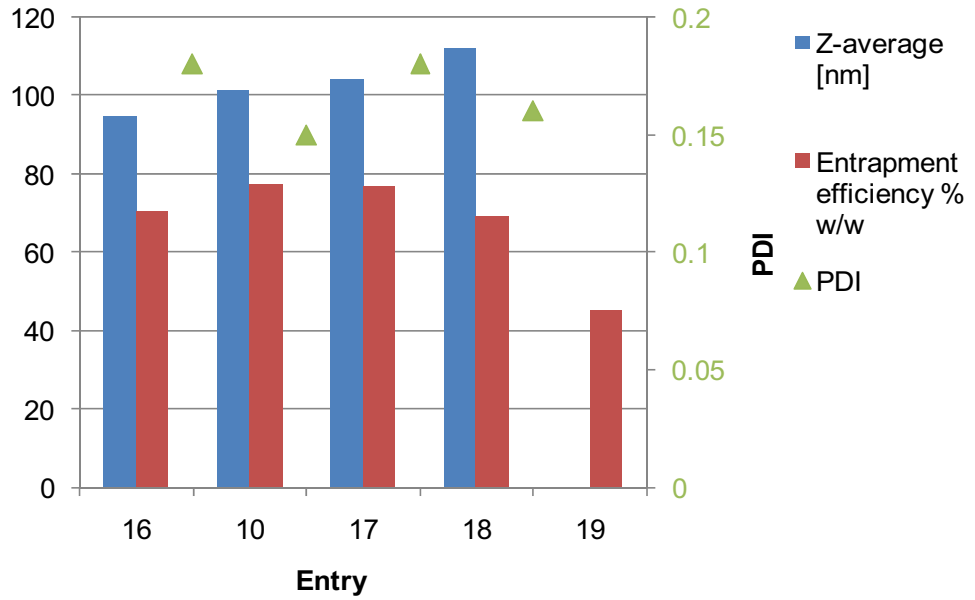

Figure 65: Representation of the Z-average size of drug-loaded nanosuspensions prepared with varying concentration of stabilizers.

Similar trend in term of EE has been determined for the NS entry 18 wherein 3.0% of lipophilic surfactant was added, whereas negligible changes on the NCs size were observed. A combination of hydrophilic and lipophilic surfactants (entry 19), had a dramatic effect on both NCs EE and size, not measured on particle sizer but visually assessed as being out of the "Ouzo boundaries" since the NS was opaque and sedimentation was noticed. As suggested by Ganachaud et al.[71], our data supports that nanoprecipitation can't be only driven by Marangoni effect since narrow size particle preparation was possible in surfactant-free NCs. Surfactants are predominantly located at the interface of the NPs and could interfere with its physicochemical characteristics[183]. Mei et al.[184] have exploited this feature and incorporated poloxamer 188 into Poly(ε-caprolactone) as a pore-forming agent and drug releasing enhancer, evidencing a porous surface on the NPs developed.

Oleic Macrogol-6 Glyceride is a lipophilic surfactant (HLB=4), and reported[116, 185] reported that polymeric particles containing a fatty acid ester have the structure of a composite matrix with channels formed by the ester. Water can diffuse through the

channels resulting in a slight swelling of the particles in the aqueous phase during their preparation and consequently a larger size[116, 185]. These observations may explain less efficient (E)-BCP entrapment (entries 16, 18 and 19), caused by facilitated steam distillation of the drug during the solvent evaporation process. This phenomenon seems to be exacerbated with increase loading of the NCs-core with oily materials (entry 19).
NCs with hydrodynamic diameter inferior to 100nm and satisfactory drug EE were prepared using small amount of hydrophilic polymeric surfactant or in surfactant-free environment.

16.7 Influence of type of polymer on drug-loaded NCs.

Eudragit®RS100 has a lower content of quaternary ammonium groups (4.5 to 6.8%), and is considered less permeable to water as compared to the more permeable RL (8.8 to 12% ammonium groups). Many researchers have utilized a combination of these two polymer to modulate the drug release from solid dispersions[186-187]. It was interesting to analyze the influence of the use of either one of these cationic polymer on the NCs size, size distribution and (E)-BCP entrapment efficiency while the total polymer-to-phase solvent ratio, the drug-to-polymer ratio, the solvent-to-solvent ratio were kept constant and similar to the standard entry 10, respectively, 10.0% (w/w), 1:13 and 0.12.

Table 35: Mean particle diameter (Z-average), size distribution and entrapment efficiency of drug-loaded nanosuspensions prepared with varying types of polymer.

Entry	Polymer type	Entrapment efficiency % (w/w) recovery	Z-average (nm) [PDI]
10	Eudragit®RS100/RL100 (1:1)	77.2	101 [0.15]
20	Eudragit®RS100	74.8	106 [0.29]
21	Eudragit®RL100	73.7	91 [0.19]

PDI: polydispersity.

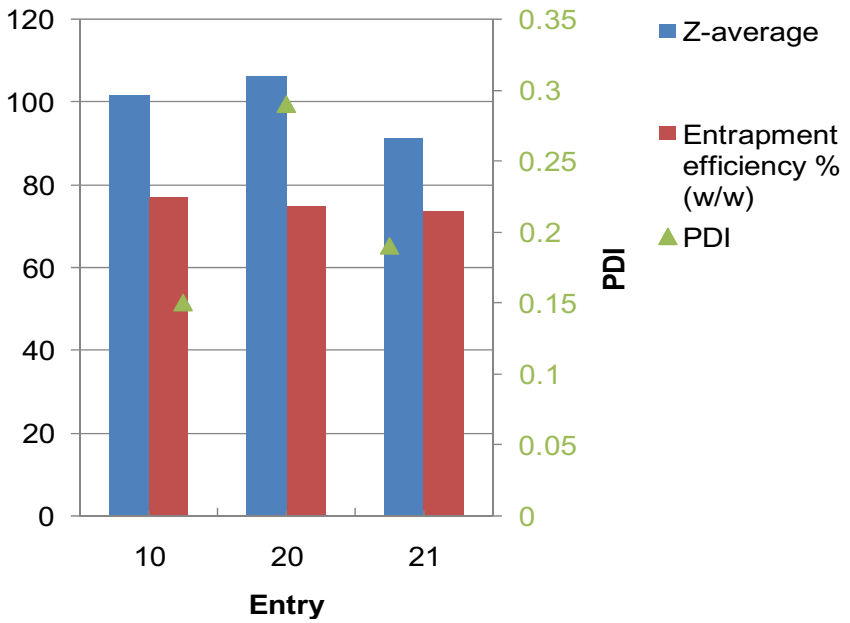

Figure 66: Representation of the Z-average size of drug-loaded nanosuspensions prepared with varying types of polymer.

The size and the (E)-BCP EE of Eudragit® RS100 containing NCs (entries 20 table 35) were not significantly disparate from their RL100 counterparts (entry 21), containing the same amount of Eudragit®, although greater polydispersity has been observed using the Eudragit® RS100. Others have also reported that the hydrodynamic radius of acetazolamide-loaded Eudragit® microspheres[188] or ciprofloxacin-loaded nanoparticles[112] were not altered by the polymer type. Conversely, using different NPs method of preparation, Pignatello et al.[114] have noticed that drug-free Eudragit® RL100 nanoparticles had a slightly greater mean diameter compared to the RS100-based nanosuspensions. Further investigations have to be performed to appreciate in which extent the Eudragit RS/RL 100 polymer ratio can affect the drug release, endowed with some flexibility since the parameters studied in this set of experiments have not been altered by the polymer type.

16.8 Influence of the incorporation of a fluorescent probe on drug-loaded NCs.

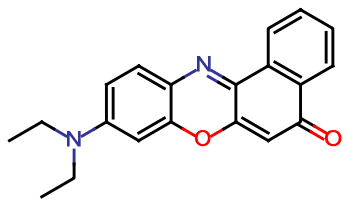

Figure 67: Nile Red chemical structure.

The objective of this experiment was to encapsulate a hydrophobic fluorescent dye, Nile Red, into the NCs core, which fluoresces in organic environment, for imaging purpose, either for diagnostic or to evaluate the biodistribution of the drug-loaded NCs. The incorporation of Nile Red at a concentration of 7.85 µM didn't lead to any modification in the composition of the standard NS (entry 10 Table 31) in term of drug loading, polymer and solvent-to-non solvent phase concentrations.

Table 36: Mean particles diameter (Z-average), size distribution and entrapment efficiency of drug-loaded nanosuspensions prepared with and without fluorescent dye.

Entry	Nile Red (µM)	(E)-BCP Entrapment efficiency % (w/w) recovery	Z-average (nm) [PDI]
10	-	77.20	101 [0.15]
22	7.85	84.30	107 [0.12]

Fluorescent labeled NCs were successfully prepared (entry 22 Table 36 and Figure 68) without any effect on the particle size or the size distribution. By contrast, the presence of Nile Red appears to have a slight positive effect on the NCs drug-loading (84.3% w/w for entry 22). The Nile Red lipophilicity (log P=5)[189] may have some influence on the (E)-BCP steam distillation yield. The fluorescence homogeneity observed in the Fig. 68 can be interpreted as efficient Nile Red encapsulation, raising encouraging perspectives for the use of the NCS developed, for imaging use. More advanced studies and characterization are required to determine the

Figure 68: Nanosuspension entry 22 under UV-lamp.

Nile Red loaded NCs release profile and *in vitro*/*in vivo* stability prior to conclude about their potential application in preclinical investigations.

16.9 Influence of macrocycles- drug-loaded NCs supramolecular assemblies on drug-loaded NCs physicochemical characteristics.

NCs bearing quaternary ammonium moieties can form supramolecular assembly through host-guest interaction or electrostatic interaction with macrocycles such as cucurbit[7]uril (CB[7])[98] and through ionic interactions with Sulfobutylether-β-cyclodextrin (SBEβCD)[92]. SBEβCD and CB[7] were selected based on their negative charge or electronegativity, high aqueous solubility and biocompatibility. Eudragit® RS100 was chosen considering the higher quaternary ammonium substitution degree (SD) (8.8%-12% w/w) compared to Eudragit® RL100 for the NCs preparation in the present study. These experiments were aiming at evaluating the feasibility of macrocycles-NCs supramolecular complexes formation based on the cationic NCs developed in our laboratory, and to obtain preliminary results in term of complexes characterization i.e. size, size distribution and EE.

Table 37: Mean particles diameter (Z-average), size distribution and entrapment efficiency of drug-loaded nanosuspensions prepared with varying type of macrocycles on drug-loaded NCs.

Entry	Macrocycles (29 mM)	Aqueous phase volume (mL)	Entrapment efficiency % (w/w) recovery	Z-average (nm) [PDI]
21	-	50.0	73.7	91 [0.19]
23	-	25.0	-	92 [0.18]
24	SBEβCD	25.0	-	5847 [0.20]
25	CB[7]	25.0	83.0	87 [0.40]

PDI: polydispersity, SBEβCD: Sulfobutylether-beta- cyclodextrin, CB[7]: cucurbit[7]uril.

Based on the substitution degree of the Eudragit® RL100 and SBEβCD, the macrocycles-NCs complexes were prepared with mass ratios calculated as follows:

For SBEβCD:

Amount of ammonium methacrylate units in 10 mg of Eudragit® RL100:
0.12 (% of ammonio methacrylate units on dry substance) x 10 (mg of polymer) = 1.2 mg.

Given that MW $_{\text{ammonium methacrylate}}$ = 172.24 g.mol^{-1} and MW $_{\text{SBEβCD}}$ = 2087 g.mol^{-1}
Amount of SBEβCD needed for interacting with 10 mg of Eudragit® RL100:
1.2 (mg of ammonio methacrylate units in 10 mg polymer) ÷ 172.24 (MW $_{\text{ammonium methacrylate}}$) x 2087 (MW $_{\text{SBEβCD}}$) = 14.54 mg of SBEβCD.

SBEβCD are randomly functionalized with sulfobutylether. SBEβCD is not a single chemical species, but comprised of a multitude of polymeric structures of varying degrees of substitution and positional/regional isomers. The average degree of substitution for the SBEβCD used is 6.5. In order to maximize the interactions between quaternary ammonium groups and SBEβCD, 14.54 mg of SBEβCD corresponding to one molar equivalent have been introduced in the NS for the proof of concept experiment.

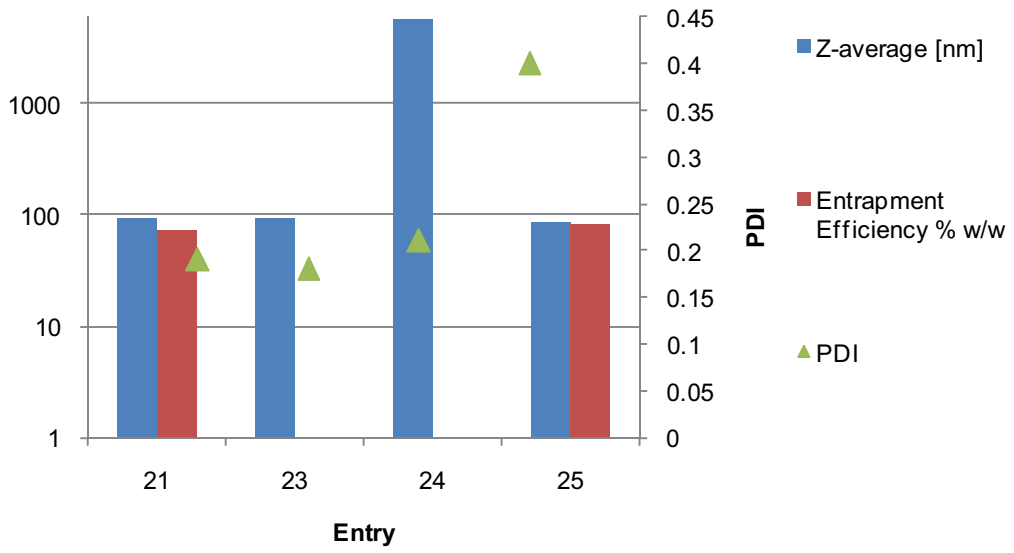

Figure 69: Representation of the Z-average size of drug-loaded nanosuspensions prepared with varying types of macrocycles on drug-loaded NCs.

For CB[7]:

Following the same steps as above and knowing that $MW_{CB[7]}$ = 1162.96 g/mol, the amount of CB[7] added was 8.0 mg for 10 mg of Eudragit® RL100.

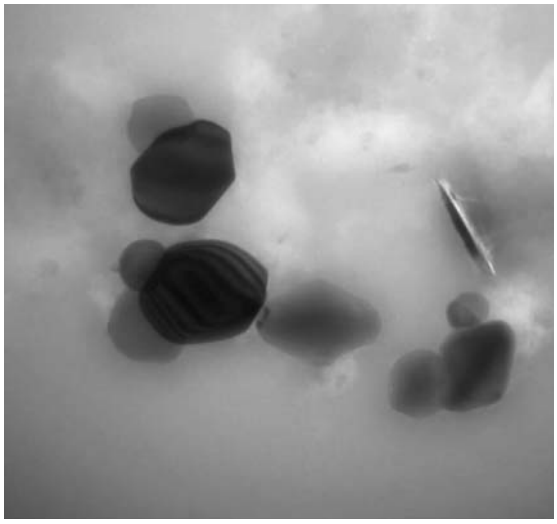

Figure 70: TEM imaging of NS entry 25, magnifying x100,000.

The amount of NS to mix with SBEβCD or CB[7] to form supramolecular complexes was calculated on the base of the amount of polymer weighed and the amount of NS obtained after solvent evaporation. The amount of NS taken was containing 10 mg of Eudragit® RL100.

Stable nanoparticles were obtained only when using the CB[7] based on NCs developed (entry 25 in Table 37). Considering that outer diameter of CB[7] is inferior to 2 nm, similar Z-average were expected for standard NCs (entry 23) and CB[7]-NCs complexes (entry 25). Observed Z-average were 92 nm and 87 nm for respectively NC and NC:CB[7] complexes, with however a rather high polydispersity distribution for entry 25. Interestingly, the complexes formed exhibited higher (E)-BCP EE than the NCs alone (entry 21). It is likely that the quaternary ammonium engaged in electrostatic interactions with the CB[7] carbonyl confer less permeability to the NPs potentially ensuing reduced steam distillation during the solvent evaporation step. Morphology study (TEM Fig. 70) revealed diamond-like shaped complexes, showing integrity despite the drying process required for TEM imaging. The CB[7]-NCs powder was re-suspended in a volume of water corresponding to the same concentration as in the NS, and stirred (approximately 15 min.) until affording a opalescent and bluish dispersion. The presence of CB[7] complexing the quaternary ammonium moieties onto the surface of the cationic NCs by electrostatic interaction may have preserved the NCs from the mechanical stress generated during the freeze-drying

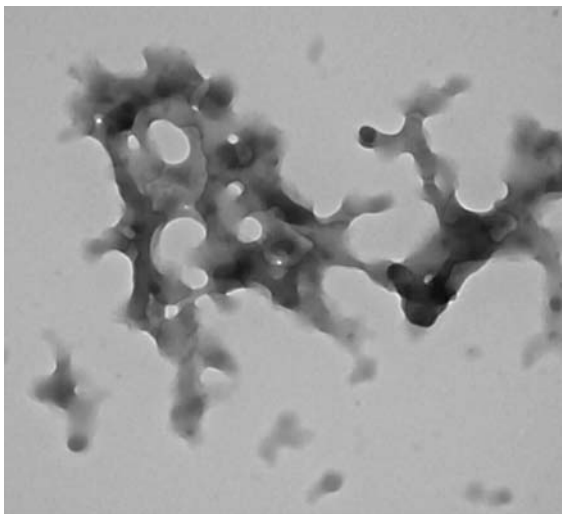

Figure 71 TEM imaging of NS entry 24, magnifying x50,000

step. No cryoprotectant was required in order to reconstitute NS from NCs powder owing to increased physical stability due to complexes formation. Long-term storage of the NCs in the form of a dry powder is known to minimize particle aggregation and drug chemical instability[151].

The supramolecular assemblies formed using SBEβCD were in the micrometric range, nonetheless, a relative monodisperse population could be observed. Because of electrostatic repulsions between the individual cyclodextrin molecules, SBEβCD are thought to not self-aggregate. However, the phase-solubility diagrams of SBEβCD are frequently of A_P-type[190], indicating formation of higher-order complexes with regard to cyclodextrin[190]. Therewith morphology studies (Fig. 71) shows a film composed of presumed SBEβCD and NCs that can be seen within. SBEβCD-NCs may form linear polymeric sequences following a pattern such as for example [NC-SBEβCD-NC-SBEβCD-NC- SBEβCD]$_n$, since SBEβCD are randomly substituted with hydroxysulfonyl on the two sides of the rim. Abdelwahed et al.[191] obtained similar TEM imaging of polyvinyl alcohol (PVA) film with polycaprolactone NCs embedded within. Further investigations using β-CD with only primary hydroxyl substitution that interacts with just one NC may prevent the formation of a continuous polymeric film and allow discerning which mechanism has been involved in SBEβCD-NCs complexes formation i.e. self-aggregation or polymerization.

Otherwise, hydrodynamic radius analysis of entries 21 and 23 in Table 37 reasserted results advanced for entries 10 (standard, 50 mL water) and 14 (standard, 25 mL water). Decrease of the non-solvent phase volume down to 25 mL didn't alter the particle size and distribution whatever was the polymer type used, a mixture of Eudragit® RL/RS 100 1:1 or RL100 only.

CB[7]-NCs complexes preliminary results raised perspectives regarding the use of these entities as potential theragnostics even though additional characterization is required in order to fully appreciate their efficacy upon *in vitro/in vivo* testing. As expected, functionalized CB[6] could be used in the future for targeting or as imaging agents complexed to cationic NC containing a drug.

16.10 Chemical stability of (E)-BCP encapsulated in polymeric nanocapsules

Chemical stability of (E)-BCP was evaluated by GC-MS using the method cited in section 12.2 on one of the batch of the NS entry 10 Table 38.

Table 38: (E)-BCP chemical stability of drug-loaded standard.

Entry	Entrapment efficiency % (w/w) recovery	
	$t_{initial}$	$t_{3\ months}$
10	74.8	80.7

After 3 months stored at 4°C, no chemical degradation of the drug had been observed (≈ 100% of (E)-BCP was recovered).

17 Summary and Conclusion

Using nanoprecipitation method, we successfully prepared nearly monodisperse polymeric NCs, characterized by an optimal size for oral absorption (<200 nm) and with satisfactory entrapment efficiency for the delivery of therapeutic dose of the lipophilic CB2 agonist (E)-BCP. The cationic Eudragit® based NCs developed, likely to be bioadhesive, allowed to improve the solubility and the chemical stability of the drug and potentially its oral bioavailability.

By varying operating conditions (i.e. rotary solvent evaporation factor, flow-rate organic phase addition) and factors (i.e. drug-to-polymer ratio, solvent phase-to-non solvent phase ratio, polymer-to-organic solvent ratio, nature and amount of surfactant, organic solvent nature, polymer nature), we determined the critical parameters to obtain nanocapsules with appropriate size, size distribution and drug entrapment efficiency for the oral delivery of lipophilic compounds. Aside from the polymer type used Eudragit® RS or/and RL, all the factors and operating conditions mentioned were of great impact on

the NCs size and drug loading. Incorporation of fluorescent dye in the core of the nanocapsules was possible and may be used as imaging tool to investigate the nanocapsules fate and drug delivery mechanisms *in vivo*.

Preliminary results on the feasibility and characterization of cucurbit[7]uril-nanocapsules complexes based on host-guest/electrostatic interactions have been generated and raised promising perspectives regarding the use of the developed NCS as theragnostic agents. The putative complexes formed resulted in hydrodynamic diameter of 87 nm (PDI 0.4) and (E)-BCP entrapment efficiency of 83.0%. Further investigations regarding the drug release, physical stability measuring potential zeta potential change and *in vivo* administration will be carried out in order to fully characterize these NCs. The cationic nanocapsules can be used to deliver other lipophilic compounds, improving their pharmaceutical properties and studying their biodistribution.

18 REFERENCES.

1. Pichierri, F. *Cucurbituril*; Tohoku University: Sendai, Japan, 2006.
2. Kreuter, J., *Nanoparticles as drug delivery systems*
American Scientific Publishers: Stevenson Ranch, U.S.A., 2004; Vol. 7, p 161–180
3. Orive, G.; Anitua, E.; Pedraz, J. L.; Emerich, D. F., Biomaterials for promoting brain protection, repair and regeneration. *Nat Rev Neurosci* **2009,** 10, (9), 682-692.
4. Mora-Huertas, C. E.; Fessi, H.; Elaissari, A., Polymer-based nanocapsules for drug delivery. *International Journal of Pharmaceutics* **2010,** 385, (1-2), 113-142.
5. Fukuda, M.; Miller, D. A.; Peppas, N. A.; McGinity, J. W., Influence of sulfobutyl ether β-cyclodextrin (Captisol®) on the dissolution properties of a poorly soluble drug from extrudates prepared by hot-melt extrusion. *International Journal of Pharmaceutics* **2008,** 350, (1–2), 188-196.
6. Irache, J. M.; Esparza, I.; Gamazo, C.; Agueros, M.; Espuelas, S., Nanomedicine: novel approaches in human and veterinary therapeutics. *Vet Parasitol* **2011,** 180, (1-2), 47-71.
7. Parveen, S.; Sahoo, S. K., Polymeric nanoparticles for cancer therapy. *Journal of Drug Targeting* **2008,** 16, (2), 108-123.
8. Cheng, F. Y.; Su, C. H.; Wu, P. C.; Yeh, C. S., Multifunctional polymeric nanoparticles for combined chemotherapeutic and near-infrared photothermal cancer therapy in vitro and in vivo. *Chem Commun* **2010,** 46, (18), 3167-3169.
9. Way, T. D.; Chang, C. J.; Lin, C. W., Bioconjugated Fluorescent Polymeric Nanoparticles for Imaging and Targeted Therapy of HER2-Overexpressing Cancer Cells. *Journal of Fluorescence* **2011,** 21, (4), 1669-1676.
10. Singh, A.; Dinawaz, F.; Mewar, S.; Sharma, U.; Jagannathan, N. R.; Sahoo, S. K., Composite Polymeric Magnetic Nanoparticles for Co-Delivery of Hydrophobic and Hydrophilic Anticancer Drugs and MRI Imaging for Cancer Therapy. *Acs Appl Mater Inter* **2011,** 3, (3), 842-856.
11. Scott, C. J.; Fay, F., Antibody targeting of polymeric nanoparticles for cancer therapy. *Drug Discovery Today* **2010,** 15, (23-24), 1087-1087.
12. Hillaireau, H.; Le Doan, T.; Couvreur, P., Polymer-based nanoparticles for the delivery of nucleoside analogues. *J Nanosci Nanotechno* **2006,** 6, (9-10), 2608-2617.
13. Chen, S.; Cheng, S. X.; Zhuo, R. X., Self-Assembly Strategy for the Preparation of Polymer-Based Nanoparticles for Drug and Gene Delivery. *Macromolecular Bioscience* **2011,** 11, (5), 576-589.
14. Bhavsar, M. D.; Amiji, M. M., Polymeric nano- and microparticle technologies for oral gene delivery. *Expert Opinion on Drug Delivery* **2007,** 4, (3), 197-213.
15. Vlieghe, P.; Khrestchatisky, M., Medicinal Chemistry Based Approaches and Nanotechnology-Based Systems to Improve CNS Drug Targeting and Delivery. *Med Res Rev* **2012**.
16. Kreuter, J., Nanoparticles--a historical perspective. *Int J Pharm* **2007,** 331, (1), 1-10.
17. Couvreur, R. G. P., Nanocapsules: Preparation, characterization and therapeutic applications. *Nanoparticulates as Drug Carriers* **2006**, (276), 255.

18. Legrand, P.; Barratt, G.; Mosqueira, V.; Fessi, H.; Devissaguet, J. P., Polymeric nanocapsules as drug delivery systems - A review. *Stp Pharma Sci* **1999,** 9, (5), 411-418.
19. Barratt, G. M., Therapeutic applications of colloidal drug carriers. *Pharm Sci Technolo Today* **2000,** 3, (5), 163-171.
20. Allémann, E.; Leroux, J.-C.; Gurny, R., Polymeric nano- and microparticles for the oral delivery of peptides and peptidomimetics. *Advanced Drug Delivery Reviews* **1998,** 34, (2-3), 171-189.
21. Bhardwaj, V.; Hariharan, S.; Bala, I.; Lamprecht, A.; Kumar, N.; Panchagnula, R.; Ravi Kumar, M. N. V., Pharmaceutical Aspects of Polymeric Nanoparticles for Oral Drug Delivery. *J Biomed Nanotechnol* **2005,** 1, (3), 235-258.
22. Davis, M. E.; Chen, Z.; Shin, D. M., Nanoparticle therapeutics: an emerging treatment modality for cancer. *Nat Rev Drug Discov* **2008,** 7, (9), 771-782.
23. Jain, K. K., Nanoparticles as targeting ligands. *Trends in Biotechnology* **2006,** 24, (4), 143-145.
24. Parveen, S.; Misra, R.; Sahoo, S. K., Nanoparticles: a boon to drug delivery, therapeutics, diagnostics and imaging. *Nanomedicine: Nanotechnology, Biology and Medicine* **2012,** 8, (2), 147-166.
25. Ochekpe, N. A.; Olorunfemi, P. O.; Ngwuluka, N. C., Nanotechnology and Drug Delivery Part 1: Background and Applications. *Tropical Journal of Pharmaceutical Research* **2009,** 8, (3), 265-274.
26. Steiniger, S. C.; Kreuter, J.; Khalansky, A. S.; Skidan, I. N.; Bobruskin, A. I.; Smirnova, Z. S.; Severin, S. E.; Uhl, R.; Kock, M.; Geiger, K. D.; Gelperina, S. E., Chemotherapy of glioblastoma in rats using doxorubicin-loaded nanoparticles. *Int J Cancer* **2004,** 109, (5), 759-67.
27. Barraud, L.; Merle, P.; Soma, E.; Lefrançois, L.; Guerret, S.; Chevallier, M.; Dubernet, C.; Couvreur, P.; Trépo, C.; Vitvitski, L., Increase of doxorubicin sensitivity by doxorubicin-loading into nanoparticles for hepatocellular carcinoma cells in vitro and in vivo. *Journal of Hepatology* **2005,** 42, (5), 736-743.
28. Zhang, C.; Zhao, L.; Dong, Y.; Zhang, X.; Lin, J.; Chen, Z., Folate-mediated poly(3-hydroxybutyrate-co-3-hydroxyoctanoate) nanoparticles for targeting drug delivery. *Eur J Pharm Biopharm* **2010,** 76, (1), 10-6.
29. Tang, J.; Xu, N.; Ji, H.; Liu, H.; Wang, Z.; Wu, L., Eudragit nanoparticles containing genistein: formulation, development, and bioavailability assessment. *Int J Nanomedicine* **2011,** 6, 2429-35.
30. Haas, S. E.; Bettoni, C. C.; de Oliveira, L. K.; Guterres, S. S.; Dalla Costa, T., Nanoencapsulation increases quinine antimalarial efficacy against Plasmodium berghei in vivo. *Int J Antimicrob Agents* **2009,** 34, (2), 156-61.
31. Nayak, B.; Panda, A. K.; Ray, P.; Ray, A. R., Formulation, characterization and evaluation of rotavirus encapsulated PLA and PLGA particles for oral vaccination. *J Microencapsul* **2009,** 26, (2), 154-65.
32. Agueros, M.; Zabaleta, V.; Espuelas, S.; Campanero, M. A.; Irache, J. M., Increased oral bioavailability of paclitaxel by its encapsulation through complex formation with cyclodextrins in poly(anhydride) nanoparticles. *J Control Release* **2010,** 145, (1), 2-8.
33. Brambilla, D.; Nicolas, J.; Le Droumaguet, B.; Andrieux, K.; Marsaud, V.; Couraud, P. O.; Couvreur, P., Design of fluorescently tagged poly(alkyl cyanoacrylate) nanoparticles for human brain endothelial cell imaging. *Chem Commun (Camb)* **2010,** 46, (15), 2602-4.

34. Mailänder, V.; Landfester, K., Interaction of Nanoparticles with Cells. *Biomacromolecules* **2009,** 10, (9), 2379-2400.
35. Xia, T.; Kovochich, M.; Liong, M.; Meng, H.; Kabehie, S.; George, S.; Zink, J. I.; Nel, A. E., Polyethyleneimine Coating Enhances the Cellular Uptake of Mesoporous Silica Nanoparticles and Allows Safe Delivery of siRNA and DNA Constructs. *ACS Nano* **2009,** 3, (10), 3273-3286.
36. des Rieux, A.; Fievez, V.; Garinot, M.; Schneider, Y.-J.; Préat, V., Nanoparticles as potential oral delivery systems of proteins and vaccines: A mechanistic approach. *Journal of Controlled Release* **2006,** 116, (1), 1-27.
37. Zhang, X.; Sun, M.; Zheng, A.; Cao, D.; Bi, Y.; Sun, J., Preparation and characterization of insulin-loaded bioadhesive PLGA nanoparticles for oral administration. *Eur J Pharm Sci* **2012,** 45, (5), 632-8.
38. Kumar, G.; Shafiq, N.; Malhotra, S., Drug-Loaded PLGA Nanoparticles for Oral Administration: Fundamental Issues and Challenges Ahead. *Crit Rev Ther Drug Carrier Syst* **2012,** 29, (2), 149-82.
39. Doggui, S.; Sahni, J. K.; Arseneault, M.; Dao, L.; Ramassamy, C., Neuronal Uptake and Neuroprotective Effect of Curcumin-Loaded PLGA Nanoparticles on the Human SK-N-SH Cell Line. *J Alzheimers Dis* **2012**.
40. Danhier, F.; Ansorena, E.; Silva, J. M.; Coco, R.; Le Breton, A.; Preat, V., PLGA-based nanoparticles: An overview of biomedical applications. *J Control Release* **2012**.
41. Xiao, R. Z.; Zeng, Z. W.; Zhou, G. L.; Wang, J. J.; Li, F. Z.; Wang, A. M., Recent advances in PEG-PLA block copolymer nanoparticles. *Int J Nanomedicine* **2010,** 5, 1057-65.
42. Thomas, C.; Rawat, A.; Hope-Weeks, L.; Ahsan, F., Aerosolized PLA and PLGA nanoparticles enhance humoral, mucosal and cytokine responses to hepatitis B vaccine. *Mol Pharm* **2011,** 8, (2), 405-15.
43. Zambaux, M. F.; Bonneaux, F.; Gref, R.; Dellacherie, E.; Vigneron, C., Preparation and characterization of protein C-loaded PLA nanoparticles. *J Control Release* **1999,** 60, (2-3), 179-88.
44. Carvalho, F. C.; Bruschi, M. L.; Evangelista, R. C.; Gremiao, M. P. D., Mucoadhesive drug delivery systems. *Braz J Pharm Sci* **2010,** 46, (1), 1-17.
45. Roy, S.; Pal, K.; Anis, A.; Pramanik, K.; Prabhakar, B., Polymer in Mucoadhesive Drug-Delivery Systems: A Brief Note. *Des Monomers Polym* **2009,** 12, (6), 483-495.
46. Behrens, I.; Pena, A. I. V.; Alonso, M. J.; Kissel, T., Comparative Uptake Studies of Bioadhesive and Non-Bioadhesive Nanoparticles in Human Intestinal Cell Lines and Rats: The Effect of Mucus on Particle Adsorption and Transport. *Pharmaceutical Research* **2002,** 19, (8), 1185-1193.
47. Das, S.; Suresh, P. K.; Desmukh, R., Design of Eudragit RL 100 nanoparticles by nanoprecipitation method for ocular drug delivery. *Nanomedicine: Nanotechnology, Biology and Medicine* **2010,** In Press, Corrected Proof.
48. Gargouri M, S. A., Bouli S, Becuwe P, Merlin JL, Maincent P, Optimization of a new non-viral vector for transfection: Eudragit nanoparticles for the delivery of a DNA plasmid.

Technol Cancer Res **2009** 8, (6),
433-44.

49. Pignatello, R.; Bucolo, C.; Puglisi, G., Ocular tolerability of Eudragit RS100® and RL100® nanosuspensions as carriers for ophthalmic controlled drug delivery. *Journal of Pharmaceutical Sciences* **2002,** 91, (12), 2636-2641.
50. Barnabas, W.; Malay, K. S.; Kumaraswamy, S.; Kumar, K. P. S.; Muthu, R.; Bhojraj, S., Chitosan nanoparticles as a new delivery system for the anti-Alzheimer drug tacrine. *Nanomedicine : the official journal of the American Academy of Nanomedicine* **2010,** 6, (1), 144-152.
51. Asane, G. S.; Nirmal, S. A.; Rasal, K. B.; Naik, A. A.; Mahadik, M. S.; Rao, Y. M., Polymer for mucoadhesive drug delivery system: a current status. *Drug Dev Ind Pharm* **2008,** 34, (11), 1246-66.
52. Roger, E.; Lagarce, F.; Garcion, E.; Benoit, J. P., Biopharmaceutical parameters to consider in order to alter the fate of nanocarriers after oral delivery. *Nanomedicine (Lond)* **2010,** 5, (2), 287-306.
53. Dodane, V.; Amin Khan, M.; Merwin, J. R., Effect of chitosan on epithelial permeability and structure. *Int J Pharm* **1999,** 182, (1), 21-32.
54. Walsh, E. G.; Adamczyk, B. E.; Chalasani, K. B.; Maher, S.; O'Toole, E. B.; Fox, J. S.; Leonard, T. W.; Brayden, D. J., Oral delivery of macromolecules: rationale underpinning Gastrointestinal Permeation Enhancement Technology (GIPET®). *Therapeutic Delivery* **2011,** 2, (12), 1595-1610.
55. Martien, R.; Loretz, B.; Schnürch, A. B., Oral gene delivery: Design of polymeric carrier systems shielding toward intestinal enzymatic attack. *Biopolymer* **2006,** 83, (4), 327-336.
56. van der Lubben, I. M.; Verhoef, J. C.; Borchard, G.; Junginger, H. E., Chitosan and its derivatives in mucosal drug and vaccine delivery. *European Journal of Pharmaceutical Sciences* **2001,** 14, (3), 201-207.
57. Badir Delf Loveymi, M. J., Parvin Zakeri-Milani, Hadi Valizadeh, Design of vancomycin RS-100 nanoparticles in order to increase the intestinal permeability. *Advanced Pharmaceutical Bulletin* **2012,** 2, (1), 43-56.
58. Chen, V. M. a. Y., Nanoparticles – A Review. *Tropical Journal of Pharmaceutical Research* **2006,** 5, (1), 561-573.
59. Garcia-Garcia, E.; Andrieux, K.; Gil, S.; Couvreur, P., Colloidal carriers and blood-brain barrier (BBB) translocation: A way to deliver drugs to the brain? *International Journal of Pharmaceutics* **2005,** 298, (2), 274-292.
60. H. Fessi, F. P., J.P. Devissaguet Procédé de préparation de systèmes colloidaux dispersibles d'une substance sous forme de nanocapsules. 1988.
61. Chorny, M.; Fishbein, I.; Danenberg, H. D.; Golomb, G., Lipophilic drug loaded nanospheres prepared by nanoprecipitation: effect of formulation variables on size, drug recovery and release kinetics. *Journal of Controlled Release* **2002,** 83, (3), 389-400.
62. Lamprecht, A.; Ubrich, N.; Yamamoto, H.; Schafer, U.; Takeuchi, H.; Lehr, C. M.; Maincent, P.; Kawashima, Y., Design of rolipram-loaded nanoparticles: comparison of two preparation methods. *Journal of Controlled Release* **2001,** 71, (3), 297-306.
63. Cauchetier, E.; Deniau, M.; Fessi, H.; Astier, A.; Paul, M., Atovaquone-loaded nanocapsules: influence of the nature of the polymer on their in vitro characteristics. *Int J Pharm* **2003,** 250, (1), 273-81.
64. Lamprecht, A., *Nanotherapeutics: Drug Delivery Concepts in Nanoscience*. Pan Stanford publishing Pte. Ltd.: Singapore, 2009.

65. Aubry, J.; Ganachaud, F.; Cohen Addad, J.-P.; Cabane, B., Nanoprecipitation of Polymethylmethacrylate by Solvent Shifting:1. Boundaries. *Langmuir* **2009,** 25, (4), 1970-1979.
66. Beck-Broichsitter, M.; Rytting, E.; Lebhardt, T.; Wang, X.; Kissel, T., Preparation of nanoparticles by solvent displacement for drug delivery: A shift in the "ouzo region" upon drug loading. *European Journal of Pharmaceutical Sciences* **2010,** 41, (2), 244-253.
67. McManamey, W. J.; Davies, J. T.; Woollen, J. M.; Coe, J. R., The influence of molecular diffusion on mass transfer between turbulent liquids. *Chem Eng Sci* **1973,** 28, (4), 1061-1069.
68. Quintanar-Guerrero, D.; Allémann, E.; Fessi, H.; Doelker, E., Preparation Techniques and Mechanisms of Formation of Biodegradable Nanoparticles from Preformed Polymer. *Drug Development and Industrial Pharmacy* **1998,** 24, (12), 1113-1128.
69. Miller, C. A., Spontaneous Emulsification Produced by Diffusion - a Review. *Colloid Surface* **1988,** 29, (1), 89-102.
70. Lopez-Montilla, J. C.; Herrera-Morales, P. E.; Pandey, S.; Shah, D. O., Spontaneous emulsification: Mechanisms, physicochemical aspects, modeling, and applications. *Journal of Dispersion Science and Technology* **2002,** 23, (1-3), 219-268.
71. Ganachaud, F.; Katz, J. L., Nanoparticles and Nanocapsules Created Using the Ouzo Effect: Spontaneous Emulsification as an Alternative to Ultrasonic and High-Shear Devices. *Chemphyschem* **2005,** 6, (2), 209-216.
72. Vitale, S. A.; Katz, J. L., Liquid droplet dispersions formed by homogeneous liquid-liquid nucleation: "The ouzo effect". *Langmuir* **2003,** 19, (10), 4105-4110.
73. Lehr, C. M., Bioadhesion technologies for the delivery of peptide and protein drugs to the gastrointestinal tract. *Crit Rev Ther Drug Carrier Syst* **1994,** 11, (2-3), 119-60.
74. Bowman, K.; Leong, K. W., Chitosan nanoparticles for oral drug and gene delivery. *International journal of nanomedicine* **2006,** 1, (2), 117-28.
75. Kast, C. E.; Bernkop-Schnurch, A., Influence of the molecular mass on the permeation enhancing effect of different poly(acrylates). *Stp Pharma Sci* **2002,** 12, (6), 351-356.
76. Martin, W.; Andreas, B.-S. r., Inhibition of Enzymes and Secretory Transport. In *Enhancement in Drug Delivery*, CRC Press: 2006.
77. Garrett, N. L.; Lalatsa, A.; Uchegbu, I.; Schätzlein, A.; Moger, J., Exploring uptake mechanisms of oral nanomedicines using multimodal nonlinear optical microscopy. *Journal of Biophotonics* **2012**, n/a-n/a.
78. Szentkuti, L., Light microscopical observations on luminally administered dyes, dextrans, nanospheres and microspheres in the pre-epithelial mucus gel layer of the rat distal colon. *Journal of Controlled Release* **1997,** 46, (3), 233-242.
79. Hussain, N.; Jaitley, V.; Florence, A. T., Recent advances in the understanding of uptake of microparticulates across the gastrointestinal lymphatics. *Advanced Drug Delivery Reviews* **2001,** 50, (1–2), 107-142.
80. Aprahamian, M.; Michel, C.; Humbert, W.; Devissaguet, J. P.; Damge, C., Transmucosal passage of polyalkylcyanoacrylate nanocapsules as a new drug carrier in the small intestine. *Biology of the Cell* **1987,** 61, (1-2), 69-76.

81. Jani, P.; Halbert, G. W.; Langridge, J.; Florence, A. T., Nanoparticle Uptake by the Rat Gastrointestinal Mucosa: Quantitation and Particle Size Dependency. *Journal of Pharmacy and Pharmacology* **1990,** 42, (12), 821-826.
82. Florence, A. T.; Hillery, A. M.; Hussain, N.; Jani, P. U., Factors Affecting the Oral Uptake and Translocation of Polystyrene Nanoparticles: Histological and Analytical Evidence. *Journal of Drug Targeting* **1995,** 3, (1), 65-70.
83. Florence, A. T.; Hillery, A. M.; Hussain, N.; Jani, P. U., Nanoparticles as carriers for oral peptide absorption: Studies on particle uptake and fate. *Journal of Controlled Release* **1995,** 36, (1–2), 39-46.
84. Desai, M. P.; Labhasetwar, V.; Amidon, G. L.; Levy, R. J., Gastrointestinal uptake of biodegradable microparticles: effect of particle size. *Pharm Res* **1996,** 13, (12), 1838-45.
85. O'Hagan, D. T., The intestinal uptake of particles and the implications for drug and antigen delivery. *J Anat* **1996,** 189 (Pt 3), 477-82.
86. Florence, A. T., The oral absorption of micro- and nanoparticulates: Neither exceptional nor unusual. *Pharmaceutical Research* **1997,** 14, (3), 259-266.
87. Hillyer, J. F.; Albrecht, R. M., Gastrointestinal persorption and tissue distribution of differently sized colloidal gold nanoparticles. *Journal of Pharmaceutical Sciences* **2001,** 90, (12), 1927-1936.
88. Delie, F., Evaluation of nano- and microparticle uptake by the gastrointestinal tract. *Advanced Drug Delivery Reviews* **1998,** 34, (2–3), 221-233.
89. Plapied, L.; Duhem, N.; des Rieux, A.; Préat, V., Fate of polymeric nanocarriers for oral drug delivery. *Current Opinion in Colloid & Interface Science* **2011,** 16, (3), 228-237.
90. Vollrath, A.; Schubert, S.; Windhab, N.; Biskup, C.; Schubert, U. S., Labeled Nanoparticles Based on Pharmaceutical EUDRAGIT® S 100 Polymer. *Macromol Rapid Comm* **2010,** 31, (23), 2053-2058.
91. Morgan, T. T.; Muddana, H. S.; Altinoglu, E. I.; Rouse, S. M.; Tabakovic, A.; Tabouillot, T.; Russin, T. J.; Shanmugavelandy, S. S.; Butler, P. J.; Eklund, P. C.; Yun, J. K.; Kester, M.; Adair, J. H., Encapsulation of Organic Molecules in Calcium Phosphate Nanocomposite Particles for Intracellular Imaging and Drug Delivery. *Nano Letters* **2008,** 8, (12), 4108-4115.
92. Ardusso, M. S.; Manzo, R. H.; Jimenez-Kairuz, A. F., Comparative study of three structurally related acid polyelectrolytes as carriers of basic drugs: Carbomer, Eudragit L-100 and S-100. *Supramol Chem* **2010,** 22, (5), 289-296.
93. Baena, Y.; Manzo, R. H.; D'Leon, L. F. P., Preparation and Physicochemical Characterization of Some Polyelectrolyte-Diclofenac Complexes. *Vitae-Columbia* **2011,** 18, (3), 304-310.
94. Jimenez-Kairuz, A. F.; Allemandi, D. A.; Manzo, R. H., The improvement of aqueous chemical stability of a model basic drug by ion pairing with acid groups of polyelectrolytes. *International Journal of Pharmaceutics* **2004,** 269, (1), 149-156.
95. Mischiati, C.; Sereni, A.; Finotti, A.; Breda, L.; Cortesi, R.; Nastruzzi, C.; Romanelli, A.; Saviano, M.; Bianchi, N.; Pedone, C.; Borgatti, M.; Gambari, R., Complexation to cationic microspheres of double-stranded peptide nucleic acid-DNA chimeras exhibiting decoy activity. *J Biomed Sci* **2004,** 11, (5), 697-704.
96. Jimenez-Kairuz, A. F.; Allemandi, D. A.; Manzo, R. H., Equilibrium properties and mechanism of kinetic release of metoclopramide from carbomer hydrogels. *Int J Pharm* **2003,** 250, (1), 129-36.

97. Rigo, M. V.; Allemandi, D. A.; Manzo, R. H., Swellable drug-polyelectrolyte matrices (SDPM) of alginic acid characterization and delivery properties. *Int J Pharm* **2006,** 322, (1-2), 36-43.
98. Isaacs, L., Cucurbit[n]urils: from mechanism to structure and function. *Chem Commun* **2009**, (6), 619-629.
99. Lagona, J.; Mukhopadhyay, P.; Chakrabarti, S.; Isaacs, L., The Cucurbit[n]uril Family. *Angewandte Chemie International Edition* **2005,** 44, (31), 4844-4870.
100. Liu, S.; Ruspic, C.; Mukhopadhyay, P.; Chakrabarti, S.; Zavalij, P. Y.; Isaacs, L., The Cucurbit[n]uril Family: Prime Components for Self-Sorting Systems. *Journal of the American Chemical Society* **2005,** 127, (45), 15959-15967.
101. Jin Jeon, Y.; Kim, S.-Y.; Ho Ko, Y.; Sakamoto, S.; Yamaguchi, K.; Kim, K., Novel molecular drug carrier: encapsulation of oxaliplatin in cucurbit[7]uril and its effects on stability and reactivity of the drug. *Organic & Biomolecular Chemistry* **2005,** 3, (11), 2122-2125.
102. Uzunova, V. D.; Cullinane, C.; Brix, K.; Nau, W. M.; Day, A. I., Toxicity of cucurbit[7]uril and cucurbit[8]uril: an exploratory in vitro and in vivo study. *Organic & Biomolecular Chemistry* **2010,** 8, (9), 2037-2042.
103. Park, I.-K.; von Recum, H. A.; Jiang, S.; Pun, S. H., Supramolecular Assembly of Cyclodextrin-Based Nanoparticles on Solid Surfaces for Gene Delivery. *Langmuir* **2006,** 22, (20), 8478-8484.
104. Xu, P.; Gullotti, E.; Tong, L.; Highley, C. B.; Errabelli, D. R.; Hasan, T.; Cheng, J.-X.; Kohane, D. S.; Yeo, Y., Intracellular Drug Delivery by Poly(lactic-co-glycolic acid) Nanoparticles, Revisited. *Molecular Pharmaceutics* **2008,** 6, (1), 190-201.
105. Mukerjee, A.; Vishwanatha, J. K., Formulation, Characterization and Evaluation of Curcumin-loaded PLGA Nanospheres for Cancer Therapy. *Anticancer Research* **2009,** 29, (10), 3867-3875.
106. White, N. S.; Errington, R. J., Fluorescence techniques for drug delivery research: theory and practice. *Adv Drug Deliv Rev* **2005,** 57, (1), 17-42.
107. Yu, X.; Chen, L.; Deng, Y.; Li, K.; Wang, Q.; Li, Y.; Xiao, S.; Zhou, L.; Luo, X.; Liu, J.; Pang, D., Fluorescence analysis with quantum dot probes for hepatoma under one- and two-photon excitation. *J Fluoresc* **2007,** 17, (2), 243-7.
108. Xue, F. L.; Chen, J. Y.; Guo, J.; Wang, C. C.; Yang, W. L.; Wang, P. N.; Lu, D. R., Enhancement of intracellular delivery of CdTe quantum dots (QDs) to living cells by Tat conjugation. *J Fluoresc* **2007,** 17, (2), 149-54.
109. Tongiani, S.; Velde, D. V.; Ozeki, T.; Stella, V. J., Sulfoalkyl ether-alkyl ether cyclodextrin derivatives, their synthesis, NMR characterization, and binding of 6 alpha-methylprednisolone. *Journal of Pharmaceutical Sciences* **2005,** 94, (11), 2380-2392.
110. Jon, S. Y.; Selvapalam, N.; Oh, D. H.; Kang, J. K.; Kim, S. Y.; Jeon, Y. J.; Lee, J. W.; Kim, K., Facile synthesis of cucurbit[n]uril derivatives via direct functionalization: Expanding utilization of cucurbit[n]uril. *Journal of the American Chemical Society* **2003,** 125, (34), 10186-10187.
111. Vikrant K Nikam, K. B. K., Vinayak M Gaware, Ramdas T Dolas, Kiran B Dhamak, Sachin B Somwanshi, Atul N Khadse, Vivekanand A. Kashid, EUDRAGIT A VERSATILE POLYMER : A REVIEW. In Pharmacologyonline: 2011; Vol. 1, pp 152-164.
112. Dillen, K.; Vandervoort, J.; Van den Mooter, G.; Ludwig, A., Evaluation of ciprofloxacin-loaded Eudragit® RS100 or RL100/PLGA nanoparticles. *International Journal of Pharmaceutics* **2006,** 314, (1), 72-82.

113. Pignatello, R.; Ricupero, N.; Bucolo, C.; Maugeri, F.; Maltese, A.; Puglisi, G., Preparation and characterization of eudragit retard nanosuspensions for the ocular delivery of cloricromene. *Aaps Pharmscitech* **2006,** 7, (1), E27.
114. Pignatello, R.; Bucolo, C.; Puglisi, G., Ocular tolerability of Eudragit RS100® and RL100® nanosuspensions as carriers for ophthalmic controlled drug delivery. *Journal of Pharmaceutical Sciences* **2002,** 91, (12), 2636-2641.
115. Bodmeier, R.; Chen, H.; Tyle, P.; Jarosz, P., Spontaneous formation of drug-containing acrylic nanoparticles. *J Microencapsul* **1991,** 8, (2), 161-70.
116. Ubrich, N.; Schmidt, C.; Bodmeier, R.; Hoffman, M.; Maincent, P., Oral evaluation in rabbits of cyclosporin-loaded Eudragit RS or RL nanoparticles. *International Journal of Pharmaceutics* **2005,** 288, (1), 169-175.
117. Miller, D. A.; DiNunzio, J. C.; Williams, R. O., Advanced Formulation Design: Improving Drug Therapies for the Management of Severe and Chronic Pain. *Drug Development and Industrial Pharmacy* **2008,** 34, (2), 117-133.
118. FDA Inactive Ingredient Search for Approved Drug Products. http://www.accessdata.fda.gov/scripts/cder/iig/getiigWEB.cfm
119. Gertsch, J.; Leonti, M.; Raduner, S.; Racz, I.; Chen, J. Z.; Xie, X. Q.; Altmann, K. H.; Karsak, M.; Zimmer, A., Beta-caryophyllene is a dietary cannabinoid. *P Natl Acad Sci USA* **2008,** 105, (26), 9099-9104.
120. Da Silva, S. L.; Figueiredo, P. M.; Yano, T., Chemotherapeutic potential of the volatile oils from Zanthoxylum rhoifolium Lam leaves. *Eur J Pharmacol* **2007,** 576, (1-3), 180-8.
121. Darmanin, S.; Wismayer, P. S.; Podesta, M. T. C.; Micallef, M. J.; Buhagiar, J. A., An extract from Ricinus communis L. leaves possesses cytotoxic properties and induces apoptosis in SK-MEL-28 human melanoma cells. *Natural Product Research* **2009,** 23, (6), 561-571.
122. Fernandes, E. S.; Passos, G. F.; Medeiros, R.; da Cunha, F. M.; Ferreira, J.; Campos, M. M.; Pianowski, L. F.; Calixto, J. B., Anti-inflammatory effects of compounds alpha-humulene and (-)-trans-caryophyllene isolated from the essential oil of Cordia verbenacea. *European Journal of Pharmacology* **2007,** 569, (3), 228-236.
123. Jirovetz, L.; Buchbauer, G.; Stoilova, I.; Stoyanova, A.; Krastanov, A.; Schmidt, E., Chemical composition and antioxidant properties of clove leaf essential oil. *J Agr Food Chem* **2006,** 54, (17), 6303-6307.
124. Russo, E. B., Taming THC: potential cannabis synergy and phytocannabinoid-terpenoid entourage effects. *British Journal of Pharmacology* **2011,** 163, (7), 1344-1364.
125. Pichette, A.; Lavoie, S.; Legault, J. Sesquiterpene formulation, kits and methods of use thereof 2008.
126. Sköld, M.; Karlberg, A.-T.; Matura, M.; Börje, A., The fragrance chemical [beta]-caryophyllene--air oxidation and skin sensitization. *Food and Chemical Toxicology* **2006,** 44, (4), 538-545.
127. Prashar, A.; Locke, I. C.; Evans, C. S., Cytotoxicity of clove (Syzygium aromaticum) oil and its major components to human skin cells. *Cell Prolif* **2006,** 39, (4), 241-8.
128. Naguib, M.; Diaz, P.; Xu, J. J.; Astruc-Diaz, F.; Craig, S.; Vivas-Mejia, P.; Brown, D. L., MDA7: a novel selective agonist for CB2 receptors that prevents allodynia in rat neuropathic pain models. *Br J Pharmacol* **2008,** 155, (7), 1104-16.

129. Rahn, E. J.; Zvonok, A. M.; Thakur, G. A.; Khanolkar, A. D.; Makriyannis, A.; Hohmann, A. G., Selective activation of cannabinoid CB2 receptors suppresses neuropathic nociception induced by treatment with the chemotherapeutic agent paclitaxel in rats. *J Pharmacol Exp Ther* **2008,** 327, (2), 584-91.
130. Veiga, V. F.; Zunino, L.; Patitucci, M. L.; Pinto, A. C.; Calixto, J. B., The inhibition of paw oedema formation caused by the oil of Copaifera multijuga Hayne and its fractions. *Journal of Pharmacy and Pharmacology* **2006,** 58, (10), 1405-1410.
131. Sylvestre, M.; Legault, J.; Dufour, D.; Pichette, A., Chemical composition and anticancer activity of leaf essential oil of Myrica gale L. *Phytomedicine* **2005,** 12, (4), 299-304.
132. Reinsvold, R. E.; Jinkerson, R. E.; Radakovits, R.; Posewitz, M. C.; Basu, C., The production of the sesquiterpene beta-caryophyllene in a transgenic strain of the cyanobacterium Synechocystis. *Journal of Plant Physiology* **2011,** 168, (8), 848-852.
133. Politeo, O.; Jukic, M.; Milos, M., Chemical composition and antioxidant activity of essential oils of twelve spice plants. *Croat Chem Acta* **2006,** 79, (4), 545-552.
134. Pereira, F. J.; Martins, F. T.; Correa, R. S.; Moreira, M. E. C.; Costa, A. M. D. D.; Dos Santos, M. H.; Polo, M.; Barbosa, L. C. A., Isolation, chemical composition and anti-inflammatory activity of Copaifera langsdorffii desf. fruit peels essential oil according to successive hydrodistillations. *Lat Am J Pharm* **2008,** 27, (3), 369-374.
135. Brown, A. E.; Riddick, E. W.; Aldrich, J. R.; Holmes, W. E., Identification of (-)-beta-caryophyllene as a gender-specific terpene produced by the multicolored Asian lady beetle. *J Chem Ecol* **2006,** 32, (11), 2489-99.
136. Fessi, H.; Puisieux, F.; Devissaguet, J. P.; Ammoury, N.; Benita, S., Nanocapsule formation by interfacial polymer deposition following solvent displacement. *International Journal of Pharmaceutics* **1989,** 55, (1), R1-R4.
137. Montasser, I.; Briançon, S.; Fessi, H., The effect of monomers on the formulation of polymeric nanocapsules based on polyureas and polyamides. *International Journal of Pharmaceutics* **2007,** 335, (1–2), 176-179.
138. Layre, A. M.; Couvreur, P.; Richard, J.; Requier, D.; Ghermani, N. E.; Gref, R., Freeze-drying of composite core-shell nanoparticles. *Drug Development and Industrial Pharmacy* **2006,** 32, (7), 839-846.
139. Lamer, V. K.; Dinegar, R. H., Theory, Production and Mechanism of Formation of Monodispersed Hydrosols. *Journal of the American Chemical Society* **1950,** 72, (11), 4847-4854.
140. Polymer, R. P., Preparatory and Associated Work. In 2012.
141. FDA, Guidance for Industry: Q3C — Tables and List. In 2003.
142. Wu, T.-H.; Yen, F.-L.; Lin, L.-T.; Tsai, T.-R.; Lin, C.-C.; Cham, T.-M., Preparation, physicochemical characterization, and antioxidant effects of quercetin nanoparticles. *International Journal of Pharmaceutics* **2008,** 346, (1–2), 160-168.
143. Bucolo, C.; Maltese, A.; Puglisi, G.; Pignatello, R., Enhanced ocular anti-inflammatory activity of ibuprofen carried by an Eudragit RS100 nanoparticle suspension. *Ophthalmic Res* **2002,** 34, (5), 319-23.
144. Pignatello, R.; Bucolo, C.; Ferrara, P.; Maltese, A.; Puleo, A.; Puglisi, G., Eudragit RS100® nanosuspensions for the ophthalmic controlled delivery of ibuprofen. *European Journal of Pharmaceutical Sciences* **2002,** 16, (1–2), 53-61.
145. Gargouri, M.; Sapin, A.; Bouali, S.; Becuwe, P.; Merlin, J. L.; Maincent, P., Optimization of a New Non-viral Vector for Transfection: Eudragit Nanoparticles for the Delivery of a DNA Plasmid. *Technol Cancer Res T* **2009,** 8, (6), 433-443.

146. Das, S.; Roy, P.; Auddy, R. G.; Mukherjee, A., Silymarin nanoparticle prevents paracetamol-induced hepatotoxicity. *Int J Nanomedicine* **2011,** 6, 1291-301.
147. Romero-Pérez, A.; García-García, E.; Zavaleta-Mancera, A.; Ramírez-Bribiesca, J.; Revilla-Vázquez, A.; Hernández-Calva, L.; López-Arellano, R.; Cruz-Monterrosa, R., Designing and evaluation of sodium selenite nanoparticles <i>in vitro</i> to improve selenium absorption in ruminants. *Veterinary Research Communications* **2010,** 34, (1), 71-79.
148. Eidi, H.; Joubert, O.; Attik, G.; Duval, R. E.; Bottin, M. C.; Hamouia, A.; Maincent, P.; Rihn, B. H., Cytotoxicity assessment of heparin nanoparticles in NR8383 macrophages. *International Journal of Pharmaceutics* **2010,** 396, (1–2), 156-165.
149. Elshafeey, A. H.; Kamel, A. O.; Awad, G. A. S., Ammonium methacrylate units polymer content and their effect on acyclovir colloidal nanoparticles properties and bioavailability in human volunteers. *Colloids and Surfaces B: Biointerfaces* **2010,** 75, (2), 398-404.
150. Date, P. V.; Samad, A.; Devarajan, P. V., Freeze thaw: a simple approach for prediction of optimal cryoprotectant for freeze drying. *Aaps Pharmscitech* **2010,** 11, (1), 304-13.
151. Abdelwahed, W.; Degobert, G.; Stainmesse, S.; Fessi, H., Freeze-drying of nanoparticles: Formulation, process and storage considerations. *Advanced Drug Delivery Reviews* **2006,** 58, (15), 1688-1713.
152. Sattler, K. D., Handbook of Nanophysics: Nanomedicine and Nanorobotics. In CRC Press: Boca Raton, FL, 2011.
153. Chattopadhyay, P.; Huff, R.; Shekunov, B. Y., Drug encapsulation using supercritical fluid extraction of emulsions. *Journal of Pharmaceutical Sciences* **2006,** 95, (3), 667-679.
154. Zheng, G.-Q.; Kenney, P. M.; Lam, L. K. T., Sesquiterpenes from Clove (Eugenia caryophyllata) as Potential Anticarcinogenic Agents. *Journal of Natural Products* **2004,** 55, (7), 999-1003.
155. Buchi *Training papers: distillation and Environnement.*; 1998.
156. Cauchetier, E.; Deniau, M.; Fessi, H.; Astier, A.; Paul, M., Atovaquone-loaded nanocapsules: influence of the nature of the polymer on their in vitro characteristics. *International Journal of Pharmaceutics* **2003,** 250, (1), 273-281.
157. Loxley, A.; Vincent, B., Preparation of Poly(methylmethacrylate) Microcapsules with Liquid Cores. *J Colloid Interf Sci* **1998,** 208, (1), 49-62.
158. Romero-Cano, M. S.; Vincent, B., Controlled release of 4-nitroanisole from poly(lactic acid) nanoparticles. *Journal of Controlled Release* **2002,** 82, (1), 127-135.
159. Poletto, F. S.; Jäger, E.; Cruz, L.; Pohlmann, A. R.; Guterres, S. S., The effect of polymeric wall on the permeability of drug-loaded nanocapsules. *Materials Science and Engineering: C* **2008,** 28, (4), 472-478.
160. Jung, T.; Breitenbach, A.; Kissel, T., Sulfobutylated poly(vinyl alcohol)-graft-poly(lactide-co-glycolide)s facilitate the preparation of small negatively charged biodegradable nanospheres. *Journal of Controlled Release* **2000,** 67, (2–3), 157-169.
161. Galindo-Rodriguez, S.; Allemann, E.; Fessi, H.; Doelker, E., Physicochemical parameters associated with nanoparticle formation in the salting-out, emulsification-diffusion, and nanoprecipitation methods. *Pharmaceutical Research* **2004,** 21, (8), 1428-1439.

162. Legrand, P.; Lesieur, S.; Bochot, A.; Gref, R.; Raatjes, W.; Barratt, G.; Vauthier, C., Influence of polymer behaviour in organic solution on the production of polylactide nanoparticles by nanoprecipitation. *International Journal of Pharmaceutics* **2007,** 344, (1-2), 33-43.
163. Thioune, O.; Fessi, H.; Devissaguet, J. P.; Puisieux, F., Preparation of pseudolatex by nanoprecipitation: Influence of the solvent nature on intrinsic viscosity and interaction constant. *International Journal of Pharmaceutics* **1997,** 146, (2), 233-238.
164. Aubry, J.; Ganachaud, F.; Cohen Addad, J. P.; Cabane, B., Nanoprecipitation of polymethylmethacrylate by solvent shifting: 1. Boundaries. *Langmuir* **2009,** 25, (4), 1970-9.
165. Stephanie Schubert , J. T. D., Jr and Ulrich S. Schubert Nanoprecipitation and nanoformulation of polymer: from history to powerful possibilities beyond poly(lactic acid) *Soft Matter* **2011**, (5).
166. Dirksen, J. A.; Ring, T. A., Fundamentals of Crystallization - Kinetic Effects on Particle-Size Distributions and Morphology. *Chem Eng Sci* **1991,** 46, (10), 2389-2427.
167. Skrdla, P. J., Roles of Nucleation, Denucleation, Coarsening, and Aggregation Kinetics in Nanoparticle Preparations and Neurological Disease. *Langmuir* **2012,** 28, (10), 4842-4857.
168. Teixeira, M.; Alonso, M. J.; Pinto, M. M.; Barbosa, C. M., Development and characterization of PLGA nanospheres and nanocapsules containing xanthone and 3-methoxyxanthone. *Eur J Pharm Biopharm* **2005,** 59, (3), 491-500.
169. Khayata, N.; Abdelwahed, W.; Chehna, M. F.; Charcosset, C.; Fessi, H., Preparation of vitamin E loaded nanocapsules by the nanoprecipitation method: From laboratory scale to large scale using a membrane contactor. *International Journal of Pharmaceutics* **2012,** 423, (2), 419-427.
170. Bilati, U.; Allemann, E.; Doelker, E., Development of a nanoprecipitation method intended for the entrapment of hydrophilic drugs into nanoparticles. *Eur J Pharm Sci* **2005,** 24, (1), 67-75.
171. Stainmesse, S.; Orecchioni, A. M.; Nakache, E.; Puisieux, F.; Fessi, H., Formation and stabilization of a biodegradable polymeric colloidal suspension of nanoparticles. *Colloid & Polymer Science* **1995,** 273, (5), 505-511.
172. Choi, S.-W.; Kwon, H.-Y.; Kim, W.-S.; Kim, J.-H., Thermodynamic parameters on poly(d,l-lactide-co-glycolide) particle size in emulsification–diffusion process. *Colloids and Surfaces A: Physicochemical and Engineering Aspects* **2002,** 201, (1–3), 283-289.
173. Sitnikova, N. L.; Sprik, R.; Wegdam, G.; Eiser, E., Spontaneously Formed trans-Anethol/Water/Alcohol Emulsions: Mechanism of Formation and Stability. *Langmuir* **2005,** 21, (16), 7083-7089.
174. Vitale, S. A.; Katz, J. L., Liquid Droplet Dispersions Formed by Homogeneous Liquid−Liquid Nucleation: “The Ouzo Effect”. *Langmuir* **2003,** 19, (10), 4105-4110.
175. Landfester, K., Miniemulsions for nanoparticle synthesis. *Top Curr Chem* **2003,** 227, 75-123.
176. Molpeceres, J.; Guzman, M.; Aberturas, M. R.; Chacon, M.; Berges, L., Application of central composite designs to the preparation of polycaprolactone nanoparticles by solvent displacement. *J Pharm Sci* **1996,** 85, (2), 206-13.

177. Fresta, M.; Puglisi, G.; Wehrli, E.; Giammona, G.; Di Marco, S., Freeze-fracture electron microscopy and light scattering studies on polyethylcyanoacrylate nanocapsule colloidal suspensions. *Il Nuovo Cimento D* **1994,** 16, (8), 1271-1276.
178. El-Shabouri, M. H., Positively charged nanoparticles for improving the oral bioavailability of cyclosporin-A. *International Journal of Pharmaceutics* **2002,** 249, (1-2), 101-108.
179. Batrakova, E. V.; Han, H. Y.; Alakhov, V.; Miller, D. W.; Kabanov, A. V., Effects of pluronic block copolymer on drug absorption in Caco-2 cell monolayers. *Pharm Res* **1998,** 15, (6), 850-5.
180. Yadav, K. S.; Chuttani, K.; Mishra, A. K.; Sawant, K. K., Long Circulating Nanoparticles of Etoposide Using PLGA-MPEG and PLGA-Pluronic Block Copolymer: Characterization, Drug-Release, Blood-Clearance, and Biodistribution Studies. *Drug Develop Res* **2010,** 71, (4), 228-239.
181. Devarajan, P. V.; Sonavane, G. S., Preparation and In Vitro/In Vivo Evaluation of Gliclazide Loaded Eudragit Nanoparticles as a Sustained Release Carriers. *Drug Development and Industrial Pharmacy* **2007,** 33, (2), 101 - 111.
182. Rao, J. P.; Geckeler, K. E., Polymer nanoparticles: Preparation techniques and size-control parameters. *Progress in Polymer Science* **2011,** 36, (7), 887-913.
183. Du, J.; O'Reilly, R. K., Advances and challenges in smart and functional polymer vesicles. *Soft Matter* **2009,** 5, (19), 3544-3561.
184. Lin Mei, Y. Z., Yi Zheng, Ge Tian, Cunxian Song, Dongye Yang, Hongli Chen, Hongfan Sun, Yan Tian, Kexin Liu, Zhen Li, and Laiqiang Huang, A Novel Docetaxel-Loaded Poly (ε-Caprolactone)/Pluronic F68 Nanoparticle Overcoming Multidrug Resistance for Breast Cancer Treatment. *Nanoscale Res Lett* **2009,** 4, (12), 1530-1539.
185. Urata, T.; Arimori, K.; Nakano, M., Modification of release rates of cyclosporin A from polyl(L-lactic acid) microspheres by fatty acid esters and in-vivo evaluation of the microspheres. *Journal of Controlled Release* **1999,** 58, (2), 133-141.
186. Aceves, J. M.; Cruz, R.; Hernandez, E., Preparation and characterization of Furosemide-Eudragit controlled release systems. *Int J Pharm* **2000,** 195, (1-2), 45-53.
187. Shivakumar, H. N.; Desai, B. G.; Deshmukh, G., Design and optimization of diclofenac sodium controlled release solid dispersions by response surface methodology. *Indian J Pharm Sci* **2008,** 70, (1), 22-30.
188. Haznedar, S.; Dortunç, B., Preparation and in vitro evaluation of Eudragit microspheres containing acetazolamide. *International Journal of Pharmaceutics* **2004,** 269, (1), 131-140.
189. Horobin, R.; Rashid, F., Interactions of molecular probes with living cells and tissues. Part 1. Some general mechanistic proposals, making use of a simplistic Chinese box model. *Histochemistry and Cell Biology* **1990,** 94, (2), 205-209.
190. Loftsson, T.; Masson, M.; Brewster, M. E., Self-association of cyclodextrins and cyclodextrin complexes. *J Pharm Sci* **2004,** 93, (5), 1091-9.
191. Abdelwahed, W.; Degobert, G.; Fessi, H., A pilot study of freeze drying of poly(epsilon-caprolactone) nanocapsules stabilized by poly(vinyl alcohol): formulation and process optimization. *Int J Pharm* **2006,** 309, (1-2), 178-88.

CHAPTER IV EXPERIMENTAL

1 MDA7 purity determination.

1.1 LC-UV-MS

1.1.1 Sample Preparation

1.0-mg/ml solution of MDA7 was made by weighing out 2.246 mg of solid MDA7 (Lot # PHD001.374F1), placing it in an amber vial, and then adding 2246 µl of methanol. This solution was then diluted 100x to a concentration of 10 µg/ml using a 10% methanol (in water) solution. Both a blank solution of 10% methanol and the 10 µg/ml solution of MDA7 were then analyzed by LC-UV-MS.

1.1.2 LC-UV-MS Methodology

The instrumentation consisted of a Waters Acquity LC system, equipped with a Waters Acquity photodiode array (PDA) detector, interfaced to a Waters TQD mass spectrometer operated in ESI positive mode. The LC analysis was performed utilizing a reversed phase gradient system with the aqueous phase A being 0.2% formic acid in water (pH 3.0) and the organic phase B being methanol. The mobile phase was delivered in a gradient mode at 0.15 mL/min at 90 % A from 0 to 30 seconds, decreased from 90.0 % to 5 % A from 30 secondes to 8 minutes, kept at 5% A from 8 to 10 minutes, returned from 5% to 90 % A from 10 to 11 minutes, and equilibrated at 90 % from 11 to 14 minutes. The LC column used was a Waters Acquity BEH C18 1.7 µm, 1.0x100mm column. The column was placed in a column heater that was maintained at 60°C. The samples were placed in a refrigerated autosampler that was maintained at 8°C. The sample (10 µL) was injected for each analysis. The UV range for the PDA was 210-500 nm. Purity was assessed at 254 nm. The Waters LC system was also coupled with a Waters TQD #1 mass spectrometer to identify MDA7. The mass spectrometer was operated in an electrospray positive mode. Major parameters were set as follows:

capillary energy 3.20 kV, cone energy 35.0 V, source temperature 125 ºC, desolvation temperature 350 °C, cone gas (nitrogen) 20 L/hr, desolvation gas (nitrogen) 650 L/hr. The mass spectrometer was scanned from 100 to 1200 *m/z*.

1.2 Results

As is shown in Fig. 71a through 71c, the UV trace of MDA7 sample at 254 nm shows no additional peaks when compared to the blank solvent (10% MeOH) other than MDA7 peak (UV retention time = 7.03 min). The purity was therefore determined to be > 99% by this method. The MS chromatogram shows the presence of a single major compound in MDA7 sample (Fig. 72), and this compound was identified as MDA7 based on the mass spectrum of this peak (Fig. 73).

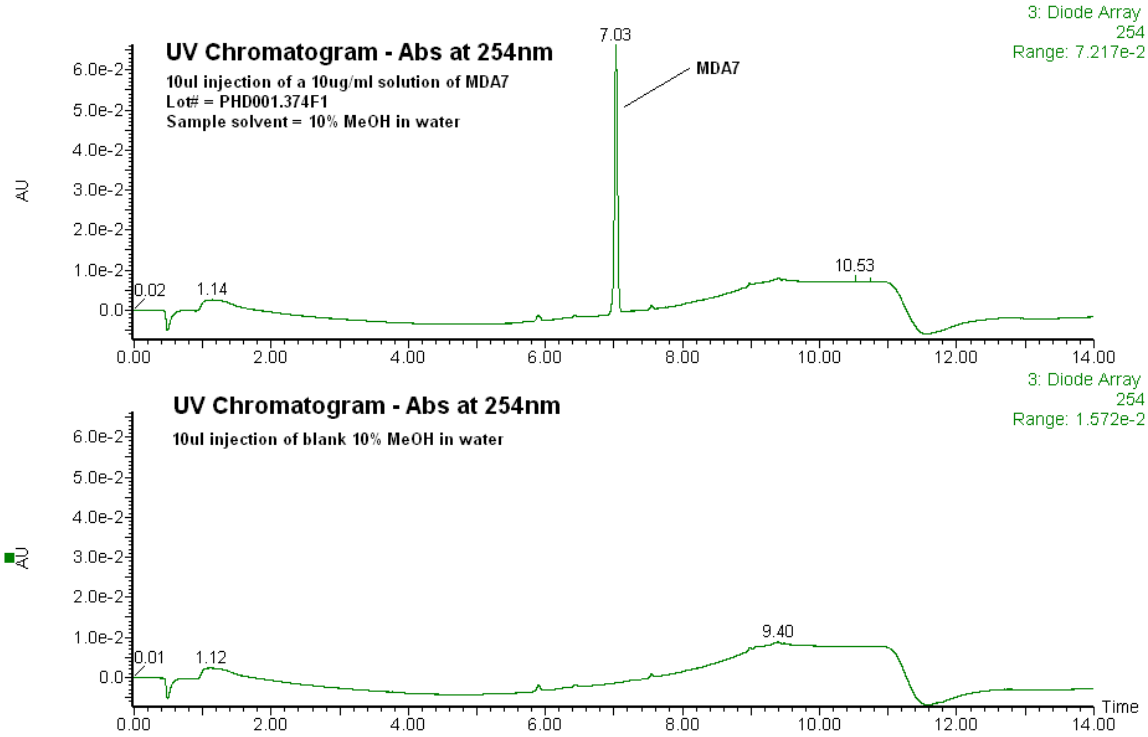

Figure 71a: UV absorption traces at λ = 254 nm. Purity is > 99%.

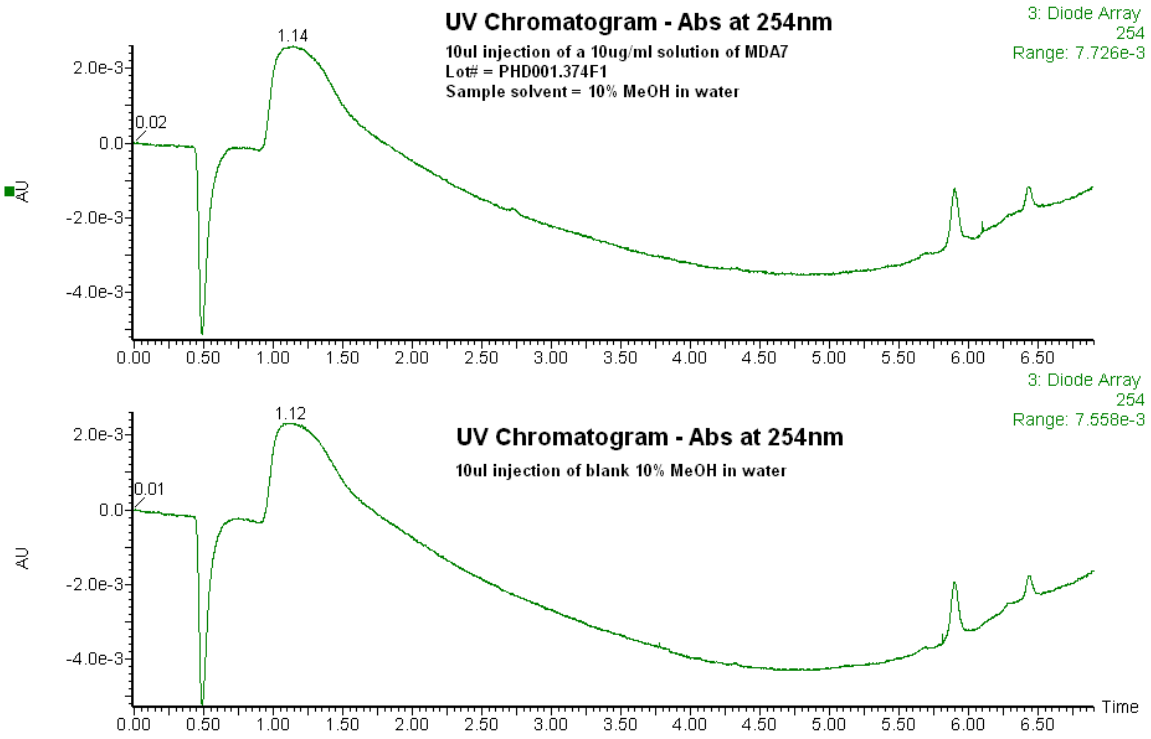

Figure 71b: UV absorption traces at λ = 254 nm expanded from 0 to 6.9 min. No differences/impurities observed. Purity is > 99%.

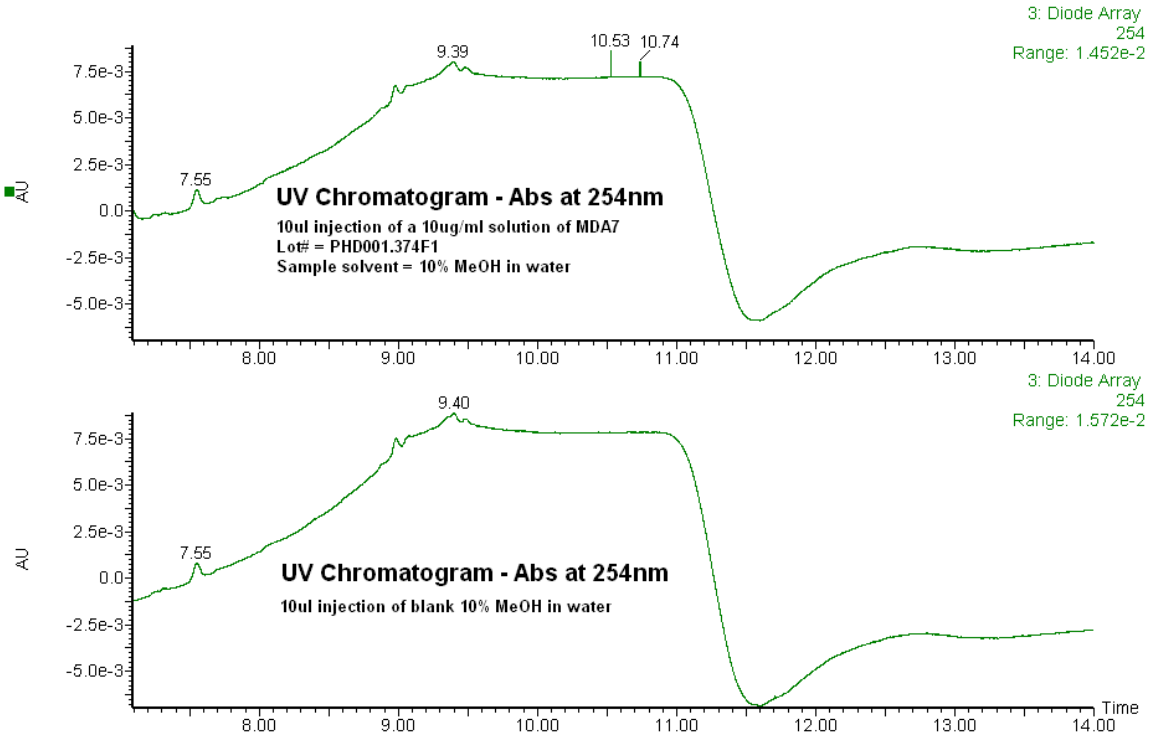

Figure 71c: UV absorption traces at λ = 254 nm expanded from 7.1 to 14 min. No differences/impurities observed. Purity is > 99%.

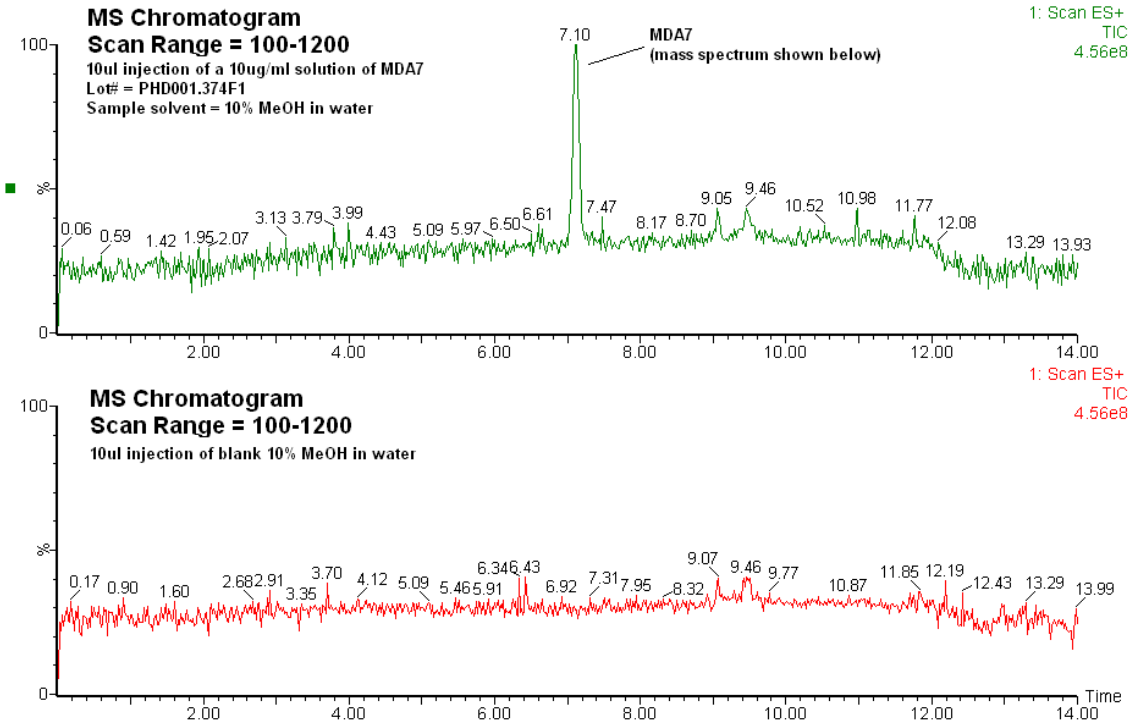

Figure 72: MS chromatograms. Scan range = 100-1200 *m/z*.

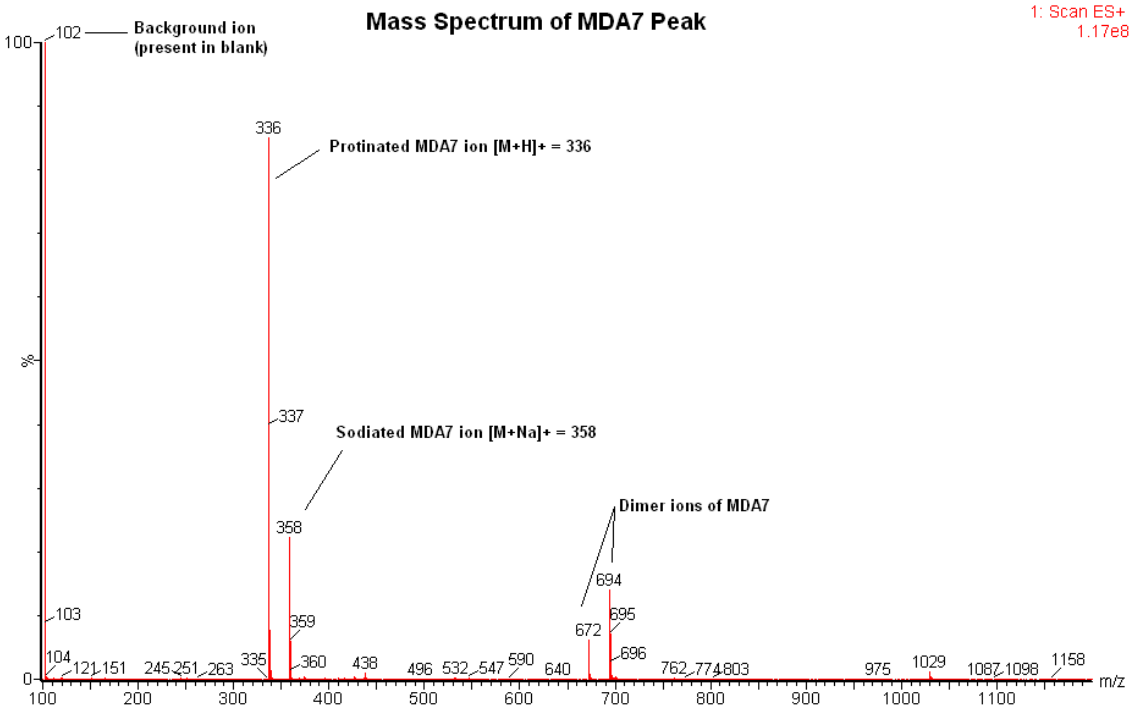

Figure 73: Mass spectrum of MDA7 peak in above MS chromatogram.

1.3 ^{1}H NMR.

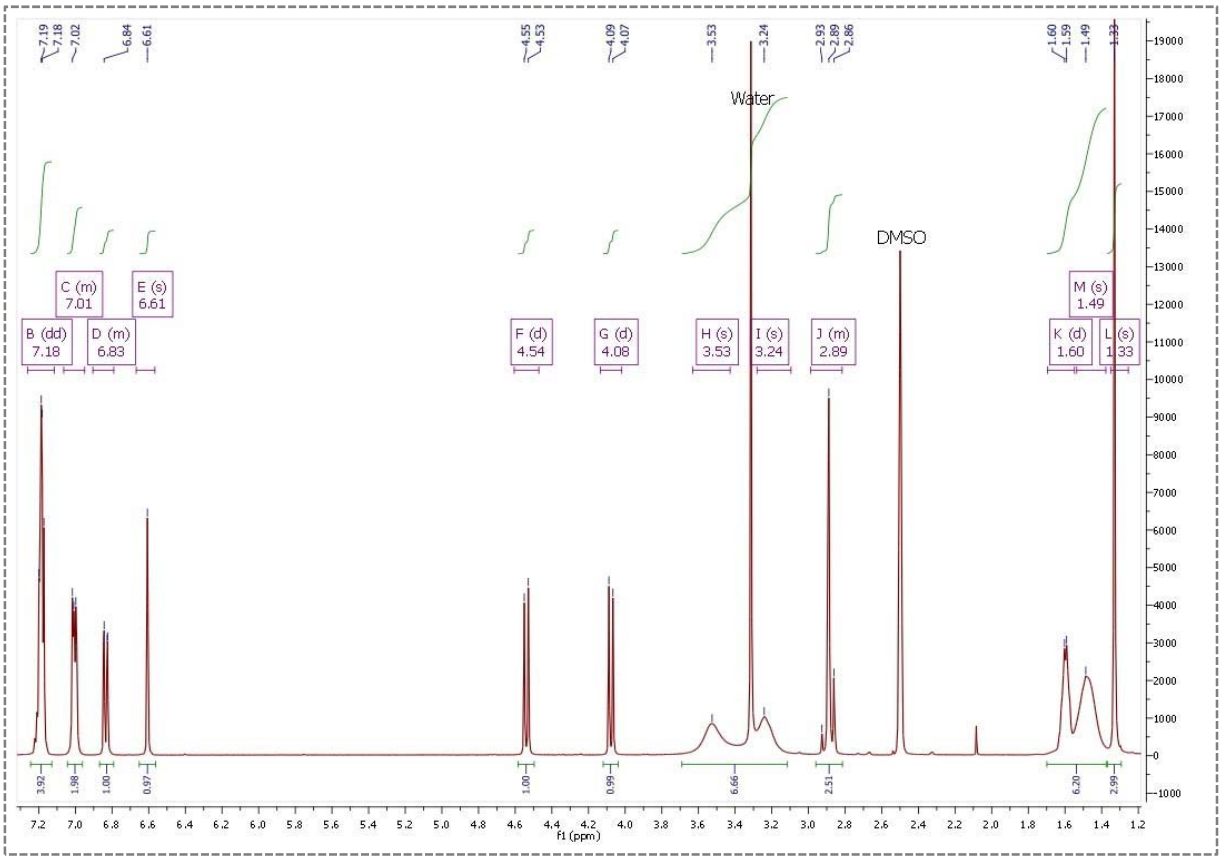

Figure 74: ^{1}H NMR MDA7 spectrum in DMSO-d_6.

2 MDA7 solubility determination.

The shake-flask method was used[1] at an equilibration of 24 hours and detection wavelength of 230 nm. Briefly, aqueous solubility (PBS Sigma, catalog number D-5652, pH 7.4) for the tested compound was determined by comparing the peak area of the principal peak in a calibration standard (200 µM in a 2% DMSO solution) containing organic solvent (methanol/water, 60/40, v/v) with the peak area of the corresponding peak in a buffer sample. In addition, chromatographic purity (%) was defined as the peak area of the principal peak relative to the total integrated peak area in the HPLC chromatogram of the calibration standard (Dionex). A chromatogram of the calibration standard for MDA7, along with a UV/VIS spectrum with labeled absorbance maxima, was generated.

3 *In vitro* MDA7 pharmacological characterization.

3.1 Materials.

MDA7 was obtained according to the methods previously described[2]. All chemicals used for the synthesis of MDA7 were purchased from Sigma-Aldrich Inc. (St Louis, MO, USA). AM251 and was SR141716A were purchased from Tocris Bioscience.

3.2 *In vitro* receptor radioligand binding studies.

3.2.1 Human CB_1 and CB_2 binding studies.

MDA7 was screened in a competitive binding experiment by using membranes of Chinese hamster ovarian cells (CHO-K1 cells) expressing the human CB_1 receptor at different MDA7 concentrations in duplicate[3]. The competitive binding experiment was performed in 96-well plates (Masterblock, catalogue number 786201, Greiner Bio-One, San Diego, CA, USA) containing binding buffer (50 mM Tris, pH 7.4, 2.5 mM EDTA, 0.5% protease-free BSA, saponin 10 µg ml^{-1}), recombinant membrane extracts (2 µg protein per well), and 1 nM [^{3}H]SR141716A (5-(4-chloro-phenyl)-1-(2,4-dichloro-phenyl)-4-methyl-1H-pyrazole-3-carboxylic acid piperidin-1-ylamide), a selective CB_1 receptor antagonist (GE Healthcare, TRK1028, 42 Ci $mmol^{-1}$, diluted in binding buffer). Nonspecific binding was determined in the presence of 10 µM CP55,940 (5-(1,1-dimethylheptyl)-2-[(1R,2R,5R)-5-hydroxy-2-(3-hydroxy-propyl)-cyclohexyl]-phenol)(Tocris Bioscience, Ellisville, MO, USA). The sample was incubated in a final volume of 0.1 ml for 60 min at 25°C and then filtered on a GF/C UniFilter microplate (Perkin Elmer, Waltham, MA, USA; catalogue number 6005177) presoaked in 0.05% Brij for 2 h at room temperature. Filters were washed six times with 4 ml of cold binding buffer, and bound [^{3}H]SR141716A was determined by liquid scintillation counting. The median inhibition concentration (IC_{50}) was determined by nonlinear regression using the one-site competition equation. The inhibition constant (K_i) values were calculated by using the

Cheng-Prusoff equation [$K_i = IC_{50}/(1 + (L/KD)$], where L = concentration of radioligand in the assay and K_D = affinity of the radioligand for the receptor.

MDA7 was also screened in a competitive binding experiment by using membranes of CHO-K1 cells selectively expressing the human CB2 receptor at different MDA7 concentrations in duplicate. The competitive binding experiment was performed in 96-well plates (Masterblock) containing binding buffer (50 mM Tris, pH 7.4, 2.5 mM EDTA, 0.5% protease-free BSA), recombinant membrane extracts (0.25 µg protein per well) and 1 nM [^{3}H]CP55,940 (Perkin Elmer, NEX-1051, 161 Ci mmol^{-1}, diluted in binding buffer). Nonspecific binding was determined in the presence of 10 µM CP55,940 (Tocris Bioscience). The sample was incubated in a final volume of 0.1 mL for 60min at 30 1C and then filtered on a GF/B UniFilter microplate (Perkin Elmer, catalogue number 6005177) presoaked in 0.5% polyethyleneimine for 2 h at room temperature. Filters were washed six times with 4 mL of cold binding buffer (50 mM Tris, pH 7.4, 2.5 mM EDTA, 0.5% protease-free BSA), and bound [^{3}H]CP55,940 was determined by liquid scintillation counting. The IC_{50} and *Ki* values were calculated as above.

3.2.2 Rat CB1 and CB2 receptor-binding studies.

MDA7 was screened in a competitive binding experiment using membranes of CHO-K1 cells selectively expressing the rat CB1 receptor at different MDA7 concentrations in duplicate[3]. The competitive binding experiment was performed in 96-well plates (Masterblock) containing binding buffer (50 mM Tris, pH 7.4, 1 mM EDTA, 0.5% protease-free BSA, 3 mM $MgCl_2$), recombinant membrane extracts (25 µg protein per well) and 1.25 nM [^{3}H]SR141716A (5-(4-chloro-phenyl)-1-(2,4-dichloro-phenyl)-4-methyl-1H-pyrazole-3-carboxylic acid piperidin-1-ylamide), a selective CB1 receptor antagonist (GE Healthcare diluted in binding buffer). Non-specific binding was determined in the presence of 10 µM AM251 (N-(piperidin-1-yl)-5-(4-iodophenyl)-1-(2,4-dichloro-phenyl)-4-methyl-*1H*-pyrazole-3-carboxamide) (Tocris Bioscience). The sample was incubated in a final volume of 0.1 mL for 60 min at 25°C and then filtered on a GF/C UniFilter microplate (Perkin Elmer, catalogue number 6005177) presoaked in 0.05% Brij for 2 h at room temperature. Filters were washed six times with 4 mL of cold binding buffer, and bound [^{3}H]SR141716A was determined by liquid scintillation counting. The IC_{50} value was

determined by nonlinear regression by using the one-site competition equation. The Ki values were calculated using the Cheng–Prusoff equation.

MDA7 was also screened in a competitive binding experiment using membranes of CHO-K1 cells selectively expressing the rat CB2 receptor at different MDA7 concentrations in duplicate[3]. The competitive binding experiment was performed in 96-well plates (Masterblock) containing binding buffer (50 mM Tris, pH 7.4, 2.5 mM EDTA, 0.5% protease-free BSA), recombinant membrane extracts (0.25 µg protein per well) and 1 nM [^{3}H]CP55,940 (Perkin Elmer, NEX-1051, 161 Ci mmol-1, diluted in binding buffer). Nonspecific binding was determined in the presence of 10 µM CP55,940 (Tocris Bioscience). The sample was incubated in a final volume of 0.1 mL for 60 min at 30°C and then filtered on a GF/B UniFilter microplate (Perkin Elmer, catalogue number 6005177) presoaked in 0.5% polyethyleneimine for 2 h at room temperature. Filters were washed six times with 4 mL of cold binding buffer (50 mM Tris, pH 7.4, 2.5 mM EDTA, 0.5% protease-free BSA), and bound [^{3}H]CP55,940 was determined by liquid scintillation counting. IC_{50} and Ki values were calculated as described previously.

3.2.3 GTPγ[^{35}S] functional assays.

Functional activity was evaluated by using a GTPγ[^{35}S] assay in CHO-K1 cell membrane extracts expressing recombinant human or rat CB1 or CB2 receptors. The assay relies on the binding of GTPγ [^{35}S], a radiolabeled nonhydrolyzable GTP analogue, to the G-protein upon binding of an agonist of the G-protein-coupled receptor. In this system, agonists stimulate GTPγ [^{35}S] binding, whereas neutral antagonists have no effect and inverse agonists decrease GTPγ [^{35}S] basal binding.

MDA7 was dissolved in 100% dimethylsulfoxide (DMSO) at a concentration of 10 mM within 4 h of the first testing session (master solution). A pre-dilution for the dose–response curve was performed in 100% DMSO, and this solution was diluted 100-fold in assay buffer to a concentration 2-fold higher than the concentration to be tested. MDA7 was tested for agonist and antagonist activities at eight concentrations in duplicate: 10, 3, 1, 0.3, 0.1, 0.03, 0.01 and 0.001 µM. CP55,940 (Tocris Bioscience) was the reference agonist. For GTPγS, 5 µg of membranes were mixed with guanosine-5'-diphosphate

diluted in assay buffer to give 30 µM solution (volume/volume), and incubated for at least 15 min on ice. In parallel, GTPγ[^{35}S] (GE Healthcare, catalogue number SJ1308) was mixed with scintillation beads (PVT-WGA, GE Healthcare, catalogue number RPNQ001), diluted in assay buffer at 50 mg mL^{-1} (0.5 mg per 10 µL^{-1}) (volume/volume) just before the reaction was started. The following reagents were successively added in the wells of an OptiPlate (Perkin Elmer): 50 µL of ligand or the reference antagonist (AM251, a CB1 receptor-selective antagonist); 20 µL of the membrane/guanosine-5'-diphosphate mix; 10 µL of the reference agonist (CP55,940) at historical EC_{80} (30 nM); and 20 µL of the GTPγ[^{35}S]:beads mix. The plates were covered with a topseal, shaken on an orbital shaker for 2 min and then incubated for 1 h at room temperature. Then the plates were centrifuged for 10 min at 800 g and counted for 1 min per well with a Perkin Elmer TopCount scintillation counter. Assay reproducibility was monitored by the use of the reference agonist, CP55,940. For replicate determinations, the maximum variability tolerated in the test was ±20% of the average of the replicates. Efficacies (E_{max}) for CB1 or CB2 receptors were expressed as a percentage relative to the efficacy of CP55,940.

4 Enabling Drug Delivery System Design and Development.

4.1 Materials.

2-Hydroxypropyl-β-cyclodextrin (HPβCD) with an average degree of molar substitution of 4.4 was purchased from CTD Inc. Ethyl Alcohol, 190 Proof, 95%, ACS/USP was purchased from PHARMCO AAPER. Dimyristoylphosphatidylcholine (DMPC) was purchased from Avanti Polar Lipids. Dimethyl sulfoxide was purchased from SIGMA-ALDRICH. PBS and maleic acid (>98%) were purchased from VWR. PBS with bovine serum albumin 1 % dry powder in pouches to dilute in 1 Liter ultrapure water was purchased from Fischer scientific. Acrodisc® Syringe Filters with Nylon Membrane were purchased from PALL Corporation. Other reagents and chemicals were obtained as gift samples, N-methyl-2-pyrrolidone (NMP or Pharmasolve™) from ISP, propylene glycol USP and Cremophor™ ELP from BASF, Super refined™ Polysorbate 20 and Super Refined™ PEG 400 from CRODA, PEG-8 capric/caprylic triglycerides (Labrasol®) and Apricot Kernel oil PEG-6 esters (Labrafil® M 1944 CS) from Gattefosse, macrogol 15-

hydroxystearate (Solutol® HS 15) from BASF . All chemicals were used as received. All experiments were carried out using ultrapure water.

4.2 Preformulation studies.

4.2.1 Kinetic solubility procedure adapted from Li et al.[4].

Approximately 5 mg of MDA7 was weighed into a vial. About 20 mg of cosolvent was added. Then, the mixture was sonicated in water-bath at 25°C for 2 min. If particles were not fully dissolved as determined by visual inspection, about 20 mg more cosolvent was added, followed by sonication under the same conditions. The above cycle was continued until all drug particles were fully dissolved. The kinetic solubility (*S*) was calculated as followed: 5 mg / (n cycles* 20 mg) * 1000 = S (mg MDA7 / g solvent)

4.3 Micellar system.

4.3.1 Preparation.

At room temperature, the appropriate amount of MDA7 was weighed for a final concentration in the micellar system ranging from 6 mg/mL to 30 mg/mL. Cosolvents were added and the resulting solution was stirred with a magnetic bar (100 rpm) until a clear solution was obtained.
Surfactant was melted at 40°C prior to the addition to the cosolvents mixture if necessary (i.e. Solutol® HS15). The resulting solution was placed under the same stirring conditions as previously described. The solution was diluted by drop wise addition of PBS using the stirring conditions described above.

4.3.2 *In vitro* static serial dilution method[5].

The testing procedure was conducted as follow:
-To 10 test tubes, 0.5 ml of phosphate buffered saline bovine serum albumin solution (a facsimile of plasma) was added.

-To tube 1, 0.5 ml of the tested formulation were added and mixed gently.
-0.5 ml of the resulting solution from tube 1 was transferred into tube 2 and mixed.
-The above step was repeated through tube 10, at which point the original formulation in tube 1 was diluted 1024 fold.
-All tubes were observed for cloudiness/precipitation.
The following criteria for formulation precipitation were assessed:
-The drug was unlikely to precipitate, if no cloudiness/precipitation was observed in all 10 tubes in 3–5 min.
-The drug was less likely to precipitate, if slight cloudiness/precipitation was observed in one or more tubes in 3–5 min.
-The drug was likely to precipitate, if cloudiness or precipitation was observed in one or more tubes in less than 1 min. and further optimization of the formulation was required.

4.3.3 Microscopic observation.

For microscopic observation, one drop of DDS was mounted on slides and observed under simple polarized light using an IX70 inverted microscope (Olympus, Melville,NY) with a Quantix charge-coupled device camera and IPLabs software (Scanalytics, Inc., Fairfax, VA).

4.3.4 Particle size measurement.

The mean particle size and size distribution of samples were determined by DLS measurements using a Nano S (Malvern Instruments, Worcestershire, England). The analysis was performed at a temperature of 25°C using samples appropriately diluted with double distilled water and filtrated (Acrodisc® Syringe Filters 0.45 µm) in order to avoid multiscattering events. DTS v. 3.0-software was used to calculate particle mean diameter (Z-Average) and the width of the fitted Gaussian distribution, which is displayed as the polydispersity index (PDI). Before each DLS scan, the samples were stabilized for 10 min. Each size measurement was performed with at least 5 runs.

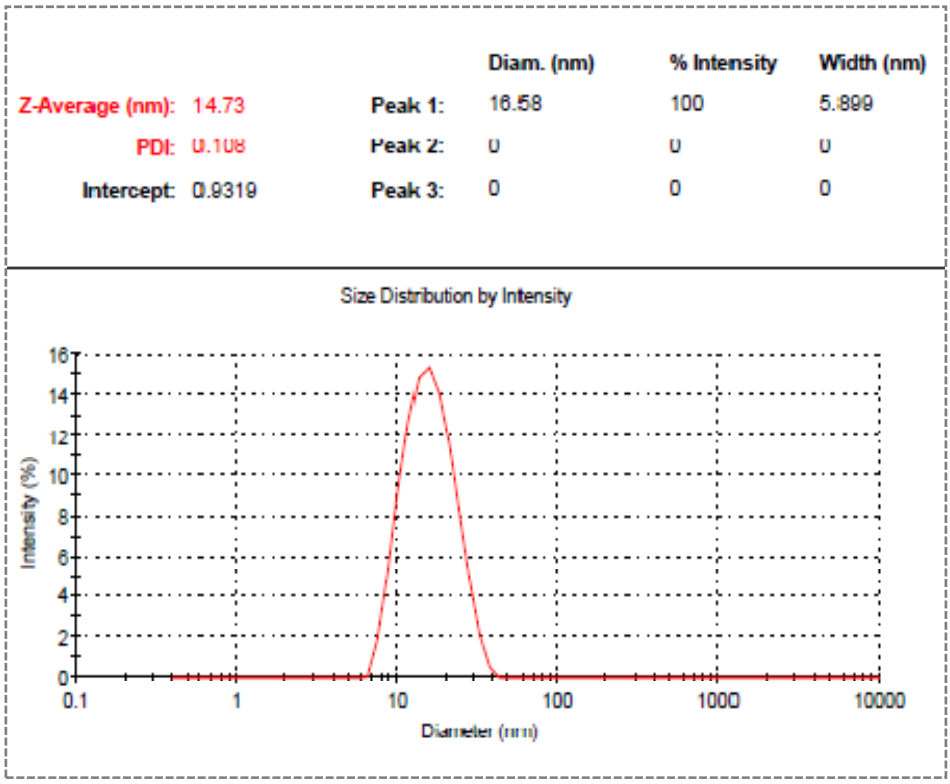

Figure 75: Particle size measurement for the micellar solution entry N in Table 14.

4.3.5 MDA7 chemical stability by ^{1}H-NMR.

^{1}H NMR spectra were recorded at room temperature on Bruker Avance III^{TM} spectrometer at 400 MHz using a 5 mm probe and a simple pulse-acquire sequence. Acquisition parameters consisted of spectral width 4000 Hz with an acquisition time 3.98 s, number of scans of 128, and relaxation delay of 1 s. All spectra were carefully baseline corrected before integration. The quantitation was accomplished using an external standard, maleic acid (MA) prepared as a 0.16 M solution in D_2O in a sealed capillary.

Approximately 900 µL of micellar solution prepared in D_20 was added to an NMR tube as well as the capillary containing the external standard. The concentration of MDA7 was calculated based on the integration ratio of the drug signal to the MA signal (δ 6.26 ppm, 2H).

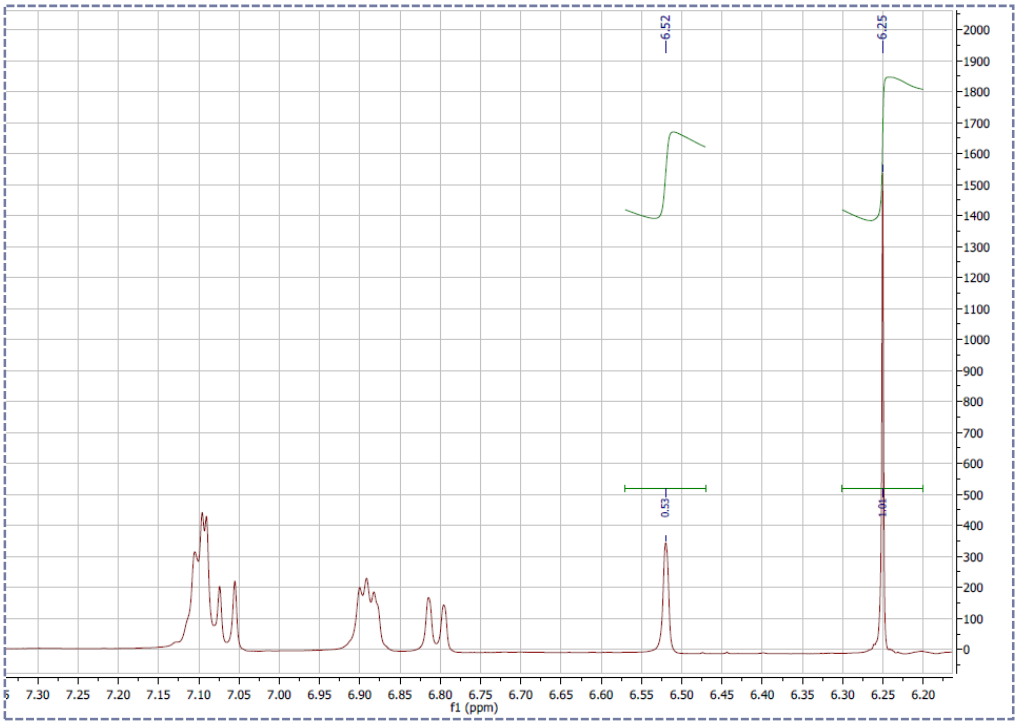

Figure 76: Micellar solution at $t_{initial}$. Quantitation of MDA7 using the peaks ratio of respectively MDA7 (6.52 ppm) and maleic acid (6.26 ppm).

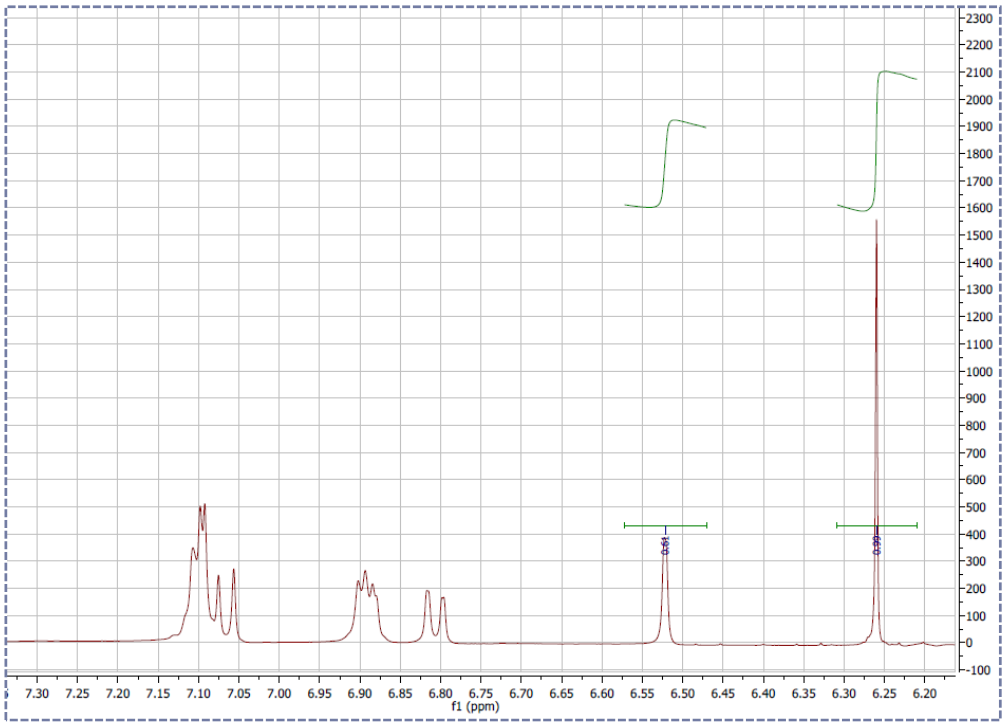

Figure 77: Micellar solution at $t_{1\ month}$. Quantitation of MDA7 using the peaks ratio of respectively MDA7 (6.52 ppm) and maleic acid (6.26 ppm).

4.3.6 MDA7 chemical stability by UPLC-MS.

4.3.6.1 Standard curve and Sample Preparation.

A stock solution of MDA7 (1 mg/mL) was prepared in methanol. Standard solutions at 1, 10, 50, 100, and 500 µg/mL (Fig. 78) were prepared by diluting the stock solution with a mixture of methanol and 0.2% formic acid in water (50: 50, v/v). A standard curve of MDA7 was constructed on the day samples were analyzed.

Before analysis, an aliquot (100 µL) of MDA7 formulated at the appropriate concentration was mixed with 900 µL of methanol in a microcentrifuge tube, vortexed for 1 minute, and centrifuged at 13,2000 rpm for 5 minutes. The upper layer was collected and was diluted in series of 10-fold dilution factor with a mixture of methanol and water (75: 25, v/v) until the accumulated dilution factor was 1: 100,000.

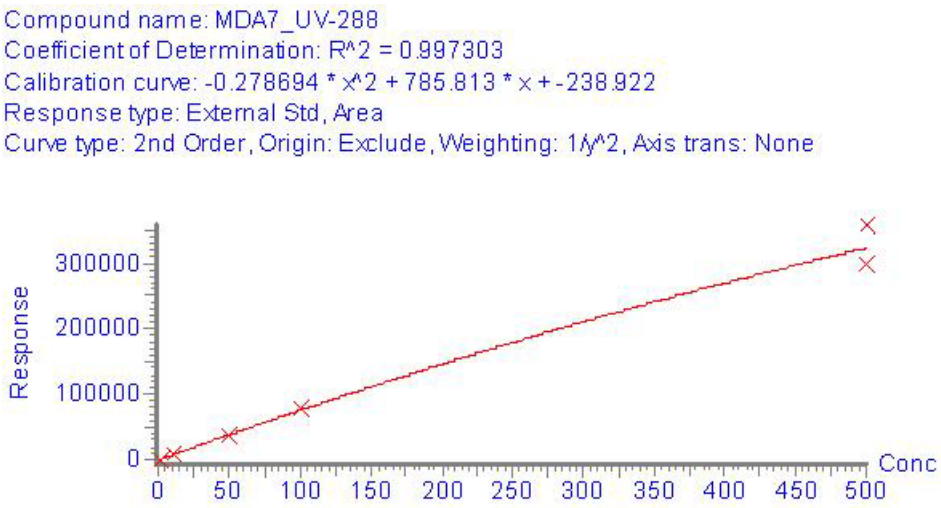

Figure 78: Standard curve of MDA7 in methanol at concentrations of 1, 10, 50,100 and 500 µg/mL.

4.3.6.2 UPLC-MS methodology.

The instrumentation consisted of a Waters Acquity UPLC system coupled with a Waters Acquity PDA detector was used. The stationary phase was a Waters Symmetry 300 C_4 column (50 x 2.1 mm, 3.5 µm particle size) protected by a 0.5 µm frit (Upchuch Scientific). The column temperature was maintained at 60°C. Solvent A was 0.2% formic acid in water (pH 3.0) and solvent B a mixture of acetonitrile and methanol (80/20, vol/vol). The mobile phase was delivered in a gradient mode at 0.350 mL/min at 75%A from 0 to 1 minute, decreased from 75% to 5%A from 1 to 3 minutes, kept at 5%A from 3 to 6 minutes, returned from 5% to 75% A from 6 to 7 minutes, and equilibrated at 75% from 7 to 10 minutes. Analytes were monitored by a photodiode array detector in the range from 190 to 350 nm. The injection volume was 20 µL. The Waters UPLC system was also coupled with a Waters Quattro Premier mass spectrometer to identify MDA7. The mass spectrometer was operated in an electrospray positive mode. Major parameters were set as follows: capillary energy 3.50 kV, cone energy 25.0 V, collision cell 25, source temperature 125 ºC, desolvation temperature 350°C, cone gas (nitrogen) 70 L/hr, desolvation gas (nitrogen) 700 L/hr, and collision gas (argon) 0.25 mL/min. MDA7 was monitored in a Multiple Reaction Mode (MRM) at *m/z*: 335.85 → 244.70.

4.3.6.3 Results

The eluate from the LC column was monitored in the range from 200 to 400 nm by a PDA detector. Fig.79 shows a representative chromatogram of MDA7 extracted at 288 nm. The UV absorption peak at 2.77 minutes was identified to be that of MDA7 by UPLC-MS/MS.

In Fig. 80 an ion spectrum extracted at retention times from 2.75 to 3.00 minutes from the chromatogram represented in Fig.79 corresponding to the major peak (*m/z* 337) of proton adduct form of MDA7 is shown.

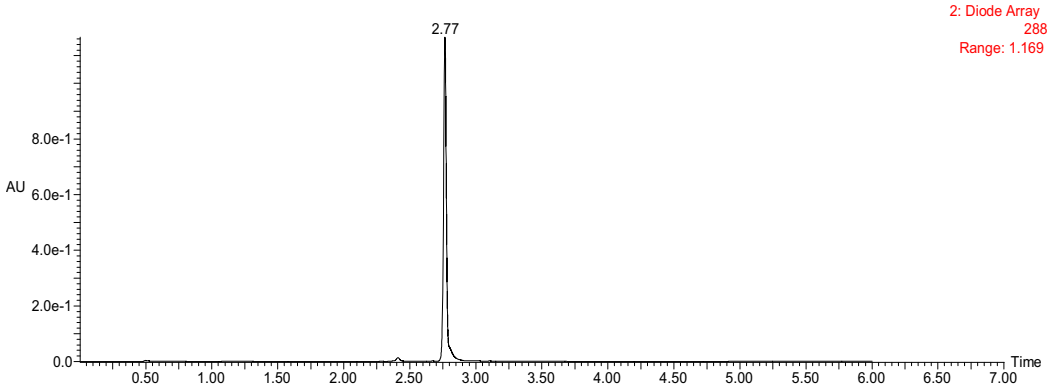

Figure 79: Chromatogram of MDA7 in methanol/0.2% formic acid in water (50: 50) extracted at 288 nm.

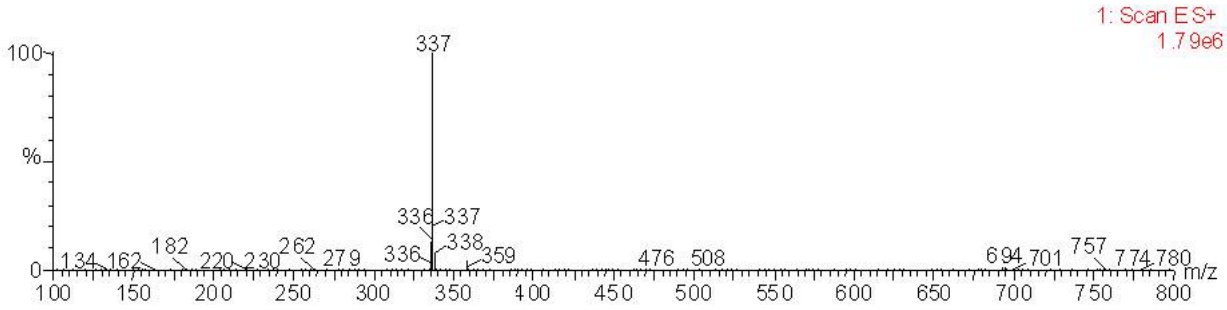

Figure 80: Ion spectrum extracted at retention times from 2.75 to 3.00 minutes from Fig. 79 chromatogram.

4.4 Oral Self-Emulsifying Drug delivery System (SEDDS).

4.4.1 Preparation.

At room temperature, the appropriate amount of MDA7 was weighted for a final concentration of 4.5 mg/mL in SEDDS. NMP was added and the resulting mixture was stirred with a magnetic bar (100 rpm) until obtaining a clear solution. Labrasol® and Labrafil® were added and the resulting placed was stirred using the conditions as described above. The solution was diluted by drop wise addition of PBS using the same stirring conditions described above.

4.4.2 Microscopic observation.

The same protocol described in section 4.3.3 was used.

4.4.3 Particle size measurement.

The same protocol described in section 4.3.4 was used.

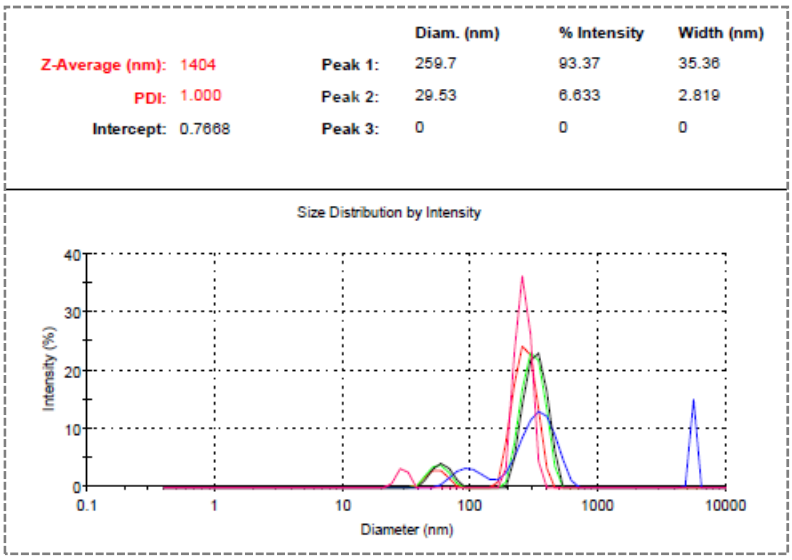

Figure 81: Particle size measurement for SEDDS entry O in Table 17.

4.4.4 MDA7 chemical stability assessment by UPLC-MS.

The same protocol described in section 4.3.6 was used.

4.5 Liposomes.

4.5.1 Preparation.

The preparation of liposomes was adapted from a method previously described by Lopez-Berestein et al[6]. MDA7 was dissolved in DMSO to afford a solution at 40 mg/mL and mixed to a solution of dimyristoylphosphatidylcholine (DMPC) at 50 mg/mL in *tert*-butanol in a molar ratio of 1:10 drug/lipids. Polysorbate 20 was added to the preparation in an amount corresponding to 5% of the total amount of MDA7+ lipids. *tert*-butanol (95 mL) was added for each 5 mL of MDA7 lipid mixture previously obtained. The resulting solution was freeze-dried (Labconco-freeze dry system/Freezone® 1) for 48h, providing a white and dried cake containing drug, lipids and surfactant. Before administration to animals, the dry drug/lipids mixture was hydrated with PBS to obtain the desired volume of administration, and stirred at 100 rpm for 20 min. at 30°C, a temperature above the gel-liquid crystal transition temperature of DMPC. This process resulted in homogeneous milky-like MLVs liposomal suspensions.

4.5.2 Morphology.

Liposomal preparation samples were placed on single slot formvar coated copper grids treated with poly-l-lysine for 1 hour. Excess samples were blotted with filter paper and then stained with filtered 1% uranyl acetate for 1 min. Stain was blotted dry from the grids with filter paper and samples were allowed to dry. Samples were then examined in a JEM 1010 transmission electron microscope (JEOL, USA, Inc., Peabody, MA) at an accelerating voltage of 80 Kv. Digital images were obtained using the AMT Imaging System (Advanced Microscopy Techniques Corp., Danvers, MA).

4.5.3 Microscopic observation.

The same protocol described in section 4.3.3 was used.

4.5.4 MDA7 chemical stability assessment by ^{1}H NMR.

The same NMR sequence and equipment described in section 4.3.5 were used. Approximately 25 mg of liposomal powder were reconstituted in 900 µL of D_2O and then added to an NMR tube as well as the capillary containing the external standard. The concentration of MDA7 was calculated based on the integration ratio of the drug signal to the MA signal (δ 6.26 ppm, 2H).

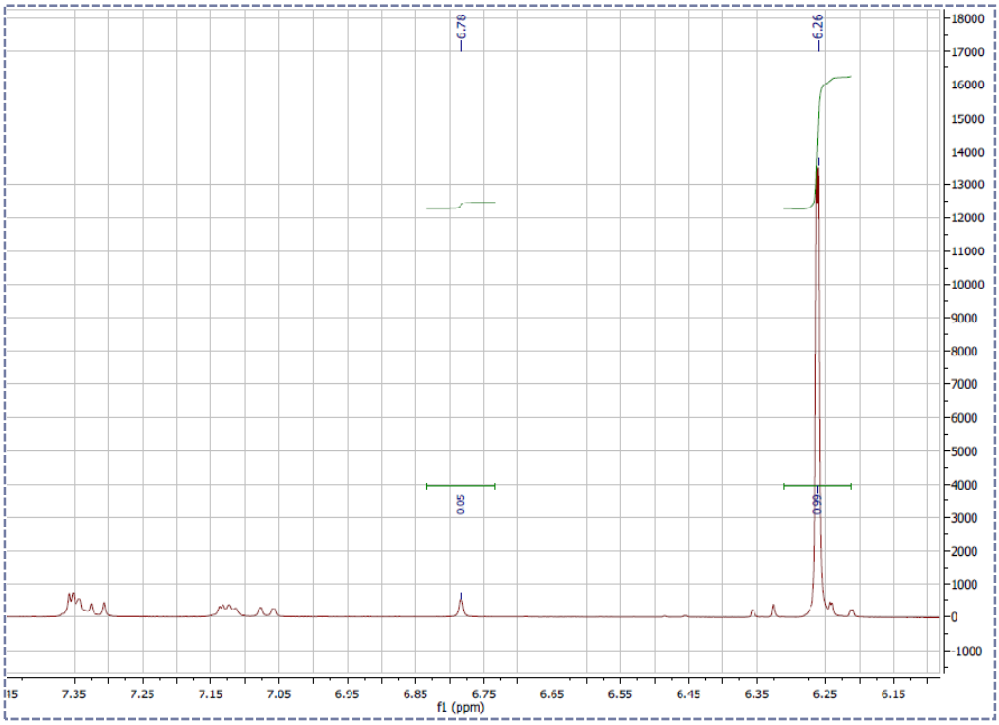

Figure 82: Liposomal dispersion at $t_{initial}$. Quantitation of MDA7 using the peaks ratio of MDA7 (6.78 ppm) and maleic acid (6.26 ppm).

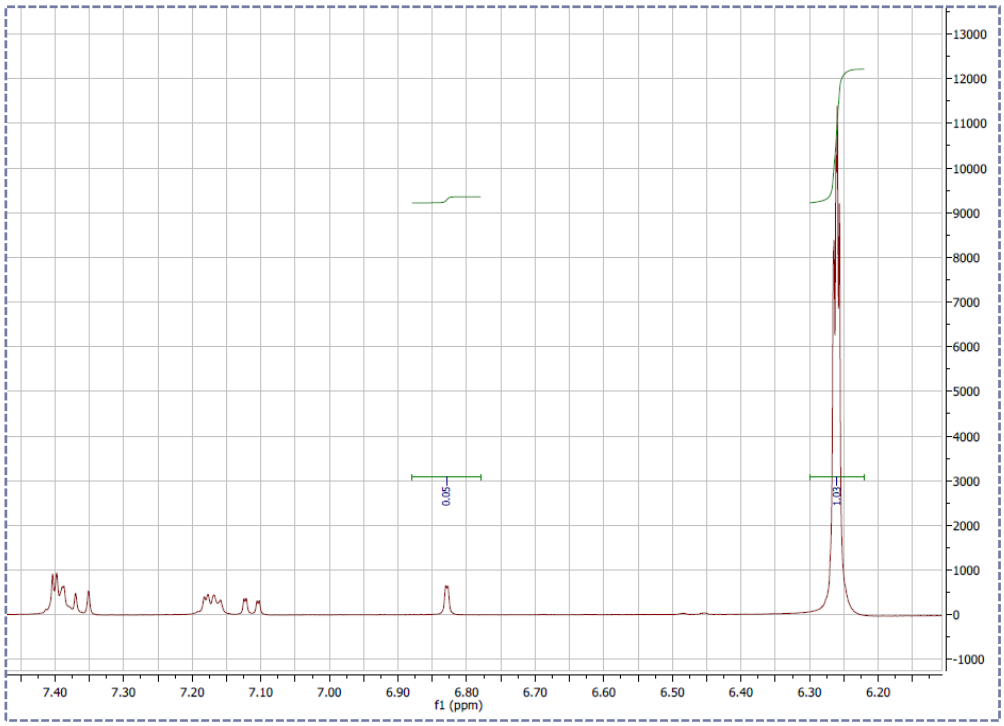

Figure 83: Liposomal solution at $t_{1\ month}$. Quantitation of MDA7 using the peaks ratio MDA7 (6.78 ppm) and maleic acid (6.26 ppm).

4.5.5 Particle size measurement.

The same protocol described in section 4.3.4 was used.

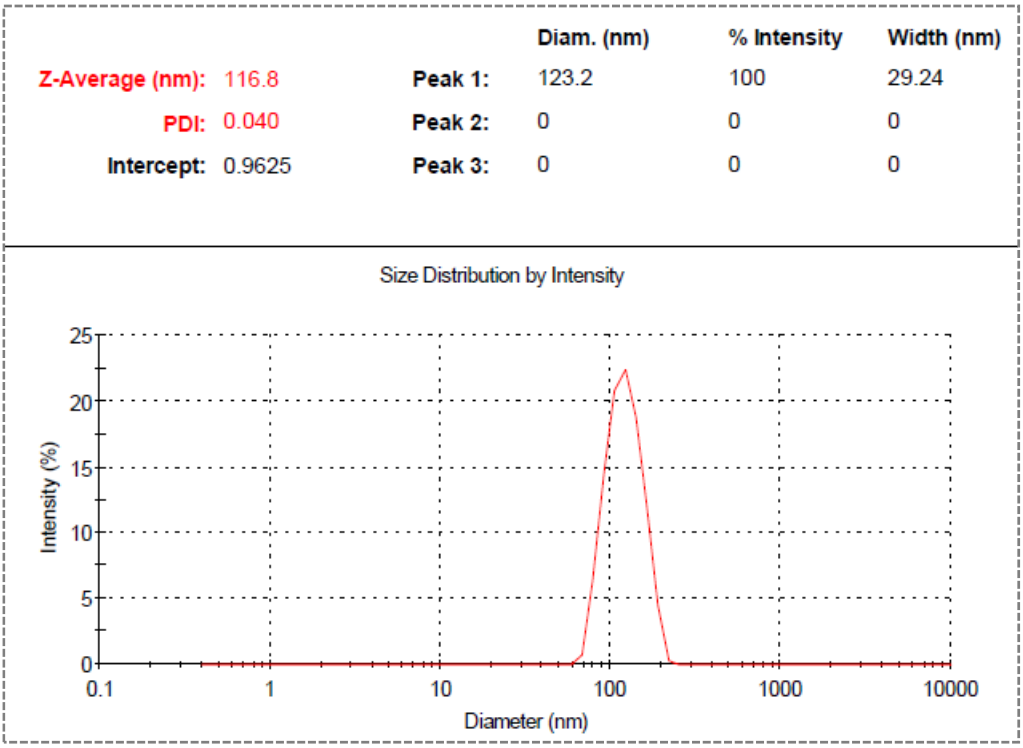

Figure 84: Particle size measurement for the liposomal dispersion entry P.

4.6 Cyclodextrins.

4.6.1 Preparation of complexes.

MDA7 and HPβCD were mixed in appropriate ratios and solvents for six days under constant magnetic agitation (200 rpm) at room temperature and protected from light.

4.6.2 NMR spectroscopy.

One-dimensional ^{1}H NMR spectra were recorded at room temperature on Bruker Avance III^{TM} spectrometer at 400 MHz using a 5 mm probe and a simple pulse-acquire sequence. Acquisition parameters consisted of spectral width 4000 Hz with an acquisition time 3.98 s, number of scans of 8, and relaxation delay of 1 s. Rotating-frame overhauser effect spectroscopy (ROESY) experiments were acquired in the phase sensitive mode with the same spectrometer and Bruker standard parameters (pulse program roesyphpr). For ROESY spectra, the time domain data was zero filled to 1024

points in F2 and 256 points in F1. The ROESY data was acquired with a spin-lock mixing time of 200 ms, and a relaxation delay of 2 s.

4.6.3 Phase solubility studies

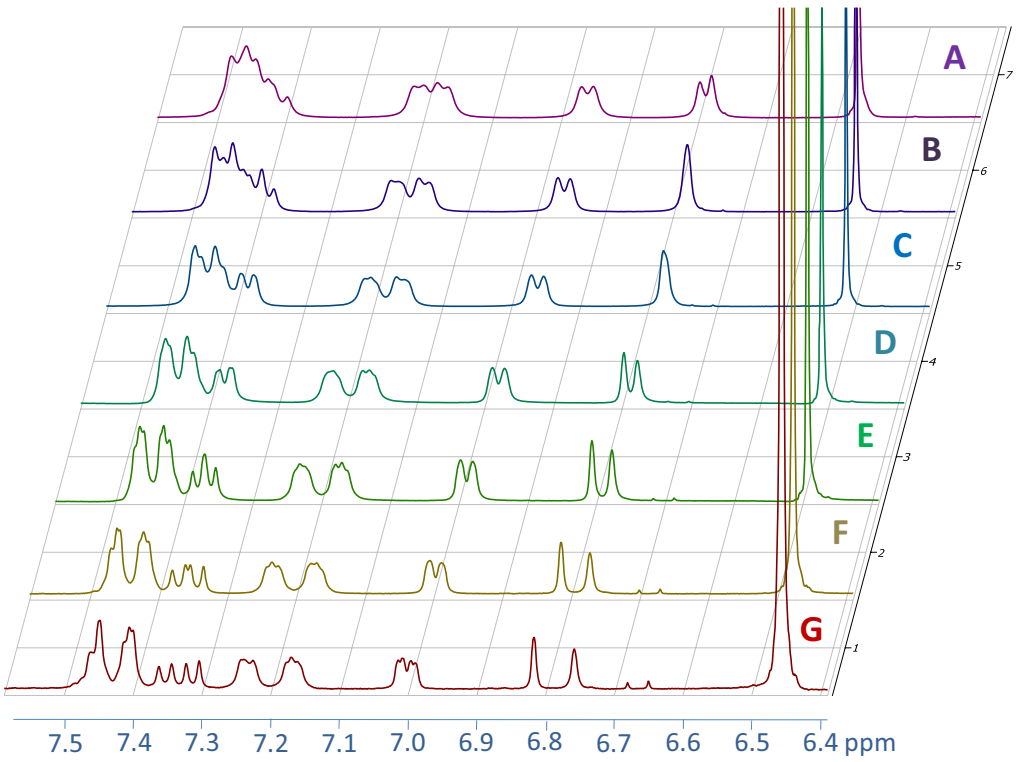

Figure 85: Aromatic proton region NMR spectra of MDA7 used for the phase solubility study upon complexation by HPβCD at in D_2O at 300 K. Molar ratio A) 1:6.7, B) 1:5, C) 1:4, D) 1:3, E) 1:2, F) 1:1 G) 1:0.5.

The phase solubility method was carried out according to Higuchi and Connors[7] method to study the effect of complexation on MDA7 solubility in water. Complexes were prepared as described above in pure water. Excess amount of MDA7 (10 mg, 29.8 µmol) were mixed with increasing concentrations of HPβCD (0.5, 1, 2, 3, 4 molar equivalent). After equilibration, undissolved MDA7 was removed from the suspension by filtration using 0.45 µm membrane filter (Acrodisc® Syringe Filters). Quantities of MDA7 dissolved were assessed using ^{1}H NMR quantification, with MA in D_2O as external standard (Fig. 85). Molar concentration of solubilized MDA7 ([MDA7]) were plotted versus molar concentration of HPβCD ([HPβCD]). From the slope of the linear fit, the apparent

association constant was determined for MDA7 and HPβCD at the linear increase of MDA7 solubility according to equation 1. Complex stoichiometry is assumed to be 1:1 for determining the apparent association constant $K_{1:1}$.

$$K_{1:1} = \frac{\text{Slope}}{[\text{MDA7}]_0(1-\text{Slope})}$$

The complexation efficiency (*CE*) was calculated as a product or the intrinsic solubility (S_0) and the association constant $K_{1:1}$.

4.6.4 Differential scanning calorimetry (DSC).

Complexes were prepared by dissolving MDA7 (15 mg, 44.7 µmol) and HPβCD as described above in 1.35 ml of pure water at 1:1, 1:4, 1:6.7 molar ratio. After equilibration undissolved MDA7 was removed from the suspension with one molar equivalent of HPβCD by filtration using 0.45 µm membrane filter (Acrodisc® Syringe Filter). MDA7 was soluble at MDA7:HPβCD molar ratio of 1:4 and 1:6.7. Solutions were freeze-dried (Labconco-freeze dry system/Freezone® 1) for 24 hours under vacuum. The resulting solid inclusion complexes were collected and analyzed. A physical mixture was prepared by thoroughly mixing MDA7 and HPβCD at 1:4 molar ratio. An excess of HPβCD was employed to reflect the molar ratio used for *in vivo* studies. The samples were placed in hermetically sealed aluminium pans and the experiments run in a calorimeter (Mettler Toledo DSC1 STARe system) at 10°C/min heating rate over 25-400°C. The instrument was calibrated with indium. Thermograms for inclusion complexes were compared to physical mixture.

4.6.5 ESI-MS analysis

Stoichiometry of the inclusion complex was confirmed by ESI-MS analysis using acetonitrile/water as mobile phase. ESI-MS experiments were performed on a Waters Micromass LCT PremierTM that utilizes a high-resolution time-of-flight (TOF) analyzer

equipped with a W-Optics and a regular and nanoelectrospray ionization sources. The sample solutions were directly infused into the ESI source with a flow rate of 0.4 mL.min^{-1}. Capillary voltage 2900 V, Sample cone voltage 95 V, Desolvation temperature 150°C, Source temperature 100°C in the negative ion mode.

4.6.6 Continuous variation method (Job's plots)

Stoichiometry of the inclusion complex was determined using a continuous variation method. The ^{1}H NMR spectrum of MDA7 in D_2O could not be determined due to its very low aqueous solubility. Therefore, a plot was created from NMR chemical shift measurements in D_2O/methanol-d_4 (1:1, v/v). The chemical shifts were referenced relative to the residual peak of MeOH-d_4 at 3.310 ppm (Fig 86). The total molar concentration of MDA7 and HPβCD were kept constant (6 mM) and their mole fraction (R) varied from 0.1 to 0.9. In order to calculate the stoichiometry, the product of molar ratio (R) by chemical shift variations ($\Delta\delta$) of the H1, H5 and $CH_{3\ HP\beta CD}$ protons of HPβCD and Ha, Hb and Hc and CH_3 protons of MDA7 were plotted versus R.

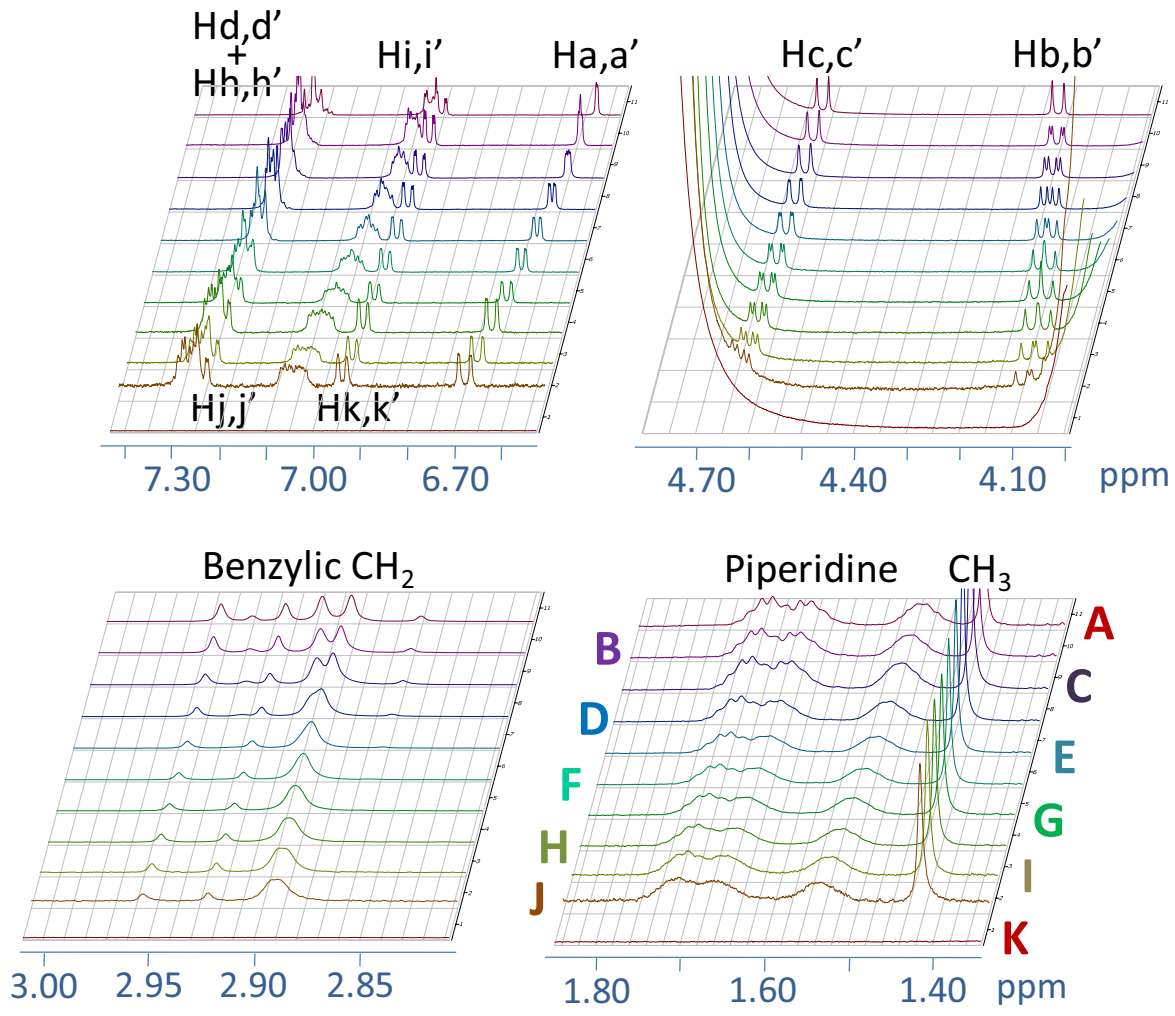

Figure 86: NMR spectra of MDA7 used for continuous variation plot study upon complexation by HP-β-CD in an equimolar solution of D_2O and methanol-d_4 at 300 K at different molar ratio MDA7:HPβCD A) 1:0, B) 0.9:0.1, C) 0.8:0.2, D) 0.7:0.3, E) 0.6:0.4, F) 0.5:0.5, G) 0.4:0.6, H) 0.3:0.7 I) 0.2:0.8, J) 0.1:0.9, K) 0:1 at 300 K.

4.6.7 Enantiomeric recognition.

Enantiomeric recognition was observed in equimolar mixture of (A) (R)-MDA7, of (B) (R,S)-MDA7 and of (C) (S)-MDA7 upon complexation by HPβCD at a concentration of 33 mM in D_2O at 300 K (see full spectra Fig. 87). The samples were prepared as in section 4.6.3. Fig. 87 shows the different external standard used, maleic acid (6.26 ppm) and sodium trimethylsilyl propionate (2.24 ppm). Maleic acid was selected according to his proximity to MDA7 aromatic signals.

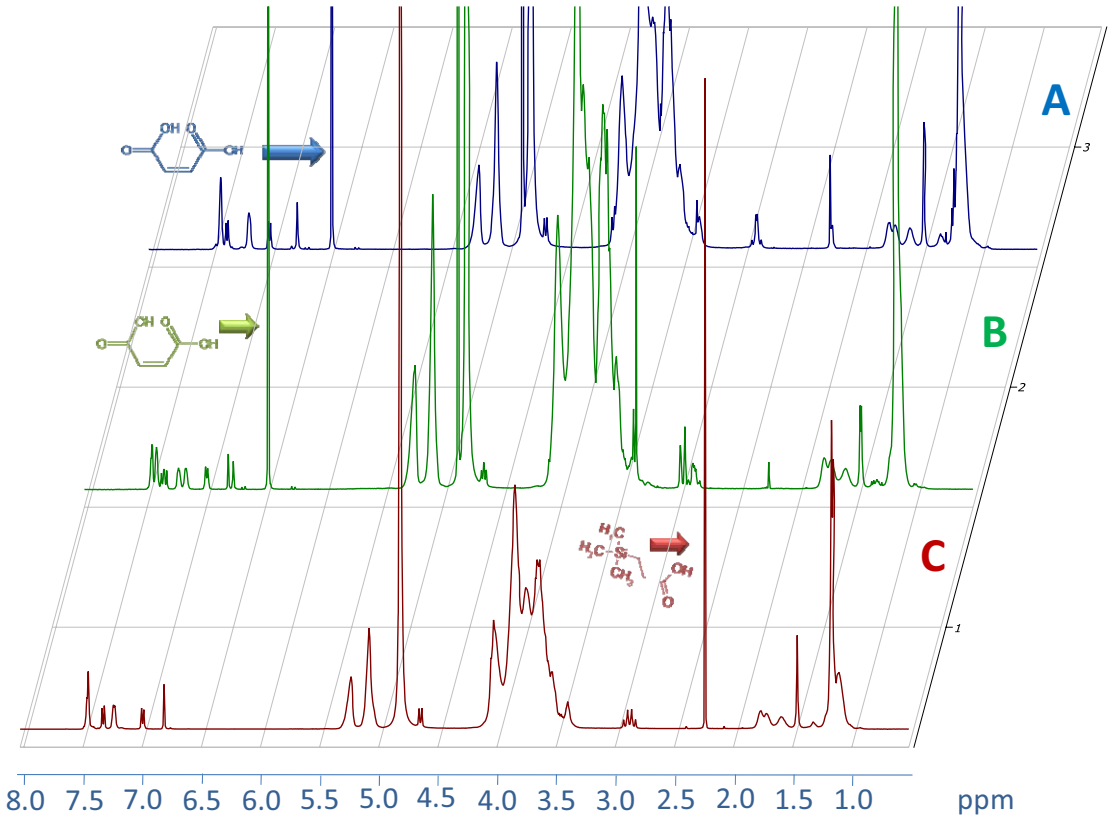

Figure 87: NMR spectra of an equimolar mixture of A) (R)-MDA7, of (B) (R,S)-MDA7 and of C) (S)-MDA7 upon complexation by HPβCD at a concentration of 33 mM in D_2O at 300 K. Two different external standards were compared, maleic acid (A and B) and sodium trimethylsilyl propionate (C).

4.6.8 Molecular modeling.

The 2-hydroxypropyl cyclodextrin structure was based on the cyclodextrin crystal structure provided by the Structural Data Base System of the Cambridge crystallographic Data Center[8]. Two 2-hydroxypropyl groups were randomly added at O-6 positions and two at O-2, O-3 positions to the crystal structure of cyclodextrin based on the expected 4 degree of substitution of HPβCD. The 2-hydroxypropyl groups were added and MDA7 was built using ChemDraw 3D. The HPβCD and MDA7 structures were individually optimized by energy minimization using a MM2 force field with a convergence criterion of 0.05 kcal/mol. The AutoDock 4.0 software was used to obtain a MDA7/HPβCD complex. A Lamarckian genetic algorithm was employed to generate a total population of 100 complexes. An initial population of 100 individuals with a maximal number of energy

evaluations of 25,000,000 and a maximal number of generations of 50,000 were the parameters used for the global search. A grid box of 70 x 70 x 70 points was used to calculate the energy maps. The points were separated from each other by 0.375 Å.

4.6.9 Transmission electron microscopy (TEM).

MDA7, HPβCD physical mixture and MDA7:HPβCD solid complexes were prepared as described above. The sample as 1 µl aliquot was placed in 4 µl of demineralized water on a formvar-coated 400 mesh copper grid. The sample was kept on the grid for 5 minutes, the liquid was wicked off with filter paper and the grid was air dried. The grid was stained by placing it on a drop of 2% Uranyl acetate for 1 minute. The stain was rinsed off by dipping the grid in demineralized water, the water removed by wicking, and the grid air dried. The grid was imaged in a Hitachi H-7100 TEM at 75kV.

4.6.10 Particle size measurement

Particle sizes were determined using DLS measurements. The DLS experiments were performed on 132 mM of pure HPβCD solution, MDA7-HPβCD solutions with concentration of 33 mM MDA7 and 33 mM of HPβCD, 33 mM MDA7 and 132 mM of HPβCD, 33 mM MDA7 and 221 mM of HPβCD (1:1, 1:4, 1:6.7 molar ratio respectively). The samples were run at 25°C using a Zetasizer nano ZS (Malvern Instruments Ltd., Malvern, UK) DLS instrument. Before each DLS scan, the samples were stabilized for 10 min.

		Size (d.n...	% Intensity	Width (d.n...
Z-Average (d.nm): 338,7	Peak 1:	299,8	71,3	77,66
PdI: 0,506	Peak 2:	76,12	15,9	14,72
Intercept: 1,00	Peak 3:	2,108	12,8	0,3533
Result quality Refer to quality report				

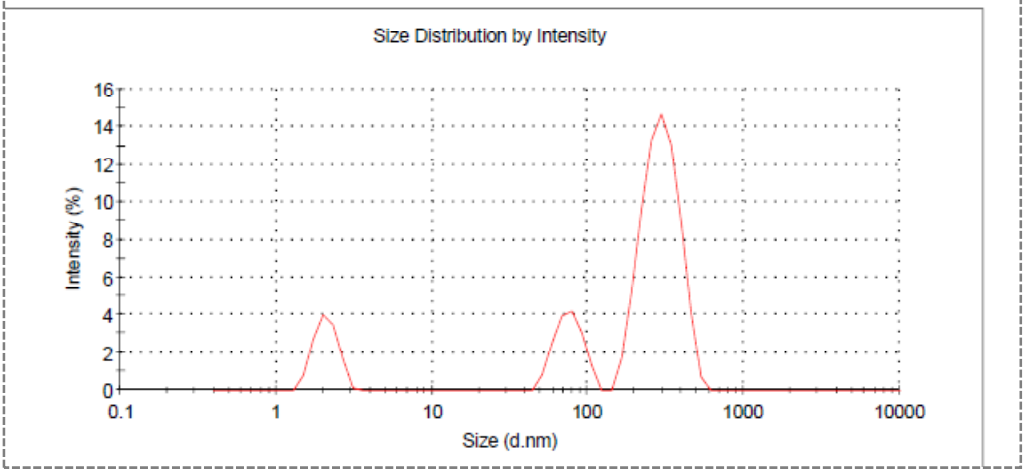

Figure 88: Particle size measurement MDA7: HPβCD (1:1) solution.

		Size (d.n...	% Intensity	Width (d.n...
Z-Average (d.nm): 919,8	Peak 1:	569,8	76,3	84,56
PdI: 0,747	Peak 2:	2,772	23,7	0,4608
Intercept: 1,04	Peak 3:	0,000	0,0	0,000
Result quality Refer to quality report				

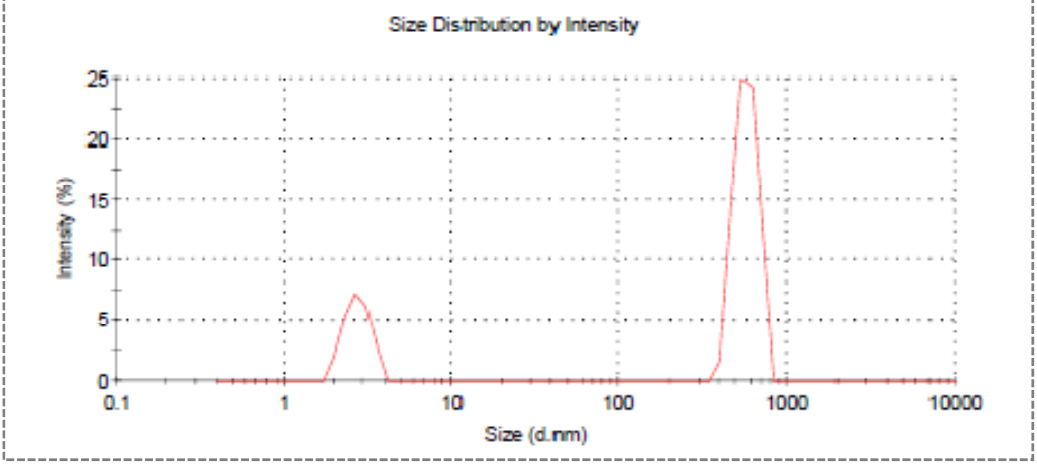

Figure 89: Particle size measurement MDA7: HPβCD (1:1) solution.

		Size (d.n...	% Intensity	Width (d.n...
Z-Average (d.nm): 1068	Peak 1:	509,7	63,3	68,78
PdI: 0,918	Peak 2:	3,441	36,7	0,6780
Intercept: 1,01	Peak 3:	0,000	0,0	0,000
Result quality Refer to quality report				

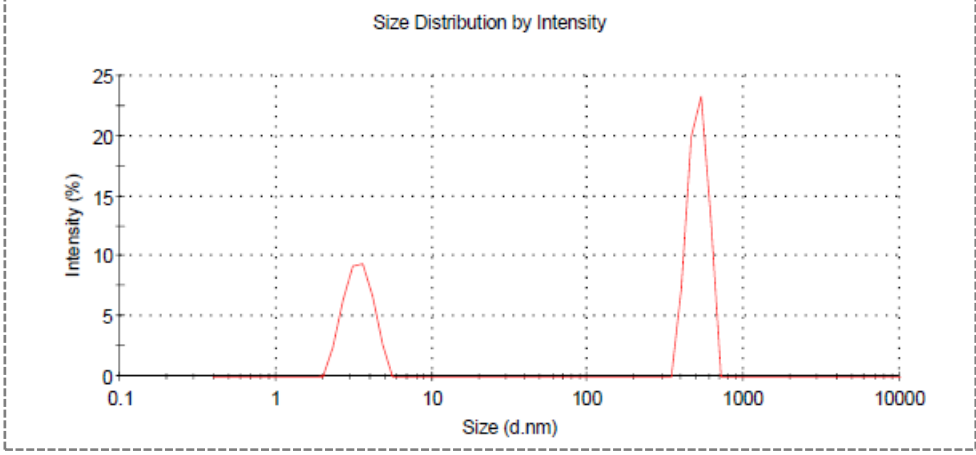

Figure 90: Particle size measurement MDA7: HPβCD (1:6.7) solution.

4.6.11 MDA7 chemical stability assessment by UPLC-MS.

The same protocol described in section 4.3.6 was used.

4.6.12 MDA7 chemical stability assessment by ^{1}H NMR.

The same protocol described in section 4.3.5 was used.

Approximately 10 mg (29.8 µmol) of MDA7 were mixed with HPβCD (6.7 molar equivalent) in D_2O. After equilibration for 6 days, the solution was added to an NMR tube as well as the capillary containing the external standard. The concentration of MDA7 was calculated based on the integration ratio of the drug signal to the MA signal (δ 6.26 ppm, 2H). The NMR tube was stored at room temperature for 1 month and MDA7 quantitation performed again.

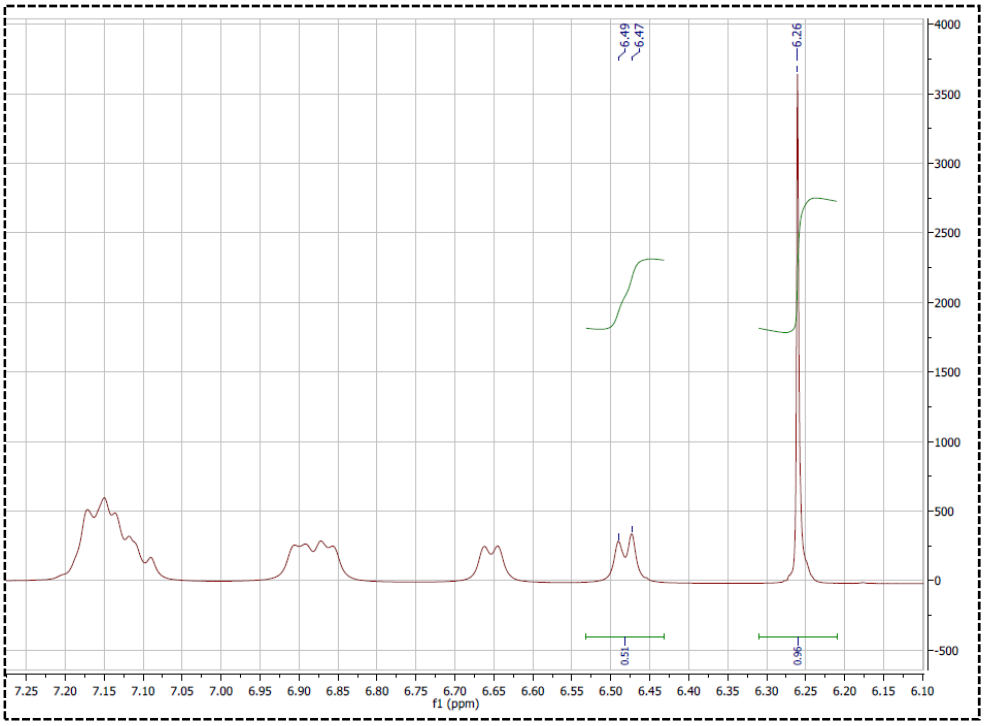

Figure 91: MDA7: HPβCD (1:6.7) solution at $t_{initial}$. Quantitation of MDA7 using the peaks ratio of MDA7 (6.48 ppm) and maleic acid (6.26 ppm).

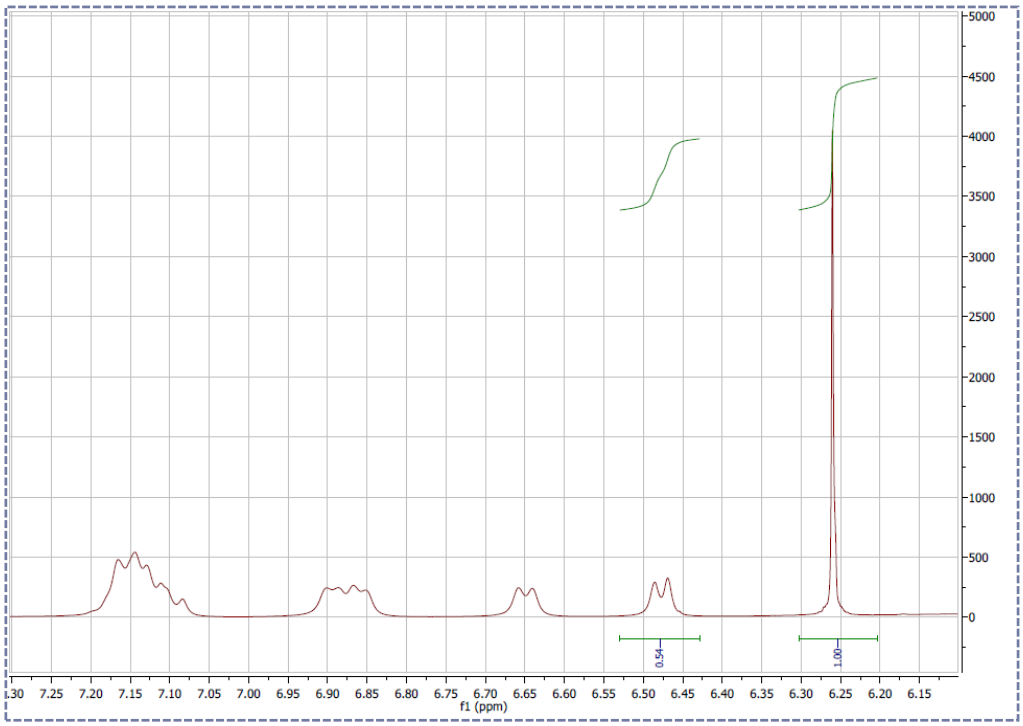

Figure 92: MDA7: HPβCD (1:6.7) solution at $t_{1\ month}$. Quantitation of MDA7 using the peaks ratio of (6.48 ppm) and maleic acid (6.26 ppm).

5 *In vivo* characterization of MDA7.

5.1 Pharmacokinetic study.

A pilot pharmacokinetic study of MDA7 in rats was conducted by the Pharmaceutical Development Center in the Department of Veterinary Medicine and Surgery (DVMS) facilities, U.T.M.D. Anderson Cancer Center, (Houston, TX). Female Sprague Dawley rats supplied by Charles River Laboratories were used in this study. Female rats (48) were assigned to an intravenous administration arm (16 sampling timepoints, 3 animals/timepoint) and 39 rats to an oral administration arm (13 timepoints, 3 animals/timepoint). Each rat received a single 15 mg/kg dose of MDA7 either intravenously via the tail vein or orally via gavage on Study Day 0. Blood samples were collected by cardiac puncture under isoflurane anesthesia at the following timepoints after intravenous dosing: 0 (pre-dose), 5, 10, 15, 30, and 45 minutes, and 1, 2, 3, 4, 6, 8, 16, 24, 48, and 72 hours. Blood samples were collected by cardiac puncture under isoflurane anesthesia at the following timepoints after oral dosing: 0 (pre-dose), 30, 45 minutes, 1, 2, 3, 4, 6, 8, 16, 24, 48, and 72 hours. Brain tissue (whole brain) was collected from all animals and rinsed, blotted, and weighed. All samples were frozen at –80°C until analyzed. Plasma and tissues were extracted using liquid-liquid extraction techniques and analyzed for MDA7 content by LC/MS/MS.

Concentration values for all collected sample timepoints above the lower limit of quantification for the LC/MS/MS method were used for the determination of pharmacokinetic parameters. These parameters were obtained by fitting a non-compartmental model (WinNonlin Version 5.2) to the mean measured plasma concentration data for each sampled timepoint in the orally dosed group. In the intravenously dosed group these data were analyzed using ADAPT II Pharmacokinetic Modeling Software (USC, Biomedical Simulations Resource) using a 2 compartment model. In all groups the mean measured concentration value for each timepoint was derived from each of 3 animals analyzed per sampling interval. All parameters were derived from the AUC (area under the concentration vs. time curve) which was calculated using a linear trapezoidal method with linear interpolation. All data were weighted as 1/y.

For the analysis of MDA7 in rat plasma and brain tissue, a Waters Acquity UPLC system coupled with a Waters Quattro Premier mass spectrometer was used. Chromatographic

separation was achieved using a Waters Symmetry 300 C4 column (50 x 2.1 mm, 3.5 µm particle size) protected by a 0.5 µm stainless stell frit (Upchuch Scientific). The column temperature was maintained at 60°C. Solvent A was 0.2% formic acid in water (pH 3.0) and solvent B a mixture of acetonitrile and methanol (80/20, vol/vol). The mobile phase was delivered in a gradient mode at 0.350 mL/min at 75%A from 0 to 1 minute, decreased from 75% to 5% A from 1 to 3 minutes, kept at 5%A from 3 to 4 minutes, returned from 5% to 75%A from 4 to 5 minutes, and equilibrated at 75% A from 5 to 6 minutes.

The Waters Quattro Premier mass spectrometer was operated in an electrospray positive mode. Major parameters were set as follows: capillary energy 3.50 kV, cone energy 25.0 V, collision cell 25, source temperature 125 ºC, desolvation temperature 350 °C, cone gas (nitrogen) 70 L/hr, desolvation gas (nitrogen) 700 L/hr, and collision gas (argon) 0.25 mL/min. MDA7 was monitored in a Multiple Reaction Mode (MRM) at m/z: 335.85 → 244.70. An instrument calibration curve was constructed over a dynamic range of 1 to 100 ng/ml for plasma and brain matrices, and used for quantitation. A 20 µl injection volume was used, and MDA7 eluted at 2.77±.05 minutes.

5.2 Influence of the DDS selected on MDA7 *in vivo* efficacy.

5.2.1 Drug administration.

All dosing solutions/dispersions were prepared within 1 h prior to injection and stored at room temperature until use. MDA7 dosing solution (250 µL) was administered at a dose of 10 mg/kg by a single bolus injection into the tail vein of the animal.

5.2.2 Assessment of mechanical withdrawal thresholds.

As described in our previous study[9], adult male Sprague-Dawley rats (Harlan Sprague Dawley, Indianapolis, IN, USA) weighing 120-150 g and were used in experimental procedures approved by the Animal Care and Use Committee of The University of Texas MD Anderson Cancer Center. Animals were housed 3 per cage on a 12/12-h light/dark cycle with water and food pellets available *ad libitum*. Rats were placed in a compartment with a wire mesh bottom and allowed to acclimate for a minimum of 30 min before

testing. Sensory thresholds for the development of allodynia to mechanical stimuli were assessed. Mechanical sensitivity was assessed by using a series of Von Frey filaments with logarithmic incremental stiffness (Stoelting Co., Wood Dale, IL, USA), as previously described[10], and 50% probability paw withdrawal thresholds were calculated with the up-down method[11]. In brief, filaments were applied to the plantar surface of a hind paw for about 6 s in an ascending or descending order after a negative or positive withdrawal response, respectively. Six consecutive responses after the first change in response were used to calculate the paw withdrawal threshold (in grams). In rats, when response thresholds occurred outside the range of detection, the paw withdrawal threshold was assigned at 15.00 g for continuous negative responses and at 0.25 g for continuous positive responses[12]. Behavioral assessment was performed by one investigator who was blinded to group allocation or the formulation used.

5.3 *In vivo* MDA7 effect administered i.p. in different models of nociception in rats.

5.3.1 Compounds and dosing solutions.

AM630 (6-iodo-2-methyl-1-[2-(4-morpholinyl)ethyl]-1H-indol-3-yl](4-methoxyphenyl)methanone) and AM251 were purchased from Tocris Bioscience. WIN 55,212-2, AM1241, naloxone, paclitaxel and all chemicals used for the synthesis of MDA7 were purchased from Sigma-Aldrich Inc. (St Louis, MO, USA). WIN 55,212-2, AM1241, AM630, AM251 and haloperidol were administered *in vivo* in 0.25 mL of 100% DMSO.

5.3.2 Animals.

All animal procedures were approved by the Animal Care and Use Committee of The University of Texas MD Anderson Cancer Center. Animals were housed three per cage on a 12/12 h light/dark cycle with water and food pellets available ad libitum. Adult male Sprague–Dawley (Harlan Sprague Dawley, Indianapolis, IN, USA) rats weighing 120–150 g were used and all experiments were performed during the light cycle.

5.3.3 Assessment of mechanical withdrawal thresholds

As described in our previous study[9], adult male Sprague-Dawley rats (Harlan Sprague Dawley, Indianapolis, IN, USA) weighing 120-150 g and were used in experimental procedures approved by the Animal Care and Use Committee of The University of Texas MD Anderson Cancer Center. Animals were housed 3 per cage on a 12/12-h light/dark cycle with water and food pellets available ad libitum. Rats were placed in a compartment with a wire mesh bottom and allowed to acclimate for a minimum of 30 min before testing. Sensory thresholds for the development of allodynia to mechanical stimuli were assessed. Mechanical sensitivity was assessed by using a series of Von Frey filaments with logarithmic incremental stiffness (Stoelting Co., Wood Dale, IL, USA), as previously described[10], and 50% probability paw withdrawal thresholds were calculated with the up-down method[11]. In brief, filaments were applied to the plantar surface of a hind paw for about 6 s in an ascending or descending order after a negative or positive withdrawal response, respectively. Six consecutive responses after the first change in response were used to calculate the paw withdrawal threshold (in grams). In rats, when response thresholds occurred outside the range of detection, the paw withdrawal threshold was assigned at 15.00 g for continuous negative responses and at 0.25 g for continuous positive responses[12].

5.3.4 Spinal nerve (L5/6) ligation model of neuropathic pain.

All surgical procedures were performed under deep isoflurane anaesthesia in 100% O_2. The spinal nerve ligation was performed as described previously[13]. Briefly, a midline incision was made above the lumbar spine to expose the left L6 transverse process. The process was then removed, the left L5 and L6 spinal nerves were isolated and both nerves were tightly ligated with 6-0 silk thread. The development of neuropathy was confirmed by daily measurement of the paw withdrawal threshold by using Von Frey filaments (see below). Behavioural experiments were conducted after neuropathy was established.

5.3.5 Paclitaxel-induced neuropathy model.

Groups of rats received either vehicle (10% Cremophor EL in saline) or 1.0 mg kg^{-1} of

paclitaxel daily i.p. for four consecutive days for a final cumulative dose of 4 mg kg^{-1} [14]; the injection volume was 1 mL kg^{-1}. Baseline responses to mechanical stimulation of the hind paw (see below) were established on day 0 and continued daily until the development of neuropathy was confirmed.

5.3.6 Assessment of mechanical withdrawal thresholds.

Rats were placed in a compartment with a wire mesh bottom, and allowed to acclimatize for a minimum of 30 min before testing. Mechanical sensitivity was assessed by using a series of Von Frey filaments with logarithmic incremental stiffness (0.41, 0.70, 1.20, 2.00, 3.63, 5.50, 8.50 and 15.1 g) (Stoelting Co., Wood Dale, IL, USA), as previously described[10] and 50% probability withdrawal thresholds were calculated with the up–down method[15]. In brief, beginning with the 2.0-g probe, filaments were applied to the plantar surface of a hind paw for 6–8 s, in an ascending or descending order after a negative or positive withdrawal response, respectively. Six consecutive responses after the first change in response were used to calculate the withdrawal threshold (in grams). When response thresholds fell outside the range of detection, the withdrawal threshold was assigned as 15 g for continuous negative responses and 0.25 g for continuous positive responses. The percentage maximal possible effect (%MPE) was calculated as ((postdrug threshold-baseline threshold)/(cutoff threshold (15 g)-baseline threshold)) x 100. The baseline threshold was determined once. Different groups were tested in the same hour on consecutive days. The only exception is the 'vehicle + vehicle' group experiment, which was performed on a different day, separate from other groups. The drug groups were not randomized. Only one experimenter performed all behavioural tests and he, therefore, was not unaware of the different treatment groups.

5.3.7 Assessment of paw withdrawal latencies in response to noxious heat.

To determine sensitivity to noxious heat, rats were placed in plexiglass enclosures on a transparent glass surface maintained at 30 °C, and allowed to acclimatize for 30 min. A thermal testing apparatus, consisting of a heat-emitting projector lamp and an electronic timer, was used. The device was activated after the lamp was placed directly beneath the plantar surface of the hind paw. The paw withdrawal latency in response to the radiant

heat (50 W) was recorded using a digital timer. A cutoff of 30 s was used to prevent tissue damage. After the baseline paw withdrawal response to noxious heat was measured, three groups of naive rats (n=10 per group) received 1, 3 or 10 mg kg^{-1} of MDA7 i.p. Response latencies were determined for each rat before i.p. drug injection and at 5, 10, 15, 30, 45, 60, 90 and 120 min after i.p. drug injection. Each paw was only stimulated once per time point.

5.3.8 Open-field chamber testing.

An automated open-field chamber (ENV-515 Test Environment, Med Associates, St Albans, VT, USA), 43.2 x 43.2 x 30.5 cm (*L* x *W* x *H*), equipped with three pairs of 16 infrared arrays that continually monitored each animal's movement, was used to determine potential CNS effects of MDA7, WIN 55,212-2 ((R)-(þ)-[2,3-dihydro-5-methyl-3-(4-morpholinylmethyl)pyrrolo[1,2,3-de)-1,4-benzoxazin-6-yl]-1-napthalenylmethanone), and haloperidol in naive rats. Rats were individually tested 15 min after i.p. drug administration. The infrared beams were set 2.5 cm apart horizontally and at a height of 3 cm above the floor, with the rearing array set at 12 cm from the floor. The area in the box was divided into four equal quadrants (zones), with data collected within each quadrant and across quadrants (zone entries). An ambulatory movement was defined as a motion of at least 5 cm and was coded by quadrant. Vertical movements were counted when the rat moves vertically at least 12 cm from the floor. Zone entries were defined as an entry into a zone from another zone. Entry into a zone was counted when the rat was far enough into the new zone to break two sets of new zone photoelectric beams during an ambulatory movement.

5.3.9 Data analysis.

Statistical analyses were carried out by using BMDP 2007 (Statistical Solutions, Saugus, MA, USA) and Graph Pad Prism (version 4.03; Graph Pad Software Inc., San Diego, CA, USA). Data were analyzed by using one-way ANOVA. If findings on ANOVA were significant, Tukey–Kramer *post hoc* analysis was used for multiple group comparison. Area under the curve (AUC) was calculated using the trapezoidal rule. The results were presented as mean±s.e.mean and were considered significant at $P<0.05$. Analyses of the dose–response curves and statistics were obtained by using the pharmacological

software programs of Tallarida and Murray (1987), and included calculation of the ED_{50} values and their 95% confidence intervals (CIs).

6 Nanocapsules

6.1 Materials

Beta-caryophyllene (#W225207) was purchased from Sigma-Aldrich. Sulfobutyl ether with an average degree of molar substitution of 6.5 was purchased from CTD Inc. Cucurbit[7]uril was purchased from Strem Chemicals Inc. Ethyl Alcohol, 190 Proof, 95%, ACS/USP was purchased from PHARMCO AAPER. Alpha-pinene (98%) was purchased from Fischer scientific. Trehalose, sucrose, glycerol, tetrahydrofuran (Omnisolv) and acetone (ACS grade) were purchased from VWR. PBS was purchased from VWR. Acrodisc® Syringe Filters with Nylon Membrane were purchased from PALL Corporation. Other reagents and chemicals were obtained as gift samples, Eudragit® RS100 and RL100 from Evonik, poloxamer 188 (Lutrol® F 68) from BASF. All chemicals were used as received. All experiments were carried out using ultrapure water.

6.2 (E)-BCP Purification.

(E)-BCP was purified with a Biotage® Isolera one flash purification system using the following parameters: collected fraction: 16mL/fraction; flow rate: 40mL/min; 3 Column Volumes of equilibration; 1.8 g of (E)-BCP injected; cartridge: Biotage® SNAP KP-Sil 100g cartridge; medium slope; 500mAU; 7 Column Volumes (1-5-1).
TLC Rf value in heptane: 0.75

6.3 (E)-BCP entrapment efficiency, drug loading and stability in nanoacapsules.

6.3.1 Equipment and instrumentation.

(E)-BCP nanocapsules analysis was performed using an Agilent 6890N Gas Chromatograph with an Agilent 5973 Mass Spectrometer. An HP-5MS column ((5%-Phenyl)-methylpolysiloxane) was used (0.25 mm ID x 30 m length x 0.25 µm film thickness). 2 µL of sample was injected for each analysis into a Split/Splitless FocusLinerTM for HP, single taper p/w quartz wool liner. Split injection was used with a split ratio of 50:1. The inlet temperature and the auxiliary transfer line temperature were set to respectively 250°C and 280°C. The temperature program started at 40°C for 1.5 minutes, ramped at 30°C/min to 190°C, 20°C/min to 210°C, and then 50°C/min to a final temperature of 300°C, which was held for 1.5 minutes. The mass spectrometer was operated with a solvent delay of 4 minutes and the mass range from 40-450 was scanned.

6.3.2 Standards preparation.

A stock solution of (E)-BCP at a stock concentration of 10mg/mL was prepared in THF and then diluted with THF to create calibration standards of the following range: 10, 25, 50 and 100 ppm.
A stock solution of α-pinene at a stock concentration of 10mg/mL was prepared in THF and added to standard solutions and unknown samples for comparative quantitation to afford a final concentration of 100 ppm.

6.3.3 Samples preparation

(E)-BCP was extracted from nanocapsules using THF. 30 mg of freeze-dried nanocapsule were placed in a vial and 1 mL of THF was added. This mixture was stirred with a magnetic stirring bar at 300 rpm for one hour. Finally, 15 µL of this solution were added to 100 µL of α-pinene and diluted with THF to obtain 1 mL of final solution which was analyzed using GC-MS.

The EBCP concentration in the sample was determined using a fresh standard curve made on each day of analysis. The entrapment efficiency and drug loading were determined using the following formulae:

Drug Entrapment efficiency (%) = (Mass of drug recovered in NC / Mass of drug incorporated in NS) X100

Drug loading (%) = (Mass of drug recovered in NC / Mass of NC recovered) X100

Examples of spectra obtained for entrapment efficiency, drug loading and stability determination are given in Chapter III section 12.2 (GC-MS method development for the determination of (E)-BCP entrapment efficiency and stability in drug-loaded nanocapsules).

6.4 Preparations of EBCP nanoparticles.

(E)-BCP nanocapsules were prepared using the nanoprecipitation method. (E)-BCP (45 mg) and Eudragit RS100/RL100 (600 mg) ratio 1:1 were dissolved in 6 mL of acetone. The internal organic phase solution was slowly injected (flow rate 1.4 ml.min.) using a syringe pump (model KDS200, KD Scientific, USA) into 50 mL of the external aqueous solution (0.02% Poloxamer 188 in purified water). The resulting mixture was then stirred using an IKA® RW 20 Digital (IKA, Germany) at 700 rpm for 10 min (solvent phase dropping time). Acetone was completely removed by rotary vacuum evaporation (Buchi R215, USA) in a water bath at 20°C for 30 min at a vacuum of 70 mb and then 10 mb for 10 min to evaporate water from the nanosuspension. Aliquots of the nanosuspensions obtained were analyzed (e.g. DLS, TEM). The remaining nanosuspension was frozen at -80°C for 8 hours, lyophilized for 72H (Labconco Freezone® 1) and analyzed by GC-MS for drug content. Blank nanocapsules were prepared following the above method without (E)-BCP.

6.5 Particle size measurement.

The same protocol described in section 4.3.4 was used.

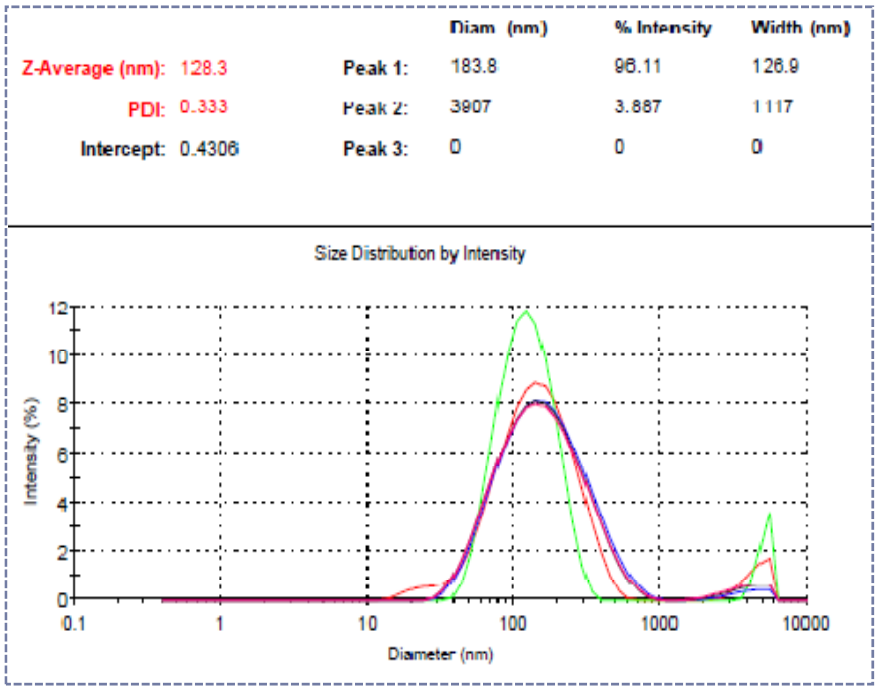

Figure 93: Particle Size distribution of entry 1 Table 29.

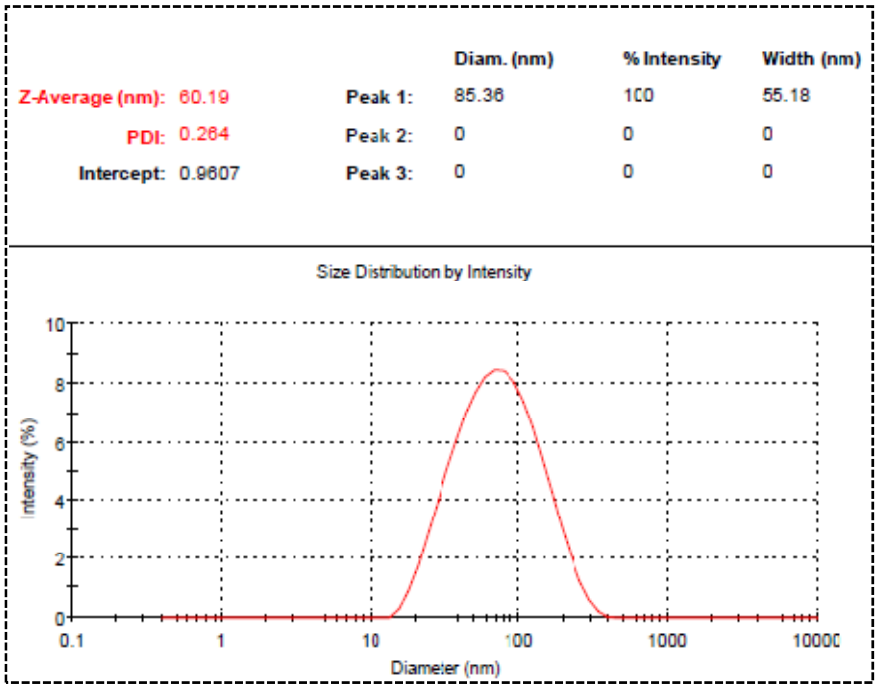

Figure 94: Particle Size distribution of entry 2 Table 29.

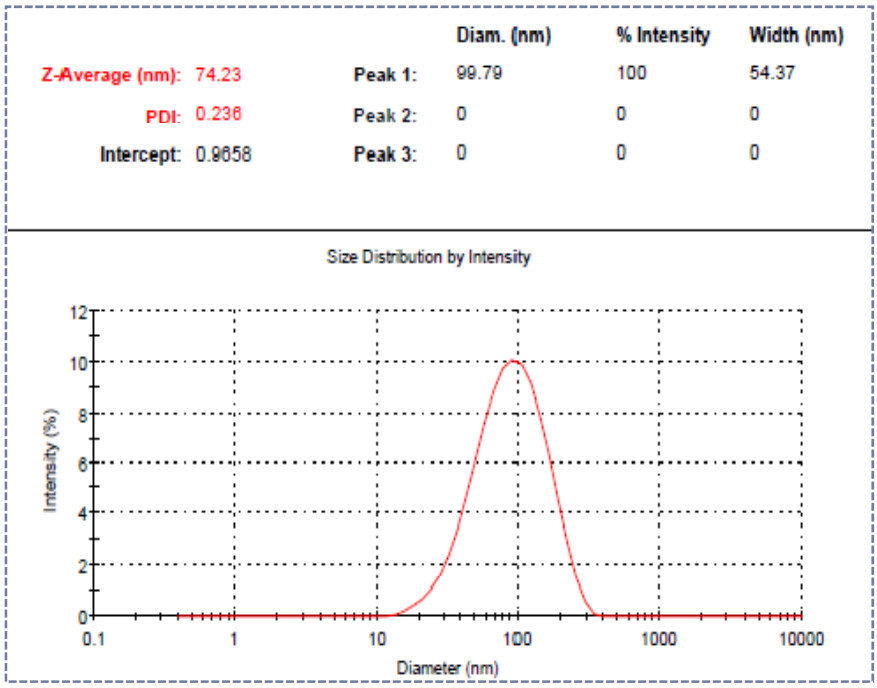

Figure 95: Particle Size distribution of entry 3 Table 29.

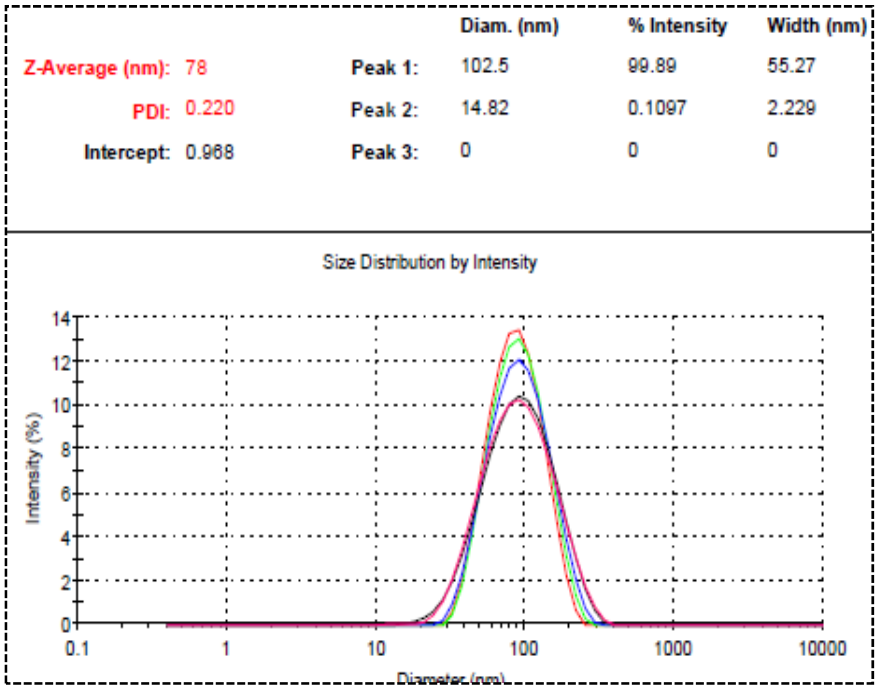

Figure 96: Particle Size distribution of entry 4 Table 29.

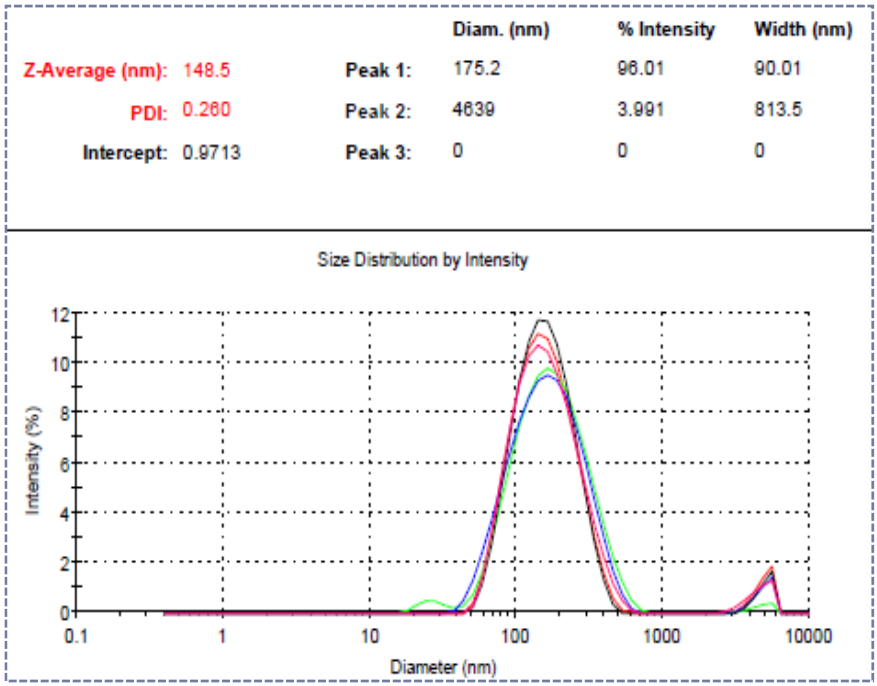

Figure 97: Particle Size distribution of entry 5 Table 29.

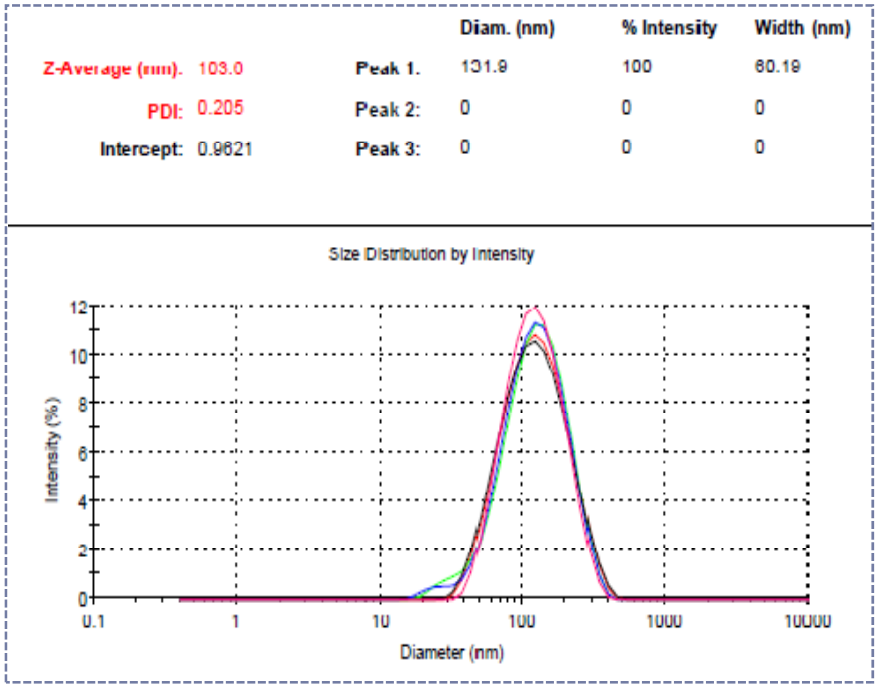

Figure 98: Particle Size distribution of entry 9 Table 31.

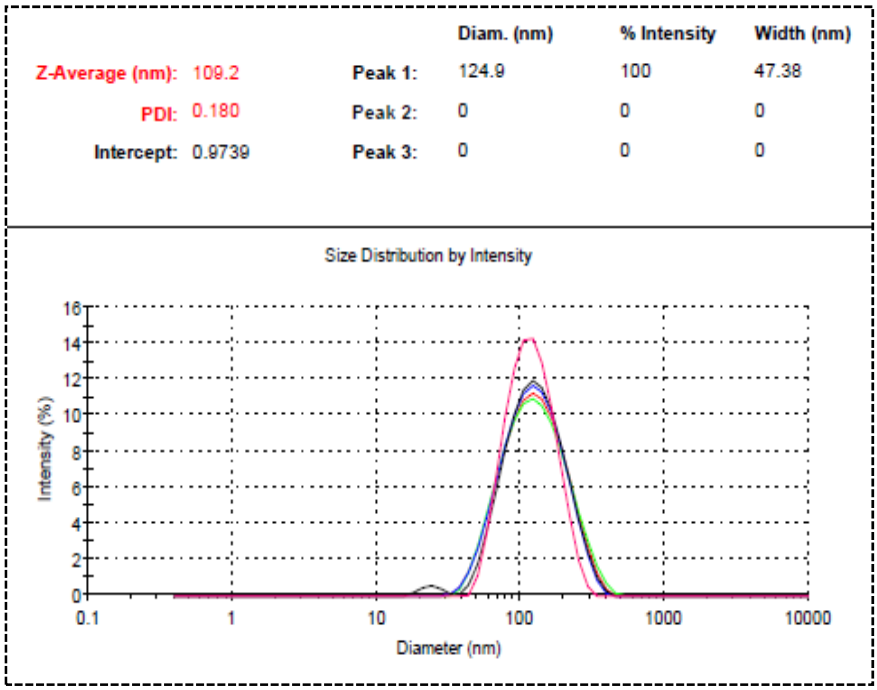

Figure 99: Particle Size distribution before rotary evaporation of entry 10 Table 31.

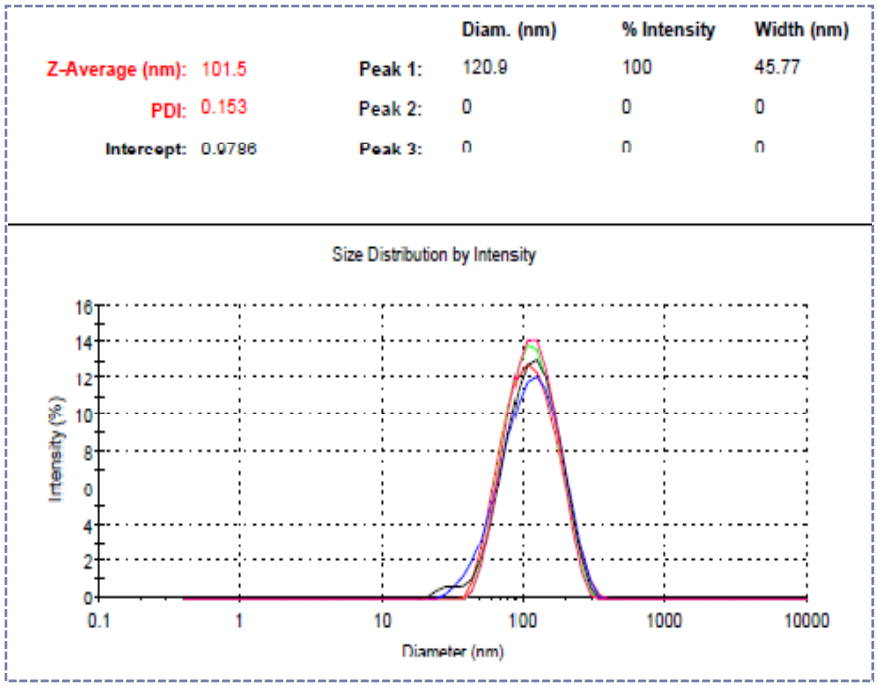

Figure 100: Particle Size distribution of entry 10 Table 31.

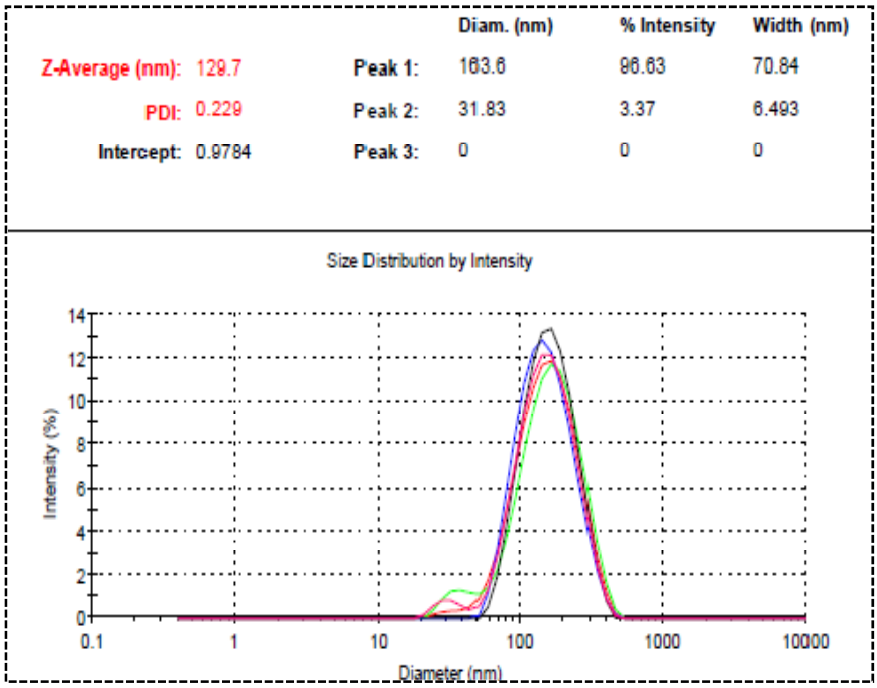

Figure 101: Particle Size distribution of entry 11 Table 31.

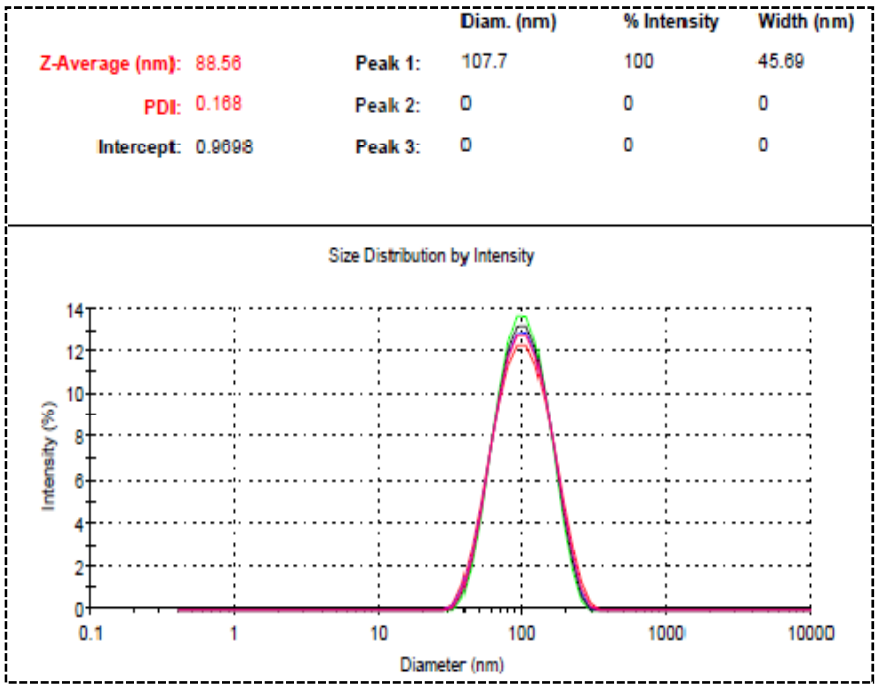

Figure 102: Particle Size distribution of entry 14 Table 33.

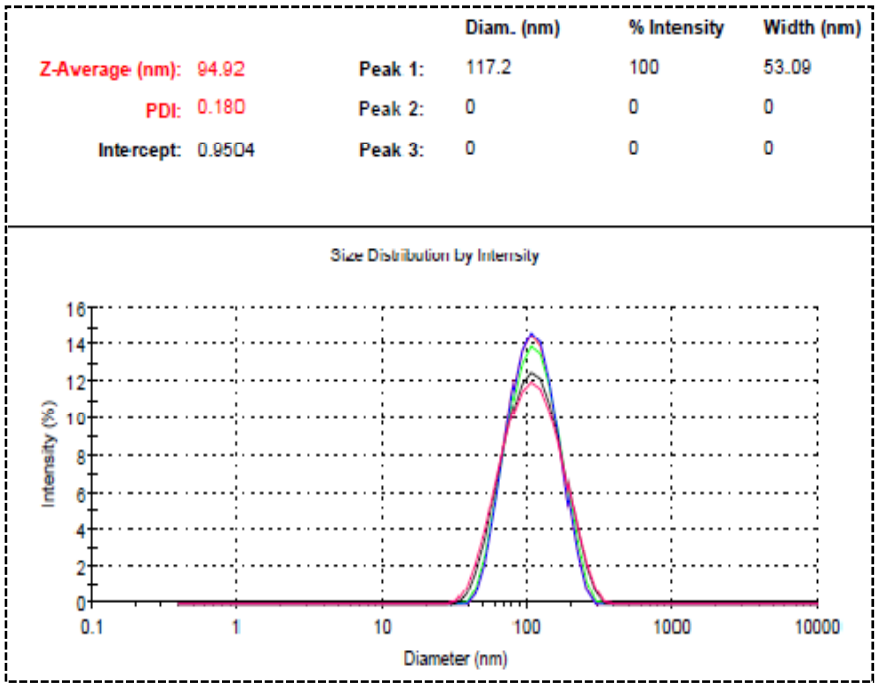

Figure 103: Particle Size distribution of entry 16 Table 34.

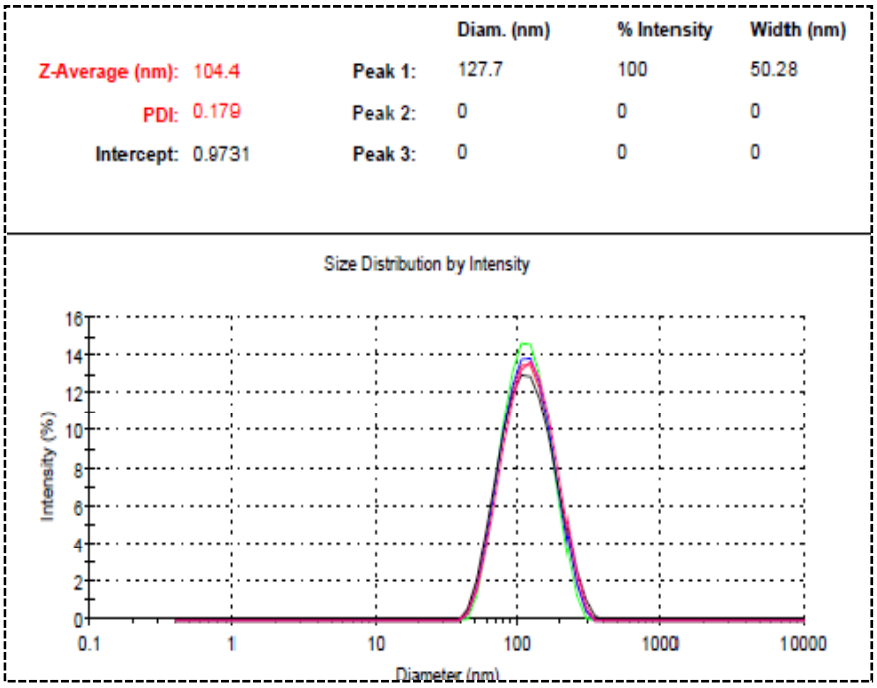

Figure 104: Particle Size distribution of entry 17 Table 34.

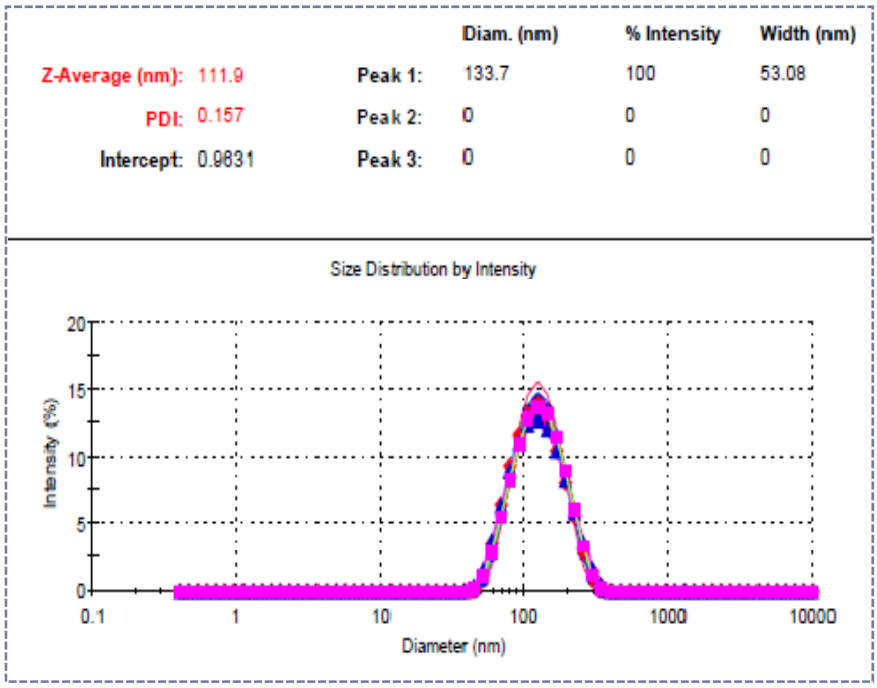

Figure 105: Particle Size distribution of entry 18 Table 34.

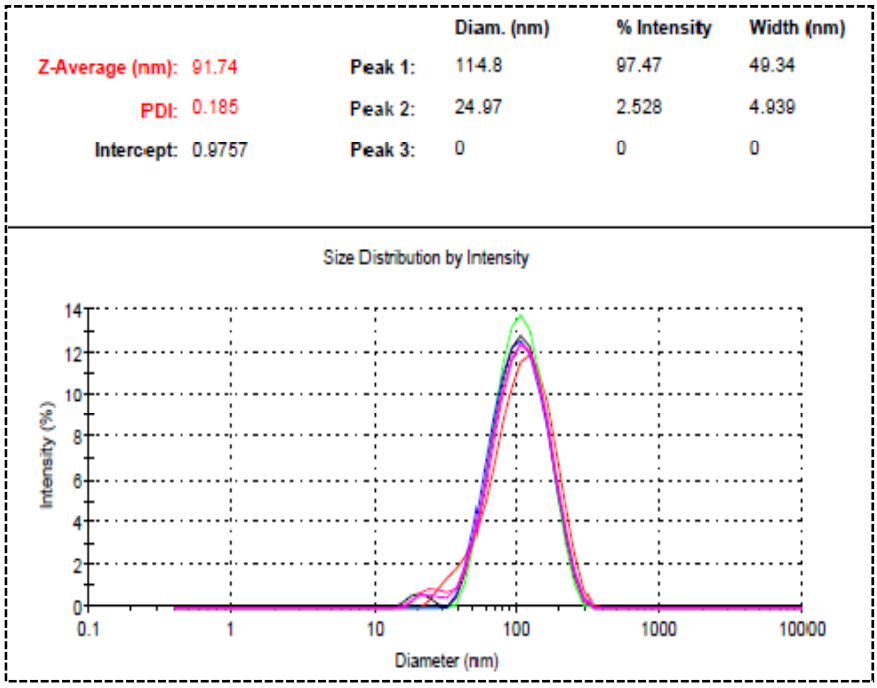

Figure 106: Particle Size distribution of entry 23 Table 37.

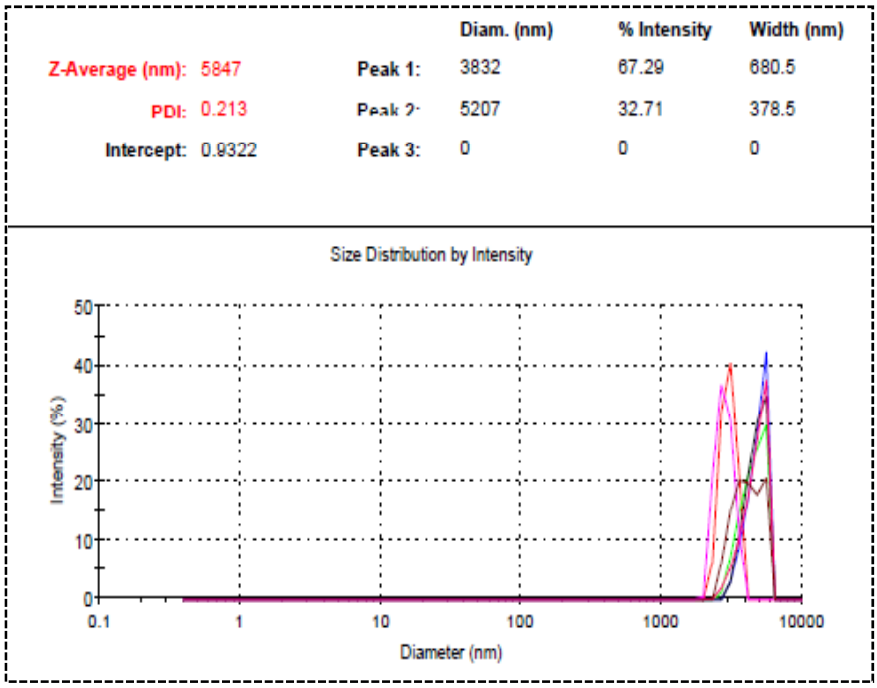

Figure 107: Particle Size distribution of entry 24 Table 37.

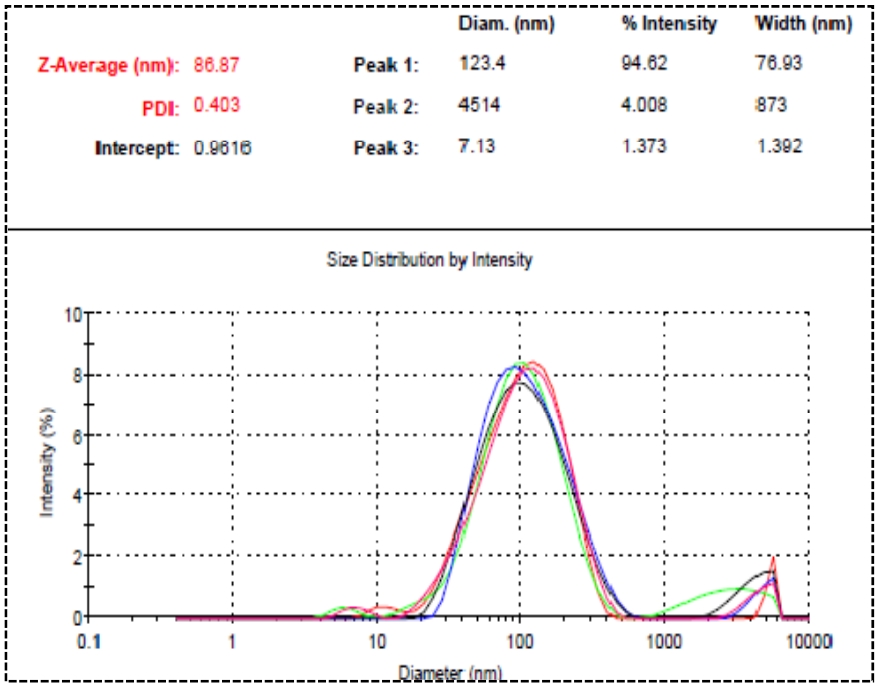

Figure 108: Particle Size distribution of entry 25 Table 37.

6.5.1 Morphological analysis.

1 µl aliquot of the fresh nanosuspension sample was placed in 4 µl of demineralized H_2O on a formvar-coated 400 mesh copper grid, forming a thin liquid film. The sample was kept on the grid for 5 minutes, the liquid was wicked off with filter paper and the grid was air dried. The grid was stained by placing it on a drop of 2% (w/v) uranyl acetate for 1 minute. The stain was rinsed off by dipping the grid in demineralized H_2O, the water removed by wicking, and the grid air-dried. The grid was imaged in a Hitachi H-7100 TEM at 75kV (Hitachi, Brisbane, USA).

7 REFERENCES.

1. Lipinski, C. A.; Lombardo, F.; Dominy, B. W.; Feeney, P. J., Experimental and computational approaches to estimate solubility and permeability in drug discovery and development setting. *Advanced Drug Delivery Reviews* **2001,** 46, 3-26.
2. Diaz, P.; Phatak, S. S.; Xu, J.; Fronczek, F. R.; Astruc-Diaz, F.; Thompson, C. M.; Cavasotto, C. N.; Naguib, M., 2,3-Dihydro-1-benzofuran derivatives as a series of potent selective cannabinoid receptor 2 agonists: design, synthesis, and binding mode prediction through ligand-steered modeling. *ChemMedChem* **2009,** 4, (10), 1615-29.
3. Mukherjee, S.; Adams, M.; Whiteaker, K.; Daza, A.; Kage, K.; Cassar, S.; Meyer, M.; Yao, B. B., Species comparison and pharmacological characterization of rat and human CB2 cannabinoid receptors. *European Journal of Pharmacology* **2004,** 505, (1–3), 1-9.
4. Li, P.; Zhao, L., Developing early formulations: Practice and perspective. *International Journal of Pharmaceutics* **2007,** 341, (1–2), 1-19.
5. Li, P.; Vishnuvajjala, R.; Tabibi, S. E.; Yalkowsky, S. H., Evaluation of in vitro precipitation methods. *Journal of Pharmaceutical Sciences* **1998,** 87, (2), 196-199.
6. Lopez-Berestein, G.; Tari, A. M.; Lim, S.-J. Method to incorporate N-(4-hydroxyphenyl) retinamide in liposomes. 2002.
7. Higuchi, T.; Connors, K. A., Advances in Analytical Chemistry and Instrumentation. *Chapter 4. Phase Solubility Studies* **1965**, 117-212.
8. Aree, T.; Schulz, B.; Reck, G., Crystal Structures of -Cyclodextrin Complexes with Formic Acid and Acetic Acid *Journal of Inclusion Phenomena and Macrocyclic Chemistry* **2003,** 47, (1-2), 39-45.
9. Naguib, M.; Diaz, P.; Xu, J. J.; Astruc-Diaz, F.; Craig, S.; Vivas-Mejia, P.; Brown, D. L., MDA7: a novel selective agonist for CB2 receptors that prevents allodynia in rat neuropathic pain models. *Br J Pharmacol* **2008,** 155, (7), 1104-16.
10. Chaplan, S. R.; Bach, F. W.; Pogrel, J. W.; Chung, J. M.; Yaksh, T. L., Quantitative assessment of tactile allodynia in the rat paw. *Journal of Neuroscience Methods* **1994,** 53, (1), 55-63.
11. Dixon, W., The up-and-down method for small samples. *J Am Stat Assoc* **1965,** 60, 967-978.
12. Brainin-Mattos, J.; Smith, N. D.; Malkmus, S.; Rew, Y.; Goodman, M.; Taulane, J.; Yaksh, T. L., Cancer-related bone pain is attenuated by a systemically available d-opioid receptor agonist. *Pain* **2006,** 122, (1-2), 174-181.
13. Kim, S. H.; Chung, J. M., An experimental model for peripheral neuropathy produced by segmental spinal nerve ligation in the rat. *Pain* **1992,** 50, (3), 355-63.
14. Polomano, R. C.; Mannes, A. J.; Clark, U. S.; Bennett, G. J., A painful peripheral neuropathy in the rat produced by the chemotherapeutic drug, paclitaxel. *Pain* **2001,** 94, (3), 293-304.
15. Dixon, W. J., The up-and-down Method for Small Samples. *J Am Stat Assoc* **1965,** 60, (312), 967-978.

CONCLUSION

Cannabinoid compounds are gaining interest as potential pharmacological agents to treat neurodegenatrative and neuroinflammatory diseases such as neuropathic pain. CB2 agonists are particularly interesting since no or few psychotropic effects have been reported when tested *in vivo* on models of acute and chronic pain. Natural and synthetic cannabinoids are generally highly lipophilic compounds, resulting in unsuitable pharmacokinetic and efficacy profile *in vivo*. In the first part of this project, we designed four DDS, namely micellar system, liposomes and inclusion complexes based on HPβCD for i.v. and i.p. injection and a SEDDS for oral administration, in order to improve the physicochemical properties (i.e. solubility) of MDA7 required for PK and PD studies. These DDS enabled sufficient and consistent systemic exposure of the novel CB2 agonists developed in our laboratory in different rat models of chronic pain. MDA7 complexed with HPβCD proved to significantly alleviate tactile allodynia and exert antinociceptive activity in a model of SNL. The HPβCD based formulation was the most efficient DDS compared to micellar and liposomal preparation administered parenterally. The FDA approved HPβCD appeared to be a well adapted enabling formulation approach for delivery of lipophilic compounds such as cannabinoids at pre-clinical stages of development and their use could be extended for the formulation of NCE tested in high throughput pharmacological screening. These host molecules present many advantages related to their safety, characterization, versatility forming easy-to-obtain inclusion complexes with various drugs and their ability to improve delivery, enhancing NCE solubility. Furthermore, the developed drug inclusion complexes can be directly used in clinical trials. We also demonstrated HPβCD could be successfully used for the delivery of chiral drugs such as MDA7 since the same proportion of each enantiomer was solubilized by the formation of a 1:1 complex and no enantiomeric discrimination in term of solubility was observed. Should the enantiomeric excess be required, determination by ^{1}H-NMR is easy and affordable after complexation of a chiral molecule such as MDA7 by HPβCD. It should be noted that the use of a cosolvent such as MeOH-d_4 used in the Job's plot analysis, can solve a potential problem of water solubility of the small guest molecule. The specific nature of the lipophilic host/guest interaction can be a weakness in that only molecule with the right size and geometry can

be complexed by HPβCD in DDS. One potential problem of drugs that show unusually high affinity for HPβCD might be that they can be retained in urine at early time after injection since cyclodextrins undergo high renal clearance with small volume of distribution and quite short half-lives. In regard with the development process, the amount of cyclodextrins incorporated in the DDS has to be optimized by a phase solubility study for each active substance to be tested. In this regard, a combination of cosolvents or polymer with cyclodextrins can respectively increase the intrinsic solubility or the constant affinity of the complex formed and thereby reducing the concentration in cyclodextrins used in the design of DDS. We already started working on this approach with some compounds from our library.

A powerful alternative for dissolving hydrophobic drugs is the use of cosolvents and surfactants forming micelles and thus increasing their bioavailability. Micelles can have prolonged blood residence time and can gradually accumulate in area with leaky vasculature. Micellar preparations are applicable to a wide range of low crystalline and lipophilic compounds. The micellar system developed has already enabled the *in vivo* testing of various cannabinoids with different physicochemical properties. However, micellar preparations often suffer from significant toxicity after parenteral administration since high concentration of cosolvent and surfactant are usually necessary to solubilize drugs, specifically when toxicological studies are carried out with increasing doses of drug. In our study MDA7, encapsulated in liposomes yielded a limited antinociceptive effect despite their propensity to distribute in tissues with discontinuous endothelium and to target phagocytocic cells. Long-circulating liposomes coated with PEG might have been more efficient as DDS while reducing mononuclear phagocyte system uptake and subsequent high clearance. Overall, the early formulation strategy adopted with liposomes, micellar system and inclusion complexes-based cyclodextrins allowed to evaluate the *in vivo* activity of a selective but non specific CB2 agonist, MDA7, in models of neuropathic pain without any vehicle effect. We currently design DDS for lipophilic small molecules with a targeted polypharmacology for the treatment of complex diseases such as neuropathic pain. The strategy developed in this work will be used resulting in the rapid design of a suitable DDS for a rapid *in vivo* testing of our NCEs.

In the second part of this project, we designed polymeric nanocapsules for the delivery of the highly lipophilic, naturally-occuring natural CB2 agonist, β-caryophyllene. The NCs prepared by nanoprecipitation resulted in enhanced solubility and chemical stability with

high entrapment efficiency of (E)-BCP (≈80%). The cationic and round-shaped NCs developed, are expected to be mucoadhesive. These NCs are nearly monodisperse and exhibit the optimal size for oral absorption in the range of 100 nm. These properties should confer consistent drug absorption through GI epithelium or increased lymphatic transport and subsequent oral bioavailability of (E)-BCP. Whether cationic nanocarriers such as our NCs when administered orally are absorbed transcellularly through the membranous epithelial cells (M cells) of the Peyer's patches in the GALT or through the gut enterocytes, or paracellularly by persorption is not well known. NPs should reach the bloodstream while keeping their native structure to target distant pharmacological targets. To date no such NPs have been described since most of the previously described cationic NPs are based on the metabolizable chitosan. Combining the use of Nile Red, a fluorescent dye encapsulated in the core of our NCs and biocompatible but non-biodegradable long-circulating polymeric NCs based on Eudragit® may provide indispensable information in regards with the mechanism of nanocarriers and drug absorption, their biodistribution and their fate in the body. Results from this study could allow further toxicological investigations and perspective concerning the potential use of these nanosystems combining delivery and imaging properties.

The cationic NCs developed are not limited to the model drug investigated and can encapsulate other lipophilic compounds after solubilzing them in an appropriate oil and raise for these substances the same opportunities as described above. In addition, we demonstrated that the NCs prepared have the properties of forming supramolecular complexes with anionic cyclodextrins or cucurbiturils macrocycles. Preliminary results have been generated for the use of these intriguing macrocycles with our cationic system which can be the base for the design of potential future theragnostic (drug delivery and imaging) systems specially promising for the selective targeting of distant pharmacological targets.

Further work might be undertaken to eventually adapt this concept using biodegradable cationic polymer such as chitosan for chronic use or to avoid any potential toxicities issues. Nevertheless the entrapment of imaging agent such as Nile Red will probably improve the understanding of the *in vivo* behaviors of these non biodegradable nanocapsules. A study to evaluate the *in vivo* antinociceptive efficacy of CB2 agonist

after oral administration in the nanocapsules developed has been planned and will be carried out in a near future.

Through this project, we set up an early formulation strategy and validated the pharmacological activity of our CB2 agonists as well as developed a complex and advanced DDS which may be used as a theragnostic tool in future drug discovery or development process. The development of cannabinoids as therapeutics has been limited for a long time because of their poor aqueous solubility, and attempts to synthesize more water-soluble cannabinoids have been undertaken but these NCE may suffer from non appropriate biodistribution in areas important for the treatment of pain such as the CNS.

Mechanism of action for CB2 agonists is yet needed to be understood and selective targeting of immune cells by the supramolecular complexes developed containing a CB2 agonist could elucidate their mode of action as well as validating the biological targets involved in neuropathic pain and immune disorders. In addition, the early formulation strategy developed may be extended to the CB1 ligands since they show significant structural analogy with CB2 compounds to better understand their mechanism of action on immune response. Otherwise cannabinoids have been described to have anticancer properties and the use of PEGylated liposomes or functionalized nanocapsules could allow increasing the knowledge regarding cannabinoids antitumoral activity by tumor-specific targeting.

Overall, this work opens perspectives for further mechanistic investigations regarding the activity of cannabinoids ligands, their pharmacological target(s) and their absorption pathway with the possibility to develop a cannabinoid compound with an improved biological profile for the clinical treatment of pain.